Volume 6, Number 3
November, 1960

THE SOVIET JOURNAL OF

ATOMIC ENERGY

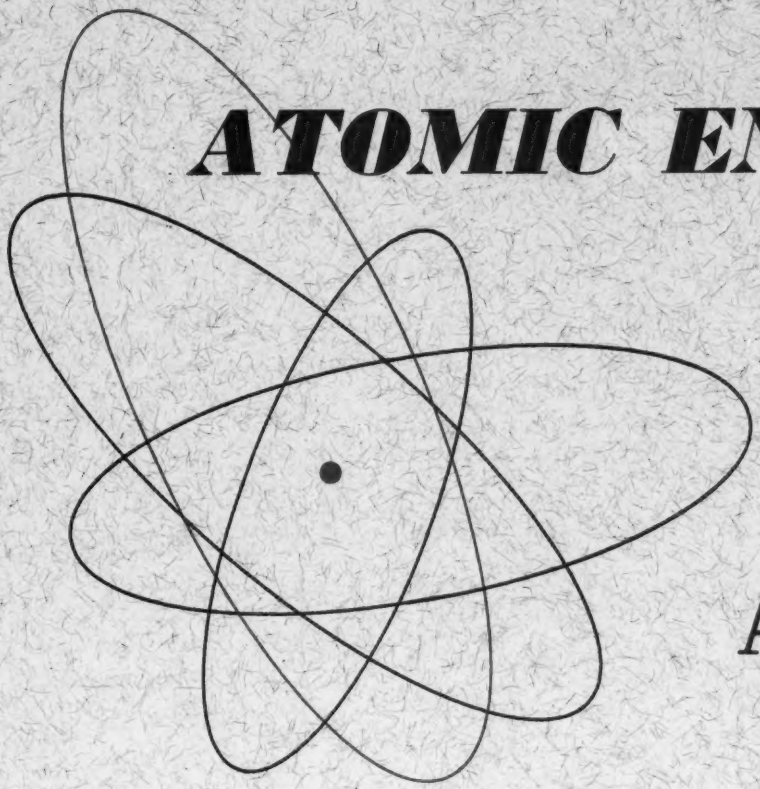

Атомная энергия

TRANSLATED FROM RUSSIAN

CONSULTANTS BUREAU

3 titles of immediate interest!

LECTURES ON NUCLEAR THEORY
by L. Landau and Ya. Smorodinsky
Translated from Russian

A concise presentation by these world-famous Soviet physicists of some of the basic concepts of nuclear theory. Originally published at $15.00 per copy.

". . . a real jewel of an elementary introduction into the main concepts of nuclear theory . . ."—NUCLEAR PHYSICS
". . . a decidedly worth-while addition to any experimental nuclear physicist's library."—E. M. Henley, PHYSICS TODAY

cloth 108 pages $5.25

Order from: **PLENUM PRESS 227 W. 17th Street, New York 11, N.Y.**

— of major interest to all researchers in low-temperature physics.

A SUPPLEMENT TO "HELIUM"
By E. M. Lifshits and E. L. Andronikashvili
Translated from Russian

This notable volume consists of two supplementary chapters, by these outstanding Soviet physicists, which were added to the Russian translation of W. H. Keesom's classic book "Helium."

The first chapter, by Lifshits, presents a concise resume of the Landau theory of superfluidity. The second chapter reports in considerable detail the experimental work conducted by Peter Kapitza and E. L. Andronikashvili.

cloth 167 pages illustrated $7.50

Order from: **CONSULTANTS BUREAU 227 W. 17th St. • New York 11, N. Y.**

A NEW METHOD IN THE THEORY OF SUPERCONDUCTIVITY
By N. N. Bogoliubov, V. V. Tolmachev and D. V. Shirkov
Translated from Russian

The Soviet authors put forth a systematic presentation of a new method in the theory of superconductivity, developed as a result of the research of N. N. Bogoliubov and V. V. Tolmachev—based on a physical and mathematical analogy with superfluidity. This new method is an immediate generalization of the method developed by Bogoliubov in formulating a microscopic theory of superfluidity.

The authors give calculations for the energy of the superconducting ground state using Frohlich's Hamiltonian, as well as of the one-fermion and collective elementary excited states. A detailed analysis of the role of the Coulomb interaction between the electrons in the theory of superconductivity is included. The authors also demonstrate how a system of fermions is treated with a fourth-order interaction Hamiltonian and establish the criterion for its superconductivity.

cloth 121 pages illustrated $5.75

Order from: **CONSULTANTS BUREAU 227 W. 17th St. • New York 11, N. Y.**

Descriptive folders upon request.

EDITORIAL BOARD OF
ATOMNAYA ÉNERGIYA
A. I. Alikhanov
A. A. Bochvar
N. A. Dollezhal
D. V. Efremov
V. S. Fursov
V. F. Kalinin
A. K. Krasin
A. V. Lebedinskii
A. I. Leipunskii
I. I. Novikov
(Editor-in-Chief)
B. V. Semenov
(Executive Secretary)
V. I. Veksler
A. P. Vinogradov
N. A. Vlasov
(Assistant Editor-in-Chief)
A. P. Zefirov

THE SOVIET JOURNAL OF

ATOMIC ENERGY

A translation of ATOMNAYA ÉNERGIYA,
a publication of the Academy of Sciences of the USSR

(Russian original dated March, 1959)

Vol. 6, No. 3 November, 1960

TABLE OF CONTENTS

	RUSS PAGE	PAGE
Aspects of Nuclear Power Economics. E. P. Anan'ev	245	137
Uranium and Its Alloys. G. Ya. Sergeev and V. V. Titova	253	143
Fuel Elements of Nuclear Reactors. A. G. Samoilov and V. S. Volkov	261	150
The Effect of Neutron Irradiation on the Structure and Properties of Ferrito-Pearlitic Steels. V. S. Lyashenko and Sh. Sh. Ibragimov	277	165
An Investigation of γ-Emission Associated with Thermal Neutron Capture. L. V. Groshev, B. I. Gavrilov, and A. M. Demidov	281	170
The Asymmetry of Nuclear Fission. B. T. Geilikman	290	178
The Excitation Energy of Fragments in Nuclear Fission. B. T. Geilikman	298	184
Possibility of Accelerating Polarized Protons in a Cyclotron. G. M. Budyanskii, Yu. A. Zavenyagin, N. D. Federov, and V. A. Khrabrov	306	190
Experimental Verification of the Theory of Neutron Diffusion in a Medium with Voids. I. F. Zhezherun	311	194
Neutron Activation Analysis of Samples of Rock and Ore Concentrates. D. I. Leipunskaya, Z. E. Gauér, and G. N. Flerov	315	198
Scintillating Glass for the Detection of Slow Neutrons V. K. Voitovetskii, N. S. Tolmacheva, and M. I. Arsaev	321	203
Letters to the Editor		
Apparatus for Fine Purification of Inert Gases from Oxygen and Water Vapor. N. S. Grachev and P. L. Kirillov	327	208
Preparation of Heavy Isotopes of Carbon, Sulfur, Krypton, and Neon by Diffusion in a Vapor Stream. I. G. Gverdtsiteli and V. K. Tskhakaya	329	211
Preparation of Plastic Scintillators. E. E. Baroni and V. M. Shoniya	330	213
β-Dosimetric Applications of Several Standard γ-Counters. B. P. Bulatov	332	215
Shielding Against γ-Radiation Leaving Through the Base of a Cyclindrical Source. D. P. Osanov	333	217
A Numerical Method for Solving Two-Dimensional Diffusion Equations. N. I. Buleev	338	222
Scientific and Technical News		
Scientific and Technical Conference on Applications of Radioactive Isotopes and Radiations in Automotive and Tractor Engineering. A. I. Nisnevich and D. I. Vysotskii	342	225
[Nuclear Energy for Rocket Engines	343]	
Soviet Electronic Instruments for Use in Nuclear Physics on Display at the 1958 World's Fair	345	228
[Buildup Factors for Shielding Glasses	350]	
Hyperfine-Grained Emulsions	352	232
Radiogenic Lead in Nonradioactive Minerals as a Criterion in the Exploration for Uranium and Thorium Deposits	352	233
[The Stellarator Program in the USA	353]	

Annual subscription $75.00
Single issue 20.00
Single article 12.50

Copyright 1960 Consultants Bureau Enterprises, Inc., 227 West 17th St., New York 11, N. Y.
Note: The sale of photostatic copies of any portion of this copyright translation is expressly prohibited by the copyright owners.

CONTENTS (continued)

	RUSS. PAGE	PAGE
[International Colloquium for 1959, 1960		
Source: Proc. Phys. Soc. 72, No. 468, 1151(1958).	355]	
Brief Communications	356	234
Information and Bibliography	358	235
New Literature	358	236
In Press	360	237
Articles in the Periodical Literature	361	238

NOTE

The Table of Contents will continue to list all material which appeared in Atomnaya Energiya, but those items which originated in the English language and are therefore not included in the translation are enclosed in brackets. Whenever possible, the source from which English copies of the omitted reports can be obtained will be given.

Consultants Bureau Enterprises, Inc.

ASPECTS OF NUCLEAR POWER ECONOMICS

E. P. Anan'ev

The article is a review of various aspects of nuclear power economics based on materials made available at the Second International Conference on the Peaceful Uses of Atomic Energy at Geneva, 1958.

Currently, discussions are under way in various countries on the economic aspects of the use of atomic energy for the production of electric power, and the scheduling of the erection of atomic-fueled electric power plants. This article provides a rundown of the various major questions related to the structure of the initial capital outlay, an analysis of plant-operation factors, and their effects on the economics of atomic electric power plants.

Problems of the economics of atomic electric power plants using fast reactors are dealt with in brief.

Data are cited indicating that the prequisities exist for the economically justified use of the heat power of thermal reactors in power utility installations.

During the three years which have elapsed since the First Geneva Conference on the Peaceful Uses of Atomic Energy, 1955, atomic power plants operating on an industrial scale have been built and commissioned in the USSR, the USA, and Great Britain. Although not enough time has elapsed to enable us to give exhaustive answers to all problems arising in the area of atomic power economics, some of the principal questions related to the structure of initial capital investment and operating costs incurred in an atomic power station may be answered now with greater confidence than could have been done three years ago.

The electric power cost structure and the factors affecting the cost per kw-hr now stand in bolder relief.

Since the economic structure of atomic and heat-power electric power stations are similar, the power developed by atomic power stations now in operation, under construction, or on the drawing boards may be compared with the power of coal-fired power plants.

At the Second International Conference on the Peaceful Uses of Atomic Energy, the economic aspects of the utilization of atomic energy for the generation of electric power were discussed. Reports on this topic were presented by the USSR [2027],* France [1131], the United Kingdom [262], the USA [1076], India [1624], Czechoslovakia [2092], Poland [1593], Rumania [1304], Japan [1318], Italy [1363], and other nations. Over 25 papers dealt solely with questions of the development of atomic power and related economics, whereas over 175 papers dealt with the engineering side of atomic power. In addition, a significant number of the papers presented discussed the physics of experimental and power-only reactors, as well as research reactors.

Some of the papers not only considered the question of the use of atomic energy for generating electric power, but also for producing heat power for industry [443] and for power utilities [136].

Both the over-all aspects of the economics and the factors involved in the development of atomic power networks were discussed [1445, 1382, 54, 2028].

In the paper presented by the Soviet delegation, entitled "The Future of Atomic Power Engineering in the USSR" [2027], concrete data were provided on the prerequisites for the development of nuclear power facilities in the USSR.

In the program under way in Great Britain for the erection of atomic-fired power plants, special attention is being devoted to dual-purpose atomic power stations incorporating Calder-Hall-type reactors, i.e., graphite-moderated, gas-cooled reactors burning natural uranium. The material presented by the British delegation indicates that one of the foremost tasks facing atomic electric power stations now in operation is the production of plutonium [1].

A paper presented by Mayer (USA) [2163] endeavors to survey the prospects for the development of atomic power in 152 countries throughout the world during the period from 1960 to 1980.

As one might expect the development of nuclear power in each country depends on the structure of its energy budget. For example, in the Soviet Union, which possesses huge energy reserves of coal fuels and appreciable hydroenergetic resources, the development of atomic power engineering will be different from that in countries lacking coal. The schedule of projected work in the Soviet Union provides mainly for the acquisition of a fund of experience in the operation of large-scale atomic power stations. Power engineers in Czechoslovakia [2092] are faced with the task of bringing about an appreciable increase in the generation of electric power without stepping up coal consumption proportionately. This may be achieved by utilizing available uranium reserves. Czechoslovakia has therefore decided to construct an industrial, atomic-fuel power station operating on natural uranium.

The papers submitted by the French delegation indicate that the prospects for the development of atomic power plants in that country are sufficiently promising to allow a step-up in the consumption of natural gas (found in deposits at Laquais), since the compensation for the expended reserves of natural gas may be made available

*Numbers enclosed in brackets are the official numbers assigned to papers delivered at the 1958 Geneva Conference.

through the generation of electric power by atomic power plants of the future [1131].

The reports submitted by Turkey, Italy, Poland, Rumania as well as other nations communicate a desire to erect atomic-fuel electric power plants.

Some years ago, several specialists in the USA relegated the construction of atomic power plants to the remote future. They felt, since coal costs for the USA were somewhat below the average world-level, that the development of nuclear power at that time did not appear to offer great economic advantages. At the 1958 Conference, however, a USA delegate presented a report [1076] outlining a program for the development of nuclear power facilities in that country, in conjunction with the erection of atomic-fuel power plants for the purposes of gaining experience in determining the most promising reactor types, as well as acquiring engineering and economic performance data [1076].

A paper by Lewis [183] indicates the possible rate of growth of nuclear power development in Canada, which would be consistent, in the opinion of the author, with the needs of the country. The program is based on the building of heavy-water reactors using natural uranium (without regeneration of the latter). The following dates have been set for operation at the lower levels indicated: 0.2-1 million kw by 1966; 0.6-1.7 million kw by 1971; 2.0-3.3 million kw by 1976; 4-7 million kw by 1981. These figures are viewed as the minimum schedule; the maximum program, also represented in the paper, anticipates considerable scaling up of those power levels.

India's requirements of power facilities (looking ahead to the year 2000) operating on the basis of the use of the thorium raw material available in the country are outlined in a paper presented by H. Bhabha [1624]. It is believed that nuclear reactors will eventually supply most of India's electric power, and present plans for the development of India's nuclear power potential allow for her estimated population increase (600,000,000 people by 2000 A.D.), as well as for the raising of her electric power consumption to the level prevailing in European countries.

The economic aspects of the development of nuclear power in small countries deficient in power resources were also discussed in the submitted reports.

Capital Expenditures

Reports presented at the Conference confirmed the widely known fact that nuclear power economics are determined by two criteria: 1) by the ratio of capital alloted for the erection of nuclear power plants to the capital allotments for the erection of electric power plants fired by conventional fossil fuels; 2) by the ratio of operating and maintenance expenses (including fuel costs), which determine for the most part the cost of the electric power generated, to the cost of electric power derived from conventional-fuel electric power plants.

Capital expenditures depend on various factors. Jukes [72] notes that, over the past three years in Great Britain, capital outlays for electric power plants in the construction or planning stage were increased on several occasions. This attests to the instability of criteria used in evaluating construction costs.

Lane [2] (USA), a specialist in the field of "nuclear" economics, pointed out that capital expenditures for 80 Mw atomic-fueled electric power stations are 3-3.5 times higher than those for coal-fired electric power stations, coming to 200-250 dollars per kw, whereas for an electric power station producing in the neighborhood of 200 Mw, capital outlays come to 150-160 dollars per kw. Consequently, capital expenditures for a high-power-level nuclear electric power plant do not differ substantially from the outlays for a conventional plant. The amount of capital expended displays little dependence on the nature of coolant used (water, gas, or liquid metal).

The effect of the power level developed by an atomic electric power station on capital expenses has been determined quite clearly by a number of authors [3-6]. It should be noted that experimental atomic power stations in the Soviet Union will have high power levels, making it possible to acquire experience in the industrial operation of reactors, and to clarify problems pertaining to economics and to the nuclear power network being created in the USSR.

It is now more or less firmly established that the relative costs of individual component elements of atomic power stations remain stable for all power levels.

In Lewis' paper [183] (Canada), the cost structure of of a nuclear electric power station using a heavy-water reactor (see below) is presented. We learn from those data that the capital outlay for steam-generating equipment is approximately equal to the outlay for turbogenerators and accessories (50%).

	Total cost, $ million	Specific cost of rated power, $/kw
Reactor and accessory equipment	10,7	53,5
Construction and operating costs	10,0	50,0
Pumps and steam generators	4,7	23,5
Turbogenerators and accessories	15,0	75,0
Total	40,4	202,0
Heavy water	11,7	58,5
Fuel reserves	8,2	41,0
Total costs	60,3	301,5

In a coal-fired electric power station, boiler room and fuel supply expenses usually exceed those for the turbogenerator facilities, and amount to roughly 50-55% of plant costs. It may therefore be safely assumed that in a nuclear power station the cost of steam-generating equipment would be comparable to boiler room costs (with accessories) in a coal-fired power station.

In one report [207] (Canada), it was demonstrated that capital costs incurred where a high interest rate was paid

back on borrowed capital (credit) may amount to about 250 dollars per kw of rated electric power.

Hydroelectric power stations require higher capital expenditures, as a rule, than do coal-fired power stations. Hydroelectric power plants now under construction in Canada require capital investments of about 300 dollars per kw (12 years ago, the costs of capital outlays came to 200 dollars per kw). The trend is toward increased capital investments. In Canada, capital costs for coal-fired stations amount to 150 dollars per kw of rated power, 130 dollars per kw for oil-fired stations and 120 dollars per kw for gas-fired electric power stations.

In another report [1446] (Great Britain), capital costs at nuclear electric power plants are compared to costs at heat-power electric plants (Table 1). Construction of the respective power stations was undertaken at approximately the same period.

The interest rate on borrowed capital is 5-6% for both nuclear and coal-fired power plants. This corresponds to total capital costs for 8% and 8.7% annually in the erection of nuclear power stations (20 years' amortizable life) and to capital costs incurred in the erection of a conventional station amounting on the average to 6.7-7.5% (depreciation period of the power station: 25 years; of the buildings: 40 years).

The amortization period of the nuclear power plant (20 years) is based on the predicted service life of the reactor. The amortization period of a coal-fired power station (equipment and buildings) is the one conventionally assumed in British practice. According to Jukes' calculations [7] (Great Britain), capital investments in atomic-fuel electric power stations similar to the power stations being built for the Central Power Administration are calculated to reach 130 pounds sterling per kw of power rating.

TABLE 1. Comparative Data for Nuclear and Coal-Fired Power Stations

	Nuclear power station		Coal-fired power station	
Year to be commissioned	1960	1962	1959	1963
Power, Mw	275—300	500	200	550—600
Capital costs, pounds sterling per kw	145	120	55	45
Service life of equipment (depreciation), years	20	20	25	

In the USA, capital investments placed in nuclear power stations now being erected fluctuate roughly from 200 to 470 dollars per kw of rated power. In standardized construction of a series of plants based on an accepted prototype, plant costs will apparently exhibit greater stability, and are expected to close the gap with the costs of coal-fired plants which, as pointed out earlier, amount to 180 dollars per kw, in existing coal-fired electric power generating stations in the USA and Canada.

Equipment costs in one of the British nuclear power stations (at Hunterston are expected, according to present estimates, to come to 125 pounds sterling per kw of rated power.

The area occupied by the power station will be essentially without effect on the construction costs of nuclear power stations but will figure prominently in the choice of the construction site and in prospecting work during the planning stage.

Comparison of the plant areas in the case of coal-fired and of nuclear power plants demonstrates that a nuclear-fuel power plant is more compact and may be accomodated in a smaller area. As we see readily from Table 2, the area occupied by a nuclear power plant producing 300 Mw power is 1.5-2 times smaller than the area occupied by a coal-fired power station.

TABLE 2. Area Occupied by Plant, for Coal and Nuclear Power Stations

	Coal-fired stations			Nuclear station		
	GRES		TETs			
Power, Mw	300	600	300	100	200	300
Area occupied, hectares	23—26	35—39	27—34	5	10÷15	
Building factor, %	9—10	12—17	16—17	—	—	—
Utilization factor of area, %	35—50	36—50	49—55	—	—	—

Operating Factors and Their Effects on the Economic Criteria Governing Nuclear Power Stations

At the present time, it is still too early to say which will prove to be the most convenient nuclear fuel: enriched, or natural, uranium, since the economic yardstick indicating the advantage inherent in the use of either form has yet to become established, and this problem may be satisfactorily solved only in conjunction with other factors.

The duration of the run, or period of operation, is a parameter exerting a material effect on the competitive capabilities of one atomic-fuel power station now under construction in the USSR (possessing a uranium-graphite reactor, steam superheat to 500°C under a steam pressure of 90 atm), as may be readily appreciated from the diagram. The diagram shows the relative dependence of the fuel component of electric power costs on the length of the operating period. The fuel proves to contribute some 30-40% of the total costs of electric power generated. It is common knowledge that in coal-fired power stations

the fuel component of the power costs per one kw-hr does not drop below 67% [8]. The comparison of the contributions due to the fuel component speaks in favor of nuclear power stations.

The length of the operating period is to a considerable degree dependent on the plutonium formed in the reactor. Plutonium isotopes Pu^{239} and Pu^{241} help lengthen the run, whereas a buildup of nonfissionable Pu^{240} isotope with its large neutron-absorption cross section leads, conversely, to reduced reactivity and, as a consequence, to a shorter operating period.

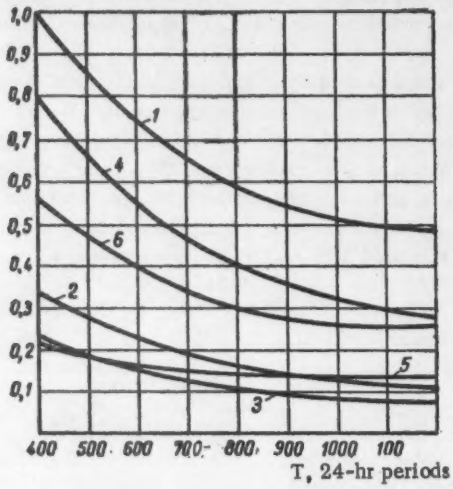

Dependence of the fuel component of electric power costs of the period of operation: 1) cost of uranium charge in pile; 2) cost of fabrication of operating channels; 3) chemical processing costs of uranium; 4) uranium costs after chemical processing; 5) cost of plutonium extracted from reactor; 6) fuel contribution to electric power costs.

In a uranium-graphite boiling water reactor with steam superheat (USSR), the amount of U^{235} consumed in the course of a run (730 days) amounts, on the basis of calculations, to 243 kg, and of Pu^{239}, to 55 kg. The plutonium so formed is partly burned in the pile and thus contributes to lengthening the operating period. The direct advantage is obvious.

The length of a run (or the extent of burnup) is also affected by the mode of core operation. For example, during the operation of the first nuclear power station in the USSR, a technique of partial charging of the operating channels was employed, which made it possible to greatly increase the amount of fuel burnup in the channels. The essentials of the method of partial chargings consisted in a constant complete burnup in the center of the pile of the poorly depleted peripheral operating channels, replacing the latter with new channels. Operation of the reactor over the course of 300 effective days required the use of 512 channels, at a rate of depletion of 1.7 channels per single effective day. The use of the partial charging technique made it possible to cut down the rated channel depletion for a single effective day to 1.2 channels, which had a favorable effect on the competitive economic capabilities of the nuclear power station, and allowed a reduction in the costs of the electric power generated.

The amount of energy comprising 10,000 Mwd/ton developed by the uranium charge in the reactor is often used as a basis for calculation of the fuel contribution to electric power costs. However, this figure is not a limiting figure; e.g., in four operating channels of the reactor installed in the USSR's first nuclear power station, the extent of U^{235} burnup was brought to 25 kg/ton, which corresponds to heat energy generated amounting to about 20,000 Mwd/ton.

An effective means for cutting electric power costs will be found in the construction of high-power nuclear stations. Two pathways are available for attaining those high power goals: 1) building reactors with high unit power; 2) the use of a combined heat cycle, viz. producing steam from the heat derived from the fission reaction and subsequent superheating of the steam by means of the heat derived from consumption of conventional organic fossil fuels. A cycle of that type is being used in an American nuclear power station now under construction (Indian Point), which provides, solely on account of saturated steam, available electric power of 163 Mw [1885]. The heat power of the reactor is 588 Mw. Steam superheat enables the electric power of the station to be raised to 112 Mw. The total electric power generated comes to 275 Mw.

If the operating data were our sole criteria of economic competitive capability then, as follows from design data, electric power costs in a cycle working only on saturated steam would come to 1.75 cents per kw-hr. By employing steam superheat, power costs may be cut down to 1.32 cents per kw-hr. Accordingly, superheating the steam by using conventional fuels will raise the power of the nuclear electric power station 70% compared to the power developed by a station operating on saturated steam alone, and in the process cuts electric power costs by 30%.

Using a cycle with steam superheat reduces the cost of the power station equipment. The design specific cost of an atomic power station amounts (without using the steam superheat) to 472 dollars per kw (the total cost being 90 million dollars). The relationships underlying fuel consumption are the following: nuclear fuel: 7.36 million dollars; liquid fuel: 3.015 million dollars.

Since the overriding purpose of the British nuclear power stations is evidently the production of plutonium, the evaluation of their economic performance data must be approached from a different angle than that used in the evaluation of the economic performance data of nuclear stations whose principal function is the generation of electric power.

Jukes presents, in one report [72], comparative economic data for British nuclear power stations now in construction or planning stages (some of these data were presented

TABLE 3. Comparative Economic Performance Data of British Nuclear Power Stations

	Data presented at the 1955 Geneva Conference	Recent data on Stations being constructed	
		Period of completion of construction work 1960-1961	Period for completion of construction work 1962
Power, Mw	150	275÷300	500
Capital expenses, including initial loading expenses, pence per kw-hr	0,36	0,51—0,52 & 0,55—0,56	0,41—0,42 &0,45—0,46
Operating costs, rated, pence per kw-hr	0,40	0,06 0,06	0,05 0,05
Fuel recharging expenses, pence per kw-hr		0,13—0,19 & 0,13—0,19	0,13—0,19 & 0,13—0,19
Credit from plutonium buyback by government, pence per kw-hr	0,33÷0,17		
Total power costs, pence per kw-hr	0,43÷0,59	0,77—0,70 & 0,74—0,81	0,59—0,66 & 0,63—0,70

at the 1955 Geneva Conference), for which see Table 3.

The fact that the cost of recharging of fuel is linked with the amount of government credit allocated to plutonium buyback for weapons use, prevents us from making a complete analysis of the true cost of a kw-hr of electric power generated. However, it may be safely assumed that if the plutonium produced at the nuclear power station is not bought back for weapons use, then the net cost of a single kw-hr of power generated would amount to 1.09 pence for a 150 Mw station, and would also be considerably above the value cited for nuclear power stations generating 500 Mw power.

An article by Hinton [9] (Great Britain) provides rather optimistic data, extrapolated 40 years ahead, on the cost of electric power generated at nuclear-fueled electric power stations, taking into account the fact that electric power costs at coal-fired power stations will increase over the same period, as expected, due to the increased cost of coal supplies.

TABLE 4. Predicted Electric Power Costs for Power Generated at Nuclear and at Coal-Fired Power Stations in Great Britain (in pence per kw-hr)

	1960	1970	1980	1990
Nuclear power stations				
Total cost	0,73	0,52	0,41	0,33
Profits from plutonium buyback	0,07	0,05	0,03	0,01
Net cost	0 66	0,47	0,38	0,32
Coal-fired electric power stations				
Total cost	0,60	0,67	0,73	0,84
With fuel costs included	0,44	0,52	0,60	0,72

Comparative data on electric power costs as produced by nuclear and by coal-fired electric power plants may be found in Table 4.

Fast Reactor Economics

The extent of fuel burnup in a fast reactor† is determined by the stability of the fuel element used. After serving out its useful life, the fuel element should be withdrawn and routed for chemical reprocessing.

Reactivity losses in a fast reactor due to fuel burnup are moderate. Therefore, the less frequently fuel elements are extracted for chemical reprocessing, the more economical will be the performance of the power station.

The competitive capabilities of a nuclear power station incorporating a fast reactor [2028] are determined by the breeding ratio. The value of the breeding ratio must take into account plutonium losses suffered during chemical reprocessing.

The technique for calculating the effectiveness of the performance of a fast reactor was outlined in one of the papers submitted by the Soviet delegation [2028]. In the present article, the intent was solely to underline the fact that, in taking into account all of the features encountered in the use of nuclear fuel in fast power reactors, the electric power costs may be rather low. Such results have been arrived at by other authors in their calculations.

At the Enrico Fermi fast reactor power station in the USA [2427], the design cost of electric power at 1% burnup amounts to 0.72 cents per kw-hr, at 2% fuel burnup to 0.35 cents per kw-hr, and at 3% burnup to 0.22 cents per kw-hr. The most reliable value of those cited is the value for 2% burnup and, accordingly, a power cost level of 3.5 mills per kw-hr may be attained without any particular difficulty.

† The extent of fuel burnup is equal to the ratio of the mean weight of fission fragments to the mean weight of the plutonium formed in the spent fuel element.

Heat-Power Utilities

It is no accident that nuclear energy attracts the attention of scientists as a competitive power source. In the problem of heat-power public utilities servicing large cities, a large role is played not only by heat cost factors, but also by over-all economic factors. Heat-power facilities place an intense demand on coal supplies during the course of the home-heating season and thereby overloads existing transportation facilities, whereas the haulage of nuclear fuel to meet the demands of a nuclear heat power and nuclear electric power generating station presents no difficulties.

The problem of developing heat power utilities from a nuclear energy source is described in papers submitted by Swedish scientists [135,136]. To supply heat needs, it is proposed to employ the "Adam" atomic facility, which will have a reactor capable of developing 75 Mw heat power, in service over 5000 hrs annually. The temperature of the hot water produced in the reactor will be 140°C. Siting the reactor facility in mountainous environs will enable two conflicting problems to be tackled successfully: safety requirements will be met and the facility will be as close as possible to the city it is servicing.

The basic design economic performance data of the Swedish heat power facility are the following: At a cost of 74 dollars/kg of natural uranium and with plutonium buy-back credit of 12 dollars for the by-product plutonium from 1 kg of uranium, the net fuel cost will level off at 62 dollars/kg. The amount of power generated will be about 4000 kwd/kg. Under such conditions, the cost of the heat power will be 0.065 cents per kw-hr.

The cost of power produced in Sweden by means of combustion of oil fuels of 9200 kcal/kg calorific value (on the basis of 22 dollars for a single cubic meter and at a thermal plant efficiency of 85%) amounts to 2.6 mills per kw-hr of heat energy. Thus, the heat generated from combustion of conventional fossil fuels is four times more expensive than the heat generated at the nuclear installation.

Even if it is assumed that those data are highly optimistic, the economic effectiveness and feasibility of such an approach to utilizing atomic energy is beyond doubt.

In conclusion, it should be noted that a more extended experience in the operation of existing large-scale nuclear electric power generating power plants and the commissioning of new large-scale stations will make it possible to provide a definitive answer to questions arising in the economics of nuclear power engineering.

LITERATURE CITED

[1] Calder Hall, Technical study. (Published in Russian by the Atomic Energy Administration of Britain, August 1958).

[2] J. A. Lane, Nuclear Power Economics. (Lecture read during the International Courses on Atomic Energy for Industrialists.) (Paris, Jan. 1957).

[3] N. A. Nikolaev, Atomnaya energiya 3, 11, 385 (1957).

[4] N. A. Dollezhal', Atomnaya energiya 3, 11, 391 (1957).

[5] I. I. Novikov, Atomnaya energiya 3, 11, 409 (1957).

[6] N. A. Dollezhal' et al, Atomnaya energiya 5, 3, 223 (1958).

[7] Appl. Atomics, 79, 3 (1957).

[8] L. Ya. Avrukh, Net Cost of Electric and Heat Power [in Russian] (Gosenergoizdat, 1957).

[9] C. Hinton, J. Brit. Nucl. Energy Conference 2, 292 (1957).

Received November 5, 1958

URANIUM AND ITS ALLOYS

G. Ya. Sergeev and V. V. Titova

A short résumé is given of the results of investigations of the physico-mechanical properties of uranium and its alloys, based on reports given at the Second International Conference on the Peaceful Uses of Atomic Energy, Geneva, 1958. The effect of irradiation on uranium and, in particular, the phenomenon of gas swelling are examined. Some examples are given of α-phase and γ-phase uranium alloys, including alloys of the fissium type. The temperature limits for the use of solid nuclear fuel based on uranium are considered. In conclusion, we give some information on the techniques for metallographic investigation of irradiated and unirradiated uranium.

In the period between the two Geneva conferences, metallographic investigations were mainly directed toward the measurement and evaluation of the physical and mechanical properties of highly pure uranium, free from the effect of the usual impurities, and of industrial uranium. The purpose of the investigations was the further study of the structure and properties of uranium and its behavior under technological processing and irradiation.

The investigations were primarily directed toward solving the most difficult problem in nuclear technology, namely, increasing the dimensional and structural stability of fuel elements under irradiation. This problem must be solved for the development of fuel materials, which can withstand the burnup of a large portion of the total atoms in the fuel at high temperatures and thus provide cheaper nuclear energy.

In many cases, in work at high temperatures and burnup, it is desirable to have nuclear fuel with high dimensional stability and resistance to corrosion. In connection with this, many alloys based on uranium were investigated.

Reports [2190 and 699]* give the results of investigations on the physico-mechanical properties of mono- and polycrystalline uranium and alloys based on uranium. The following were examined quite thoroughly: problems of the thermal and thermomechanical treatment of uranium [713, 2307, 1433], the effect of radiation on the properties of uranium and its alloys [2192], [1878, 1890, 2191, 618, 50, 619], and the properties of uranium during irradiation [2191, 1163]. The Soviet report [2043] gave the results of detailed investigations of the structure of alloys and the phase diagrams of some ternary systems, including uranium, thorium, and their high-melting compounds.

French scientists presented a series of extensive reports on individual problems of uranium metallography [1258, 1163, 1158, 1164, 1167]. Considerable interest was evoked in a report by Japanese investigators [1324].

Data on the action of radiation on metal fuel elements at high temperatures, on the causes of instability in fuel elements, and the use of various materials for their preparation are given in reports [1878, 616, 617, 81, 622, 792]. The work described in the British [791, 306, 317, 1523, 44, 29], French [1157], Soviet [2191] and other reports was also in this direction.

The most interesting information on the metallography of uranium is summarized below.

Investigation of the Structure and Physico-mechanical Properties of Uranium:

Properties of Uranium Monocrystals. Many of the physical and mechanical properties of polycrystalline uranium are determined in rhombic α-uranium by the anisotropy of the properties of the individual crystals. Therefore, a knowledge of the properties of monocrystals is especially useful as it provides a foundation for correcting the properties of polycrystalline material. Such investigations on the properties of monocrystalline uranium, described in reports [713 and 1258], are of considerable interest.

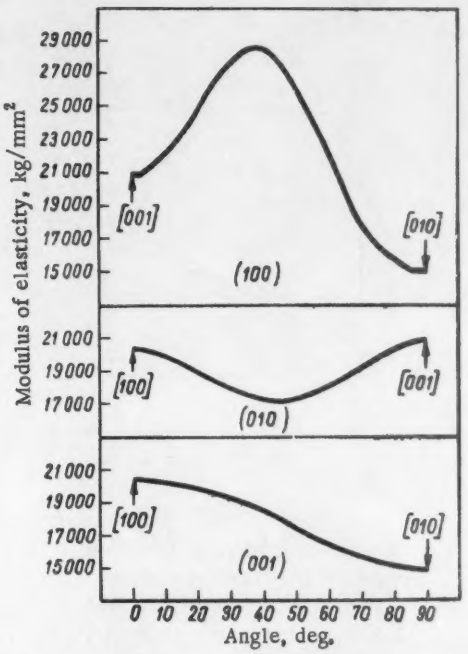

Fig. 1. Changes in Young's modulus in relation to the crystallographic direction [713].

The electrical and magnetic properties of monocrystals were determined along the three main crystallographic directions at 273 and 4.2° K, and the thermal ex-

*The numbers of the reports given at the conference are in brackets.

pansion of uranium monocrystals was studied in the temperature range from -253 to +640°C. The volume changes during $\alpha \rightarrow \beta$ and $\beta \rightarrow \gamma$ conversions were determined more accurately. They equal 1.15 and 0.71%, respectively.

The elasticity constants of uranium were determined by a method using ultrasonic pulse techniques, specially modified to deal with small crystals. The anisotropy of the elastic properties of α-uranium was evaluated quantitatively: Young's modulus had the minimum value in the (010) direction and the maximum in a direction lying at an angle of 38° to the (001) direction in the (100) plane. The Young's modulus value of uranium monocrystals may vary by a factor of almost 2, depending on the crystallographic direction (Fig. 1). A study of the mechanism of the plastic deformation of uranium in the upper temperature range of the α-phase is being continued. Fig. 2 shows graphically the anisotropy of the tensile characteristics of a uranium monocrystal [1258].

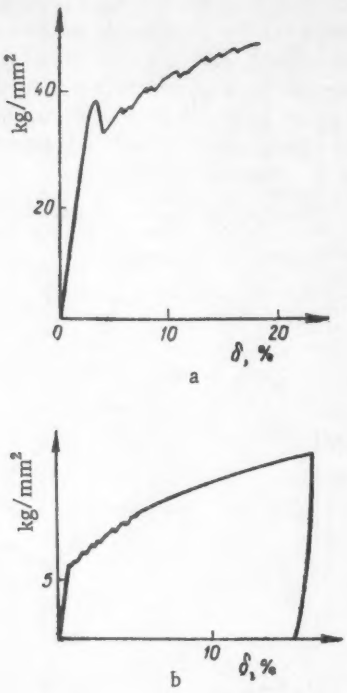

Fig. 2. The beginning of the elongation curve of monocrystals: a) direction (193) coincides with the elongation axis; b) direction (274) coincides with the elongation axis [1258].

Properties of Polycrystalline Uranium:

Changes in uranium strucutre produced by heat treatment. In the reports much attention was paid to the problem of changes in the structure and properties of polycrystalline uranium. Problems related to changes in the structure and properties of uranium, produced by heat treatment, were examined most thoroughly in the Soviet report [2307].

The great refinement in structure during tempering from the β - and γ - phases was demonstrated, and the relation of grain size in the tempered uranium to the foreign body content (mainly iron, silicon, and aluminum) was established.

It is reported in [713] that the grain size does not depend on temperature (within the range over which the β -phase exists) and duration of tempering. It was noted that further refinement of the grains was produced by several temperings. In practice, several temperings are used as a means of breaking the perimeter of acicular crystals formed during tempering. At present it is considered that tempering from the γ -phase has no advantages over tempering from the β -phase and, in general, even gives less satisfactory results [713, 2191]. Investigation of the recrystallization processes in tempered uranium is of considerable interest. Recrystallization by annealing a tempered metal in the α-phase, without the former undergoing deformation, is an operation used lately in heat treatment. The authors of report [713] consider that in this case the motive force for the recrystallization is deformation produced in the uranium by tempering and connected with the anisotropy of the linear expansion coefficient, as is confirmed by the relation of this phenomenon to the cooling rate. Recrystallization annealing after tempering from the β -phase makes it possible to decrease the grain size considerably and to obtain uranium with a fine-grained, equiaxial structure, i.e., increase its quasi-isotropy.

Report [2307] gives the results of investigations of structural changes in uranium arising during deformation in the α-phase followed by recrystallization annealing. A recrystallization diagram is given for uranium. As deformed and recrystallized uranium has a texture which controls its directed growth under irradiation, particular attention was paid to the development of methods for liquidating texture and the anisotropy of the properties connected with it.

Heat treatment in the β -phase is recommended as a method for eliminating the anisotropy of the thermal expansion of uranium. It was shown here that the degree of elimination of the anisotropy depends not only on temperature and time but also on the rate of cooling from the given temperature [713].

Mechanical properties of uranium at high temperatures. The mechanical properties of uranium were examined before, at the time of, and after, irradiation to evaluate the behavior of uranium under conditions of stress, which arise during the use of nuclear fuel. For example, it was established that in the vertical fuel elements in Calder Hall reactors, the fuel rods of cast uranium bent at a rate which depended on the resistance of the material to creep under irradiation [50, 317].

The fullest data on the mechanical properties of unirradiated uranium are given in reports [2307 and 49]. It was shown in the first report that the mechanical properties depend on temperature in short and prolonged (creep) tests. The changes in mechanical properties in relation to the tempering parameters (heating temperature, duration, rate of cooling, etc.) were investigated thoroughly. The effect of additives on the mechanical properties of tempered uranium was studied. The properties of uranium alloys at high temperatures were reported in [49]. The creep tests, whose results were given in reports [713 and 49], were carried out very carefully and were accompanied by special investigations on the effect of thermal cycles, arising due to fluctuations in temperature during the tests, on the accuracy of the results. Special attention was paid to a study of the effect of uranium grain size on the creep rate. Twinning occurred in uranium deformed below 350°C and consequently there was deformation within the grains, while above this temperature, deformation occurred along the grain boundaries. Therefore, at lower temperatures, fine-grained material has greater resistance to creep, while at and above 400°C, the opposite is true [2307].

The effects of radiation on uranium†. The effect of radiation on uranium prepared by different technical methods was investigated. Uranium rolled at 300°C had a texture for which parallelism of direction (010) to the rolling axis was characteristic. When irradiated, such metal grew considerably in the (010) direction. Uranium rolled with a definite degree of deformation at 600°C had a mixed texture, which could result in elimination of the growth or even compression under irradiation.

The Soviet report [2191] gave the relation of the growth coefficient of textured uranium, with 0.02% burnup, to the degree of deformation and grain size, as well as the effect of various modifications of tempering on the relation of dimensional changes in samples to the degree of burnup. Also for the first time, the results of determining the mechanical properties of uranium directly during irradiation were given, which showed that after the uranium had been in a neutron field ($nv=1.5\cdot 10^{13}$ neutr./cm^2·sec) for even a short period, its relative elongation decreased somewhat, and its tensile strength increased noticeably.

In connection with high burnup and high temperatures in fuel elements, much attention has been paid lately to the study of the so-called swelling phenomenon, i.e., gas swelling resulting in a change in form and volume and a decrease in density of the fuel under the action of irradiation. This phenomenon is described quite thoroughly in American [618, 616 and 617] and British [81, 791] reports. Most scientists agree that a distinction is required between growth and gas swelling in metallic fuel systems. Growth may be defined as a change in the form of the fuel under the action of radiation (with the minimum change in density) [617]. The usual rate of uranium growth reaches a maximum at 200°C, decreases with a further increase in temperature, and then equals zero at 400 - 500°C; consequently there is no swelling produced by growth, at 400 - 500°C (Figs. 3 and 4).

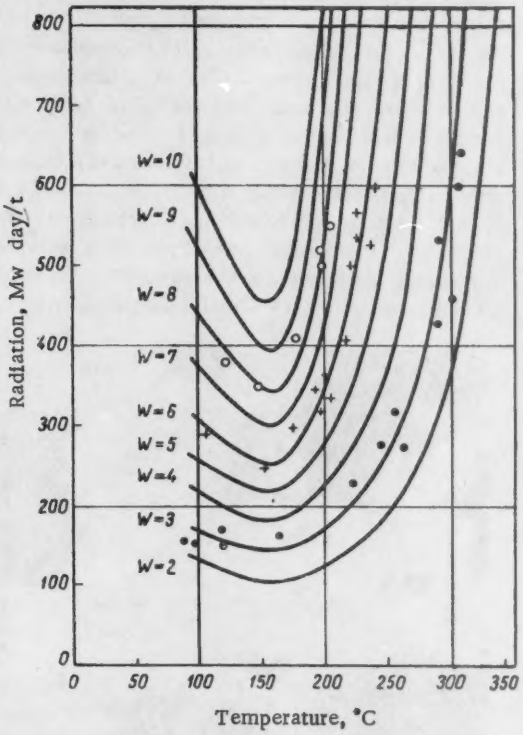

Fig. 3. Change in wrinkling relative to radiation and temperature [50]; W ‡) wrinkling parameter; ● — W = 2.5-3.5; + — W = 5.5-6.5; ○ — W = 7.5-8.5.

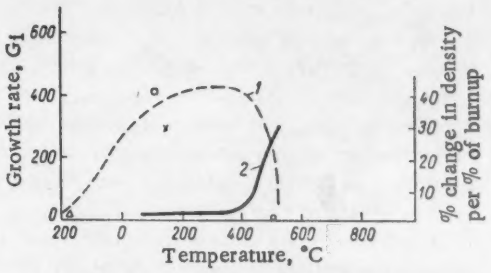

Fig. 4. Effect of temperature on rate of growth and gas swelling of irradiated uranium [618]: 1) growth curve; 2) gas swelling curve; ×) Turkalo's data; ○) Pleyl's data; △) Kuntz and Holden's data; □) Kittel and Paine's data.

The phenomenon of gas swelling usually occurs at temperatures above 350°C (from 350 to 650°C, depending

† More detailed data is given in the resume by Yu. N. Sokurskii, J.A.E. 6, 4 (1959)

‡ Deviations (without considering the sign) of separate measurements of the diameter, carried out at 1 cm intervals, from the average diameter.

on a number of factors and the composition of the fuel) and is overlapped by growth over a certain temperature range. It is considered that gas swelling occurs as a result of the formation of cavities in the uranium, which are due to the continuous formation of gaseous fission products, krypton and xenon (Fig. 5). Since these cavities are filled with pressurized gas at high temperatures, the phenomenon of gas swelling depends on the resistance of the fuel to creep, and it increases rapidly with temperature after a certain limit, which is characteristic of each material. Up to 500°C, gas swelling is accompanied by the formation of small pores of almost the same dimensions. At temperatures above 500°C, the pores formed in uranium have very different dimensions.

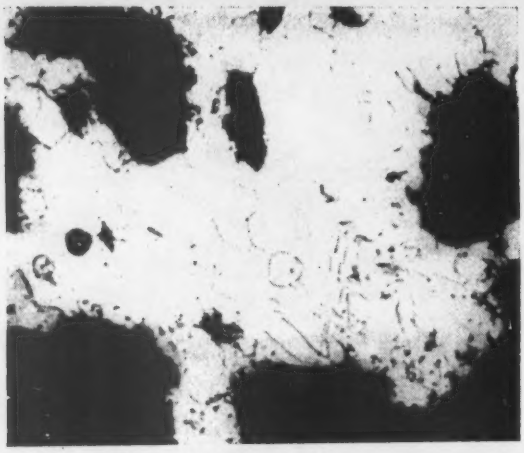

Fig. 5. Microstructure of uranium after strong irradiation [81].

The scale of gas swelling depends on the magnitude of burnup and the irradiation temperature. The increase in volume may be considerable. An increase in volume from 10% to over 100% (per % of burnup) is typical. Some experimental data on gas swelling are given in the table [81].

It is considered that the rate of burnup should affect the increase in volume of uranium in the range 350-500°C. With the same burnup , greater gas swelling occurs with the greater rate of burnup .

The following are some of the methods used for decreasing gas swelling or arresting its harmful effect: alloying, compression of the fuel materials from all sides (demonstrated successfully in the Argonne National Laboratory), increase in the channel cross section of the coolant, and dispersion of the fission material.

Uranium Alloys

To increase the dimensional stability of uranium at various temperatures, investigations were carried out on an extensive number of binary and ternary alloys of uranium with different elements; for example, binary alloys of uranium with Al, Cr, Mo, Nb, Si, Ti, V, Zr or ternary alloys such as U-Mo-Cr, U-Cr-Fe, U-Cr-Al, U-Mo-Fe, U-Zr-Nb, U-Si-Fe, U-Zr-Mo, U-Nb-Mo, Th-U-C.

Mainly two groups of alloys were developed: with the structure of α-uranium (α-phase alloys) and with the structure of γ-uranium (γ-phase alloys). The former alloys based on natural or slightly enriched uranium are more suitable for use in thermal neutron reactors; the latter are suitable for fast neutron reactors, as they require a high alloy content and, consequently, considerable enrichment.

The most promising are alloys of uranium with chromium, molybdenum, and zirconium, ternary alloys of uranium-zirconium-niobium [2043], and uranium-fissium alloys.**

The following are examples of α-phase alloys:

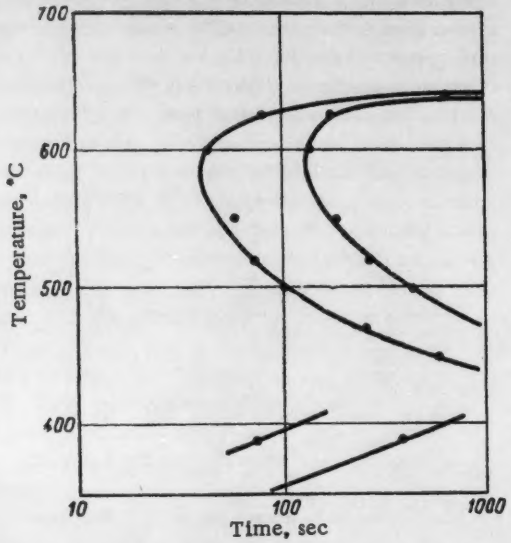

Fig. 6. C-shaped diagram for alloys of uranium with 0.5 at. % of chromium [27].

Alloys with small additions of chromium are α-phase alloys and the additions improve the dimensional stability of uranium under irradiation and cyclic heat treatment. For example, an alloy with 0.39 wt.% of chromium, after isothermal treatment at 475°C, showed less than 0.5% elongation under thermal cycling; under the same conditions, unalloyed uranium was elongated 6%. Samples of alloys with 0.1 wt. % (0.5 at. %) and 0.4 wt. % of chromium were treated with heat before irradiation, first isothermally at 580°C and then at 500°C (Figs. 6 and 7). Such samples elongated approximately the same as uranium tempered from the β-phase during irradiation; however, they had a considerably smoother surface. An alloy with 0.4 wt. % of chromium was less stable and samples became rough after only 0.1% burnup .

Uranium-molybdenum alloys. A 1.5 - 2 wt. % content of molybdenum sharply decreased the form changes of uranium. Alloys of the uranium-molybdenum

** Fissium (Fs) is the material remaining after the pyrometallurgical treatment of fission products. The composition of fissium is determined by the yields of these elements during fission [Ed. note].

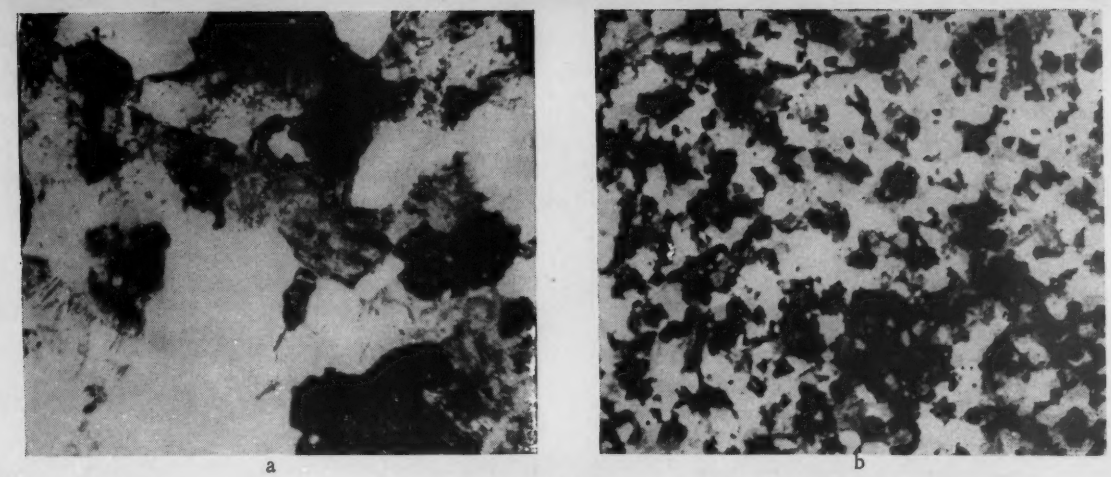

Fig. 7. Microstructure of an alloy of uranium with 0.5 at. % of chromium [27]. a) After casting, × 35; b) after isothermal processing at 550°, × 35.

system were also investigated thoroughly in the USA, Britain, and especially in France.

Uranium-zirconium alloys. More than 2 wt.% of zirconium is required for dimensional stability of uranium under cyclic heat treatment. For example, 5.4 wt. % of zirconium limited elongation due to cyclic heat treatment to less than 0.2%.

The best dimensional stability under irradiation was observed after isothermal treatment. Thus, after several hours of isothermal treatment at 690°C, after tempering from 800°C, the growth coefficient G_i=3.

The best results for an alloy containing 5 wt. % of zirconium and 1.5 wt. % of niobium were obtained after isothermal treatment, for example, γ-treatment followed by annealing for 24 hours at 650°C. This alloy was intended for the EBWR reactor with a fuel element surface temperature of 280°C.

Examples of γ-phase uranium alloys are the alloys of the uranium-molybdenum system with a 9 - 10 wt.% of molybdenum. It should be noted that molybdenum has an especially advantageous effect on uranium's resistance to creep, which indicates that these alloys should have a good resistance to gas swelling. Elements of uranium alloys with 10 wt. % of molybdenum are used in the "Enrico Fermi" reactor (fuel-element surface temperature 500°C). It was reported in [2043] that the widest field of ternary solid solutions based on γ-uranium is found in the uranium-zirconium-niobium system. This system is of great interest in connection with the search for stable uranium alloys for atomic reactor fuel elements. According to the data given by Dr. Chiswik in his oral report, the best alloy for resisting gas swelling is that of uranium with 10 wt.% of niobium and 4 wt. % of zirconium.

Uranium-fissium alloys were discussed in detail at the conference [713, 1890]. During the pyrometallurgical purification of fuel elements, unloaded from a fast neutron reactor, a group of elements from fission products could not be separated after several fuel purification cycles, and these impurities accumulated in a definite equilibrium. The elements in this group (arbitrarily called fissium and denoted by Fs) are the following (in wt. %):

Zr . . .	0,1	Ru . . .	2,6
Nb . . .	0,01	Rh . . .	0,47
Mo . . .	3,42	Pd . . .	0,3
Tc . . .	0,99	U . . .	92,09

Report [713] describes various types of fissium alloys, for example, Fs 5 with the composition (in wt. %):

U . . .	95	Ru . . .	1,5
Mo . . .	2,5	Rh . . .	0,5
Zr . . .	0,2	Pd . . .	0,5

These alloys are used as fuel elements in the EBR-II fast neutron reactor. The temperature of the fuel element walls is 525°C.

Other alloys of the fissium type, which maintain the ratio of these elements, differ from each other in their total amount. The main components of fissium are molybdenum and ruthenium, and therefore the conversions and resultant structures of fissium alloys are examined as a ternary uranium-ruthenium-molybdenum system, a system which is considered in report [713]. The stability of fissium-type alloys under irradiation depends to a large extent on heat treatment. The growth coefficient, G_i, for γ-annealed samples of uranium with 3 wt. % of Fs falls from 50 to 0.1 after annealing for 24 hours at 650°C.

The introduction of an additional amount of molybdenum into fissium-type alloys results in the radiation growth coefficient of these alloys no longer depending on heat treatment. For example, an alloy of uranium with 5.0 wt. % of Fs and 2.5 wt. % of molybdenum showed a growth coefficient which was approximately equal to 2, regardless of whether the alloy was tempered from the γ-phase or cooled slowly. Similar behavior was observed for an alloy of uranium with 5.0 wt.% of Fs and 7.5 wt.%

Uranium, arc smelted			
irradiation temp., °C	burnup, %	volume growth, %	% of volume change per % of burnup
630	0.29	9.8	34
700	0.27	11.5	43
800	0.34	84.5	248

of molybdenum. Data on the properties of fissium-type alloys are given in report [713]. Besides the fact that alloys of the fissium type have good dimensional stability under cyclic heat treatment and irradiation, their use as fuel in reactors greatly simplifies the process of fuel purification.

Temperature Limits for the Use of Nuclear Fuels Based on Uranium. On the basis of results of investigations on uranium and its alloys, reported at the conference, we may assume the following temperature ranges for the possible use of various types of nuclear fuels based on uranium to be generally accepted:

from 350 - 450°C – unalloyed, heat-treated uranium with a fine grain and improved mechanical properties;

from 350 - 450°C to 650°C – alloyed, heat-treated uranium;

above 650°C – only heat-stable ceramic compositions of uranium oxides and carbides.

The upper temperature for the use of uranium alloys is determined by the extreme development of gas swelling. Metallic fuel systems have certain advantages over ceramic ones, for example, a greater concentration of uranium atoms per unit volume and greater heat conductivity. These are important factors as they directly affect the dimensions of the reactor.

Contemporary Procedures for Metallographic Investigations of Irradiated and Unirradiated Uranium [1855]. The metallography of uranium is one of the experimental methods of investigation that could be usefully applied to the study of the peculiarities of nuclear fuel in reactors. After establishing the relation between the microstructure and other physico-mechanical properties of a nuclear fuel, one may, in a number of cases, deduce the reliability of using a given metal or alloy in a reactor. However, due to the strong radioactivity of irradiated uranium, various changes must be introduced into the usual metallographic methods and apparatuses used. For example, etching, which is usually used successfully in investigating unirradiated uranium, does not give satisfactory results with irradiated uranium as the surface of the section rapidly deteriorates.

The microstructure is readily investigated by means of ion bombardment. For example, samples, etched with argon at a pressure of 40μ and a dc voltage of ~2000 v at a current strength of 2-3 ma, may be investigated directly at all levels of magnification, or replicas may be used. Special apparatuses exist for the remote etching of sections by ion bombardment or for the remote taking of replicas. In order to take a replica, a cellulose acetate strip is remotely dipped into acetone for 20 sec and then placed on the sample. The sample together with the strip are removed from the acetone and dried in air for 20 min, after which, the replica is removed from the sample with special pincers on a manipulator. It may be shadowed with a layer of aluminum. This method makes it possible to determine if there had been any unusual growth in the grain, to study the structure of deformed zones of fuel elements, to determine the existence of cracks and surface deformation of damaged fuel elements, etc.

However, normal metallographic analysis (even using ion bombardment etching) cannot fully show the microstructural changes induced by thermal cycles and radiation destruction. This is explained by the fact that structural changes produced by radiation may mask microstructural changes occurring during the preparation of the section and also those due to changes in the irradiation parameters. Therefore, in studying the structural changes produced by irradiation, methods for the preliminary metallographic characterization of the surface and fractography were applied.

The first method was used for studying the kinetics of structural change produced by irradiation in the same section. For this purpose, the polished surface of a microsection was etched by ion bombardment and then a cellulose-acetate replica of it taken. The sections were placed in special capsules (filled with a sodium-potassium alloy for improving heat conductivity) made of zircalloy-2, which were then placed in the reactor. It was first shown that heating in a sodium-potassium alloy for 400 hours at a temperature below 600°C did not deteriorate the surface of uranium and did not cause considerable grain growth and roughening of the surface of uranium samples. After irradiation in the reactor to various stages of burnup, the samples were removed from the capsules and replicas again taken of their surfaces (which had been characterized metallographically and a replica taken previously). By comparison of the replicas taken before and after ir-

radiation, it was possible to establish exactly the spots where microstructural changes had occurred. By this method it is possible to observe changes in twinning dimensions, the formation of new twins, changes in grain boundaries, displacement of grains, and to investigate in detail with an electron microscope the changes in microstructure.

The fractography method consists of an investigation of cellulose-acetate replicas, taken of the surface of a fracture in irradiated samples broken by impact, and differ in that they do not require the preparation of special samples. The surface of the fracture characterizes the internal structure of the sample, deformed only by impact breakage. The fine pores, formed by the accumulation of vacancies or the evolution of gases, are quite visible and are not harmed during the break. This cannot be achieved by applying the usual metallographic techniques which require polishing of the surfaces, nor for the same reason, by methods of preliminary metallographic characterization. In order to compare the data from fractographic analysis with those of normal metallographic investigation, a metallographic section is prepared at a distance of 3 mm from the fracture and a replica is taken of the section's surface.

In conclusion, we may note that judging by the range of subjects, experimental techniques, and data obtained the state of the metallography of uranium and its alloys in those countries presenting pertinent material at the conference is at approximately the same level. One of the main problems, namely that of determining the mechanism of growth under the action of radiation and thermal cycles, remains unsolved.

In connection with the tendency to increase the degree and rate of burnup and working temperatures of fuel elements in reactors, the development of methods for counteracting the phenomenon of gas swelling by producing nuclear fuel, based on uranium, that is heat resistant under neutron irradiation, assumes an ever-increasing importance.

Received December 25, 1958

FUEL ELEMENTS OF NUCLEAR REACTORS

A. G. Samoilov and V. S. Volkov

On the basis of foreign reports presented at the Second International Conference on the Peaceful Uses of Atomic Energy, Geneva, 1958, the characteristics of construction of fuel elements (FE) and basic data relating to them for a series of reactors are given. Problems on the selection of fuel and construction materials as well as the technology of preparing FE for various types of nuclear reactor are examined.

Construction of fuel elements

Fuel elements are made in the form of rods, plates, or pipes (ring FE).

The rod FE consist of a core of fissile material hermetically sealed in a jacket. In reactors with a high specific energy output, small diameter FE are used (in order to avoid excessive temperature gradients along the radius) and several are usually assembled together. Spacing is achieved by the use of jackets with straight or spiral ribs, forming a spiral around the FE with wire, spot welded to the jacket, or welding spacing collars at regular intervals.

Thus, the FE of the EBR-II reactor (USA) are spaced by spiral wire ribs [1782]*. The fuel-element assemblies in the Canadian NPD-2 reactor are designed in the form of a bundle of 7 rods, each of which, excluding the central one, has two Zircalloy-2 wires wound spirally around it (with a pitch of 49.5 cm in different directions for adjacent rods), and these are used for spacing and for mixing the coolant [209]. The FE in the American EBR-I reactor (third charge) are spaced by three Zircalloy-2 wires of 1.17-mm diameter, welded along each rod at 120° to each other [1845]. In the fuel element assembly of the "Yankee" atomic power station (USA), collars 19 mm high placed between the rods at 350-mm intervals are used for spacing [1038].

Plate FE are usually assembled in several pieces parallel to each other and formed into one unit by being welded together or to side, nonfuel element plates. This solves the problem of fixing and spacing the FE plates. Such assemblies are used in both of the following: power reactors, experimental and test reactors.

Plate FE have been developed for the breeding zone of the Shippingport PWR reactor (second charge). The dimensions of a plate are 60 x 286 x 3.26 mm; each contains 15 square tablets of UO_2. The tablets are separated by partitions 2 mm thick. The jacket and the partitions are made from Zircalloy-2 [2380].

Ring FE consist of a bundle of tubes of small diameter or of concentric tubes of relatively large diameters. For example, the fuel-element assembly in the Belgian BR-2 reactor consists of six coaxial fuel-element tubes with 33 - 76-mm diameters [1679].

To ensure good heat contact between the fuel-element core and the jacket, a diffusion bond is produced in many FE during production. Various methods of squeezing or pressing are used to decrease the gap between the core and the jacket, or this gap is filled with a good heat conductor. Thus, in the FE of the EBR-II reactor, the gap between the fuel and the jacket is filled with sodium [1782]. In the "Enrico Fermi" reactor (USA) a diffusion bond is produced between the fuel and the jacket in the FE by extruding the fuel and jacket together [792 and 2427].

Ribbing the jacket is widely used in gas reactors to improve heat transfer from the FE to the coolant. In these reactors the jackets are mostly made of alloys based on magnesium which has a good coefficient of heat conductivity, and therefore, an increase in the surface to be cooled by ribbing is extremely effective. However, with too sharp and too close a pitch of the ribbing, the coefficient of heat transfer falls due to the decrease of the gas speed in the narrow slits and its higher temperature. At the same time, sharp spiral and circular ribs improve heat transfer considerably due to the mixing of the gas as eddies are formed when a gas stream passes perpendicular to them. Therefore, double ribbing of FE is often used, and this consists of spiral ribs intersected by higher straight ribs and achieves a mixing of the gas and an increase in the heat-transferring surface. The British atomic power stations at Hunterstone, Berkeley, and Bradwell have double-ribbed FE [48, 74, 263, and 264].

An FE has been designed for a high-temperature gas reactor, in the Federal German Republic, which consists of a graphite sphere 5 - 6 cm in diameter filled with a fissile material, uranium carbide, or a breeding material, thorium carbide [1005].

In order to lower the cost of atomic energy, FE are being designed for a high degree of burnup, a high specific energy release, and high operating temperatures. The average burnup of a metallic element reaches 3500 Mw. d/t and ceramic ones, up to 10,000 mw d/t. Specific heat fluxes from 1.10^6 to 3.10^6 kcal/m^2 hr are permissible.

The main data on FE for a series of nuclear reactors are given in the table (see pp. 154-163).

*The numbers in square brackets refer to reports given at the conference.

Nuclear fuel

When the temperature of the fuel in gas-cooled reactors does not exceed ~ 400 - 500°C, use is made of metallic uranium that is specially heat treated to increase its stability under irradiation. With much higher temperatures, when the form and volume of ordinary uranium undergo considerable changes due to radiation damage and the formation of internal pores caused by the evolution of gaseous fission products and low creep resistance (so-called swelling), uranium alloys and ceramic and cermetic fuels are used. Thus, in the German high-temperature reactor it is planned to use uranium carbide as fuel since it has a high melting point and satisfactory heat conductivity, which may be raised by mixing the uranium carbide with graphite [1005 and 1054]. For the British experimental high-temperature gas reactor, AGR, the FE were designed in the form of UO_2 rods with beryllium [312].

In reactors with water, liquid metal, and organic coolants, UO_2 is used widely as a fuel due to its exceptional stability under radiation, high melting point, resistance to corrosion, and compatibility with many constructional materials. Uranium dioxide is used either in the form of compressed and fired tablets or in the form of a powder dispersed in a matrix of nonfissile material. Fuel in the form of baked UO_2 tablets is to be used in the American "Yankee" and Dresden reactors [1038 and 2372], in the SGR reactor with sodium cooling, and a graphite moderator [608], and in the Belgian 125 Mw boiling reactor [1801]. Plate FE with UO_2 dispersed in a stainless steel matrix are used in the APPR reactor (USA) [1925]. The composition of the core (in % of total) is 19.04% of UO_2, 0.5% of B_4C, and 82.4% of stainless steel. Plates of UO_2 in a stainless steel matrix are also used in the OMRE reactor (USA) with an organic moderator [421]. Plates of U_3O_8, dispersed in an aluminum matrix, are used in the "Argonaut" experimental reactor (USA) [1019].

Alloys of uranium with molybdenum, zirconium, aluminum, chromium, niobium, and nickel, which increase the stability of uranium under irradiation, and alloys of relatively little uranium with various elements are also used widely in water and liquid-metal reactors. Thus, the "Enrico Fermi" reactor uses as fuel an alloy of uranium with 10 wt. % of molybdenum [792]; for the third charge the EBR-I reactor uses a uranium alloy with 2 wt. % of zirconium [791 and 1845]; and the Dounreay reactor (Great Britain), a uranium alloy with 0.1 wt. % ($\frac{1}{2}$ atom %) of chromium [44]. The EBWR reactor (USA) uses a uranium alloy with 5 wt. % of zirconium and 1.5 wt. % of niobium [1038]. An alloy with 6.7 wt. % of uranium with Zircalloy-2 was selected for the seed FE of the PWR reactor [787], and an alloy with 17.6 wt. % of uranium with an aluminum-nickel alloy for the ALPR reactor (USA) [455].

A new development in fuel materials is the use of uranium containing fission products that remain after the reprocessing of irradiated uranium. This type of alloy (called fissium), with a high radiation stability, was selected for the EBR-II experimental breeder reactor. The composition of the fissium alloy (in wt. %) is 95% of uranium, 0.2% of zirconium, 2.5% of molybdenum, 1.5% of ruthenium, 0.3% of rubidium, and 0.5% of palladium [1782]. Tangible measures are being taken for using plutonium and thorium as fuel material.

In the Canadian NRX reactor, part of the uranium FE were replaced by FE of a plutonium-aluminum alloy. At first three FE were prepared, each consisting of 11 small blocks (plutonium-aluminum alloy) of 25.4-mm diameter. The blocks had an aluminum jacket 4.55 mm thick and were connected to form a rod 3000 mm long, which in its turn was enclosed in an aluminum tube 2 mm thick. The plutonium content of the blocks varied and increased from 0.5 wt. % in the end blocks to 20 wt. % in the central block. These elements were kept in the reactor successfully to 55 - 60 wt. % burnup of plutonium or 1.5 wt. % of all the atoms of the fuel alloy. Then 23 elements of similar construction were prepared, but they had only three central blocks of the plutonium alloy with 20 wt. % of plutonium. The end blocks were of uranium. These elements operated for various times in the reactor, some failing.

Similar elements were replaced by differently constructed elements, which consisted of 12 blocks, 34.5 mm in diameter, of a plutonium-aluminum alloy (3.7 wt. % of plutonium). The blocks were enclosed in an aluminum tube with 2 mm thick walls. Eleven such elements have already remained in the reactor from 4 to 15 months and will operate until a plutonium burnup of 60 - 70 wt. %. It is planned to add FE of a plutonium-aluminum alloy every year with a total plutonium content of up to 3 kg [191].

An experimental plutonium regeneration reactor, PRTR, is being built in the USA for studying problems of nuclear physics, the technology of plutonium fuel, and the regeneration of exhausted FE. FE have been designed for it from a plutonium-aluminum alloy (1.7 wt. % of plutonium) in the form of rods, 12.7 mm in diameter and 2.1 mm in length, enclosed in a Zircalloy-2 jacket. There was a discussion of the possibility of using as fuel mixtures UO_2 with PuO_2 and also mixtures of PuO_2 or UO_2 - PuO_2 with Al_2O_3, MgO, SiO_2, BeO, and ThO as diluents [447 and 1776].

A combination of fuel element assemblies is being developed for the MTR reactor at Hanford. Each assembly consists of 16 welded fuel element plates. A plutonium-aluminum alloy (14 wt. % of plutonium) is used as fuel [1776].

The advantage of thorium is that it has a high melting point (1700°C) and has no phase conversions up to 1400°C; its disadvantage is the need to add an enriched fissile material.

The American reactor BORAX uses a UO_2-ThO_2 mixture as fuel [2379]. A method of preparing FE from a uranium-thorium alloy (7.6 wt. % of uranium) was developed for the SRE reactor [785]. A homogeneous mixture of UO_2 and ThO_2 was selected for use as fuel in the atomic power station of

the American company "Consolidated Edison". Thorium is the breeding material, while ThO_2 is used for its good radiation stability, high resistance to corrosion in hot water, and compatibility with UO_2 and the stainless steel of the jacket [1885].

A new fuel-moderator composition was developed for the American experimental reactor, TRIGA. It is a urano-zirconium hydride, containing up to 8 wt. % of uranium, enriched up to 20 wt. %. In this mixture there is approximately one hydrogen atom to every zirconium atom. The mixture has a density approximately equal to that of metallic zirconium [1017].

Construction materials

Zircalloy-2 and various stainless steels are widely used for making FE jackets. A large number of existing water-cooled reactors have FE with zircalloy jackets, and many of the projected reactors are to have Zircalloy-2 and stainless steel FE jackets. In most cases alloys based on magnesium are used for preparing FE jackets for reactors with gas cooling. It is considered more economical in the USA to use enriched fuel in gas reactors. In this case constructional materials may be used which, even though they have high neutron capture cross sections, still tolerate high temperatures. Thus, stainless steel was selected for FE jackets for the gas reactor GCR-2 [450].

The use of new construction materials is being planned for many projected reactors. Thus, for the Dounreay reactor, a ring type of FE has been developed, which has a niobium tube for the outer covering and a vanadium tube for the inner one. It is designed to operate at temperatures of 300 - 600°C. The purpose of preparing a jacket from two materials of different melting points is to ensure safe working of the reactor: in the case of a breakdown in the cooling system and overheating of the FE, the inner vanadium tube melts. The molten fuel flows out of the active zone through the niobium tube without mixing with the fuel of the other FE, thus eliminating the possibility of a critical mass [44].

New materials which would allow higher operating temperatures are being sought for the jackets of gas reactor FE. In Britain a project is being developed for a high temperature gas reactor having FE with beryllium jackets. The maximum temperature of such an FE jacket is 600°C [312]. In Sweden FE are also being developed with beryllium jackets which tolerate a surface temperature of up to 533°C [2419]. FE with beryllium jackets are to be designed for the atomic power station at Hunterstone [1523].

FE using graphite jackets have been planned for the British experimental high-temperature reactor of 10 Mw. Up to 800 - 900°C is a permissible temperature for a graphite jacket and the average temperature of the fuel is up to 1000°C. The gas temperature at the outlet from the reactor reaches 750°C, which makes it possible to use a standard turbine.

The use of graphite for FE jackets is attractive as graphite has a high resistance to radiation, good heat conductivity, and the capacity to tolerate very high temperatures and high thermal gradients. The disadvantage of such a jacket is the possibility of gaseous fission products diffusing through it [314].

A design for FE with graphite jackets for use in a high temperature gas reactor has also been developed in the Federal German Republic. It is considered that the maximum temperature on the surface of such a jacket will reach 1100°C [1005, 1054].

A number of reports examined the possibility of using alloys based on aluminum for FE jackets. Aluminum has several advantages: it is inexpensive, readily accessible, processed easily, and has a low neutron capture cross section. However, it has two critical disadvantages which limit its use in reactors, its low ultimate strength and high creep rate at elevated temperatures, and its low resistance to corrosion. Although aluminum has been used for many years in low-temperature water reactors, the problem of using it in high-temperature power reactors has only been seriously considered now, since a series of alloys based on aluminum which have a high corrosion resistance and strength has been developed.

FE with a jacket of an aluminum-nickel alloy that tolerates a surface temperature of up to 230°C have been developed for the boiling reactor ALPR [45, 1430]. There are indications that for a series of reactors, the FE jackets which were to have been made of zirconium may possibly be made from aluminum alloys.

In order to increase the operating period of the reactor, some apparatuses have FE with burnup additives, which first suppress part of the reactivity and then, as they burn out, increase it. Most often boron in the pure state or in the form of various compounds is used as the burnup additive. It may be introduced into the fuel, the jacket, or special parts of the fuel element assembly. Boron carbide in the amount of 0.14 wt. % was introduced into the core of the fuel element plates of the APPR reactor [1925]. Natural boron (1.5 g) was introduced into each FE of the ETR-A experimental reactor (USA) for engineering tests [414]. In the ALPR reactor, boron is introduced not into the FE themselves, but into a special strip, which is spot welded to the side plate of the fuel element assembly [455]. For the TRIGA reactor (USA), it is proposed to use samarium as a burnup additive, and this would be in the form of the oxide in an aluminum disk placed inside the FE [1017].

Fuel element preparation technology

The methods of preparing FE, described in the reports to the Second Geneva Conference, are generally known. A number of new and most interesting technical methods should be noted.

French scientists presented interesting material on vacuum welding of various metals.† The metals to be

† Vacuum welding by electron beam. Commissariat a l'energie atomique, Departament de metallurgie et de chimie appliqué. ONU, France, Exposition de Geneva, September 1958.

welded are heated by a beam of fast electrons which is produced and focused by well-known methods. In welding fine parts, the beam may be reduced to such an extent that its cross-sectional area is only a small fraction of a square millimeter, thus giving an accuracy that cannot be obtained in arc welding.

In welding large metal parts (target area of 6 - 8 mm^2), a power of 50 kw is reached. Welding in vacuum eliminates the possibility of oxidation or other contamination. Good results were obtained with such metals as tungsten, molybdenum, tantalum, zirconium, beryllium, and uranium. Electronic welding was used in preparing FE for the French EL-3 reactor, and these consisted of uranium rods with a spiral channel, enclosed in an aluminum jacket which was pressed around the rods hydrostatically. The zirconium tank of the homogeneous reactor "Proserpina" (France) was also made using vacuum electronic welding.‡

In manufacturing the plate elements of the breeder zone of the PWR reactor, a method of eutectic-diffusion welding was used for Zircalloy parts. A thin layer of pure metal, forming a eutectic with zirconium, was deposited on the surface of these parts. The parts were heated to the melting point of the layer. The film of molten, eutectic alloy was maintained at this temperature until the eutectic diffused into the metal and the low-melting eutectic layer disappeared. As binding elements, nickel, copper, and iron may be used, and the melting points of their eutectics with zirconium are 961, 885, and 934°C, respectively, which are considerably lower than the melting point of zirconium (1750°C). The solubility of these elements in β-zirconium in the solid state (1.9, 3.8, and 5.5 wt. %) ensures good diffusion during welding. Although nickel and iron are included in the composition of Zircalloy, and their use would not introduce other elements into the alloy, copper was used due to the lower melting point of the eutectic. The thickness of the diffusion layer was 0.004 - 0.005 mm [2380].

The method of obtaining a diffusion bond between the core and jacket as well as between various parts by means of compression with gas at the bonding temperature is interesting. By use of this method, one may readily make complicated forms, occasionally required for reactors, cover friable materials with a jacket, and control the dimensions of parts accurately. The parts to be joined had cleaned surfaces and were enclosed in an evacuated jacket and heated in gas under a pressure of 700 atmos. to a temperature at which diffusion bonding occurred. By means of gas compression, a pressed mixture of titanium and boron was covered with a titanium coating and cermets of uranium alloys with UO_2 were covered with a molybdenium and niobium coating. Cellular FE (in the form of thick plates) were prepared from UO_2 with a covering and spacers from Zircalloy.

Diffusion bonding was obtained after 4 hours at a pressure of 700 atmos. and a temperature of 843°C. A similar method was used to prepare rod FE with a core of a zirconium alloy with 22 wt. % of uranium and a zirconium jacket. A coating of zirconium was put onto uranium which had been electropolished and nickel plated. The best bond between electropolished uranium and zirconium was obtained at a pressure of 700 kg/cm^2 with heating to 650°C for 6 hours, and for nickel-plated uranium, at a pressure of 700 kg/cm^2 with heating up to 650°C for 6 hours or heating at 732°C for 30 minutes [788]

The method of preparing FE by continuous casting or zone melting is interesting. The element consists of a uranium collar with an inner tube of Zircalloy-2, along which pressurized coolant flows. This method is based on the fact that Zircalloy-2 has a high melting point, is quite stable at the melting point of uranium, and forms a very good metallic bond with molten uranium. Preliminarily cast uranium cylinders are fitted onto a Zircalloy-2 tube. The assembly is placed in a suitable form and in order to obtain a diffusion bond between the fissile material and the jacket, rapid zone melting is carried out in vacuum with the minimal molten zone. A high-frequency generator serves as a heater. It is possible to use graphite rings between uranium collars. The rings have certain advantages during work with uranium alloys: They prevent liquation, while during operation in the reactor, they absorb to a certain degree the swelling of the fuel. These rings should have an opening so that the molten uranium can fill the whole form.

Zone melting gives a defect-free, solid bond between uranium and Zircalloy-2. The interdiffusion of uranium and Zircalloy-2 makes an almost continuous transition from a zone with a high uranium concentration to a zone with a high Zircalloy-2 concentration. When the process is carried out correctly, no friable intermediate layer is formed. Metallic bonding with these properties is obtained if the initial carbon content of the uranium is small and does not increase during melting in a graphite mold. If the opposite is the case, a very friable intermediate layer may form, which during the operation of the reactor and swelling of the uranium could break and thus result in local overheating. Carbonization can be prevented by placing a thin-walled tube of Zircalloy-2 between the uranium and the graphite mold [240].

The Argentine delegation gave a report on the manufacture of FE for the RA-I reactor (similar to the "Argonaut" reactor). The FE were prepared by extrusion of the core and jacket together. A mixture of U_3O_8 and aluminum powders were placed in an aluminum pot with slightly conical walls, closed with an aluminum stopper, and extruded through a slit matrix. The finished plates had a core of 45 wt. % of U_3O_8 and 55 wt. % of aluminum in an aluminum jacket 610 mm long, 73 mm wide, and 2.75 mm thick [1555].

‡ Vacuum welding by electron beam. Commissariat a l'energie atomique, Departament de metallurgie et de chimie applique. ONU, France, Exposition de Geneva, September 1958.

Basic Parameters of FE

No.	Location of reactor, literature source; type of reactor, its purpose and thermal power	Type of FE and its length	Jacket material; thickness; surface temperature	Fuel; diameter or thickness through fuel; maximum temperature	Energy release of fuel; heat flux from surface; burnup of fuel	Coolant; rate; inlet temperature — outlet temperature; pressure
			Rod FE			
1	Great Britain, atomic power station at Hunterstone (being built) [74, 1523]; thermal, heterogeneous, 435 Mw	Rod 63 cm long with double ribbing (held in a graphite collar)	Magnesium alloy — 454°C	Natural uranium; Ø 28.2 mm; 569°C	2.16 Mw/t — 3600 Mw d/t	CO_2; — 204-391°C; 10.5 kg/cm²
2	Great Britain, atomic power station at Hinkley Point [75]; thermal, heterogeneous, 966 Mw	Rod with spiral ribs	Magnesium alloy — 430°C	Natural uranium heat treated; Ø 28.6 mm –	– – –	CO_2; — 179-373°C; 13 kg/cm²
3	Great Britain, atomic power station at Bradwell (being built) [263];thermal, hetereogeneous, 531 Mw	Rod 91 cm long with double ribbing	Magnesium alloy =	Natural uranium; Ø 29.4 mm	Maximum 3.65 Mw/t — 3000 Mw·d/t	CO_2; — 160-345°C; 10 kg/cm²
4	Great Britain, atomic power station at Berkley (being built) [264]; thermal, hetereogeneous, 556 Mw	Rod 63 cm long with double ribbing (held in a graphite collar)	Magnesium alloy — 430°C	Natural uranium — 550°C	= = 4500 Mw·d/t	CO_2; — 160-345°C; 8.8 kg/cm²
5	France [1134]; G-2 and G-3 reactor projects for the production of plutonium and electrical energy, 200 Mw	Rod 30 cm long with 16 longitudinal ribs	Alloy of magnesium with 0.8% zirconium; 1.5 mm; 400°C	Natural uranium; Ø 28 and 31 mm; 550°C	Average 1.82, maximum 3.3 Mw/t = =	CO_2; 80-305°C (in the central channels), 150-354°C (in the peripheral channels) 15 kg/cm²
6	Belgium [1673]; RR-I, an experimental reactor, 4 Mw	Rod 20.4 cm long; a layer of AlSi between jacket and fuel to prevent diffusion	Aluminum =	Uranium Ø 25.4 mm; 250°C	= = =	Air 6-80°C – –

No.	Location of reactor, literature source; type of reactor, its purpose and thermal power	Type of FE and its length	Jacket material; thickness; surface temperature	Fuel; diameter or thickness through fuel; maximum temperature	Energy release of fuel; heat flux from surface; burnup of fuel	Coolant; rate; inlet temperature—outlet temperature; pressure
7	Federal German Republic [1630]; FR-2 project - research reactor at Karlsruhe (being built), 12 Mw	Rod 261 cm long	Aluminum; 1 mm; 80°C	Uranium, some rods of thorium; ⌀ 16 mm —	— Maximum $0.775 \cdot 10^6$ kcal/m² · g —	D_2O; — 36-45°C —
8	USA [792, 1850, 2427]; "Enrico Fermi" fast neutron power reactor (being built), 300 Mw	Active zone: rods 76 cm long in assemblies of 144 units, jacket diffusion bonded to fuel	Zirconium 0,127 mm; 569°C	Uranium alloy with 10 wt. % of molybdenum, enriched with 27% of U^{235} ⌀ 3.76 mm 713°C	140 Mw/t; average $1,88 \cdot 10^6$, maximum $3,26 \cdot 10^6$ kcal/(m² · hour); 10,900 Mw · d/t	Sodium; 9,8 m/sec; Tmax = 543°C —
		Breeding zone: rod 178 cm long; sodium layer 0,1 mm thick between uranium and jacket	Stainless steel; 0,225 mm —	Impoverished uranium with 2,75 wt. % molybdenum; ⌀ 10,5 mm —	Side FE of breeding zone $0,03 \cdot 10^6$ kcal/(m² · · hr), upper and lower FE of breeding zone $0,098 \cdot 10^6$ kcal/(m² · · hour), 4900 Mw · d/t	— — — —
9	USA [791]; EBR-I project, an experimental reactor, fast neutron breeder (third charge)	Active zone: rods 21,5 cm long in assemblies of 36 units in a cell; jacket diffusion bonded to fuel	Zircalloy-2; 0,5 mm —	Alloy of highly enriched uranium with 2 wt. % of zirconium; ⌀ 9,25 mm —	— — —	Sodium; — — — —
		Breeding zone: rods assembled from 36 sections in a cell	Zircalloy-2; 0,5 mm —	Alloy of natural uranium with 2 wt. % zirconium	— — —	— — —
10	USA [1782]; EBR-II - experimental power reactor - fast neutron breeder (being built), 62,5 Mw	Active zone: rods 36 cm long; sodium layer 0,15 mm thick between jacket and fuel	Stainless steel; 0,228 mm —	Alloy of uranium with fission products remaining after processing of irradiated uranium (in wt. %): U - 95, Zr - 0,2, Mo - 2,5, Ru - 1,5, Rb - 0,3, Pd - 0,5; ⌀ 3,66 mm	314 Mw/t; maximum $2,78 \cdot 10^6$, average $1,84 \cdot 10^6$ kcal/(m² · · hour) —	Sodium; 7,95 m/sec; 371-482°C —

No.	Location of reactor, literature source; type of reactor, its purpose and thermal power	Type of FE and its length	Jacket material; thickness; surface temperature	Fuel; diameter or thickness through fuel; maximum temperature	Energy release of fuel; heat flux from surface; burnup of fuel	Coolant; rate; inlet temperature—outlet temperature; pressure
		Breeding zone: rods 140 cm long assembled from 19 sections; sodium layer 0.3 mm thick between jacket and fuel	Stainless steel; 0.455 mm —	Impoverished uranium; ⌀ 11 mm —	— — —	— — — —
11	Great Britain [312]; AGR project - experimental high-temperature gas reactor, 100 Mw	Rod —	Beryllium — 600°C	UO_2; enriched with 1.65% U^{235} — —	Average 6.83, maximum 15.9 Mw/t — —	CO_2; — 250-500, later 325-575°C; 19 kg/cm²
12	Great Britain [314]; experimental high-temperature reactor project, 10 Mw	Hexahedral rods 185 cm long, assemblies of 7 sections	Graphite; 7 mm; t_{av} = 830°C	Rings from a mixture of uranium and thorium carbides and graphite; external diameter 37 mm, internal - 23 mm; atomic concentration of fuel; Th: U = 7.4, graphite: uranium = 2860; 14.2 kg U^{235} — t_{av} = 1030°C	— — —	Helium; — 350-750°C; 10 kg/cm²
13	USA; GCR-2 project [450], [Nucl. Eng., July 1958] - prototype gas power reactor 687 Mw	Rods 100 cm long, assemblies of 7 units	Stainless steel type 304; 0.51 mm; t_{max} = 649°C	UO_2 in the form of rings; 2% enrichment ⌀ 19 mm (external), 8.1 mm (internal); 1200°C	— Average $0.152 \cdot 10^6$, maximum $0.26 \cdot 10^6$ kcal/(m² · hour); 7350 Mw · d/t	Helium; — 238-538°C; 21 kg/cm²
14	Sweden [2419]; 3 reactor projects for large power stations: 1st reactor with tubes under pressure, moderator —D_2O, 525 Mw	a) Rods 450 cm long in assemblies of 19 units, jacket with ribbing	Magnesium; 0.8 mm; 442°C	First natural uranium, later natural UO_2; ⌀ 10 mm; 525-550°C	Average 9.0 Mw/t; average $0.175 \cdot 10^6$, maximum $0.36 \cdot 10^6$ kcal/(m² · hour); 3000-6000 Mw · d/t	CO_2; 17.6 m/sec; 115-410°C; 102 kg/cm²
		b) rods 450 cm long in assemblies of 19 units	Beryllium; 1.0 mm; 533°C	UO_2; ⌀ 12.6 mm —	Average 10.1 Mw/t; average $0.175 \cdot 10^6$, maximum $0.36 \cdot 10^6$ kcal/(m² · hour); 9000 Mw · d/t	CO_2; 21 m/sec; 115-500°C; 102 kg/cm²

No.	Location of reactor, literature source; type of reactor, its purpose and thermal power	Type of FE and its length	Jacket material; thickness; surface temperature	Fuel; diameter or thickness through fuel; maximum temperature	Energy release of fuel; heat flux from surface; burnup of fuel	Coolant; rate; inlet temperature — outlet temperature; pressure
	2nd reactor with a tank under pressure, moderator - D_2O, 525 Mw	a) Bunch of 19 rods, 223 cm long	Stainless steel; (18% Cr, 8% Ni); 0.12 mm; 574°C	Sintered tablets of natural UO_2; ⌀ 12.6 mm —	Average 10.3 Mw/t; average $0.282 \cdot 10^6$, maximum $0.745 \cdot 10^6$ kcal/(m^2·hour)	CO_2; 39 m/sec; 208-500°C; 71 kg/cm^2
		b) Bunch of 19 rods 223 cm long; 8 ribs 4 mm high on the jacket of each rod	Magnesium; 0.8 mm; 422°C	Metallic uranium; ⌀ 10 mm —	Average 9.08 Mw/t; average $0.129 \cdot 10^6$, maximum $0.34 \cdot 10^6$ kcal/(m^2·hour); ~ 3000 Mw·d/t	CO_2; 25 m/sec; 156-400°C; 71 kg/cm^2
	3rd reactor in rock, moderator - graphite, 1000 Mw	Bunches of 4 rods 640 cm long; the jacket of each rod has 12 spiral ribs 8.7 mm high	Magnesium; 1.0 mm; 440°C	Metallic uranium; ⌀ 14.6 mm 550-580°C	Average 6.8 Mw/t; average $0.107 \cdot 10^6$, maximum $0.284 \cdot 10^6$ kcal/m^2·hour	CO_2; 23 m/sec; 150-400°C; 60 kg/cm^2
15	Sweden [135]; R-3 project; a power reactor; thermal, heterogeneous (being built) 1st stage 65 Mw	Bunches of 19 rods 60 cm long	Zircalloy-2; 0.7 mm; 224°C	UO_2 tablets; ⌀ 17 mm —	Average 3 Mw/t; maximum $0.28 \cdot 10^6$ kcal/(m^2·hour); 3200 Mw·d/t	D_2O; 3.55 m/sec; 205-220°C; 36 kg/cm^2
	2nd stage 125 Mw	The same	Zircalloy-2; 0.7 mm; 148°C	The same	Average 5.75 Mw/t; maximum $0.54 \cdot 10^6$ kcal/(m^2·hour); 4200 Mw·d/t	D_2O; 5.5 m/sec; 205-220°C; 36 kg/cm^2
16	Sweden [136]; "Adam" project, a power reactor; thermal, heterogeneous, 75 Mw	Bunch of 19 rods; jackets have spiral ribs for spacing	Aluminum; 0.75 mm; 148°C	Tablets of sintered UO_2; ⌀ 13.5 mm —	Average 4.7, maximum 13.6 Mw/t; maximum $0.39 \cdot 10^6$ kcal/(m^2·hour); 2290 Mw·d/t	D_2O — 80-140°C; 17 kg/cm^2
	100 Mw	Bunch of 19 rods	Aluminum; 0.75 mm; 169°c	The same	Average 6.3, maximum 18.1 Mw/t; maximum $0.515 \cdot 10^6$ kcal/(m^2·hour); 2290 Mw·d/t	D_2O; — 80-160°C; 17 kg/cm^2

No.	Location of reactor, literature source; type of reactor, its purpose and thermal power	Type of FE and its length	Jacket material; thickness; surface temperature	Fuel; diameter or thickness through fuel; maximum temperature	Energy release of fuel; heat flux from surface; burnup of fuel	Coolant; rate; inlet temperature — outlet temperature; pressure
17	Canada [208]; heavy water power reactor project, 794 Mw	Bunch of 31 rods 30.5 cm long	Zircalloy-2; 0.5 mm, 282°C	UO_2; 2200°C	Maximum 39.7 Mw/t; maximum $0.9 \cdot 10^6$ kcal/(m^2 · hour)	D_2O; — 221-274°C
18	Canada [209]; NPD-2 project, an atomic electrical power station; reactor with tubes under pressure	Rods 49.5 cm long in assemblies of 7 units; wire wound around each rod for spacing	Zircalloy-2; 0.635 mm	Tablets of sintered UO_2; ⌀ 24.1 mm —	— — —	D_2O; — 252-277°C; 70 kg/cm^2
19	USA, atomic electrical power station at Shippingport [2462, 2380]; PWR, a pressurized water reactor, operating from December 1957, 60 Mw (elect.)	Breeding zone: rods 260 mm long and 10.45 mm in diameter in assemblies of 113 units. Seed and laminated elements of breeding zone (second charge) See No. 29	Zircalloy-2; 0.57 mm —	UO_2 tablets; 9 mm —	— — —	H_2O; — — —
20	USA [1038]; "Yankee" atomic electrical power station (being built), 392 Mw	Rods in assemblies of 305-306 units	Stainless steel; 0.534 mm; 343°C	Tablets of sintered UO_2; ⌀ 7.35 mm; 2600°C	Average of $0.234 \cdot 10^6$, maximum $1.2 \cdot 10^6$ kcal/(m^2 · hour); 7200 Mw · d/t	H_2O; 4.25 m/sec; 260-381°C; 140 kg/cm^2
21	Japan [1319]; nuclear reactor project for cobalt, 180 Mw	Rods 48.6 cm long in assemblies of 300 units each	Zircalloy-2; 0.6 mm —	UO_2 tablets, enriched with 1.5 wt.% U^{235} ⌀ 9 mm; 1490°C	Average 60 w/cm^3; average $0.375 \cdot 10^6$ kcal/(m^2 · hour); 9200 Mw · d/t	H_2O; 4.8 m/sec; 259-281°C; 140 kg/cm^2
22	USA [1885]; Consolidated Edison atomic electrical power station (being built), 585 Mw	Rods 250 cm long in assemblies of 206 units	Stainless steel; 0.508 mm —	Tablets of a homogeneous mixture of UO_2 and ThO_2 (19,200 kg of ThO_2 and 1080 kg of fully enriched UO_2); ⌀ 7 mm —	— — 18,000 Mw · d/t	H_2O; — 252-270°C —

No.	Location of reactor, literature source; type of reactor, its purpose and thermal power	Type of FE and its length	Jacket material; thickness; surface temperature	Fuel; diameter or thickness through fuel; maximum temperature	Energy release of fuel; heat flux from surface; burnup of fuel	Coolant; rate; inlet temperature — outlet temperature; pressure
23	Belgium [1801]; boiling power reactor project with indirect cycle; 241.9 Mw (thermal) 125 Mw (elect.)	Rods in assemblies of 49 units	Stainless steel; — —	UO_2, 2.5 % enriched; ⌀ 10 mm —	25.5 kw/dm^3 — 10,000 Mw · d/t	H_2O — water at inlet 272, steam 285°C; 70 kg/cm^2
24	USA [2372]; Dresden atomic electrical power station project (being built); boiling reactor, 626 Mw	Rods 267 cm long in assemblies of 36 units	Zircalloy-2; 0.76 mm —	UO_2 tablets, 1.5 % enriched; ⌀ 12.5 mm; 2510°C	50,000 kw/m^3; average $0.254 \cdot 10^6$; maximum $0.935 \cdot 10^6$ kcal/(m^2 · hour); 10,000 Mw · d/t	H_2O; forced circulation 2 m/sec — 71.5 kg/cm^2; steam 44.5 vol. %
25	Belgium [416]; BR-3, a power reactor (supplied by USA, to begin operating in December 1959), 43 Mw	Rods 142 cm long and 8.7 mm in diameter in assemblies of 110-111 units	Stainless steel; 0.53 mm —	UO_2 tablets, 15.2 mm high, 4.43% enriched in the outer zone and 3.29% in the inner; ⌀ 7.6 mm —	Average $0.268 \cdot 10^6$, maximum $1.25 \cdot 10^6$ kcal/(m^2 · hour) —	H_2O; — t_{in} = 255°C, t_{av} = 263°C; 140 kg/cm^2
26	USA [608, 785]; SGR project, an atomic electrical power station, reactor with graphite moderator and sodium cooling, 254 Mw (thermal) 75 Mw (elect.)	Rods in assemblies of 19 units	Stainless steel; 0.25 mm —	UO_2, 3.5% enriched; ⌀ 12.7 mm; 2760°C	— Maximum $0.81 \cdot 10^6$ kcal/(m^2 · hour); average 10,000, maximum 16,000 Mw · d/t	Sodium — 320-507°C —
27	USA [1017]; TRIGA project, a reactor for research and isotope production, 0.01 Mw	Rod 36 cm long	Aluminum; 0.76 mm —	Uranium-zirconium hydride, containing up to 8% uranium and 20% enriched; ~⌀ 36 mm —	— — —	H_2O — natural convection —

No.	Location of reactor, literature source; type of reactor, its purpose and thermal power	Type of FE and its length	Jacket material; thickness; surface temperature	Fuel; diameter or thickness through fuel; maximum temperature	Energy release of fuel; heat flux from surface; burnup of fuel	Coolant; rate; inlet temperature — outlet temperature; pressure
			Plate FE			
28	Canada [211]; NPU, a high-power research reactor, 200 Mw	5 thick uranium plates, 300 mm long, placed in a round tube	Aluminum; — 102°C	Natural uranium; 4.5 and 4.34 mm; 193°C	Maximum $1.71 \cdot 10^6$ kcal/(m^2 · hour) —	D_2O; 10 m/sec; — 49-75°C —
29	USA atomic electrical power station at Shippingport [2380, 787, 2462]; RWR, a pressurized water reactor. Second charge of the breeding zone will be loaded in 1961. Power will be increased to 100 Mw (elect.)	Breeding zone: (second charge): plates measuring 60.2 × 286 × 3.26 mm, containing 15 tablets each of UO_2, separated by spacers 2 mm thick	Zircalloy-2; 0.63 mm —	Rectangular UO_2 tablets (measuring 6.35 × 76 × × 2.03 mm); 2.03 mm —	— — —	H_2O — — —
		Seed elements, plates in assemblies of 15 × 4 units. Rod elements of breeder zone (first charge) see No. 29	Zircalloy-2; 0.38 mm —	Alloy of enriched uranium with Zircalloy--2; uranium content 6.7 wt. % — —	— — —	— — — —
30	Brazil [2274]; test reactor of the swimming-pool type, 5 Mw	Packet of 19 plates		Uranium-aluminum alloy — —	— — —	H_2O — — —
31	USA [455]; ALPR, a prototype of small-scale boiling water reactor (being built), 3 Mw	Packet of 19 plates, plate dimensions 3.05 × 96 × × 705 mm	Aluminum-nickel alloy 0.9 mm, 227°C	Aluminum-nickel-uranium alloy with 17.6 wt.% of uranium, ⌀ 1.25 mm 232°C	Average 17.5 kw/dm^3; average $0.61 \cdot 10^6$ kcal/(m^2 · hour)	H_2O; feed water - 58°C; steam 216°C; 21 kg/cm^2
32	USA [414]; ETR-A, a test reactor	Packet of 19 plates —	Aluminum; — 138°C	Alloy of fully enriched uranium with aluminum (1 wt. % uranium), boron added —	— Maximum $3.15 \cdot 10^6$ kcal/(m^2 · hour) —	H_2O; 10.7 m/sec — 13 kg/cm^2

No.	Location of reactor, literature source; type of reactor, its purpose and thermal power	Type of FE and its length	Jacket material; thickness; surface temperature	Fuel; diameter or thickness through fuel; maximum temperature	Energy release of fuel; heat flux from surface; burnup of fuel	Coolant; rate; inlet temperature — outlet temperature; pressure
33	Great Britain [313]; Merlin research reactor (being built), 5 Mw	Packet of 14 plates; plate dimensions 1.47 × 73 × × 635 mm; 3.3 mm slit for water	— — —	Uranium-aluminum alloy (20 wt. % uranium, 93% enriched); 0.46 mm —	— — —	H_2O — 35-45°C —
34	USA [421]; OMRE, an experimental reactor with organic moderator and coolant, 14.8 Mw	Packet of 16 plates; plate dimensions 3.04 × 63.5 × × 920 mm; 3.4 mm slit for water	Stainless steel; 0.127 mm —	Fully enriched UO_2 in a matrix of stainless steel; 0.51 mm —	Average 580, maximum 1830 kw/kg; average $0.2 \cdot 10^6$, maximum $0.62 \cdot 10^6$ kcal/(m · hour)	Mixture of polyphenols — 260-274°C —
35	Great Britain [1464]; research reactor with light water as moderator (being built), 5 Mw	Packet of 14 plates	Aluminum; — 103°C	Alloy of highly enriched uranium with aluminum — —	— — —	H_2O — 53°C —
36	Argentine [1584, 1555]; RA-1, a thermal, heterogeneous reactor	Packet of 17 plates; plate dimensions 2.2 × 72 × × 600 mm; 6 mm slit for water	Aluminum; 0.27 mm —	U_3O_8 in an aluminum matrix (45% U_3O_8), 20% enriched; 2.2 mm —	— — —	H_2O — — —
			Ring FE			
37	Belgium [1679]; BR-2, a test reactor, thermal, heterogeneous (being built), 50 Mw	Assembly of six concentric tubes 76.2 cm long, increasing in diameter from 33 to 76.2 mm; slit for water 2.97 mm	Aluminum; 0.38 mm —	Uranium-aluminum alloy (20-25 wt. % uranium), 90% enriched, 0.5 mm —	Maximum $3.28 \cdot 10^6$ kcal/m² · hour —	H_2O — 40.6-47.2°C 12.6 kg/cm²
38	USA [610]; projects for power reactors with heavy water moderator and coolant; 1st: 435 Mw	Tube 36.4 × 52.4 mm diameter	Zircalloy-2; 1.52 mm; 300°C	Uranium alloy with 2 wt. % zirconium; 6.4 mm; 526°C	Average 34.4 Mw/t; maximum $1.96 \cdot 10^6$ kcal/m² · hour; 3250 Mw · d/t	D_2O; 5.4; 3.8 m/sec; 98-111°C —

No.	Location of reactor, literature source; type of reactor, its purpose and thermal power	Type of FE and its length	Jacket material; thickness; surface temperature	Fuel; diameter or thickness through fuel; maximum temperature	Energy release of fuel; heat flux from surface; burnup of fuel	Coolant; rate; inlet temperature — outlet temperature; pressure
	2nd: 439 Mw	The same	Zircalloy-2; 1.52 mm; 312°C (local surface boiling)	Uranium alloy with 2 wt. % zirconium; 6.4 mm; 550°C	Average 38.6 Mw/t; maximum $2.3 \cdot 10^6$ kcal/m^2 · hour; 3200 Mw · d/t	D_2O; 14.6; 6.4 m/sec; 95-112°C; 7 kg/cm^2
	3rd: 479 Mw	The same	Zircalloy-2; 1.52 mm; 320°C (local surface boiling)	Uranium alloy with 2 wt.% zirconium; 6.4 mm; 560°C	Average 36.0 Mw/t; maximum $2.07 \cdot 10^6$ kcal/m^2 · hour; 4500 Mw · d/t	D_2O; 5.18; 3.62 m/sec; 107-119°C; 7 kg/cm^2
	4th: 433 Mw (reactor with tubes under pressure)	The same	Zircalloy-2; 1.52 mm; 320°C	Uranium alloy with 2 wt. % of zirconium; 6.4 mm; 594°C	Average 41.5 Mw/t; maximum $2.4 \cdot 10^6$ kcal/(m^2 · hour); 3500 Mw · d/t	D_2O; 7.5; 4.7 m/sec; 106-123°C; 70 kg/cm^2
39	USA [447]; PRTR, a plutonium regeneration test reactor (being built), thermal, heterogeneous, with tubes under pressure, 70 Mw	FE, concentric tubes; seed FE, an assembly of 19 rods, 12.7 mm diameter and ~210 mm long; possible construction of ring type	Zircalloy-2 — —	Sintered UO_2; seed FE, an alloy of plutonium with aluminum or Silumin (1.7 wt. % plutonium)	— Maximum $1.08 \cdot 10^6$ kcal/(m^2 · hour) —	D_2O; — 249-277°C; 74 kg/cm^2
40	USA [423]; "Mighty Mouse", a research reactor with high neutron flux, 250 Mw	Tube 8.02 × 9.95 mm diameter and 91.5 cm long; tubes in 8 assemblies of 455 units	Magnesium alloy; 0.25 mm; 140°C	Highly enriched uranium in a magnesium matrix; 0.5 mm —	— Maximum $2.06 \cdot 10^6$ (inside tube), $1.64 \cdot 10^6$ kcal/(m^2 · hour) (outside tube)	D_2O; 7.6 m/sec (inside tube), 5.8 m/sec (outside tube); 43-66°C; 7 kg/cm^2
41	Switzerland [246]; project for prototype heavy water power reactor (firm of "Sulzer"), 300 Mw	Assembly of 8 annular elements; inner diameter of 13 mm; water under pressure flows along the inner cavity	Zircalloy-2; 1.5 mm —	Natural uranium; small number of elements with uranium enriched up to 1% — —	— — —	D_2O — 190-220°C; 60 kg/cm^2

No.	Location of reactor, literature source; type of reactor, its purpose and thermal power	Type of FE and its length	Jacket material; thickness; surface temperature	Fuel; diameter or thickness through fuel; maximum temperature	Energy release of fuel; heat flux from surface; burnup of fuel	Coolant; rate; inlet temperature — outlet temperature; pressure
42	Switzerland [259]; project for prototype reactor with heavy water moderator and organic coolant, 100 Mw	Tube 10 × 38 mm in diameter	Magnesium; 1.0 mm —	Natural uranium; 8 mm; 600°C	Maximum 353, average 140 w/cm^3; maximum $1.6 \cdot 10^6$, average $0.48 \cdot 10^6$ kcal/(m^2 · hour)	Diphenyl; 10 m/sec (inside tube), 4.6 m/sec (outside tube); 260-324°C; 20 kg/cm^2
	Canada [210]; project for power reactor with heavy water moderator and organic coolant, 150 Mw (elect.)	Two concentric tubes and one (in the center) rod, 2.05 mm long; 2.03 mm slit for coolant	Aluminum; 0.78 mm; 445°C	Sintered UO_2 — —	— Maximum $1.22 \cdot 10^6$ kcal/(m^2 · hour); 6000 Mw · d/t	Mixture of polyphenyls; 8.6 m/sec; 302-427°C —

SUMMARY

FE are being developed very extensively for all types of reactors, since up to now the most promising type of reactor has not yet been established.

The main focus of attention in the development of FE for power reactors is that of raising the operating parameters. In connection with this, intensive searches are being made for new construction materials that are heat and corrosion resistant at high temperatures. In the range of fissile materials, a fuel composition with high radiation stability and corrosion resistance is being sought. Plutonium and thorium have been put into practical use.

There is also a tendency toward the fabrication of FE which do not allow very high operating parameters, but which use jackets of readily available and cheap materials, for example, alloys based on aluminum.

In the preparation of FE, a series of new technical methods have been developed, for example, electronic vacuum welding. There are no particularly original results in the field of FE construction. FE are fabricated mainly along established lines with a predominance of rod FE.

Received December 25, 1958

THE EFFECT OF NEUTRON IRRADIATION ON THE STRUCTURE AND PROPERTIES OF FERRITO-PEARLITIC STEELS

V. S. Lyashenko and Sh. Sh. Ibragimov

Specimens of steels 1Kh17N2, 2Kh13, and 30KhMA, which are susceptible to heat treatment, and of steel 1Kh17 containing niobium, which is not susceptible to heat treatment were subjected to irradiation with fast neutrons at temperatures of 70° and 500-600°C.

As a result of irradiation at 500-600°C the mechanical properties of steels 1Kh17N2, 2Kh13, and 30KhMA undergo considerable change, but no change is observed in steel 1Kh17 containing niobium. Metallographic examination shows that the increases in the strength properties of the steels mentioned during irradiation at 500-600°C is connected with a change in structure. In the opinion of the authors the observed changes in microstructure are due to the formation of displacement spikes in the irradiated material.

The bombardment of a solid, in particular of a metal, with a stream of fast particles sets up defects in the crystal lattice that lead to a considerable change in the physical and mechanical properties of the material. The nature of these defects is very complex and notwithstanding the large number of theoretical and experimental researches in this field, unanimity has not yet been reached.

According to Seitz's theory [1], the change in properties of metals on irradiation is due to the formation of Frenkel defect pairs (vacancies and interstitial atoms) in the crystal lattice and to the breakdown of the uniform crystal structure of microvolumes as a result of the formation of thermal spikes.

According to Brinkman's theory [2], the nature of radiation damage in heavy elements is different from that in light elements, the change in properties of heavy metals on irradiation being due mainly to the formation of displacement spikes, i.e., microregions where, because of the high temperature (considerably above the melting point of any refractory metal) and the adequate diffusion time, atoms can be displaced over several interatomic distances.

The experimental data in references [3, 4, 5], which are regarded as conclusive evidence of the formation of thermal spikes during neutron irradiation, relate to fissile material (uranium containing 9% molybdenum) in which the possibility of such spikes being formed is considerably greater on account of the formation of fission fragments with large kinetic energy.

The authors of the present paper have studied the changes in microstructure and properties of steels 1Kh17N2, 2Kh13, and 30KhMA and of steel 1Kh17 containing niobium after irradiation with fast neutrons at temperatures of 70 and 500 - 600°C. The specimens were heat treated before being placed in the reactor.

The properties of the steels before and after irradiation are presented in Table 1, from which it can be seen that the mechanical properties of all the steels after irradiation at 70°C change approximately by the same amount. The ultimate strength, the yield strength, and also the hardness of the steels increase while the plasticity falls. An increase in the integrated flux from $8 \cdot 10^{19}$ to $1.8 \cdot 10^{20}$ neutrons/cm^2 does not lead to any further change in the mechanical properties of steel 2Kh13, although for steel 1Kh17 containing niobium, saturation is not reached even after irradiation with an integrated flux of $1.4 \cdot 10^{20}$ neutrons/cm^2 (Table 2).

On irradiation at 500-600°C the properties of the steels investigated should remain practically unchanged owing to the recovery from radiation damage at the elevated temperature. The properties of steel 1Kh17 containing niobium are almost unchanged after irradiation at 500-600°C. The properties of the specimens of steels irradiated at 70°C are completely restored by heat treatment at 350°C, as can be seen from the data in Table 2, giving the properties of steel 1Kh17 containing niobium after irradiation and heat treatment.

The mechanical properties of steels 1Kh17N2, 2Kh13, and 30KhMA after irradiation at 500-600°C vary by a considerable amount, though the electrical conductivity remains almost unchanged, a fact which is difficult to explain by Seitz's theory. The strength properties of steels 1Kh17N2 and 30KhMA are even somewhat greater after irradiation at 500-600°C than after irradiation at 70°C.

Such a change in the mechanical properties of the steels can be largely accounted for by the change in structure of the alloys, as can be seen, for example, in Fig. 1. Before irradiation steel 1Kh17N2 consists of temper sorbite and rounded ferrite grains; after irradiation at 500-600°C the ferrite constituent disappears and an isothermal-quench structure develops with austenite grain boundaries. The microhardness increases by 90 kg/mm^2.

Figures 2 and 3 show the microstructures of steels 2Kh13 and 30KhMA before and after irradiation at 500-600°C. The microstructure of the steels is considerably changed after irradiation. In steel 2Kh13 the austenite grain boundaries are seen more clearly.

The appearance of the austenite grain boundaries, which show up well in the microstructure of steels 1Kh-

TABLE 1. The Effect of Irradiation on the Properties of Steels

Type of steel	Initial condition of the material	Integrated flux of fast neutrons per cm^2	Ultimate strength, kg/mm^2			Yield strength, kg/mm^2			Elongation, %			Microhardness, kg/mm^2			Specific electrical resistivity, microhm·cm		
			Before irradiation	after irradiation		before irradiation	after irradiation		before irradiation	after irradiation		before irradiation	after irradiation		before irradiation	after irradiation	
				at 70° C	at 500–600° C		at 70° C	at 500–600° C		at 70° C	at 500–600° C		at 70° C	at 500–600° C		at 70° C	at 500–600° C
1Kh17N2	Quenched from 1100°C and tempered at 650°C	$8 \cdot 10^{19}$	106	126	132	88	114	119	12	8	9	268	350	358	64	—	63,4
1Kh17 with ~1% niobium	Normalized at 900°C	$1,4 \cdot 10^{20}$	70	86	71 *	—	—	—	27	16	12 *	228	285	236	85	86	—
2Kh13	Quenched from 1000°C and tempered at 600°C	$8 \cdot 10^{19}$	95	114	106	84	90	86	13	7	12	290	—	315	55,1	—	54,9
2Kh13	Quenched from 1000°C and tempered at 650°C	$1,8 \cdot 10^{20}$	94,5	113	—	—	—	—	19	12	—	267	316	—	57,8	58,9	—
30KhMA	Quenched from 850°C and tempered at 650°C	$8 \cdot 10^{19}$	90	115	119	74	107	106	14	9	12	—	—	—	19,2	20,5 **	19,2

* Integrated flux: $3,4 \cdot 10^{20}$ slow neutrons per cm^2 and about 25% of higher-energy neutrons.

** At 250°C.

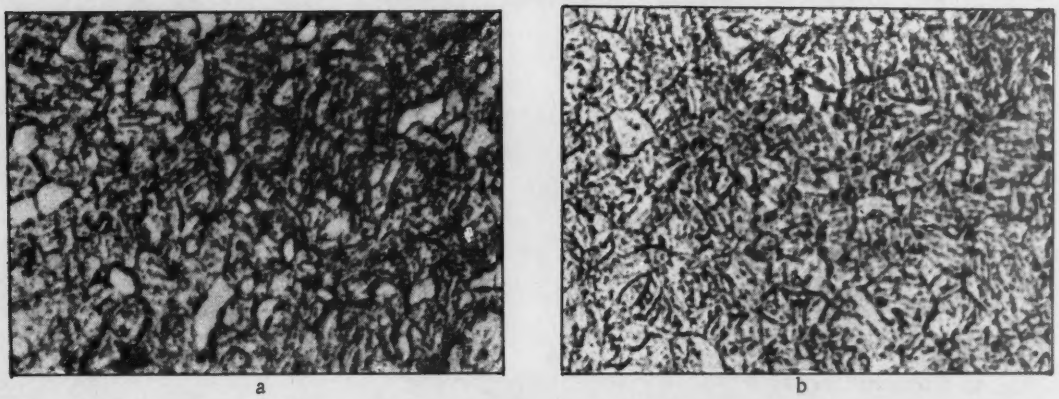

a b

Fig. 1. Microstructure of steel 1Kh17N2, × 1000: a) before irradiation; b) after irradiation at 500-600°C.

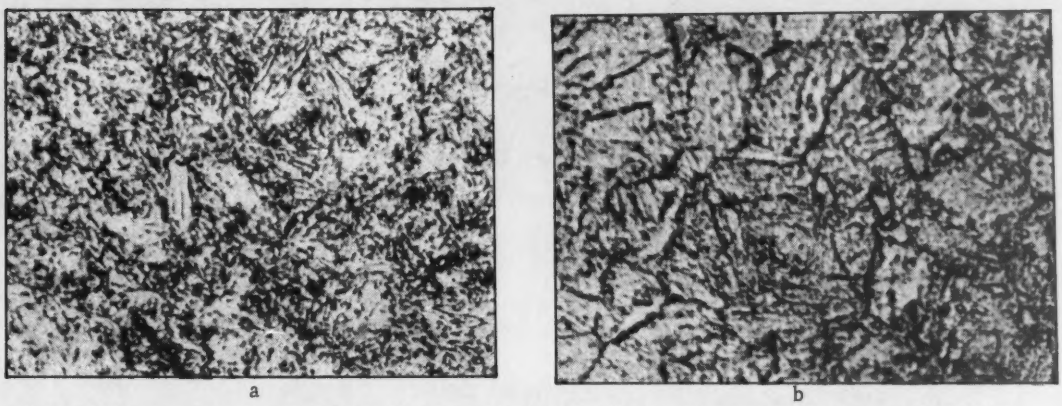

a b

Fig. 2. Microstructure of steel 2Kh13, × 1000: a) before irradiation; b) after irradiation at 500-600°C.

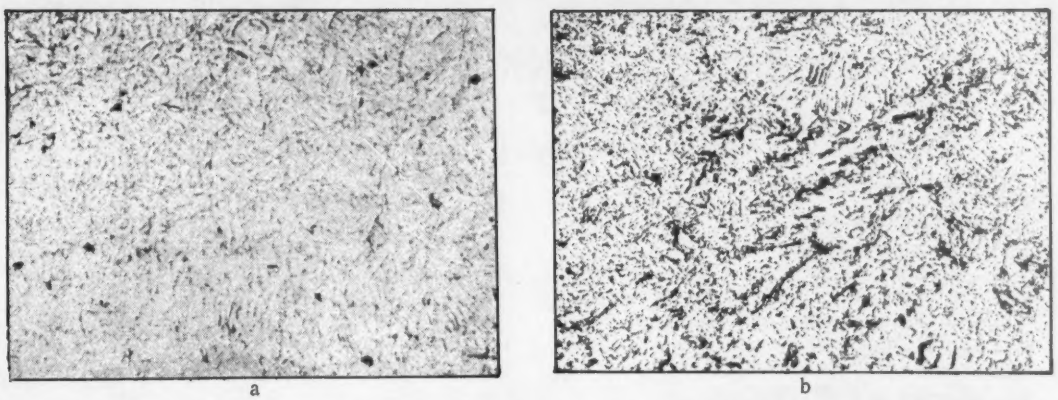

a b

Fig. 3. Microstructure of steel 30KhMA, × 1000: a) before irradiation; b) after irradiation at 500-600°C.

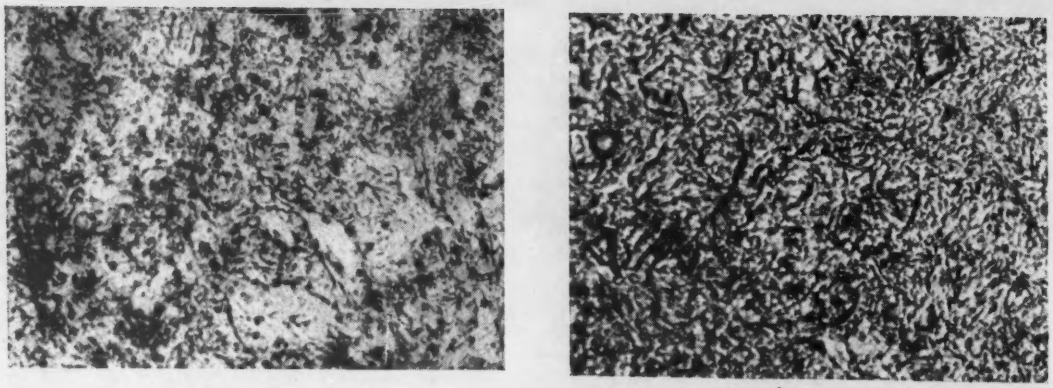

a b

Fig. 4. Microstructure of steel 2Kh13, × 1000: a) before irradiation; b) after irradiation at 70°C.

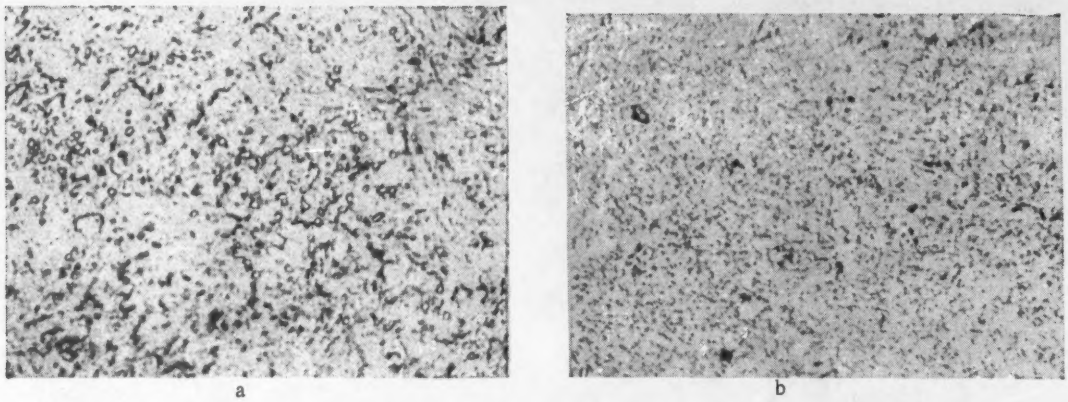

a b

Fig. 5. Distribution of carbides in steel 2Kh13, × 1000: a) before irradiation; b) after irradiation at 70°C.

TABLE 2. The Properties of Steel 1Kh17 Containing Niobium

Treatment	Ultimate strength, kg/mm^2	Elongation, %	Microhardness, kg/mm^2	Specific electrical resistivity, microhm · cm
Irradiation with fast neutrons at 70°C. Integrated flux $1.8 \cdot 10^{20}$ neutrons/cm^2	88	13.5	291	86.5
The same with heat treatment at 350°C for 100 hr	71	24	234	85
Normalization at 900°C and heat treatment at 350°C for 100 hr	72	23	235	85

17N2 and 2Kh13; the change in the sorbitic structure in these steels and also in steel 30KhMA; the increase in the strength properties of the steels after irradiation at 500-600°C as compared with the initial state – all these facts can be accounted for by the formation of thermal spikes, i.e., the heating of microvolumes by the action of the neutron flux up to the quenching temperature (the austenitic range) and higher, with subsequent quenching of these volumes by rapid cooling to the irradiation temperature (500-600°C). On this basis it is easy to explain the observed refinement and redistribution of carbides in steel 2Kh13 resulting from irradiation at 70°C. The microstructure of this steel before and after irradiation by an integrated flux of $1.8 \cdot 10^{20}$ fast neutrons per cm^2 at 70°C and the distribution of the carbides in this steel are shown in Figs. 4 and 5.

It may be assumed that during irradiation, as a result of the formation of microvolumes at a high temperature and their rapid cooling to 70°C, martensitic particles are formed which on further bombardment decompose with precipitation of carbides. The precipitated carbides then coagulate, although the degree of coagulation is less than that of carbides during the tempering of chilled steel at 650°C.

1. As a result of the irradiation of steels with fast neutrons at temperatures of 70 and 500-600°C, a considerable change is observed in the properties of steels 1Kh17N2, 2Kh13, and 30KhMA, a change which is connected not only with "radiation hardening" of the material but also with a change in the microstructure of the alloys.

2. The observed changes in the microstructure and properties of steels 1Kh17N2, 2Kh13, and 30KhMA after irradiation at 500-600°C point to the formation in the irradiated material of microvolumes with a high temperature (the austenitic range and above). Although the elevated temperature persists in such regions for only a very short time, there is always the possibility of further diffusion of the atoms, as a result of which (on subsequent cooling of the material to the irradiation temperature) the structural condition of such microvolumes must differ considerably from the initial condition.

3. It is clear that fast neutrons have a considerable effect on the kinetics of decomposition of the martensitic phase in the steels investigated. Under the action of fast neutrons the martensitic regions, whose formation has been assumed in this paper, decompose even at temperatures of ~70°C and the precipitated carbides coagulate.

LITERATURE CITED

[1] F. Seitz, Phys. Today 5, 6, 6 (1952).

[2] J. A. Brinkman, J. Appl. Phys. 25, 961 (1954).

[3] S. T. Konobeevskii, N. F. Pravdyuk, and V. I. Kutaitsev, "Studies in the field of geology, chemistry, and metallurgy (Reports of the Soviet Delegation to the International Conference on the Peaceful Uses of Atomic Energy)" [in Russian] (Academy of Sciences Press, 1955) p. 263.

[4] S. T. Konobeevskii, J. Atomic Energy (USSR) 2, 63 (1956).

[5] S. T. Konobeevskii, J. Atomic Energy (USSR) 4, 1, 34 (1958).

Received September 12, 1958

AN INVESTIGATION OF γ-EMISSION ASSOCIATED WITH THERMAL NEUTRON CAPTURE

L. V. Groshev, B. I Gavrilov, and A. M Demidov

A number of spectra of γ-rays from the (n, γ) reaction brought about by irradiation by thermal neutrons were investigated with the use of a magnetic Compton spectrometer at the VVR reactor of AN SSSR. The conditions of the experiment are described, as well as the results of measurements made on the γ-spectra of tin and antimony.

In addition to the spectra obtained at the RFT reactor of AN SSSR (using a spectrometer, of which a description has been published [2]) which were included in a recently published table of data [1] on the gamma-spectra associated with radiative, thermal neutron capture, spectra for a number of elements were also included which were studied by means of another spectrometer set up at the VVR reactor of AN SSSR.

A description is given below of the apparatus, and of the conditions under which the measurement was made of the spectra of P, Sc, Cr, Cu, and Zn which were included in the table of data mentioned above. The recently obtained γ-ray spectra of Sn and Sb are also described.

Construction of the Spectrometer and Method of Measurement of the γ-Spectra

The basic difference between the present apparatus and the one used at RFT lies in the different conditions of observation of the γ-rays (Fig. 1). The vertical channel trometer is placed in such a way as to ensure that the spectrometer does not "see" the active zone of the reactor. Such a placement of the channel enables one to dispense with the thick lead or bismuth block which in the RFT apparatus, lies between the sample and active zone of the reactor and attenuates the neutron beam incident on the sample. The gamma rays incident on the sample from the active zone do not introduce especial complications into the measurements, since they can enter the spectrometer only after having been scattered through 90°, and having an energy of less than 0.5 Mev. At the bottom of the vertical channel there is a block of lead which absorbs the γ-rays which emanate from the reactor shield. Along the length of the vertical channel are distributed seven lead collimators, which are spaced in such a way that the radiator of the spectrometer will not "illuminate" the walls of the channel. The sample being investigated, which is in a graphite container, is placed in the horizontal channel, and is mounted against the vertical channel.

The present spectrometer, which is of the magnetic Compton type, does not differ very much from the apparatus used in our earlier experiments [2]. The radius of its basic orbit r_0 is equal to 150 mm, while the air gap between the poles of the magnet is about 100 mm. The poles of the magnet are arranged vertically. The diameter of the pole pieces is equal to 520 mm. The magnetic field in the gap diminishes radially not only for $r < r_0$, but also for $r > r_0$, which permits the use of a plane radiator. The necessary form of the magnetic field was obtained by means of shaping the pole piece surfaces in such a manner that they coincided with the equipotential surfaces of the field. The magnetic field which was obtained differs from the theoretical in the region $110 < r < 210$ mm by less than 0.5%. Special devices provide for changing radiators and variation of the width of the slots in front of the β-counters in the spectrometer chamber without loss of the vacuum in it.

The electromagnet of the spectrometer is fed by an EMU-25 electromechanical amplifier, the current of which can be varied from 0.6 to 20 amp. Stabilization of the current was accomplished by comparison of the voltage drop across a constant resistance in series with the windings of the magnet, to the voltage of a battery. The signal from the comparison circuit, after having been transformed into a changed voltage, is amplified and fed to a phase detector, from which it then proceeds to the excitation winding of the EMU-25. Such a circuit keeps the current variations down to an order of about 0.01%.

Relative measurements of the value of the magnetic field are made by the use of the method of a saturated magnetic probe (of a Permalloy transformer) placed on a coil, the magnetic field of which compensates the field of the magnet. The stabilization of the current in the compensating coil is of the order of $5 \cdot 10^{-5}$. The compensating coil is placed in the leakage field of the magnet.*

Figure 2 gives the background γ-ray spectrum which was measured in the absence of a sample. For this measurement, the graphite container with the bakelite chamber which was enclosed in it (wall thickness, 2 mm) was in operating position. Such a bakelite chamber was used in studying the γ-rays from samples of Sc_2O_3 (see below).

The insufficient shielding of the reactor, which results in an increased background level of radiation in the working space, constitutes a weak point of the apparatus. Therefore, the whole spectrometer is enclosed in containers of water or paraffin, while the chamber of the spectrometer is shielded by a layer of lead about 10 cm thick.

*The changes described above in the construction of the spectrometer and the instrument for measuring the magnetic field were introduced into the spectrometer at the RFT reactor of AN SSSR in 1956. The system for stabilization and measurement of the magnetic field was developed under the direction of A. S. Volkov.

However, even this additional shielding is not enough, and there are many single counts of the β -counters. The numerous counts of the β -counters lead to the appearance of a considerable number of accidental coincidences, the contribution of which in the regions of the γ -spectra between the lines varies from 5% for large Eγ to 25 % for Eγ ≤ 1 Mev. This contribution varies slightly from one sample under investigation to another, in so far as the increase in flux of γ -rays through the spectrometer increases the load of the first counter and as a result increases the number of both real as well as accidental coincidences. It should be noted that for intense lines of γ -spectra, the contribution of accidental coincidences is not more than 1%. It will be recalled that although extra shielding was not used in the spectrometer in the RFT apparatus, there were no accidental coincidences. In addition, the increase in γ -ray flux through this spectrometer does not lead to the appearance of accidental coincidences, since the load of the second counter remains insignificant.

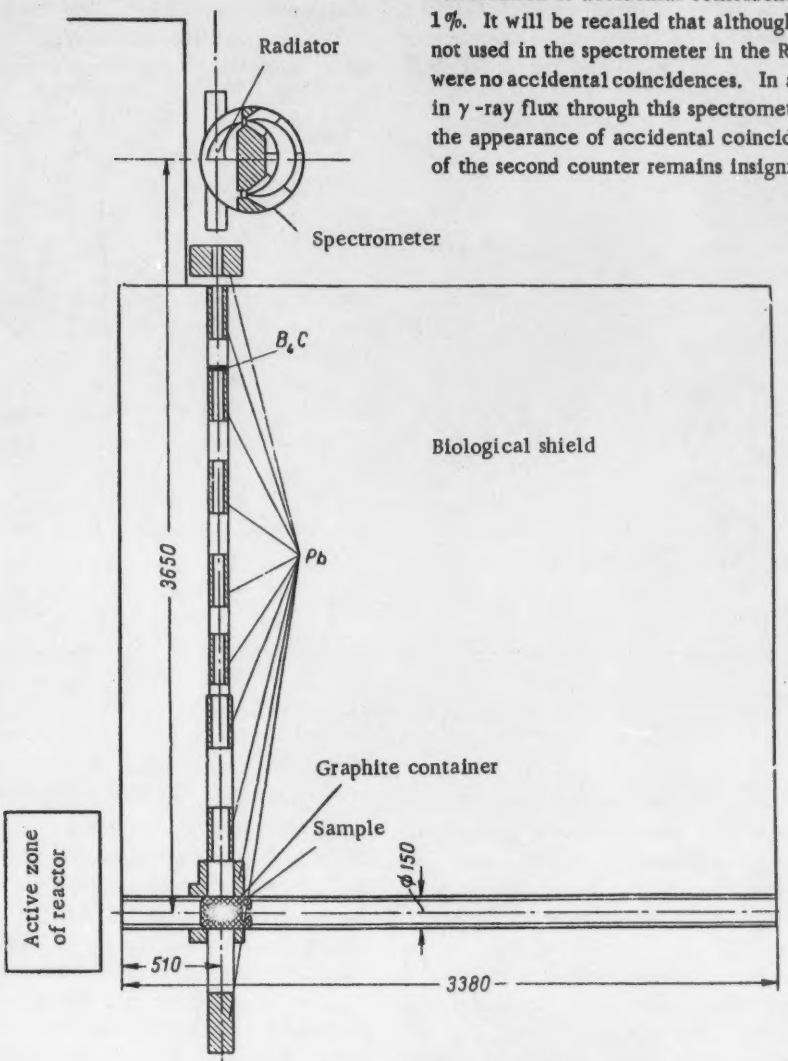

Fig. 1. General layout of the apparatus.

γ -Ray Spectra of Tin and Antimony

Antimony. The weight of the sample was 1 kg. A plate of metallic antimony 15 mm thick was placed at an angle of 45° to the neutron beam. The γ -ray spectrum was studied in the range from 0.3 to 7 Mev. Figure 3† gives the spectrum of γ -rays of antimony which were taken with the apparatus. The numbers of coincidences in five minutes are plotted on the vertical axis: these were obtained after subtracting accidental coincidences and background (the number of coincidences from the sample when surrounded by a layer of boron carbide), and also making corrections for the presence of electrons from the electron-position pairs formed in the radiator by the γ -rays along with the Compton electrons. The measurements were made with a radiator 80 microns thick.

Figure 4 gives the corrected spectrum of the γ -rays of antimony. The values of $\nu(E\gamma)/\rho$, where $\nu(E\gamma)$ is the number of γ -quanta per neutron capture and per unit energy interval (1 Mev), are plotted on the vertical axis. In going from the raw spectrum to the corrected spectrum,

† The numbers of the lines in the figures correspond to their index numbers in the tables.

corrections are introduced for the spectral sensitivity of the apparatus, for the absorption of γ-rays along the path from the sample to the radiator and for the absorption of γ-rays in the sample itself.

Table 1 shows values of the energies and intensities of the γ-rays from antimony which were obtained by us, along with those obtained by Bartholomew et al. [3]. The intensities of the line in numbers of γ-quanta per neutron capture were determined by normalizing the total energy emitted by the antimony nuclei to the neutron binding energy. It is seen from the table that there is satisfactory agreement between our data and the other results [3]. Unfortunately, the interpretation of the lines furnished by the spectrum is made difficult by the fact that the spectrum is dependent on the neutron absorption of the two isotopes of antimony. Also, little is as yet known of the levels of the nuclei being studied, Sb^{122} and Sb^{124}. The neutron binding energies for these isotopes are only approximately known.

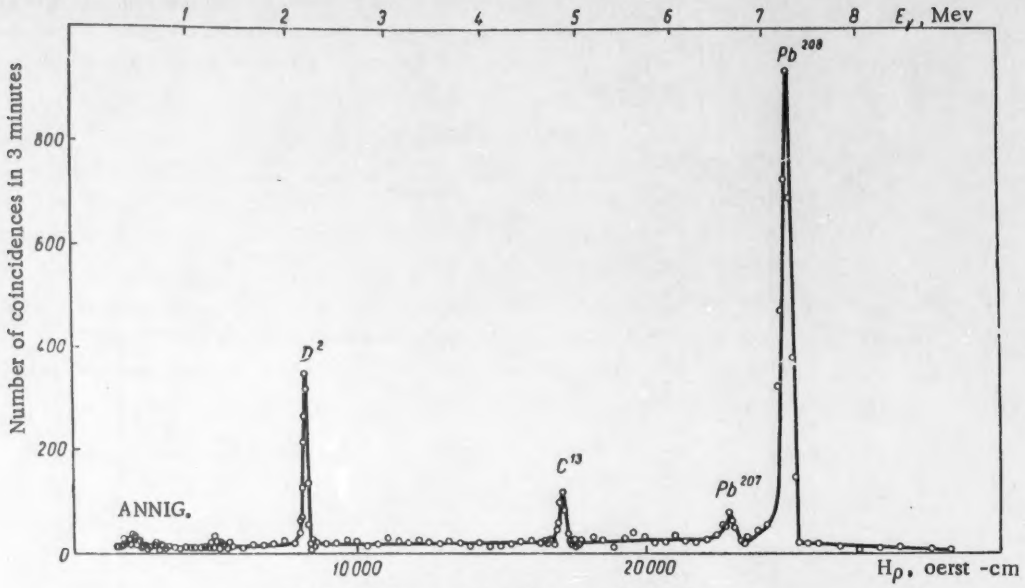

Fig. 2. Background γ-ray spectra of apparatus.

The only thing one can safely assert is that line 1 belongs to Sb^{122} and corresponds to a transition to the ground state. The forbidden portion of the spectrum is quite similar in form to the forbidden portions of the spectra of several other odd-odd isotopes studied, for example, Rh^{104}, $Ag^{108,110}$, In^{116}, and Ta^{182}.

Tin. The sample was a metal cylinder 110 mm in diameter and 80 mm long. The weight of the sample was 5 kg. The γ-spectrum was studied in the region from 0.3 to 11 Mev. Figures 5 and 6 show the raw and corrected spectra of the γ-rays of tin. Values of energy and intensities of the γ-lines of tin obtained from the spectrum are given in Table 2. The intensities of the lines were determined by the method of normalizing the spectrum to the neutron binding energy.

Table 3 lists the percent abundances of the isotopes naturally occurring in tin, the cross section for capture of thermal neutrons in the isotopes σisot, the contribution of the isotopes to the total cross section for capture of thermal neutrons in the natural isotopic mixture σ, and the binding energy of the last neutron in the product nucleus Bn. According to the data of this table, thermal neutrons are captured by the four isotopes Sn^{114}, Sn^{115}, Sn^{117}, and Sn^{119} in 86% of the cases.

In the γ-ray spectrum of tin, lines 3 and 4, and 5 are of interest. The portion of the spectrum containing these lines is shown separately in Fig. 7. Table 4 lists values of the energy of the first excited levels of Sn^{116}, Sn^{118}, and Sn^{120}, taken from various authors.

It is known that the first excited levels of even-even nuclei, as a rule, are heavily occupied as a result of γ-transitions of the nucleus after thermal neutron capture. This last circumstance, and also the coincidence of the energies of γ-lines 3, 4, and 5 with the energies of the first excited levels in Sn^{116}, Sn^{118}, and Sn^{120}, respectively, furnished us the basis to ascribe these lines to the isotopes in question.

In the heavy elements ($A > 90$) with even atomic number, the odd-A isotopes usually make the main contribution to the absorption of thermal neutrons in a natural mixture of isotopes. One can, therefore, presume that the isotope Sn^{114}, which is 0.65% abundant, will make a small contribution to the total cross section for neutron capture in a natural isotopic mixture of tin.

In order that the isotope Sn^{114} may make an appreciable contribution to the total cross section for thermal neutron capture by tin, one must assume that its cross section is equal to ~ 50 barn. Such a possibility for an even-even nucleus with $Z = 50$ is known to be excluded.

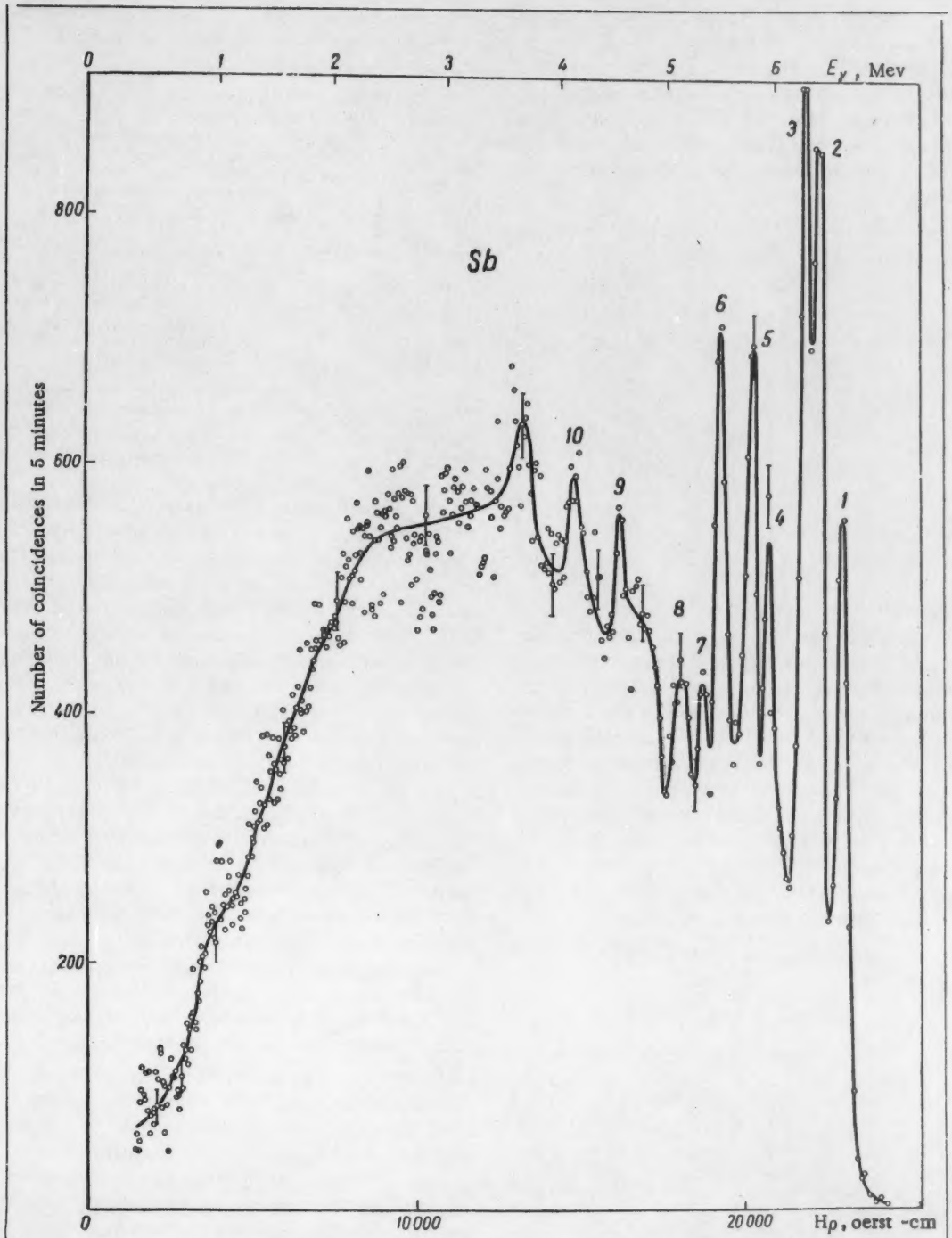

Fig. 3. Spectrum of γ-rays of antimony taken by the apparatus.

If this is taken into account and it is assumed that the population of the first excited states in γ - transition following thermal neutron capture is approximately equal in the isotopes Sn^{116}, Sn^{118}, and Sn^{120}, then, by using the data of Table 2, the cross section for capture of thermal neutrons by the isotopes Sn^{115}, Sn^{117}, and Sn^{119} can be estimated. They are equal to 50 ± 20; 2.6 ± 1.0; 2.3 ± 1.0 barns, respectively, for Sn^{115}, Sn^{117}, and Sn^{119}. The cross section for capture of thermal neutrons in a natural isotopic mixture of tin was taken equal to (0.65 ± 0.05) barns in these calculations. (The errors in the listed cross sections include the possible deviation in the population of the first excited levels.)

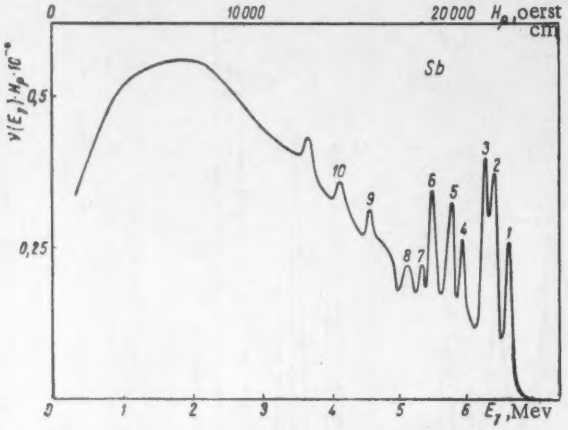

Fig. 4. Corrected spectrum of the γ -rays of antimony.

Let us note that peak 1 in the γ -spectrum of tin for an energy of about 8 Mev is much wider than the standard peak from the monochromatic γ -line. This may be connected with the fact that the energies of the principal γ -transitions in Sn^{116}, Sn^{118}, and Sn^{120} are near this value. Since the binding energy of the last neutron must increase with a decrease in the number of neutrons (Z constant), when N is far from a magic number, the γ -transition with an energy of 9.43 ± 0.05 Mev must correspond to the principal γ -transition in Sn^{116}.

TABLE 1. Energy and Intensity of γ -rays Accompanying Capture of Thermal Neutrons in Antimony

Number of line	Data of Bartholomew et al. [3]		Data of the present exp.	
	E_γ, Mev	I_γ*	E_γ, Mev	I_γ*
1	$6,80 \pm 0,04$	0,7	$6,78 \pm 0,02$	1,3
2	$6,50 \pm 0,03$	1,6	$6,52 \pm 0,02$	1,9
3	$6,33 \pm 0,04$	1,1	$6,35 \pm 0,03$	1,7
4	$6,11 \pm 0,06$	1	$6,07 \pm 0,05$	0,6
5	$5,89 \pm 0,04$	1	$5,86 \pm 0,03$	1,1
6	$5,61 \pm 0,03$	1	$5,65 \pm 0,03$	1,3
7	$5,43 \pm 0,03$	0,5	$5,45 \pm 0,04$	0,5
8	—	—	$\sim 5,1$	—
9	—	—	$\sim 4,6$	—
10	—	—	$\sim 4,1$	—

*Intensities given in numbers of γ-quanta per 100 captures in a natural mixture of isotopes.

As was already noted earlier [11], the magic number Z=50 does not appear‡ in the spectra of the γ-rays of the (n, γ) reaction with thermal neutrons. Actually, for the odd-odd emitting isotopes of In and Sb, which are neighbors to Sn, the forms of the γ-spectra are almost the same as the forms of the γ-spectra of other odd-odd nuclei. There is also no essential difference between the forms of the γ-spectra of Sn and Cd.

TABLE 2. Energies and Intensities of γ-rays Accompanying Capture of Thermal Neutrons in Tin

Number of line	Radiating isotope	Data of Kinsey et al. [4]		Data of the present exp.	
		E_γ, Mev	I_γ*	E_γ, Mev	I_γ*
1	Sn^{116}	$9,35 \pm 0,08$	0,4	$9,43 \pm 0,05$	0,5
2	—	—	—	$3,27 \pm 0,02$**	2
3	Sn^{116}	—	—	$1,29 \pm 0,01$	15
4	Sn^{118}	—	—	$1,22 \pm 0,01$	18
5	Sn^{120}	—	—	$1,17 \pm 0,01$	18

*Intensities given in numbers of γ-quanta per 100 captures of neutrons in a natural mixture of isotopes.

**The existence of this γ-line is not established with complete certitude.

Let us recall that near the magic numbers Z=82 and N=126, a decided change in the form of the γ-spectra is observed, which is connected with the appearance of $3p$-levels near the ground state and to some extent with a decrease in level density in this region of atomic weights [12]. An increase in the intensity of γ-lines with high energy is also observed in the spectra of nuclei for which N=83, namely in the γ-spectra of Ba, La, and Pr. But the change in the form of the γ-spectra of these nuclei is completely explained by the low binding energy of the 83rd neutron and by the level density [12].

In contrast to the cases mentioned above, in the Z=50 region there are no p-levels near the ground state, and the binding energies for emitting nuclei have the normal values: ~6.5, ~6.8, and ~9.3 Mev for In, Sb, and Sn respectively. Evidently the decrease in level density for Z=50 nuclei is not so large as to change the form of the γ-ray spectrum in the (n,γ) reaction with thermal neutrons.

Some information concerning the change in the level density on approaching a magic number can be obtained from the change in the density of the neutron s-resonances. Such information is contained, for example, in reference

‡Generally speaking, the magic number Z = 50 appears in an increase in the energies of the intense γ-lines which correspond to γ-transitions from the first excited levels of Sn to the ground state by comparison with the energies of the analogous γ-transitions in other nonmagic even-even nuclei. However, here we have in mind the absence of both a change of the general form of the spectrum and of an increase in the intensities of the γ-transitions with high energies which is observed for N = 82 and N = 126.

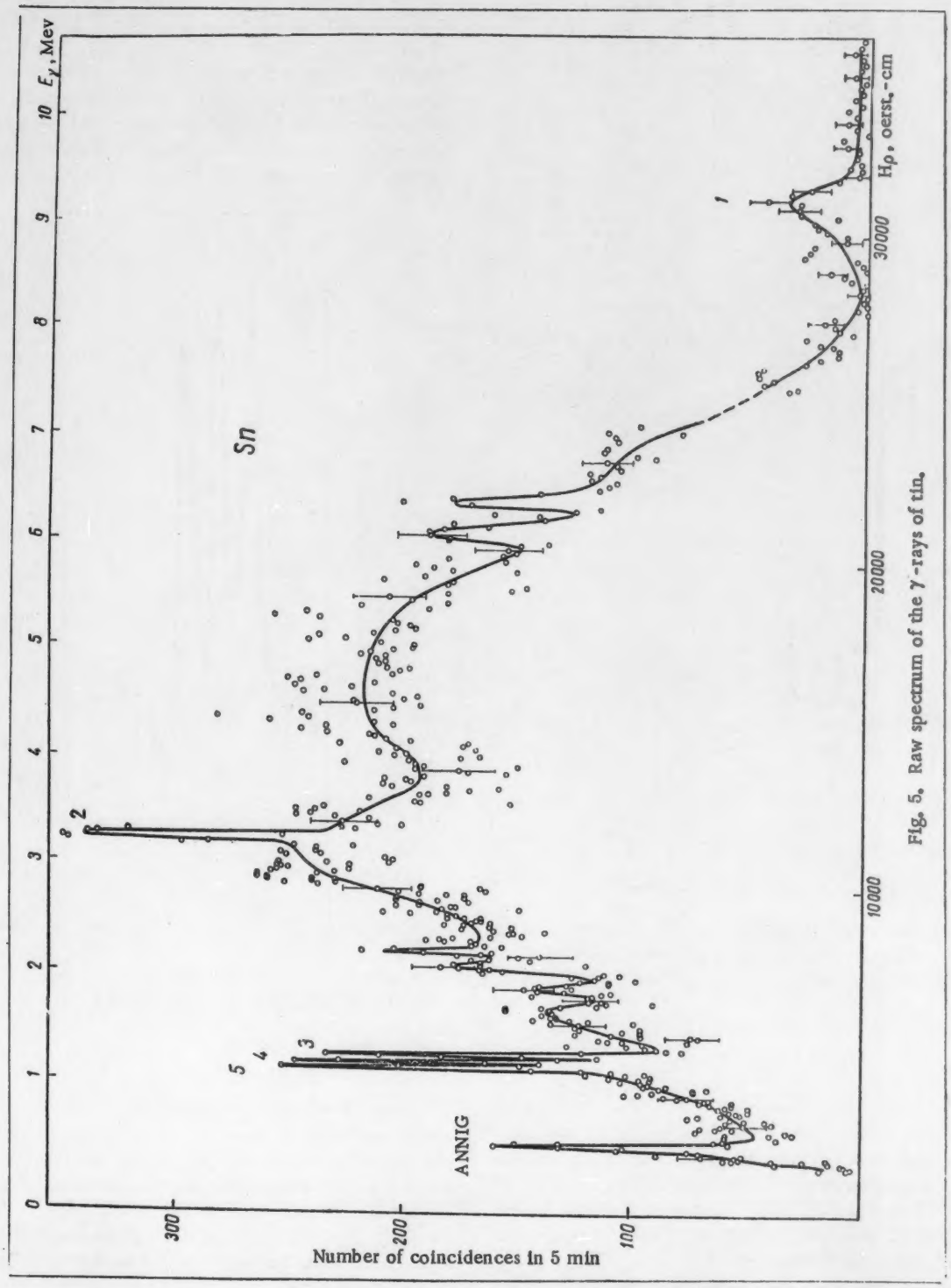

Fig. 5. Raw spectrum of the γ-rays of tin.

TABLE 3. Some Data on the Isotopes of Tin

Isotope	Percent abundance	σ_{isot}, barn	Contribution of isotope to σ, %	Bn in product-nucleus, Mev	Source in literature for Bn values
Sn^{112}	0,95	1,3±0,3	2	8,4±0,3	[5]
Sn^{114}	0,65	—	—	7,9±0,6	[5]
Sn^{115}	0,34	—	—	9,9±0,4	[5]
Sn^{116}	14,24	$(6\pm2)\cdot10^{-3}$	0,14	7,3±0,2	[5]
Sn^{117}	7,57	—	—	9,24±0,15	[6]
Sn^{118}	24,01	$(10\pm6)\cdot10^{-3}$	0,4	6,54±0,12	[6]
Sn^{119}	8,58	—	—	9,1±0,3	[5]
Sn^{120}	32,97	0,14±0,03	8	6,14±0,07	[6]
Sn^{122}	4,71	0,16±0,04	1	6,0±0,4	[5]
Sn^{124}	5,98	0,2±0,1	2	5,75±0,07	[6]

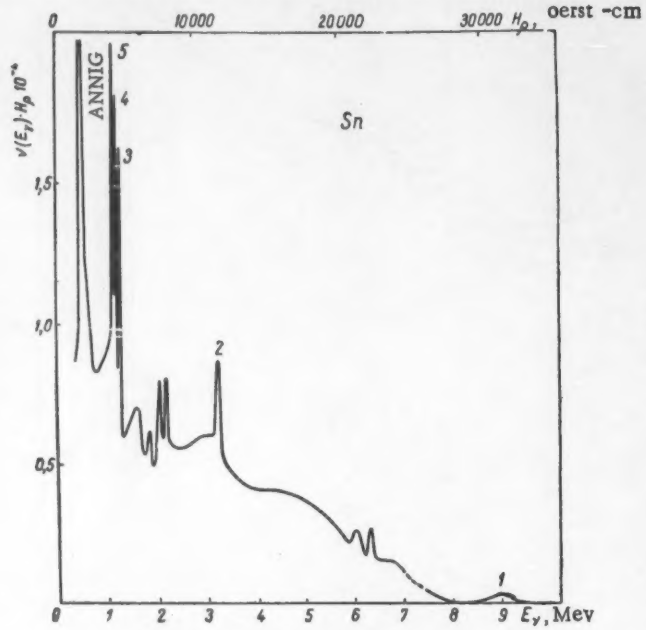

Fig. 6. Corrected spectrum of γ-rays of tin.

[13], from which it follows that for nuclei near Z=50 no sharp change in the density of neutrons s-resonances is observed, in contrast to the regions with N=82 and N=126.

Conditions of Measurement of the Spectra of the γ-Rays from the P_2O_5, Sc_2O_3, Cr_2O_3, Cu, and Zn Samples

The spectra of the γ-rays obtained in the measurements of these samples with the VVR apparatus, as well as the schemes of the γ-transitions of the P^{32}, Sc^{46}, $Cr^{53,54}$, $Cu^{64,66}$, and $Zn^{65,67,68,69}$ nuclei which we drew up, were cluded in the atlas of the spectra of the γ-rays of radiative capture of thermal neutrons [1] and will not, therefore, be given here. The following are just a few observations concerning the indicated measurements.

P_2O_5. In order to prevent the sample from absorbing moisture from the air, it was enclosed in a hermetically sealed bakelite container, and then placed in a special container with aluminum walls 1 mm thick. The diameter of the sample was 140 mm, its length was 120 mm, and its weight was 1.5 kg. The presence in the spectrum of a background of intense lines of γ-rays which were emitted upon neutron capture by hydrogen, lead, and aluminum prevented a detailed examination of the part of the spectrum of $E\gamma \approx 2.23$ Mev and $E\gamma > 7$ Mev; consequently, these portions are indicated in the corresponding figures in the atlas by a dotted line.

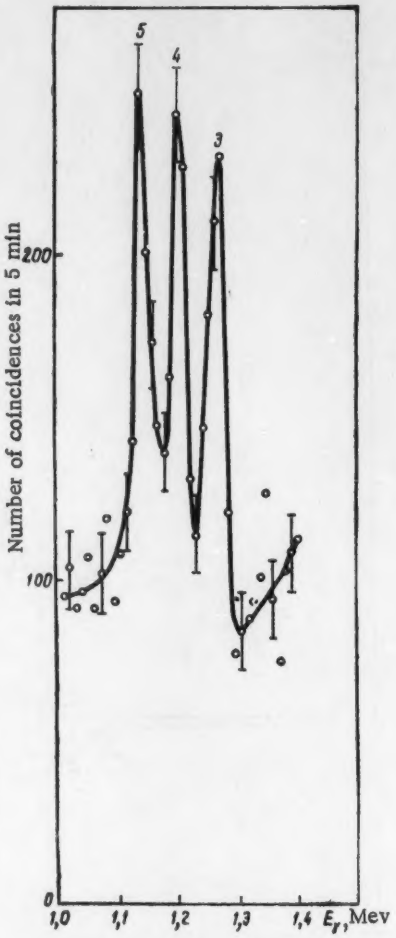

Fig. 7. A section of the raw spectrum of the γ-rays of tin.

Sc_2O_3. The sample diameter was 100 mm, while its weight was 25 g. A graphite container was used for this and all the subsequent samples. In addition, the sample was placed in a thin-walled bakelite container. A detailed investigation of the portions of the spectrum for $E\gamma \approx 2.23$ Mev and $E\gamma \approx 7.38$ Mev was not possible, due to the presence in the spectrum of a background of intense lines of the γ-rays of the H(n,γ)D and Pb^{207}, (n,γ) Pb^{208} reactions.

Cr_2O_3. The sample diameter was 120 mm, its length was 100 mm, and it weighed 1 kg. Due to the presence of

7.38-Mev γ-rays in the background, the part of the spectrum near this energy could not be examined.

TABLE 4. Data for the First Excited Levels of the Isotopes of Tin

Isotope	Energy, Mev	Literature
Sn^{116}	1,268±0,010	[7]
	1,274	[8]
	1,300	[8]
	1,29	[9]
Sn^{118}	1,219±0,010	[7]
	1,22	[9]
Sn^{120}	1,155±0,010	[7]
	1,180±0,010	[10]
	1,18	[8]
	1,18	[9]

Cu and Zn. The samples were in the form of disks 110 mm in diameter and 20 mm thick. The disks were placed at an angle of 45°, duplicating the arrangement in the case of antimony. The weights of the copper and zinc samples were 1.7 kg and 1.3 kg, respectively. In the present case, the background peak at an energy of 7.38 Mev was considerably less intense than the corresponding portions of the spectra of the Cu and Zn samples, and was taken into account in analyzing the results of the measurements.

In conclusion, we wish to thank A. S. Volkov for constructing the electronic apparatus and providing for its stable operation; also, we thank the maintenance organization of VVR AN SSSR.

LITERATURE CITED

[1] L. V. Groshev, A. M. Demidov, V. N. Lutsenko, and V. I. Pelekhov, Atlas of the γ-Ray Spectra of Radiative Capture of Thermal Neutrons [in Russian] (Atomizdat, 1958).

[2] L. V. Groshev, B. P. Ad'yasevich, and A. M. Demidov, Physical Investigations: Reports of the Soviet Delegation to the International Conference for the Peaceful Uses of Atomic Energy [in Russian] (Izd-vo AN SSSR, 1955) p. 252.

[3] G. A. Bartholomew and B. B. Kinsey, Can. J. Phys. 31, 1025 (1953).

[4] B. B. Kinsey and G. A. Bartholomew, Can. J. Phys. 31, 1051 (1953).

[5] D. M. Van Patter and W. Whaling, Rev. Mod. Phys. 26, 402 (1954).

[6] V. A. Kravtsov, Uspekhi Fiz. Nauk 54, 3 (1954).

[7] P. H. Stelson and F. K. McGowan, Bull. Am. Phys. Soc. 2, 69 (1957).

[8] B. S. Dzhelepov and L. K. Peker, Decay Schemes of Radioactive Isotopes [in Russian] (Izd-vo AN SSSR, 1957).

[9] D. G. Alkhazov, D. S. Andreev, L. N. Gal'perin, A. P. Grinberg, G. M. Gusinskii, K. I. Erokhina, and I. Kh. Lemberg, Theses of the Proceedings of the All-Union Conference on High- and Low-Energy Nuclear Reactions [in Russian] (Izd-vo AN SSSR, 1957) p. 42.

[10] C. L. McGinnis, Phys. Rev. 109, 888 (1958).

[11] B. B. Kinsey, G. A. Bartholomew, Phys. Rev. 93, 1260 (1954).

[12] G. A. Bartholomew, P. I. Campion, I. W. Knowles, and G. Manning, Report at the Columbia Conference on the Interactions of Neutrons with Nuclei (New York, September, 1957).

[13] T. D. Newton, Can. J. Phys. 34, 804 (1956).

Received November 17, 1958

THE ASYMMETRY OF NUCLEAR FISSION

B. T. Geilikman

One of the essential characteristics of nuclear fission and of processes occuring in nuclear reactors is the distribution of fission fragments by mass. According to the drop model of the nucleus, a symmetrical mass distribution of the fragments is most probable, but this, however, is contrary to experiment.

To find the mass distribution of the fragments, in this work we calculated the energy of the fissionable nucleus before rupture of the neck, taking into account shell effects, for several nuclei. It was shown that the energy minimum corresponds to asymmetric fission.

1. Two very interesting explanations have recently been put forward for the asymmetry of nuclear fission. Nosov [1], and Businaro and Gallone [2] showed on the basis of the drop model that after passing through a saddle point but apparently before rupture of the neck, a nucleus becomes unstable as regards asymmetric deformations, determined by the parameter α_3, i.e., at a certain value of the symmetric deformation parameter $\alpha_2 = \alpha_{2k}$ the second derivative of the nuclear energy with respect to α_3

$$\frac{\partial^2 U(\alpha_2, \alpha_3, \ldots)}{\partial \alpha_3^2}\Big|_{\alpha_3=0} \text{ reduces to zero}$$

$$\left(\text{when } \alpha_2 < \alpha_{2k} \quad \frac{\partial^2 U}{\partial \alpha_3^2}\Big|_{\alpha_3=0} > 0;\right.$$

$$\left.\text{when } \alpha_2 > \alpha_{2k} \quad \frac{\partial^2 U}{\partial \alpha_3^2}\Big|_{\alpha_3=0} < 0\right).$$

As paper [1] shows, this instability is absolute: when $\alpha_2 > \alpha_{2k}$ at any value of $\alpha_3 \neq 0$, the energy $U(\alpha_2, \alpha_3 \ldots)$ decreases with an increase in $|\alpha_3|$.

However, such an absolute instability with respect to α_3 can hardly explain the asymmetry of fission observed experimentally. In the case of fission close to the threshold, the nucleus has a low energy (≤ 1 Mev) in passing through the saddle point and therefore at this point the oscillator, corresponding to the degree of freedom of α_3, is in the ground state. Due to the quasistationary state of the deformation process after passing through the saddle point [3, 4], the probability of excitation of oscillator α_3 is very low. Therefore, to find the distribution with respect to α_3 at the point of neck rupture, we should examine essentially the quantum and not the classical problem of the wave packet spread in the field $U(\alpha_2, \alpha_3)$ when $\alpha_2 \geq \alpha_{2k}$ with the basic condition

$$\psi(\alpha_2, \alpha_3)|_{\alpha_2 \approx \alpha_{2k}} = \varphi_0(\alpha_3),$$

where $\varphi_0(\alpha_3)$ is the φ-function of the oscillator in the ground state. Using the evaluations of α_{2k} in [1] and the evaluations of the rate of symmetric deformation on descending from the saddle point according to [5, 6], one can show that the distance between α_{2k} and the point of neck rupture α_{2p} is not sufficiently large for a very extensive spread of the packet to occur there. Thus, the distribution with respect to α_3 at the point of neck rupture is somewhat wider than $[\varphi_0(\alpha_3)]^2$ where $\alpha_2 = \alpha_{2k}$, but as before it has a maximum at $\alpha_3 = 0$, which corresponds to symmetrical fission.

Fong [7, 8] offered another explanation for the asymmetry of fission, assuming that the probability of fission is determined only by the statistical weight of the final state. As a basis he used the Heppert-Mayer idea that a greater energy is evolved in the formation of magic and close to magic fragments than in the formation of nonmagic fragments (in the case of symmetrical fission). As the statistical weight increases greatly with an increase in excitation energy of the fragments, then the probability of fission is greatest with asymmetrical fission that results in the formation of magic fragments.

However, one can hardly consider that in fission close to the threshold the probability of the process is determined completely by the statistical weight ρ_E[4]. As is known, according to the perturbation theory the probability of the process is $\omega = 2\pi |V_{ab}|^2 \rho_E / h$. If the energy is very great, then due to the exponential dependence of ρ_E on E, the factor which changes more slowly, the square of the matrix element $|V_{ab}|^2$, may be neglected, but generally speaking both factors have the same role close to the threshold. These concepts remain correct even when the perturbation theory is not used.

Newton [9] pointed out another defect in Fong's work [8]. In this it was assumed that the density of the states for all fragment pairs was determined by the same formula. At the same time, the density of states for magic fragments is less than that of nonmagic fragments at the same excitation energy. This effect, which promotes symmetrical fission, compensates for, or even exceeds, the effect of the energy advantage in the case of magic fragments. Finally it should be noted that in [8] the coulombic interaction energy of the fragments is also calculated very inaccurately. In particular, it is assumed that for fragments $\alpha_2^{frag} = 0$ and only $\alpha_3^{frag} \neq 0$. It will be shown below that at the point of neck rupture $\alpha_2^{frag} > \alpha_3^{frag}$

The distribution of fragment masses for U^{235} fission under the action of neutrons was calculated in paper [8]. The results agreed well with experimental data. However, in paper [10] on the basis of the statistical theory, a four-humped curve was obtained for fission of Pu^{239} by neutrons or, after introducing changes into Fong's formula, a two-humped one, which did not agree with experiment.

However, shell effects undoubtedly play an essential role in the fission process. Apparently it is for this reason that the one-drop model used in [1 and 2] could not explain the asymmetry of fission. In considering shell ef-

fects one should investigate fully the dynamics of the fission process and not limit oneself to statistical examinations.

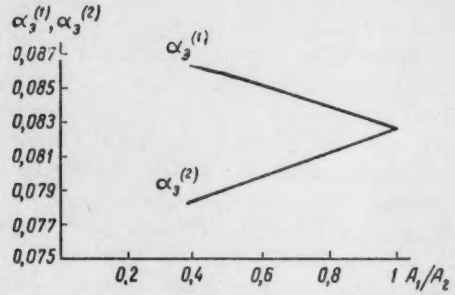

Fig. 1. The relation of the parameters $\alpha_3^{(1)}$ and $\alpha_3^{(2)}$ before rupture of the neck of the nucleus to A_1/A_2.

2. For a full solution to the problem one must know the energy of the nucleus $U(\alpha_2, \alpha_3, \ldots)$ up to neck rupture, taking into account shell effects, as a function of $\alpha_2\alpha_3\ldots$ The most interesting relation is that of U to α_3 in the region close to neck rupture. The energy U in this region may be evaluated in the following way. If the neck is sufficiently narrow, one may consider that a shell has formed in each half of the nucleus as after passing the saddle point, the deformation process is close to quasistatic [3, 4]. It will be shown below that the deformation of each half of the nucleus, i.e., future fragment, is not very great as compared with a sphere of equal volume ($\alpha_2^{\text{frag}} \approx 0.25$; $\alpha_3^{\text{frag}} \leq 0.1$; Fig. 1). Therefore, the energy of the initial nucleus on approaching the point of neck rupture may be represented as the sum of: 1) the energy of two spherical nuclei with the atomic weights of the future fragments according to Weizsäcker-Williams' formula and taking into account shell effects, 2) the deformation energy of these nuclei, and 3) coulombic interaction energy of the two deformed nuclei. The coulombic interaction of two touching deformed nuclei as a function of their deformation parameters $\alpha_2^{(1)}$, $\alpha_3^{(1)}$, $\alpha_2^{(2)}$, $\alpha_3^{(2)}$ with an accuracy of up to second-order terms in $\alpha_2^{(i)}$ and $\alpha_3^{(i)}$ was calculated in [3] (see appendix as [3] has two printing errors).

The Weizsäcker-Williams' formula with the shell effect taken into account was proposed in papers [8] and [11]. Neither of the formulas can be considered sufficiently accurate, but they are quite useful for obtaining qualitative results. We used Fong's formula [8]. Bohr and Wheeler [12] have already found the deformation energy of future fragments U_d as a second-order approximation within the framework of the drop model. Thus, the energy of the initial nucleus close to the point of neck rupture will have the form

$$U = M_1(A_1, Z_1) + M_2(A_2, Z_2) + U_{d1} + U_{d2} + U_{\text{inter}}. \qquad (1)$$

where

$$M(A, Z) = \left\{ 931 \left[1{,}01464A + 0{,}014A^{2/3} - 0{,}041905Z_A + \frac{0{,}0141905\,(Z - Z_A - \Delta Z_A)^2}{Z_A} + \Delta M_A \cdot 10^{-3} + \delta_A \right] + \mu \right\} \text{ Mev};$$

$$Z_A = A\,(1{,}98067 + 0{,}0149624A^{2/3})^{-1};$$

$$\delta_A = \frac{0{,}036}{A^{3/4}} \times \begin{cases} 1 & \text{even } A, \text{ odd } Z \\ 0 & \text{odd } A \\ -1 & \text{even A and Z;} \end{cases}$$

$\mu = -2.0$ for A - Z = 50 or 82; $\mu = -1.1$ for Z = 50, and $\mu = 0$ for the rest of the values of A and Z;

$$U_{di} = \frac{e^2}{r_0}\left\{ \frac{3}{25}\left(\varepsilon A_i^{2/3} - Z_i^2/A_i^{1/3}\right)[\alpha_2^{(i)}]^2 + \frac{3}{14}\left(\varepsilon A_i^{2/3} - \frac{4}{7}Z_i^2/A_i^{1/3}\right)[\alpha_3^{(i)}]^2 \right\};$$

$$\varepsilon = \left(\frac{Z^2}{A}\right)_{\text{cr}} = 48 - 50; \quad i = 1,\ 2.$$

$$U_{\text{inter}} = \frac{Z_1 Z_2}{a}\frac{e^2}{r_0}\left\{ 1 + \frac{3}{5a^2}\sum_{i=1}^{2}\alpha_2^{(i)}A_i^{2/3} + \frac{3}{7a^3}\sum_{i=1}^{2}\alpha_3^{(i)}A_i + \frac{3}{35a^2}\sum_{i=1}^{2}[\alpha_2^{(i)}]^2\left(4A_i^{2/3} + \frac{3A_i^{4/3}}{a^2}\right) + \frac{3}{7a^2}\sum_{i=1}^{2}[\alpha_3^{(i)}]^2\left(\frac{8}{15}A_i^{2/3} + \frac{3}{11}\frac{A_i^{4/3}}{a^2} + \frac{200}{429}\frac{A_i^2}{a^4}\right) + \sum_{i=1}^{2}\alpha_2^{(i)}\alpha_3^{(i)}\left(\frac{4}{7}\frac{A_i}{a^3} + \frac{5}{11}\frac{A_i^{5/3}}{a^5}\right) + \frac{18}{7a^5}\left(\alpha_2^{(1)}\alpha_3^{(2)}A_1^{2/3}A_2 + \alpha_2^{(2)}\alpha_3^{(1)}A_1A_2^{2/3}\right) + \frac{54}{25}\frac{\alpha_2^{(1)}\alpha_2^{(2)}(A_1A_2)^{2/3}}{a^4} + \frac{180}{49}\frac{\alpha_3^{(1)}\alpha_3^{(2)}A_1A_2}{a^6}\right\}; \qquad (2)$$

$R_i = A_i^{1/3}r_0$; $r_0 = (1{,}2 - 1{,}5)10^{-13}$ cm; $d = ar_0$ is the distance between the centers of gravity of the fragments. Formula (2) is derived in the appendix.

As experiments on coulombic excitation show [13], the elasticity coefficients in U_{di} found for the drop model are on the average somewhat higher than the actual ones.

In formula (2), besides resolution with respect to $\alpha_2^{(i)}$ and $\alpha_3^{(i)}$, resolution with respect to $A_i^{1/3}/a$ was also carried out. It will be shown below that $a \approx 2.5A^{1/3}$, and consequently $A_1^{1/3}/a \approx 1/(2.5 \cdot 2^{1/3})$. Therefore in (2) we confine ourselves to terms containing only a^{-6}.

The graphical dependence of ΔZ_A and ΔM_A on A, found from an analysis of experimental data, is given in [8].

In order to find $\alpha_2^{(1)}$, $\alpha_3^{(1)}$, $\alpha_2^{(2)}$, $\alpha_3^{(2)}$ for a given A_1/A_2, we will use the expressions for the forms of a deformed fissioning nucleus, obtained from the numerical calculations of Frankel and Metropolis [5]. In [5] the form of the nucleus was calculated for symmetrical deformation on

the basis of the drop model only. With very extensive deformations of a nucleus, corresponding to the saddle point and particularly to neck rupture, the shells of the initial nucleus disappear and therefore, in calculating the energy and forms of a nucleus, the drop model can be used. However, as was shown above, the existence of fragment shells is of considerable importance in neck rupture. Their effect may be considered in the following way: in symmetrical fission, the drop model gives correct results as when $A_1 = A_2$; shell effects are negligible (the fragments are far from being magic). For unsymmetrical fission, however, α_3 are very small ($\alpha_3 \leq 0.1$; see below); therefore the true form differs little from the one found in [5]. We should note that in general the expression for the form of the nucleus should not change very greatly with changes in the appearance of the energy of the nucleus, as it is determined to a considerable extent by purely geometrical factors. As was shown in [5 and 6], the form of a nucleus for any symmetrical deformation of the nucleus in the drop model would appear as

$$\frac{r(\vartheta)}{R} = C\left[1 + \sum_{l=0}^{4} \alpha_{2l} P_{2l}(\cos\vartheta)\right] \qquad (3)$$

where

$$\alpha_0 = -y^2[1{,}06 + 9{,}76\cdot 10^{-4}(0{,}49 - y)^{-4}];$$

$$\alpha_2 = y\,[2{,}3 + 5{,}42\cdot 10^{-4}(0{,}49 - y)^{-4}];$$

$\alpha_4 = y^2\{1{,}6 + y[3{,}0 + 2{,}84\cdot 10^{-3}(0{,}49 - y)^{-4}]\}$; $\alpha_6 = -2{,}36\cdot 10^{-5}(0{,}49 - y)^{-4}$; $\alpha_8 = -4{,}72 \times 10^{-5}(0{,}49 - y)^{-4}$; $P_n(\cos\vartheta)$ are Legendre polynomials; y is a parameter determining the deformation of the nucleus; C is a normalization constant; C is close to unity, for example, when $A_1 = A_2$ at a neck thickness, d_{neck}, equal to zero, $C \approx 0.92$.

We find that $y = y_k$ for which d_{neck} is equal to zero. It was found that $y_k \approx 0.358$.

Then let us assume that into the expression $r(\vartheta)/RC$ is added the item $\alpha_3[P_3(\cos\vartheta) + {}^3/_2\ P_1(\cos\vartheta)] \equiv {}^5/_2\ \alpha_3\cos^3\vartheta$, then as before $y = 0.358$. If α_3 is small, then the nuclear form thus obtained is close to the true one. For each value of α_3 we find C from the condition that $\int_{-1}^{1}[r(\mu)/R]^3\,d\mu = 2$ (condition that the volume is constant). For each value of α_3 we find the ratio of the volumes of the two parts of the nucleus, i.e., the ratio of the atomic weights of the future fragments A_1/A_2 (for example, when $\alpha_3 = 0.06$, $A_1/A_2 \approx 0.7$). Then for each value of A_1/A_2 we also find the distance from origin of the coordinates (i.e., the point at which the thickness of the neck equals zero) to the centers of gravity of the two fragments $d_1 = b_1 r_0 A^{1/3}$ and $d_2 = b_2 r_0 A^{1/3}$ ($A = A_1 + A_2$) and the resolution coefficients $\alpha_n^{(1)}$, $\alpha_n^{(2)}$ of the radius-vectors of the future fragments $r_1(\vartheta_1)$ and $r_2(\vartheta_2)$ with respect to the Legendre polynomials from n=0 to n=3, relative to the origin of the coordinates at the center of gravity of the fragment (Fig. 2). The functions $r_1(\vartheta_1)$ and $r_2(\vartheta_2)$ are normalized for the volumes of spheres with atomic weights A_1 and A_2. The values b_1, b_2 and $\alpha_3^{(1)}$, $\alpha_3^{(2)}$, thus calculated, are given in Figs. 1 and 3; $\alpha_2^{(1)} = \alpha_2^{(2)} \approx 0.26$ is quite accurate when $0.4 \leq A_1/A_2 \leq 1$. (These graphs are more accurate than those in [14] as here the terms with P_6 and P_8 in formula (3) are allowed for; due to this $\alpha_2^{(i)}$ is smaller.) In particular, for $A_1 = A_2$; $b_1 + b_2 \approx 2.58$; $\alpha_3^{(i)} \approx 0.08$. Z_1 and Z_2 for each pair of values of A_1 and A_2 are calculated by the formula $Z_1/Z_2 = A_1/A_2$ and then the values are corrected for coulombic repulsion, which makes Z_1 somewhat greater for smaller A_1. At the present time numerical calculations have been completed for the difference in energy $\Delta U(A_1/A_2) = U(A_1/A_2) - \langle U(1)\rangle$ for U^{236}, Pu^{240}, Cm^{242}, Cf^{252}, Cf^{244} with values of $r_0 = 1.22\cdot 10^{-13}$ cm and $\epsilon = 50.1$ [15]; $\langle U(1)\rangle$ is the value of $U(A_1/A_2)$ averaged over the range $0.95 \leq A_1/A_2 \leq 1$.

The results of the calculations are shown in Figs. 4 and 5. Figures 4 and 5 do not show some irregularities of the curves for ΔU, which may be due to the fine structural yield of fragments.

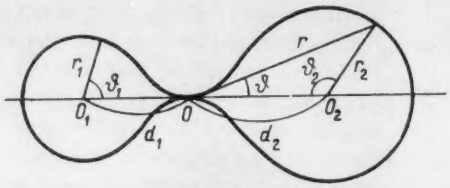

Fig. 2. Nucleus before neck rupture.

At values of A_2/A_1 exceeding 2, the calculations become extremely inaccurate, as here the form of the initial nucleus obtained from the symmetrical form (3) by the addition of the asymmetrical deformation may differ appreciably from the true one.

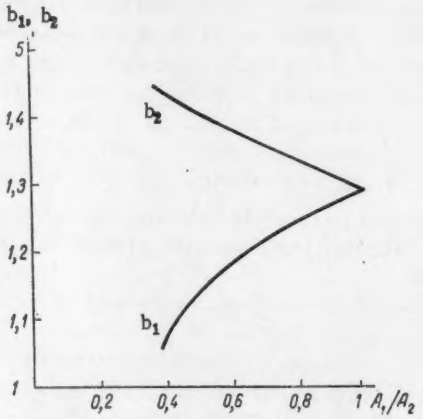

Fig. 3. The relation of b_1 and b_2 to A_1/A_2.

As can be seen from Fig. 4, the energy of the nucleus at the point of neck rupture has a minimum at A_1/A_2, which does not equal unity. With an increase in Z^2/A, the minimum is shifted towards $A_1/A_2 = 1$, while its depth decreases. According to Swiatecki's empirical formula, the difference in atomic weight of the fragments, corres-

ponding to the two maxima on the two-humped curve, equals [16]:

$$A_1 - A_2 = 0{,}09\left(40{,}2 \mp 0{,}7 - \frac{Z^2}{A}\right)^{1/2} A, \qquad (4)$$

i.e., $A_2 - A_1$ decreases with an increase in Z^2/A and at $Z^2/A \approx 40.2$ fission should become symmetrical. According to our calculations, even for Cf^{252} the minimum ΔU corresponds to $A_1 = A_2$, i.e., to symmetrical fission (for Cf^{252} $Z^2/A \approx 38.1$). A shallow minimum is also obtained for Cf^{244} at $A_1 \neq A_2$, but due to the inaccuracy of the calculations it is difficult to say to what extent this result is reliable.

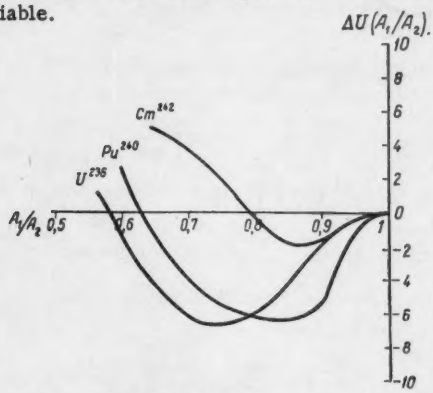

Fig. 4. The relation of the energy ΔU to A_1/A_2.

Our calculations are as yet very rough, and we cannot claim great accuracy. The deformation of future fragments is not very small ($\alpha_2^{(i)} \approx 0.25$) and representing the energy of each fragment as the sum of the energy of a spherical nucleus, allowing for shell effects, and the deformation energy in a second-order approximation with respect to $\alpha_2^{(i)}$ and $\alpha_3^{(i)}$ cannot be considered as accurate.

However, if the shells of deformed nuclei actually shift and apparently correspond to somewhat different A_1, A_2 and Z_1, Z_2, then for qualitative results on the essential role of shell effects such a rough calculation will suffice. An appreciable inaccuracy is also introduced by the fact that in calculating the deformation and coulombic interaction energies, we confined ourselves to second-order approximations. This inaccuracy may be eliminated if, as the first approximation, we take an ellipsoid rather than a sphere (as the symmetrical deformation determined by the parameter $\alpha_2^{(i)}$ has the greatest value; see [1] and [2]). The greatest error arises from the inaccuracy of Weizsackers formula with the shell effects considered, particularly due to the large errors in determining the parameter ΔZ_A. A more accurate Weizsäcker formula would make it possible to calculate more reliably the energy of the nucleus before neck rupture.

Thus we found the relation of the energy of the initial nucleus to the asymmetry of deformation directly before the rupture of the neck. The same type of calculation may be carried out for a fissioning nucleus with a neck diameter other than zero. Obviously, the method given above for calculating the energy of a nucleus is not suitably used with quite a large neck diameter. However, one can see from the expression for the energy at the point of neck rupture that instead of absolute instability in relation to asymmetrical deformation α_3, which one obtains

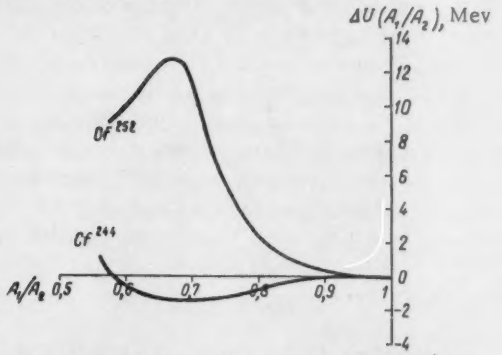

Fig. 5. The relation of the energy ΔU to A_1/A_2.

with a drop model [1, 2], in a model which takes into account shell effects, there is bifurcation of the central dip in the energy surface. Regrettably we cannot find the point of bifurcation of the dip. If the shell effects occur and with not too small a neck thickness, then the corresponding value of α_{2k}', may be small than α_{2k} in a drop model.

Due to the presence of dips during the spread of the packet for α_3 after $\alpha_2 = \alpha_{2k}'$ besides a fall in the maximum $\alpha_3 = 0$, new maxima for the function $\Psi(\alpha_3)$ will arise at values of $\alpha_3 = \pm\, \alpha_3^0(\alpha_2)$ that will correspond to the position of the dips. If the distance from α_{2k}' to α_{2p} is sufficiently great, then at the point of neck rupture, the α_{2p} maximum at $\alpha_3 = 0$ will be considerably less than the maximum at $\alpha_3 = \pm\, \alpha_3^0(\alpha_{2p})$ (or will be completely absent). Due to the existence of energy minima at $\alpha_3 = \pm\, \alpha_3^0(\alpha_2)$, this distance from α_{2k}' to α_{2p} may be considerably smaller than the distance $\alpha_{2p} - \alpha_{2k}'$ for the spread of the central maximum up to the same values in the case of no dips. Since the energy of the nucleus cannot as yet be calculated as a function of α_2 and α_3 at all values of α_2, we will examine only a limiting case, corresponding to a sufficiently large distance $\alpha_{2p} - \alpha_{2k}'$. In this case one can assume that the central maximum has no effect and then the mass distribution of the fragments will be determined by the square of the Ψ-function of the oscillator in a ground state close to $\alpha_3 = \alpha_3^0(\alpha_{2p})$ at the point of neck rupture $[\varphi_0(\alpha_3 - \alpha_3^0(\alpha_{2p}))]^2$, i.e., a Gaussian distribution. With a more accurate calculation of $U(\alpha_2, \alpha_3)$ one could find the parameters of this distribution.

One should note that attempts to explain the asymmetry of fission on the basis of an analysis of the state of the nucleus at the saddle point are incomplete, since actual mass division occurs at the point of neck rupture. Therefore, if at the saddle point, the energy of the nucleus favors a certain mass division, then it will actually occur only if the energy of the nucleus at the point of neck rupture also corresponds to the same mass division. Thus, the deciding role for mass division is played by the region close to the point of neck rupture.

3. The form of the energy $U(\alpha_2, \alpha_3)$ at $\alpha_2 \geq \alpha_{2k}'$ corresponds to fission close to the threshold. If fission occurs

with a high level of nuclear excitation, for which shell effects are very small, then, apparently, the energy of the nucleus U will be determined by the drop model [1, 2], i.e., fission will be symmetrical. This is apparently explained by the rapid growth of symmetrical fission with an increase in the nuclear excitation energy (more rapid than would be expected from simple statistical considerations, see [4]). In analyzing experimental data, one should differentiate between nuclei which have a neutron width G_n greater than the fission width G_f and nuclei which have $G_f > G_n$. For the former nuclei $x < x_0$ usually, while for the latter nuclei $x > x_0$, where x_0 is a certain critical value of the parameter $x \equiv \frac{Z^2A}{(Z^2/A)_{cr}}$. When $x = x_0$, $G_f \approx G_n$.

In the case of an excited nucleus with $x < x_0$, the emission of a certain number of neutrons mainly occurs with a low probability of fission. If the excitation energy is sufficiently great that after emission of all the neutrons, the parameter x becomes equal to x_0, then at the end fission of the cold nucleus would occur with high probability (emission fission). In this case, superposition of symmetrical fission would occur with low probability after the emission of each neutron by the excited nucleus, and after the asymmetric fission of the cold nucleus. Therefore an accurate calculation of mass distribution is hardly possible. Such superposition of symmetric and asymmetric fission may explain the mass distribution of the fragments in the fission of gold with nitrogen ions of 115 Mev energy [17]. If the excitation energy is small then fission of the cold nucleus with high probability is impossible and fission will be symmetric. Apparently this explains the symmetric character of the fission of bismuth with 22 Mev deuterons [18].

Central and side maxima may also be observed simultaneously in the fission of a weakly excited nucleus when the distance $\alpha_{2p} - \alpha'_{2k}$ is small. If $\alpha_{2p} - \alpha'_{2k}$ is so small that the central maximum has insufficient time to spread fully to the point of neck rupture (see above) then the fragment mass distribution curve may have three maxima. As the difference $\alpha_{2p} - \alpha'_{2k}$ increases with an increase in x (see [1, 5]), then the appearance of such a triple-humped curve could be expected at comparitively small values of x (if in this case fission is not of the emission type). It is possible that this explains the triple-humped curve in the case of fission of Ra^{226} with 11 Mev protons [19].

If for the initial nucleus, $x > x_0$, then fission from the excited state would occur at first with great probability and not neutron emission. Therefore, the contribution of symmetric fission should in this case be even greater than when $x < x_0$.

In conclusion I would like to thank I. G. Krutikova for carrying out the numerical calculations and S. T. Belyaev and A. B. Migdal for their interesting discussion.

APPENDIX

Let us find the electrostatic interaction of two deformed nuclei with atomic weights A_1 and A_2 and the atomic numbers Z_1 and Z_2, whose centers of gravity are at a distance of $d = ar_0$ from each other. The equation for the surface of the nuclei has the form

$$r_i(\vartheta_i) = R_i\left(1 + \sum_{n=0}^{3} \alpha_n^{(i)} P_n(\cos\vartheta_i)\right); \quad R_i = r_0 A_i^{1/3} \quad (i = 1, 2).$$

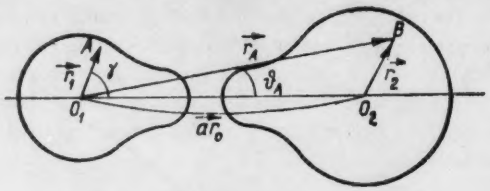

Fig. 6. Fission fragments.

In calculating the interaction energy, we will confine ourselves to second-order terms in $\alpha_n^{(i)}$. In this approximation for $\alpha_0^{(i)}$ and $\alpha_1^{(i)}$ from the conditions of the conservation of volume and the position of the center of gravity of the nuclei, we obtain the expression:

$$\alpha_0^{(i)} = -\sum_{n=2} [\alpha_n^{(i)}]^2/(2n+1);$$

$$\alpha_1^{(i)} = -9\sum_{n=2} \frac{n+1}{(2n+1)(2n+3)} \alpha_n^{(i)} \alpha_{n+1}^{(i)}.$$

The potential energy of the second nucleus in the field of the first equals

$$U_2 = \frac{1}{2}\int \rho_2(r_2)\,\Phi_1(r_A)\,dV_2; \quad \vec{r}_A = \vec{ar_0} + \vec{r}_2,$$

where Φ_1 is the potential of the first nucleus inside the volume of the second (Fig. 6). Let us resolve $\Phi_1(|\vec{ar_0} + \vec{r_2}|)$ into a series in powers of x_2, y_2, z_2.

$$U_2 = \frac{3}{2}\frac{Z_2 e}{4\pi R_2^3}\left\{\Phi_1(ar_0)\frac{4\pi R_2^3}{3} + \right.$$

$$+\frac{1}{2}\left(\frac{\partial^2\Phi_1}{\partial z_2^2}\right)_{r_2=0}\int_{V_2}(z_2^2 - x_2^2)\,dV_2 +$$

$$\left.+\frac{1}{6}\left(\frac{\partial^3\Phi_1}{\partial z_2^3}\right)_{r_2=0}\int_{V_2}(z_2^3 - 3z_2x_2^2)\,dV_2\right\} =$$

$$= \frac{Z_2 e}{2}\left\{\Phi_1(r_0 a) + \right.$$

$$+\frac{3}{10}\left(\frac{\partial^2\Phi_1}{\partial z_2^2}\right)_{r_2=0} R_2^2\left(\alpha_2^{(2)} + \frac{4}{7}[\alpha_2^{(2)}]^2 + \frac{8}{21}[\alpha_3^{(2)}]^2\right) +$$

$$\left.+\frac{1}{14}\left(\frac{\partial^3\Phi_1}{\partial z_2^3}\right)_{r_2=0} R_2^3\left(\alpha_3^{(2)} + \frac{4}{3}\alpha_2^{(2)}\alpha_3^{(2)}\right)\right\}. \quad \text{(Pt. 1)}$$

Let us now find the potential $\Phi_1(r_A)$:

$$\Phi_1 = \int_{V_1}\frac{\rho_1 dV_1}{r_A\sqrt{1 - 2\cos\gamma\, r_1/r_A + r_1^2/r_A^2}} =$$

$$= \frac{3}{2}\frac{Z_1 e}{R_1^3}\sum_{n=0}^{\alpha}\int_{V_1}\frac{r_1^{n+2}}{r_A^{n+1}}\,d\cos\vartheta_1\,dr_1 P_n(\cos\vartheta_1)P_n(\cos\vartheta_1) =$$

$$= \frac{Z_1 e}{r_A}\left\{1 + \frac{3}{5}\frac{R_1^2}{r_A^2}\left(\alpha_2^{(1)} + \frac{4}{7}[\alpha_2^{(1)}]^2 + \right.\right.$$

$$+\frac{8}{21}[\alpha_3^{(1)}]^2\Big)P_2(\cos\vartheta_A)+\frac{3}{7}\frac{R_1^3}{r_A^3}\Big(\alpha_3^{(1)}+$$

$$+\frac{4}{3}\alpha_2^{(1)}\alpha_3^{(1)}\Big)P_3(\cos\vartheta_A)+\frac{18}{35}\frac{R_1^4}{r_A^4}\Big([\alpha_2^{(1)}]^2+$$

$$+\frac{5}{11}[\alpha_3^{(1)}]^2\Big)P_4(\cos\vartheta_A)+\frac{10}{11}\frac{R_1^5}{r_A^5}\alpha_2^{(1)}\alpha_3^{(1)}P_5(\cos\vartheta_A)+$$

$$+\frac{1200}{3003}\frac{R_1^6}{r_A^6}[\alpha_3^{(1)}]^2P_6(\cos\vartheta_A)\Big\}. \qquad \text{(Pt.2)}$$

where $r_A=\sqrt{r_0^2a^2+r_2^2-2r_0az_2}$ and $\cos\vartheta_A=(ar_0-z_2)/r_A$.

From Pt. 2 we find $\frac{\partial^2\Phi_1}{\partial z_2^2}$ and $\frac{\partial^3\Phi_1}{\partial z_2^3}$. In this we can use a simple identity, which can be proved readily by the recurrent formulas for $P_n(\mu)$:

$$\frac{\partial}{\partial z_2}\left(\frac{P_n(\cos\vartheta_A)}{r_A^{n+1}}\right)=\frac{n+1}{r_A^{n+2}}P_n(\cos\vartheta_A).$$

We find

$$\frac{\partial^2\Phi_1}{\partial z_2^2}=\frac{3Z_1e}{r_A^3}\Big\{\frac{2}{3}P_2(\cos\vartheta_A)+$$

$$+\frac{12}{5}\frac{P_4(\cos\vartheta)R_1^2}{r_A^2}\Big(\alpha_2^{(1)}+\frac{4}{7}[\alpha_2^{(1)}]^2+\frac{8}{21}[\alpha_3^{(1)}]^2\Big)+$$

$$+\frac{20}{7}\frac{R_1^3}{r_A^3}P_5(\cos\vartheta_A)\Big(\alpha_3^{(1)}+\frac{4}{3}\alpha_2^{(1)}\alpha_3^{(1)}\Big)+$$

$$+\frac{36}{7}\frac{R_1^4}{r_A^4}P_6(\cos\vartheta_A)\Big([\alpha_2^{(1)}]^2+\frac{5}{11}[\alpha_3^{(1)}]^2\Big)+$$

$$+\frac{140}{11}\frac{R_1^5}{r_A^5}P_7(\cos\vartheta_A)\alpha_2^{(1)}\alpha_3^{(1)}+$$

$$+\frac{3200}{429}\frac{R_1^6}{r_A^6}P_8(\cos\vartheta_A)[\alpha_3^{(1)}]^2\Big\}. \qquad \text{(Pt. 3)}$$

We find $\frac{\partial^3\Phi}{\partial z_2^3}$ similarly.

Substituting (Pt. 2) and (Pt. 3) in (Pt. 1) we find U_2. We obtain U_1 from U_2 by transposing the indices 1 and 2. The full interaction energy of the two nuclei, $U_{inter.}=U_1+U_2$, is found to be equal to expression (2).

LITERATURE CITED

[1] V. G. Nosov, "Physical investigations," Reports of the Soviet Delegation to the International Conference on the Peaceful Uses of Atomic Energy, (Acad. Sci. USSR Press, Moscow, 1955) p. 303.

[2] U. Businaro and S. Gallone, Nuovo Cimento, 1, 629, 1277 (1955).

[3] B. T. Geilikman, "Physical investigations," Reports of the Soviet Delegation to the International Conference on the Peaceful Uses of Atomic Energy, (Acad. Sci. USSR Press, Moscow, 1955) p. 310.

[4] B. T. Geilikman, Appendix No. 1 to the journal "Atomic Energy," (Atom. Press, 1957) p. 5.

[5] S. Frankel and N. Metropolis, Phys. Rev. 72, 914 (1947).

[6] D. Hill and J. Wheeler, Phys. Rev. 89, 1102 (1953).

[7] P. Fong, Pnys. Rev. 89, 332 (1953).

[8] P. Fong, Phys. Rev. 102, 435 (1950).

[9] T. Newton, Symposium of Physics Fission (Chalk River, 1956) p. 307.

[10] J. Perring and J. Story, Phys. Rev. 98, 1525 (1955).

[11] K. Kumar and M. A. Preston, Can. J. Phys. 33, 298 (1955).

[12] N. Bohr and J. Wheeler, Phys. Rev. 56, 426 (1939).

[13] G. Temmer and N. Heydenburg, Phys. Rev. 104, 967 (1956).

[14] B. T. Geilikman, Report No. 2474 at the Second International Conference on the Peaceful Uses of Atomic Energy (Geneva, 1958).

[15] T. Maris, Phys. Rev. 101, 147 (1956).

[16] W. Swiatecki, Phys. Rev. 100, 936 (1955).

[17] N. I. Tarantin, G. N. Flerov, et al., J. Exp. and Theoret. Phys. 34, 316 (1958).

[18] A. W. Fairhall, Phys. Rev. 102, 1335 (1956).

[19] R. P. Jensen and A. W. Fairhall, Phys. Rev. 109, 942 (1958).

Received August 5, 1958

THE EXCITATION ENERGY OF FRAGMENTS IN NUCLEAR FISSION

B. T. Geilikman

The multiplication factor for chain reactions in a nuclear reactor depends essentially on the number of secondary neutrons emitted during fission, and this is determined completely by the excitation energy of the fragments. Therefore, calculation of the excitation energy of the fragments as a function of the atomic number Z and the atomic weight A of the fissioning nucleus is of considerable interest in atomic energy.

In the work it was shown that the excitation energy of the fragments may be found by solving a system of equations for the deformation parameters of the fragments and the distance between them. The basic excitation energies of the fragments were found for some nuclei. An investigation was made of the dependence of the excitation energy on Z and A of the fissioning nucleus.

1. As is known, in the case of fission close to the threshold, after passing through the saddle point, the deformation process of the fissioning nucleus is approximately quasistatic with respect to the internal degrees of freedom of the nucleus. Therefore the probability of excitation of these degrees of freedom to the point of neck rupture is small. The probability of excitation of the internal degrees of freedom of the fragments only becomes appreciable during the essentially nonquasistatic stage of neck rupture [1].

The most interesting aspect for comparison with experiment is the calculation of the dependence of the fragments' excitation energy on the ratio of the fragment masses, A_1/A_2, for the given nucleus and on Z and A of the fissioning nucleus for a given ratio of A_1/A_2. To calculate the excitation energy of the fragments it is necessary to know the total potential energy of the fragments as a function of the deformation parameters $\alpha_n^{(1)}$ and $\alpha_n^{(2)}$ and the distance d between the centers of gravity of the fragments.

Let us suppose that the equation for the surface of the fragments has the form

$$r_i(\vartheta_i) = R_i\left(1 + \sum_{n=0}^{3} \alpha_n^{(i)} P_n(\cos\vartheta_i)\right);$$

$$R_i = r_0 A_i^{1/3};\ r_0 \approx (1{,}2 \div 1{,}5)\,10^{-13}\ \text{cm}\ (i = 1, 2).$$

$\alpha_0^{(1)}$ and $\alpha_1^{(i)}$ are expressed in terms of $\alpha_2^{(i)}$ and $\alpha_3^{(i)}$ from the condition of the conservation of volumes and the position of the centers of gravity of the fragments. The coulombic interaction energy of the two fragments is determined by formula (2) in the previous article [2] with an accuracy up to second-order terms in $\alpha_n^{(1)}$ and $\alpha_n^{(2)}$. Thee deformation energy of each fragment U_d with the same second-order approximation was found by Bohr and Wheeler [3] and is also presented in article [2].

2. As is known, the excitation energy of each fragment is considerably greater than the quanta of surface vibrations $\hbar\omega$. Therefore to calculate the excitation of the fragments, it is possible to use not the quantum, but the classical equations of motion for the variables $\alpha_2^{(1)}$, $\alpha_3^{(1)}$, $\alpha_2^{(2)}$, $\alpha_3^{(2)}$, a(a = d/r_0; d is the distance between the centers of gravity of the fragments):

$$\mu\ddot{a} = -\frac{\partial V}{\partial a};$$

$$\left.\begin{aligned}
\frac{3}{10}M_1A_1^{2/3}\ddot{\alpha}_2^{(1)} &= -\frac{\partial V}{\partial\alpha_2^{(1)}} - p_{22}^{(1)}\dot{\alpha}_2^{(1)} - p_{23}^{(1)}\dot{\alpha}_3^{(1)};\\
\frac{3}{10}M_2A_2^{2/3}\ddot{\alpha}_2^{(2)} &= -\frac{\partial V}{\partial\alpha_2^{(2)}} - p_{22}^{(2)}\dot{\alpha}_2^{(2)} - p_{23}^{(2)}\dot{\alpha}_3^{(2)};\\
\frac{1}{7}M_1A_1^{2/3}\ddot{\alpha}_3^{(1)} &= -\frac{\partial V}{\partial\alpha_3^{(1)}} - p_{33}^{(1)}\dot{\alpha}_3^{(1)} - p_{32}^{(1)}\dot{\alpha}_2^{(1)};\\
\frac{1}{7}M_2A_2^{2/3}\ddot{\alpha}_3^{(2)} &= -\frac{\partial V}{\partial\alpha_3^{(2)}} - p_{33}^{(2)}\dot{\alpha}_3^{(2)} - p_{32}^{(2)}\dot{\alpha}_2^{(2)},
\end{aligned}\right\} \quad (1)$$

where $V = (U_{ex} + U_{d1} + U_{d2})/\frac{e^2}{r_0}$; $\ddot{\alpha}_n^{(i)} \equiv \frac{d^2\alpha_n^{(i)}}{d\tau^2}$; $\tau = t\Big/\left(\frac{mr_0^3}{e^2}\right)^{1/2}$; m is an atomic mass unit; $\mu = \frac{M_1M_2}{M_1+M_2}$; M_i is the mass of the i-th nucleus in atomic mass units; $p_{kl}^{(i)}$ is the coefficient of friction. The mass coefficients $\mu_2 = \frac{3}{10}M$ and $\mu_3 = \frac{1}{7}M$ ($\mu_n = \frac{3M}{n(2n+1)}$ were found in paper [4].

Equations (1) may be solved by successive approximations. An evaluation showed that the term Z_1Z_2/a^2 in the right-hand side of the equation for a (see formula (2) in [2]) is a factor of approximately 10 greater than the rest of the items (even at t = 0). If these items are rejected, the equation for a is readily solved (Kepler's problem). Substituting the relation of a to τ found in the rest of the equations, we can find $\alpha_2^{(1)}$ and $\alpha_3^{(1)}$ as functions of τ. After this it is easy to find $\alpha(\tau)$ in a second-order approximation.

Frictional forces are included in Eqs. (1) for the degrees of freedom $\alpha_2^{(i)}$, $\alpha_3^{(i)}$. The existence of such frictional forces is related to the possibility of transfer of the surface oscillation energy to nucleon degrees of freedom. If $\tau_{nucl} \ll \tau_{osc}$ ($\tau_{nucl} = \hbar/\Delta E_{nucl}$; $\tau_{osc} = \hbar/\Delta E_{osc}$; ΔE_{nucl} is the distance between nucleon levels; $\Delta E_{osc} = \hbar\omega$) then the oscillations will be slow in relation to the movement of the nucleons and the probability of excitation of the nucleon degrees of freedom will be small. In this case the frictional force may be considered equal to zero. If, however,

$\tau_{nucl} \gg \tau_{osc}$ then the frictional force, f_{fr} will be other than zero. In fission close to the threshold, immediately after neck rupture $\Delta E_{nucl} > \hbar\omega$, i.e., $\tau_{nucl} < \tau_{osc}$ and $f_{fr} \approx 0$. As transfer of energy to nucleon degrees of freedom will occur anyway, though slowly, then with an increase in the excitation energy of the fragments it may be that $\tau_{nucl} > \tau_{osc}$. In this case the frictional force cannot be considered equal to zero. We see that with an increase in the excitation energy of fragments, the frictional force also increases. In the fission of a strongly excited nucleus, at the very beginning $\Delta E_{nucl} \ll \hbar\omega$ and the frictional force is other than zero. Let us examine the system of equations (1) in two limiting cases:

1) $f_{fr} = 0$, i.e. $p_{kl}^{(i)} = 0$ and 2) $p_{22}^{(i)} = p_{32}^{(i)} = 0$;

$$\frac{5p_{22}^{(i)}}{3M_iA_i^{2/3}} \gg \omega_2^{(i)}; \quad \frac{7}{2}\frac{p_{33}^{(i)}}{M_iA_i^{2/3}} \gg \omega_3^{(i)},$$

where ω_2 is the frequency of quadrupole oscillations; ω_3 is the frequency of octupole oscillations.

In the first case the additional excitation energy of the fragments (besides the thermal energy, which the fragments had at the moment of neck rupture) will be equal to the oscillation energy at $a \to \infty$ (in units of e^2/r_0):

$$\left.\begin{aligned} E_\infty^{(i)} &= \frac{3}{20}M_iA_i^{2/3}[\dot{\alpha}_2^{(i)}]^2 + \frac{1}{14}M_iA_i^{2/3}[\dot{\alpha}_3^{(i)}]^2 + \\ &+ \frac{3}{25}(sA_i^{2/3} - Z_i^2/A_i^{1/3})[\alpha_2^{(i)}]^2 + \\ &+ \frac{3}{14}(sA_i^{2/3} - \frac{4}{7}Z_i^2/A_i^{1/3})[\alpha_3^{(i)}]^2; \\ E_\infty &= E_\infty^{(1)} + E_\infty^{(2)}. \end{aligned}\right\} \quad (2)$$

After sufficient time this oscillation energy will be converted into kinetic energy of the nucleons.

In the second case the additional excitation energy of fragments is equal to the full operation of the frictional forces:

$$\left.\begin{aligned} W^{(i)} &= p_{22}^{(i)}\int_0^\infty [\dot{\alpha}_2^{(i)}]^2\,d\tau + p_{33}^{(i)}\int_0^\infty [\dot{\alpha}_3^{(i)}]^2\,d\tau; \\ W &= W^{(1)} + W^{(2)}. \end{aligned}\right\} \quad (3)$$

It can readily be seen that the value of the excitation energy will differ little between the two limiting cases. Actually in the first approximation the equations for a coincide at $f_{fr} = 0$ and $f_{fr} \neq 0$. There is a difference only in the second approximation. Numerical calculation shows that in the first case the excitation energy of the fragments is only 15 - 20% greater than in the second case. Fission close to the threshold is apparently closer to the first case as excitation of oscillations occurs during several oscillation periods when the frictional force is still small. Fission of an excited nucleus corresponds to the second case.

3. Let us find the starting conditions for the system of equations (1). Apparently the values of $\alpha_2^{(1)}$, $\alpha_3^{(1)}$ $\alpha_2^{(2)}$, $\alpha_3^{(2)}$, $a = (b_1 + b_2)A^{1/3}$, obtained for a neck thickness equal to or close to zero, should be taken as the basic conditions for the system of equations (1) (the method of finding these values is described in paper [2]). We thus obtain only the initial values of the coordinates of $\alpha_2^{(i)}$, $\alpha_3^{(i)}$, a. It may readily be seen that $\alpha_{20}^{(i)}$, $\alpha_{30}^{(i)}$, $\frac{a_0}{A^{1/3}}$ do not depend on A and Z of the fissile nucleus, but depend only on the ratio A_1/A_2.

The initial values of the rates $\dot{\alpha}_2^{(i)}$, $\dot{\alpha}_3^{(i)}$, a are essentially different for 1) fission by neutrons close to the threshold, 2) spontaneous fission, and 3) fission of an excited nucleus. In the first and second cases, during deformation before neck rupture, the nucleus is cold and $\tau_{nucl} \ll \tau_{def}$ (τ_{def} is the time of moving from the saddle point to the point of neck rupture [1]). Therefore the frictional force for the degree of freedom α_2 may be considered equal to zero. Here the potential energy of the fissile nucleus, equal in the first case to the difference between the potential energy at the saddle point and that at the point of neck rupture, and in the second case to the difference between the energy of the nondeformed nucleus and that at the point of neck rupture, is completely converted into kinetic energy of the degrees of freedom α_n at the moment of neck rupture.

Let us find the initial values of the rates in the case of spontaneous and threshold fission. As was shown in paper [2], in descending from the saddle point, the movement of the nucleus for the degree of freedom α_3 is an oscillation near the equilibrium point. The equilibrium position before bifurcation of the dip on the energy surface corresponds to $\alpha_3 = 0$ and after bifurcation of the dip, to certain values of $\pm\alpha_3^0(\alpha_2)$, other than zero, which increase with an increase in α_2. The oscillator for α_3 is in the ground state [2]. Therefore its energy is very small in comparison with T_2.

The rate of α_3, which is connected with the change in the equilibrium position α_3^0, may be evaluated in the following way:

$$\dot{\alpha}_{3p}/\dot{\alpha}_{2p} \approx (1-2)\cdot\frac{\alpha_{3p}}{\alpha_{2p}-\alpha_{2s}} \approx 0{,}07-0{,}12$$

($\alpha_{np} \equiv \alpha_n$ at the point of neck rupture, $\alpha_{ns} \equiv \alpha_n$ at the saddle point; α_{2p} and α_{2s} were calculated for $x = \frac{Z^2/A}{(Z^2/A)_{cr}} \approx 0.7 - 0.8$). Thus $\alpha_3 \approx 0$.

As the deformation of the nucleus after the saddle point occurs slowly, one may consider that the nucleus passes through the values α_2, α_4, α_6, α_8, corresponding to the potential energy minimum, i.e., determined by expression (3) in paper [2]. We then find from it

$\dot{\alpha}_n = \dot{y}\,d\alpha_n/dy$; therefore $\dot{\alpha}_n = \dot{\alpha}_2\frac{d\alpha_n/dy}{d\alpha_2/dy}$

for n = 4, 6, and 8.

In order to express the rates $\dot{\alpha}_2^{(i)}$, $\alpha_3^{(i)}$, a after neck rupture in terms of the rates $\dot{\alpha}_2$, $\dot{\alpha}_4$, . . . before neck rupture, we will use the fact that the time of neck rupture, τ_{rupt}, is very small in comparison with τ_{def} and τ_{osc}. Then

the change in rate $\Delta\vec{v}_k$ of any element of nuclear mass Δm_k during the time τ_{rupt} will equal:

$$\Delta\vec{v}_k = \frac{1}{\Delta m_k}\int_0^{\tau_{rupt}} \vec{f}_k\,dt \simeq \vec{f}_k\tau_{rupt}/\Delta m_k;$$

is $\tau_{rupt} \ll \tau_{def}$ [$\tau_{def} \approx (f_k/\Delta m_k v_k)$], then $\Delta v_k/v_k \ll 1$, i.e., the rates before and after rupture are equal. This corresponds to the so-called shaking method. Consequently

$$\operatorname{grad}\varphi[x, y, z(z_i)] = \vec{v}_c^{(i)} + \operatorname{grad}\varphi_i(x, y, z_i); \quad i = 1, 2. \tag{4}$$

Here $\varphi[x, y, z(z_i)]$ is the potential of nuclear rates before neck rupture, transposed to the origin of the coordinates of the i-th fragment (i.e., z is taken to be equal to $\pm(z_i - d_c^{(i)})$, where $d_c^{(1)} = (d_1 + d_2)A_2/A$ and $d_c^{(2)} = (d_1 + d_2)A_1/A$ are the distances from the center of gravity of the nucleus to the centers of gravity of the fragments) $\varphi_1 - (x, y, z_i)$ is the potential of the rates of the i-th fragment after neck rupture. $\vec{v}_c^{(i)}$ is the rate of the center of gravity of the i-th fragment after neck rupture,*

$$\varphi = \sum_{n=2} \frac{d\alpha_n}{dt}\frac{P_n(\cos\vartheta)}{nR^{n-2}}r^n;$$

$$\varphi_i = \sum_{n=2}^{4} \frac{d\alpha_n^{(i)}}{dt}\frac{P_n(\cos\vartheta_i)}{nR_i^{n-2}}r_i^n.$$

Converting to Cartesian coordinates in expressions φ, φ_1, and φ_2 and substituting φ, φ_1 and φ_2 in (4) we find (in dimensionless units):

$$\dot\alpha_2^{(i)} = \dot\alpha_2 \pm 2\dot\alpha_3 b_{ci} + 3\dot\alpha_4 b_{ci}^2 \pm \ldots$$
$$\ldots + (n-1)\dot\alpha_n(\pm 1)^n b_{ci}^{n-2} + \ldots;$$

$$\dot\alpha_3^{(i)} = -\left(\frac{A_i}{A}\right)^{1/3}\left(\pm\dot\alpha_3 + 3b_{ci}\dot\alpha_4 \pm \ldots\right.$$
$$\left.\ldots + \frac{(n-1)(n-2)}{2!}\dot\alpha_n(\pm 1)^n b_{ci}^{n-3} + \ldots\right);$$

$$\dot\alpha_4^{(i)} = \left(\frac{A_i}{A}\right)^{2/3}\left(\dot\alpha_4 \pm \ldots\right.$$
$$\left.\ldots + \frac{(n-1)(n-2)(n-3)}{3!}\dot\alpha_n(\pm 1)^n b_{ci}^{n-4} + \ldots\right);$$

$$v_c = v_c^{(1)} + v_c^{(2)};\quad v_c^{(i)} =$$
$$= (\dot\alpha_2 b_{ci} \pm \dot\alpha_3 b_{ci}^2 + \dot\alpha_4 b_{ci}^3 \pm \ldots$$
$$\ldots + (\pm 1)^n\dot\alpha_n b_{ci}^{n-1} + \ldots)A^{1/3} \tag{5}$$

(the minus corresponds to i = 1 and the plus to -i = 2);

$$b_{c1} = (b_1 + b_2)A_2/A = \frac{d_c^{(1)}}{R};$$

$$b_{c2} = (b_1 + b_2)A_1/A = \frac{d_c^{(2)}}{R}$$

The kinetic energy of the degrees of freedom $\alpha_n^{(i)}$ of fragments $T^{(i)}$ has the form: $T^{(i)} = \sum_{n,m} T_{nm}^{(i)}$. As $T_{nn} \gg T_{nm}$ $(n \neq m)$, then $T^{(i)} \approx \Sigma T_n^{(i)}$; $(T_n^{(i)} \equiv T_{nn}^{(i)})$.

In e^2/r_0 units

$$T_n^{(i)} = \frac{3A_i^{5/3}}{2n(2n+1)}[\dot\alpha_n^{(i)}]^2 I_n^{(i)};$$

$$I_n^{(i)} = \frac{n}{2}\int_{-1}^{1}\left[\frac{1}{n^2}\left(\frac{dP_n}{d\mu}(\mu)\right)^2(1-\mu^2) + P_n^2(\mu)\right][r_i(\mu)/R_i]^{2n+1}\,d\mu.$$

Let us evaluate $T_4^{(i)}/T_2^{(i)}$ when $A_1 \approx A_2$, neglecting at first terms in $\dot\alpha_6$ and $\dot\alpha_8$ in Eqs. (5). We find:

$$T_4^{(i)}/T_2^{(i)} \approx (2-5)\cdot 10^{-2}.$$

However, if terms $\dot\alpha_6$ and $\dot\alpha_8$ remain in (5) then $T_4^{(i)}$ may be discounted by increasing $T_2^{(i)}$ by a value equal to $T_4^{(i)}$, i.e., by increasing $\dot\alpha_2^{(i)}$ appropriately. The values $T_n^{(i)}$ with n > 4 may be neglected in this case as well.

As is shown above, $\dot\alpha_3 \ll \dot\alpha_2$ and therefore the value $\dot\alpha_3$ may be neglected. However, in contrast to paper [8] we will not neglect the values $\dot\alpha_4$, $\dot\alpha_6$, $\dot\alpha_8$. Then from (5) we find the basic conditions for the rates:

$$\left.\begin{aligned}
&\dot\alpha_2^{(i)}|_{t=0} = \dot\alpha_2 S_2^{(i)};\\
&S_2^{(i)} = \left[(1 + 3\beta_4 b_{ci}^2 + 5\beta_6 b_{ci}^4 + 7\beta_8 b_{ci}^6)^2 + \right.\\
&\left. + \frac{5}{2^{1/3}\cdot 36}\frac{I_4^{(i)}}{I_2^{(i)}}(\beta_4 + 10\beta_6 b_{ci}^2 + 35\beta_8 b_{ci}^4)^2\right]^{1/2};\\
&\dot\alpha_3^{(i)}|_{t=0} = -\dot\alpha_2 S_3^{(i)};\\
&S_3^{(i)} = (3\beta_4 + 10\beta_6 b_{ci}^2 + 21\beta_8 b_{ci}^4)\,b_{ci}\left(\frac{A_i}{A}\right)^{1/3};\\
&\dot a|_{t=0} = \dot\alpha_2 S;\quad S = [(b_{c1} + b_{c2}) + \beta_4(b_{c1}^3 + b_{c2}^3) + \beta_6(b_{c1}^5 + b_{c2}^5) + \beta_8(b_{c1}^7 + b_{c2}^7)]\,A^{1/3}.
\end{aligned}\right\} \tag{6}$$

Here $\beta_n = \left(\frac{\frac{d\alpha_n}{dy}}{\frac{d\alpha_2}{dy}}\right)_{y=y_k}$; $\beta_8 = 2\beta_6$; $\frac{d\alpha_n}{dy}$ is found from formula (3) in paper [2].

As is known, the law of conservation of energy is not completely obeyed in the method of shaking. If one considers the law of conservation of energy, then $\dot\alpha_2$ in (6) should be replaced by some effective value $(\dot\alpha_2)_{eff}$. In spontaneous and threshold fission we find $(\dot\alpha_2)_{eff}$ by comparing $T_{c_1} + \sum_{i=1}^{2}(T_2^{(i)} + T_3^{(i)})$ directly with the potential energy of the fissioning nucleus.

* The formation of vortexes may be neglected due to the low values of the flow rates of $\dot\alpha_n$.

Within the framework of the drop model, the potential energy of the deformed nucleus was found for $A_1 = A_2$ in papers [5] and [6]:

$$U = \frac{3}{10} A^{2/3} \varepsilon \xi(x, y) \frac{e^2}{r_0};$$

$$\xi(x, y) = 2{,}178(1-x)y^2 - 4{,}09(1-0{,}645x)y^3 + 18{,}64(1-0{,}894x)y^4 - 13{,}33y^5.$$

The fission barrier corresponds to y = 1 - x. However, in this the shell effect is not considered and therefore the lowest energy at the point of neck rupture corresponded to symmetric fission. The shells of the initial nucleus have no effect [2] while a consideration of the shell effect of the fragments results in a decrease in the energy of the nucleus in asymmetric fission as compared with symmetric fission. The difference in energy at the point of neck rupture for $A_1 \neq A_2$ and $A_1 = A_2$

$$\Delta U\left(\frac{A_1}{A_2}\right) = U\left(\frac{A_1}{A_2}\right) - U\,(1)$$

was found as a function of A_1/A_2 in paper [2].

From the equality $T_c + \Sigma^2(T_2^{(i)} + T_3^{(i)})$ and the potential energy of the fissioning nucleus we find $(\dot{\alpha}_2)_{eff}$:

$$(\dot{\alpha}_2)_{eff} = \left(\frac{3}{10} A^{2/3} \varepsilon \xi_{1,2} - \frac{\Delta U\left(\frac{A_1}{A_2}\right)}{\frac{e^2}{r_0}}\right)^{1/2} \left[\frac{\mu S^2}{2} + \frac{3}{20} \sum_{i=1}^{2} I_2^{(i)} (S_2^{(i)})^2 A_i^{5/3} + \frac{1}{14} \sum_{i=1}^{2} I_3^{(i)} (S_3^{(i)})^2 A_i^{5/3}\right]^{-1/2}. \qquad (7)$$

Thus, the basic conditions for the rates have the form of Eq. (6) with $\dot{\alpha}_2 = (\dot{\alpha}_2)_{eff}$, determined according to E_q. (7)

In fission close to the threshold

$$\xi_1 = \xi(x; 1-x) - \xi(x; y_k) = 0{,}728(1-x)^3 - 0{,}661(1-x)^4 + 3{,}33(1-x)^5 - \xi(x; y_k),$$

while in the case of spontaneous fission [we neglect $\frac{\hbar\omega}{2}$ as $\frac{\hbar\omega}{2} \ll U(x; y_k)$]

$$\xi_2 = -\xi(x; y_n)\ (\xi_2 > 0);\ y_n \approx 0{,}358.$$

In contrast to the initial values of the coordinates $\alpha_2^{(i)}$, $\alpha_3^{(i)}$, $\underline{a}$, the initial values of the rates $\dot{\alpha}_2^{(i)}$, $\dot{\alpha}_3^{(i)}$, $\underline{\dot{a}}$ depend not only on A_1/A_2 but also on Z^2/A.

The problem can also be solved with ξ_1 and ξ_2 found from experimental data for fission thresholds and not from theoretical calculations.

4. Let us now examine the fission of a strongly excited nucleus. In this case $\tau_{nucl} \gg \tau_{def}$ and the frictional force in descending from the saddle point is other than zero. Therefore we can consider that the potential energy in descending from the saddle point is converted wholly into nucleon heat energy. Apparently with this, the initial values of $\dot{\alpha}_2^{(i)}$, $\dot{\alpha}_3^{(i)}$, $\underline{\dot{a}}$ should be considered equal to zero. The full excitation energy of each fragment will now consist of the sum $W^{(i)}$ (3) and the corresponding part of the thermal energy of the initial nucleus E_T. E_T is equal to the excitation energy at the saddle point and the difference between the potential energy at the saddle point and at the point of neck rupture, i.e., the excitation energy of a nondeformed nucleus and the difference in the potential energy of a nondeformed nucleus and the energy at the point of neck rupture. We can also consider that in the case of an excited nucleus, there is sufficient time for a thermal equilibrium to be set up at each point during the time of deformation. Therefore the temperature is approximately constant inside the fissioning nucleus. Thus, the heat energy will be divided among the fragments in proportion to their atomic weight

$$E_T^{(1)} = \frac{A_1}{A} E_T; \quad E_T^{(2)} = \frac{A_2}{A} E_T.$$

The mechanical part of the excitation energy, equal to the operation of the frictional force $W^{(i)} = \frac{e^2}{r_0} \int_0^\infty (p_{22}^{(i)} [\dot{\alpha}_2^{(i)}]^2 + p_{33}^{(i)} [\dot{\alpha}_3^{(i)}]^2)\, d\tau$, may be divided in a completely different way and does not have to be proportional to A_1 and A_2 (see below).

In the intermediate case of a weakly excited nucleus, a sequential solution of the problem is impossible and we can only interpolate.

In the equations for fragment motion after neck rupture we ignored the possibility of a rotational motion of the fragments, in particular, the possibility of the two fragments rotating in opposite directions about an axis perpendicular to the line connecting their centers (axis of symmetry). In this case, the potential energy $U(\alpha_2^{(i)}, \alpha_3^{(i)}, \underline{a})$ should also depend on the Euler angles of the two fragments. (The rotation of the fragments around their common axis of symmetry and also the rotation of the two fragments as a whole, apparently, does not change the results obtained previously.) One can readily see, however, that in calculating the excitation energy such rotational motion can be neglected.

Actually, the period of rotation $\tau_{rev} \approx \frac{\hbar}{\Delta E_{rev}} = \frac{I}{\hbar}$ due to the large value of deformation and, consequently, the large value of the moment of inertia of fragment $\underline{I}$, is considerably greater than the period of oscillation τ_{osc}:

$$\Delta E_{rev} \approx 20 - 50\,\text{kev},\ \Delta E_{osc} \approx (1-2)\,\text{Mev}$$

$$\frac{\tau_{rev}}{\tau_{osc}} \approx (3-8) \cdot 10.$$

Therefore the rotation of the fragment during a time equal to several oscillation periods, during which practically complete excitation of the fragments occurs, may be neglected.

5. Thus, to calculate the excitation energy of the fragments, the system of equations (1) should be solved for the following cases:

1. for different values of Z and A with a definite ratio of A_1/A_2, for example, for values of A_1/A_2 corresponding to the maxima of the double humped curve, or for $A_1 = A_2$. The latter case is less interesting, but the system of equations (1) at $A_1/A_2 = 1$ is considerably simplified as $\alpha_2^{(1)} = \alpha_2^{(2)}$, $\alpha_3^{(1)} = \alpha_3^{(2)}$ and instead of five equations we obtain three. The relation of the excitation energy to Z^2/A we thus obtained may be compared with experimental data on the number and energy of secondary neutrons (see [9]).

2. for definite values of Z and A, but for different values of the ratio A_1/A_2. The results of such a calculation may be compared with experimental data on the number of secondary neutrons as a function of A_1/A_2 [10].

These two problems should be solved for the following variants:

a) spontaneous fission (no frictional force and the initial conditions contain ξ_2);

b) fission close to the threshold (frictional force equal to zero and the initial conditions contain ξ_1);

c) fission of an excited nucleus (frictional force other than zero and the initial rate values equal zero).

At the present time only the value E_∞ has been found (in a second-order approximation with respect to $\alpha_2^{(i)}$ and $\alpha_3^{(i)}$ for $T^{(i)}$ and V) for four nuclei in the case of threshold and spontaneous fission ($f_{fr} = 0$) when $A_1 = A_2$. It is difficult to establish accurately at what neck thickness d_{neck} the rupture occurs. As an evaluation shows, if d_{neck} is appreciably greater than 0.1R, for T_c when $a \to \infty$ we obtain a value which considerably exceeds the experimental values. Therefore, the calculations were carried out with the assumption that neck rupture occurring at d_{neck} equals zero and 0.1R. Similar results are obtained in the two cases. Therefore only the data for $d_{neck} = 0$ are given below. For a comparison we calculated as an approximate evaluation of the excitation energy of the fragments the sum of the deformation energy and the kinetic energy of the two fragments at the point of neck rupture:

$$E_0 = U_\partial^{(1)} + U_\partial^{(2)} + T^{(1)} + T^{(2)} = E^{(1)} + E^{(2)}$$

(also in the case of spontaneous and threshold fission at $A_1 = A_2$). Thus, as seen from (6), the ratio of the kinetic energy of the centers of gravity of the fragments $T_c = \mu a^2/2$ to $T^{(1)} + T^{(2)}$ equals

$$\frac{T_c}{(T^{(1)}+T^{(2)})} = \frac{2^{-1/3}A^{-2/3}S^2}{\left[\frac{3}{10} I_2^{(1)} (S_2^{(1)})^2 + \frac{1}{7} I_3^{(1)} (S_3^{(1)})^2\right]}.$$

According to numerical calculations $b_1 + b_2 \approx 2.58$; $I_2^{(1)} \approx 1.4$; $I_3^{(1)} \approx 1.9$; $I_4^{(1)} \approx 2.6$. Then $\frac{T_c}{(T^{(1)}+T^{(2)})} \approx 10^{-2}$, i.e., $T^{(1)} + T^{(2)}$ is approximately 100% of the potential energy $U(y_0) - U(y_k)(y_0$ is equal to zero or 1 - x). If, however, the terms with $\dot{\alpha}_6, \dot{\alpha}_8 (\beta_6 = \beta_8 = 0)$ are not considered in (6), then $T^{(1)} + T^{(2)}$ is approximately 45% of the total energy $U(y_0) - U(y_k)$. As the terms with α_6 and α_8 are determined inaccurately as yet [7] we will examine both variants in more detail.

The table gives the values of E_∞ and E_0, calculated with new values of r_0 and ϵ [11]: $r_0 = 1.22 \cdot 10^{-13}$ cm and $\epsilon = 50.1$. Here we calculate E_0 and E_∞ directly in units of e^2/r_0; when $r_0 = 1.22 \cdot 10^{-13}$ cm, e^2/r_0 1.18 Mev. It is possible that the value of $\epsilon = 50.1$ is somewhat high; if the previous value of $\epsilon = 48$ is taken, then $T^{(1)} + T^{(2)}$ increases more rapidly with an increase in Z^2/A (see below).

The table shows that the excitation energy of the fragments consists of three parts: 1) potential deformation energy U_d when t = 0; 2) kinetic energy $T^{(1)} + T^{(2)}$ when t = 0; and 3) additional excitation energy after neck rupture $E_\infty - E_0$. $E_\infty - E_0$ hardly changes with a change in Z and A and is equal to ~2.5 - 4 Mev for threshold fission at $\beta_6 \neq 0$; for spontaneous fission $E_\infty - E_0 \approx 5$ Mev. $U_d = U_d^{(1)} + U_d^{(2)}$ also changes little with an increase in Z^2/A. Thus the growth of E_0 and E_∞ is completely bound to the increase in $T^{(1)} + T^{(2)}$, i.e., $(Uy_0) - U(y_k)$. The rapid growth of $|U(y_k)|$ is readily seen in Fig. 3 in paper [7]; it is determined by the terms Z_1Z_2/a and consequently is not related to the drop model.

It follows from experimental data on the number of secondary neutrons ν that the increase in the excitation energy of the fragments corresponds to $\beta_6 \neq 0$ rather than $\beta_6 = 0$ with an increase in Z^2/A (see [9]). We note that the slower growth of $T^{(1)} + T^{(2)}$, i.e., $|U(y_k)|$, when $\epsilon = 50.1$, as compared with that when $\epsilon = 48$ (see [8]) is related to the decrease in the values of the parameter $x = \frac{Z^2}{A\epsilon}$.

It follows from experiments on coulombic excitation [12] that the mass coefficients μ_n are substantially greater than the theoretical values of μ_n according to the drop model. Therefore $E_\infty - E_0$ may be less. From [12] it also follows that the elasticity constants in U_d are on the average somewhat less than those from the drop model. Therefore with the same values of $\alpha_2^{(i)}$, $\alpha_3^{(i)}$, U_d will be somewhat less. Changes in μ_n do not affect the value $T^{(1)} + T^{(2)}$ as it is determined by the energy of the initial nucleus $U(y_0) - U(y_k)$.

With the given Z^2/A let us now try to evaluate the ratio of the excitation energies of the two fragments, or approximately $E_0^{(1)}/E_0^{(2)}$, as a function of A_1/A_2. As numerical calculations show, $U_d^{(1)}/U_d^{(2)}$ depends weakly on A_1/A_2 (it decreases slowly with a decrease in A_1/A_2

Element		U^{238}		Pu^{240}		Cm^{242}		Cf^{252}	
type of fission		threshold	spontaneous	threshold	spontaneous	threshold	spontaneous	threshold	spontaneous
$U_\partial = U_\partial^{(1)} + U_\partial^{(2)}$, Mev		18,7		18,7		18,5		19,0	
$T^{(1)} + T^{(2)}$, Mev	$\beta_6 \neq 0$	4,9	0	8,0	0	12,4	5,3	12,8	5,6
	$\beta_6 = 0$	2,2	0	3,8	0	5,8	2,5	6,0	2,6
E_0, Mev	$\beta_6 \neq 0$	23,6	18,7	26,7	18,7	30,9	23,8	31,8	24,6
	$\beta_6 = 0$	20,9	18,7	22,5	18,7	23,3	21,0	25,0	21,6
E_∞, Mev	$\beta_6 \neq 0$	27,7	—	30,4	—	33,4	28,9	34,4	30,0
	$\beta_6 = 0$	26,8	—	28,1	—	29,6	27,2	30,4	28,2

when $A_1/A_2 \leq 1$). But as $b_{c2}/b_{c1} \approx A_2/A_1$ (the distance of the center of gravity of the light fragment from the over-all center of gravity is greater than that of the heavy fragment) then $\dot{\alpha}_n^{(1)} > \dot{\alpha}_n^{(2)}$ when $A_1 < A_2$ (see [5]). Therefore, regardless of the fact that $A_1^{5/3} < A_2^{5/3}$, it is nonetheless found that $T^{(1)} > T^{(2)}$. Due to this, when $A_1 \leq A_2$, $E_0^{(1)}$ is found to be greater than $E_0^{(2)}$ (this corresponds to experimental data in paper [10]). With a further increase in A_2/A_1 the ratio $E_0^{(1)}/E_0^{(2)}$ becomes smaller due to the rapid decrease of $U_d^{(1)} / U_d^{(2)}$.

Thus, in this case too, $T^{(i)}$ and not $U_d^{(i)}$ plays the main role in explaining the basic effect ($E_0^{(1)} > E_0^{(2)}$ when $A_1 < A_2$).

In conclusion, the author would like to thank V. M. Galitskii and V. M. Strutinskii for an interesting discussion and I. G. Krutikova for carrying out the numerical calculations.

LITERATURE CITED

[1] B. T. Geilikman, "Physical Investigations," Reports of the Soviet Delegation at the International Conference on the Peaceful Uses of Atomic Energy, Geneva, 1955 (Acad. Sci. USSR Press, Moscow, 1955) p. 310.

[2] B. T. Geilikman, J. Atomic Energy 6, 2, 290 (1959).

[3] N. Bohr and J. A. Wheeler, Phys. Rev. 56, 426 (1939).

[4] R. Present, and J. Knipp, Phys. Rev. 57, 751 (1940).

[5] Ya. I. Frenkel', J. Exp. Theoret. Phys. 9, 641 (1939).

[6] S. Frankel and N. Metropolis, Phys. Rev. 72, 914 (1947).

[7] D. Hill and J. A. Wheeler, Phys. 89, 110 (1953).

[8] B. T. Geilikman, Report No. 2473 at the Second International Conference on the Peaceful Uses of Atomic Energy (Geneva, 1958).

[9] R. B. Leachman, Phys. Rev. 101, 1005 (1956).

[10] I. Fraser and J. Milton, Phys. Rev. 93, 818 (1954).

[11] T. Maris, Phys. Rev. 101, 147 (1956).

[12] G. Temmer and N. Heydenburg, Phys. Rev. 104, 967 (1956).

Received August 5, 1958

POSSIBILITY OF ACCELERATING POLARIZED PROTONS IN A CYCLOTRON*

G. M. Budyanskii, Yu. A. Zavenyagin, N. D. Federov, and V. A. Khrabrov

An estimate is made of the probability of spin reorientation in the acceleration of polarized protons in a cyclotron, the magnetic field of which falls off with radius and exhibits an azimuthal variation. The extraction of the beam from the chamber is considered. It is shown that the probability for depolarization in acceleration and extraction of the particles is small.

INTRODUCTION

In studying interactions and in attempting to understand the nature of nuclear forces it is necessary to carry out experiments with polarized particles. At the present time, polarized particles are produced by scattering, and the intensity of beams of this kind is small. Experiments with polarized particles in which one studies double and triple scattering are extremely difficult to carry out and sometimes, indeed, impossible because of the small magnitudes of the effects being measured.

When consideration is given to the development of a source of polarized ions [1], the following question arises: Is it possible to accelerate and extract these ions in a cyclotron? If acceleration if feasible, it means that scattering is not required, and if the source is a good one, it should be possible to obtain a high-intensity beam of polarized particles. Below are given some approximate analyses of the acceleration and extraction of polarized protons in a cyclotron.

The Schrodinger equation for a spin function $\underline{S}$ in the customary notation is of the form [2]

$$ih\frac{dS}{dt} = -(HM)S. \tag{1}$$

The spin function $\underline{S}$ is represented by a two-row matrix so that Eq. (1) can be written in the form

$$\left.\begin{aligned}\frac{dS_1}{dt} &= \frac{i\mu H_z}{h}S_1 + \frac{i\mu}{h}(H_x - iH_y)S_2,\\ \frac{dS_2}{dt} &= \frac{i\mu}{h}(H_x + iH_y)S_1 - \frac{i\mu H_z}{h}S_2,\end{aligned}\right\} \tag{2}$$

where $\mu = \gamma\frac{eh}{2mc}$ (for the proton $\gamma \simeq 2.8$).

If at the initial time (t = 0) the projection of the spin on the $\underline{z}$-axis is positive ($S_1(0) = 1$; $S_2(0)=0$), the probability for finding a particle with spin oriented in the opposite direction at any time $\underline{t}$, i.e., the depolarization probability, is given by the expression $P(t) = |S_2(t)|^2$.

If H_x and H_y are harmonic functions

$$\left.\begin{aligned}H_x &= H_1\cos\omega t,\\ H_y &= H_1\sin\omega t,\end{aligned}\right\} \tag{3}$$

solving Eq. (2) we obtain the following formula for the depolarization probability.†

$$P(t) = \frac{q^2\sin^2\vartheta}{1+q^2-2q\cos\vartheta}\sin^2\times \\ \times\left\{\frac{\omega}{2}(1+q^2-2q\cos\vartheta)^{1/2}t\right\}, \tag{4}$$

where

$$\left.\begin{aligned}q^2 &= \left(\frac{\nu}{\omega}\right)^2(1+4\Delta^2),\\ \Delta &= H_1/2H_0,\\ \operatorname{tg}\vartheta &= H_1/H_0 = 2\Delta.\end{aligned}\right\}$$

The quantity ν which appears in these expressions is the precession frequency of the spin in a field of intensity H_0:

$$\nu = 2\mu H_0/h. \tag{6}$$

Since the angular frequency of rotation of ions in the cyclotron is $\omega_c = \frac{eH_0}{mc}$, it follows that $\nu = \gamma\omega_c$. Usually $\Delta = H_1/2H_0 \ll 1$, $\operatorname{tg}\vartheta \approx \sin\vartheta \approx \vartheta \approx 2\Delta$, so that after some simple transformations Eq. (4) can be written in the form

$$P(t) = \frac{4\Delta^2}{(\omega/\gamma\omega_c - 1)^2 + 4\Delta^2}\sin^2\times \\ \times\left\{\frac{\omega}{2}\left[(1-\gamma\omega_c/\omega)^2 + 4\Delta^2(\gamma\omega_c/\omega)^2\right]^{1/2}t\right\}. \tag{7}$$

At resonance

$$\omega = \nu = \gamma\omega_c, \tag{8}$$

so that the depolarization probability amplitude becomes unity and

$$P(t) = \sin^2(\omega\Delta t). \tag{9}$$

Proton Depolarization in Acceleration

Using the formulas derived above we now determine the probability of depolarization for acceleration of protons in a cyclotron, the magnetic field of which falls off radially and which has a azimuthal variation. The field components H_Z, H_r, and H_ϑ are not explicit functions of time (neglecting field fluctuations due to fluctuations in

*This work was carried out in the beginning of 1956.

†Lit. Cit. [2] in the formula for P(t) the factor q^2 does not appear.

the power lines) and depend on time only through the coordinates r, ϑ, and z, regardless of the particle acceleration process.

Let $$H_z = -H_{00}[1-\delta(r)+A(r)\cos k\vartheta], \qquad (10)$$

where $\delta(r)$ takes account of the radial variations of the magnetic field, and A(r) characterizes the azimuthal variation of the field.

For small departures from the median plane of the magnetic field

$$\left.\begin{aligned} H_r &= z\frac{\partial H_z}{\partial r} = zH_{00}\left(\frac{d\delta}{dr} - \frac{dA}{dr}\cos k\vartheta\right), \\ H_\vartheta &= \frac{z}{r}\frac{\partial H_z}{\partial \vartheta} = \frac{z}{r}H_{00}kA(r)\sin k\vartheta. \end{aligned}\right\} \qquad (11)$$

Transforming to Cartesian coordinates by means of the expressions

$$\left.\begin{aligned} H_x &= H_r\cos\vartheta - H_\vartheta\sin\vartheta, \\ H_y &= H_r\sin\vartheta + H_\vartheta\cos\vartheta \end{aligned}\right\} \qquad (12)$$

and introducing the notation

$$\left.\begin{aligned} N &= {}^1\!/_2(kA/r + dA/dr), \\ M &= {}^1\!/_2(kA/r - dA/dr), \end{aligned}\right\} \qquad (13)$$

we have

$$\left.\begin{aligned} H_x &= zH_{00}\left[\frac{d\delta}{dr}\cos k\vartheta - \right. \\ &\left. - N\cos(k-1)\vartheta + M\cos(k+1)\vartheta\right], \\ H_y &= zH_{00}\left[\frac{d\delta}{dr}\sin k\vartheta + \right. \\ &\left. + N\sin(k-1)\vartheta + M\sin(k+1)\vartheta\right]. \end{aligned}\right\} \qquad (14)$$

Because of the vertical oscillations of particles in the cyclotron

$$z = z_m\cos\omega_v t, \qquad (15)$$

where z_m is the amplitude of the oscillations and is a function of radius while ω_v is the frequency of the vertical oscillations. For free oscillations induced by the reduction in the magnetic field

$$\omega_v = \sqrt{n}\,\omega_c, \qquad (16)$$

where $n = -\frac{r}{H_z}\frac{dH_z}{dr}$ is the logarithmic field decay index. In a cyclotron $n < 1$, so that ω_v is always smaller than the particle rotation frequency ω_c. It may be assumed that at the terminal radius

$$n \approx 0{,}1 \div 0{,}2; \quad \omega_v \approx (0{,}3 \div 0{,}5)\omega_c.$$

For small values of r Eq. (16) does not apply. Here the vertical oscillations are determined basically by the electric field of the dees. In the general case it may be assumed that $\omega_v = p\omega_c$, where $p \lesssim 0.5$.

Taking account of the vertical oscillations and assuming that $\vartheta = \omega_c t$, Eq. (14) can be written in the form

$$\left.\begin{aligned} H_x &= {}^1\!/_2 z_m H_{00}\left\{\frac{d\delta}{dr}[\cos(1-p)\omega_c t + \right. \\ &+ \cos(1+p)\omega_c t] - \\ &- N[\cos(k-p-1)\omega_c t + \\ &+ \cos(k+p-1)\omega_c t] + \\ &+ M[\cos(k-p+1)\omega_c t + \\ &\left. + \cos(k+p+1)\omega_c t\right\}, \\ H_y &= {}^1\!/_2 z_m H_{00}\left\{\frac{d\delta}{dr}[\sin(1-p)\omega_c t + \right. \\ &+ \sin(1+p)\omega_c t + \\ &+ N[\sin(k-p-1)\omega_c t + \\ &+ \sin(k+p-1)\omega_c t + \\ &+ M[\sin(k-p+1)\omega_c t + \\ &\left. + \sin(k+p+1)\omega_c t\right\}. \end{aligned}\right\} \qquad (17)$$

Spin reorientation can be produced only by a perturbing field, the direction of which follows the spin precession. In the coordinate system used here, this coincidence occurs when the signs of the perturbing field components H_x and H_y are the same. Hence, in the following analysis, terms in Eq. (17) which contain the factor N need not be taken into account. In accordance with the condition in (8), resonance obtains when

$$1 \pm p = \gamma \qquad (18)$$

or

$$k \pm p \pm 1 = \gamma. \qquad (19)$$

The condition in (18) is sometimes not satisfied in a cyclotron since $p < 1$, and γ is 2.8 for the proton. We now estimate the probability for depolarization of the proton, for example with p = 0.4. For the case being considered here, from Eq. (5) we have $\Delta = \frac{z_m}{4}\frac{d\delta}{dr}$. Assuming that $\delta = b(r/R)^\beta$, $b = 0{,}02$, $\beta = 10$, $z_m = 3$ cm, and $r = R = 70$ cm (terminal radius for acceleration) we find $\Delta = 3 \times 10^{-3}$. The amplitude of the depolarization probability is found to be very small ($P \approx 5 \times 10^{-5}$).

However, it is possible that the resonance conditions given in (19) can obtain in the cyclotron. In this case $p = \gamma \pm k \pm 1$. Since k is a whole number while p is the positive quantity and not greater than approximately 0.5, the resonance value of p can be achieved only when k = 2 (p = 0.2).

In conventional cyclotrons the amplitude of the second harmonic of the azimuthal nonuniformity (k = 2) is very small (approximately 0.1% of the field); in cyclotrons with an azimuthal variation we have $k > 2$. Nonetheless this resonance is still dangerous. In accordance with Eq. (9) resonance ($\omega = \gamma\omega_c$), the maximum value of the proton depolarization probability is reached when

$$\omega\Delta t = \pi/2, \qquad (20)$$

that is, the time

$$t = T/4\gamma\Delta, \qquad (21)$$

where T is the period of rotation of the particle and is approximately equal to the period of the radio-frequency voltage of the dees. At resonance the amplitude of the field components is determined from Eq. (17) and is given by

$$H_1 = {}^1/_2 z_m H_{00} M = {}^1/_8 z_m H_{00} (A/r - dA/dr). \qquad (22)$$

If $A = a(r/R)^\alpha$, we find $\Delta = H_1/2H_0 = {}^1/_8 a z_m \times$

$\times \left[2/r\,(r/R)^\alpha - \frac{\alpha}{r}\left(\frac{r}{R}\right)^{\alpha-1} \right]$. When $\alpha = 2$ the quantity Δ vanishes and t becomes infinitely large. Thus, when the particle passes through the resonance danger zone reorientation of the spin does not occur. Another field variation may be characterized by ($\alpha = 1$) $\Delta = az_m/4R$. Assuming $z_m = 3$ cm, R = 70 cm, and $a = 10^{-2}$, we find $\Delta \approx 10^{-4}$ and $t \approx 10^{3}$ T. In cyclotrons, the acceleration time usually corresponds to 50-100 RF periods. Hence, even with $\alpha = 1$ there is no danger of a change in the orientation of the spin.

Since the values of Δ which are obtained are small it is not necessary to consider other variations of the quantity A(r).

Taking account of the higher-order terms in the expression for the components of the magnetic field does not lead to any noticeable effect on the probability for depolarization aside from the appearance of new frequencies in Eq. (17). Actually, the amplitudes of the additional harmonic terms turn out to be very small as compared with those calculated before. This explains the smallness of the quantity Δ, which determines the time the particles can remain in the variable magnetic field. Thus the allowable number of periods T in Eq. (21) increases while the depolarization probability is reduced.

If the source is located at the center of the magnet there is a displacement of the center of the orbit; this can be taken into account by introducing a first azimuthal harmonic (k = 1). In this case, as in the example considered above, the quantity A(r) [c.f. Eq. (10)] is small and its depolarization effect can be neglected.

Proton Depolarization in Beam Extraction

The particle beam when being extracted, moves in a highly inhomogeneous magnetic field. Both calculations and experiment indicate that in the fringing field the ions execute approximately a single vertical oscillation regardless of the initial conditions (distance from the median plane z_0 and initial phase at entrance into the deflector). Under these conditions the ions pass through the median plane approximately in the region of maximum magnetic field gradient (Figure).

The radial field component H_z can be given by the approximation

$$H_r(l) = z\frac{\partial H_z}{\partial r} = \frac{\partial H_z}{\partial r} z_0 \sin 2\pi l/l_k \qquad (23)$$

Since $l = vt$, $H_r(l) = z_0 \frac{\partial H_z}{\partial r} \sin \varkappa t$ where $\varkappa = 2\pi v/l_k$.

During the time in which the particle traverses the path l_k from entrance to the deflector (radius r_i) to the terminal point of the path (exit from the chamber, radius r_c), the instantaneous frequency $\dot{\varphi}$ varies within the limits

$$v/r_i \geq \dot{\varphi} \geq v/r_c$$

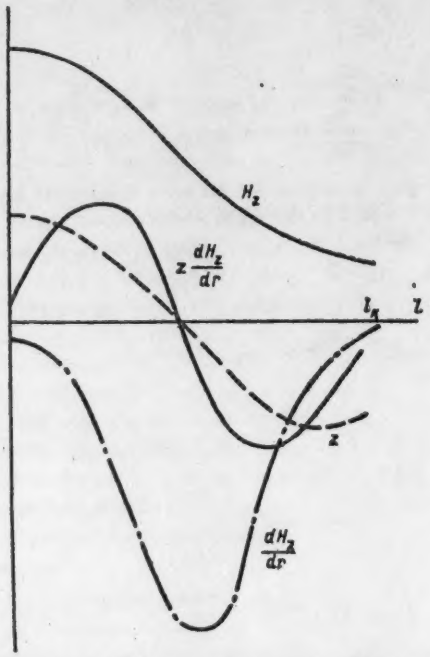

Variation of field intensity H_z, the radial derivative $\frac{dH_z}{dr}$, the vertical coordinate z, and the quantity $\frac{dH_z}{dr}z$ along the path l for an average ion trajectory in the deflected beam ($l = 0$ corresponds to the origin of the deflection beam).

The quantity v/r_i is equal to the frequency of rotation of the proton before it enters the deflector (ω_c) and $r_k \approx 2r_i$ so that the angular velocity $\dot{\varphi}$ at ejection lies between the limits ω_c and 0.5 ω_c. In order to estimate the depolarization we use the field components

$$\left.\begin{aligned} H_x &= H_r \cos\dot{\varphi}t = z_0 \frac{\partial H_z}{\partial r} \sin \varkappa t \cos \dot{\varphi} t, \\ H_y &= H_r \sin\dot{\varphi}t = z_0 \frac{\partial H_z}{\partial r} \sin \varkappa t \sin \dot{\varphi} t. \end{aligned}\right\} \qquad (24)$$

Thus, in the expressions for the components of the perturbing field there are frequencies

$$\Omega_{1,2} = \varkappa \pm \dot{\varphi}, \qquad (25)$$

where the quantities κ and ω_c are comparable. The frequency of spin precession $\nu = \gamma \frac{eH_z}{mc}$ during the particle extraction process varies between the limits

$$\gamma\omega_c \geqslant \nu \geqslant \gamma\,(eH_z/mc)_{r=r_c}. \qquad (26)$$

Comparing Eq. (25) and (26) one observes that upon ejection of the particle it is possible to have one or two points (if at $t = 0$, $\kappa + \omega_c < \gamma\omega_c$) at which the frequencies $\Omega_{1,2}$ are equal to the spin precession frequency ν (resonance points).

In order to make a very conservative estimate of the amount of depolarization we shall assume that resonance obtains not at the points noted here but over a wide range of values of l (from $l = \frac{1}{4} l_t$ to $l = l^3/4 l_t$). The time during which the particle moves in this region is $t = \frac{1}{2}\cdot\frac{l_t}{v}$.

We shall assume that the field intensity is equal to some average value $H_0 \approx \frac{1}{2} H_i$ (H_i is the field at $l = 0$) while the frequency Ω is the maximum value $\Omega_{max} = \kappa + \omega_c$. Thus, the probability for reorientation of the spin, [as is seen from Eq. (9)] is $P = \sin^2 \Omega_{max} \Delta t$.

For the cyclotron at the Institute for Atomic Energy, Academy of Sciences, USSR., at which protons are accelerated to an energy of 12 Mev, the following parameters obtain: $v = 0.16c$, $H_i = 7.6$ kilogauss, $\omega_c = 75 \times 10^6$ 1/sec, $\kappa = 10^6$ 1/sec, $l_t \approx 300$ cm, and $t = 3 \times 10^{-8}$/sec.

The quantity $\Delta = z_0 \partial H_z \partial r \cdot \frac{1}{2} H_0$ when $z_0\, \partial H_z / \partial r \approx 200$ gauss and is found to be approximately 0.03. For the values chosen here we find that Ω max and $t P = 0.03$. In actual fact it is much smaller than the value assumed earlier, and the proton depolarization upon extraction from the cyclotron is many times smaller than the value indicated by the estimate made here.

Various methods can be used to obtain polarized ions at the central region of the cyclotron. The choice of the most effective method for providing a beam of accelerated polarized ions of maximum intensity can be made only after a special analysis has been carried out.

LITERATURE CITED

[1] B. P. Ad'yasevich, S. T. Belyaev, and Yu. P. Polunin, Report to the All-Union Conference on the Physics of High-Energy Particles [in Russian] (Moscow, 1956).

[2] D. I. Blokhintsev, Fundamentals of Quantum Mechanics [in Russian] (State Technical Press, 1949) p.257.

Received September 20, 1958

EXPERIMENTAL VERIFICATION OF THE THEORY OF NEUTRON DIFFUSION IN A MEDIUM WITH VOIDS

I. F. Zhezherun

Experiments are described which have been carried out to verify the theory of diffusion of thermal neutrons in a graphite medium. Measurements of the neutron fluxes in continuous graphite media and in a graphite medium with channels verify the theoretical formulas which relate in a medium with empty channels, the effective diffusion coefficients (and the diffusion lengths) of the thermal neutrons with the lattice parameters of the channels, and the corresponding diffusion coefficient (and diffusion length) in a continuous medium.

INTRODUCTION

In making reactor calculations (especially for heterogeneous reactors), it is sometimes necessary to know the effect of a cavity in the moderator on neutron diffusion. This problem has been theoretically considered a long time ago by V. S. Fursov and S. L. Sobolev for the particular case in which the cavities in the moderator are parallel, cylindrical channels, possessing radii smaller than the neutron scattering length in the moderator λ_s, and a cross-sectional area much smaller than the cross-sectional area of the moderator removed from one channel. Under these conditions the channels have a small effect on the neutron field; however, diffusion of neutrons in directions parallel and perpendicular to the channels will be different, that is to say, the medium becomes anisotropic.

The diffusion coefficient and the diffusion length for neutrons in such a medium (if we consider distances much larger than the distances between channels) will be tensors which are symmetric with respect to channel axes. The density of thermal neutrons from a point source, n, is given by the following expression (for an infinite medium).

$$n(x, y, z) = \frac{\text{const}}{\sqrt{\left(\frac{x}{L_\perp}\right)^2+\left(\frac{y}{L_\perp}\right)^2+\left(\frac{z}{L_\parallel}\right)^2}} \left(-\sqrt{\left(\frac{x}{L_\perp}\right)^2+\left(\frac{y}{L_\perp}\right)^2+\left(\frac{z}{L_\parallel}\right)^2}\right), \quad (1)$$

where $L_\parallel$ and $L_\perp$ are the effective diffusion lengths in the directions parallel and perpendicular to the channels, respectively, and where the Z axis is in the direction of the channels, and the origin of coordinates is taken at the source.

Fursov has derived expressions which relate $L_\parallel$ and $L_\perp$ (for a medium with channels) with the diffusion length L_0 (corresponding to a continuous medium) and the parameters which characterize the channel geometry:

$$L_\parallel = L_0\left[1+\frac{\pi R^2}{a^2}\left(1+\frac{3\pi}{4}\frac{R}{2\lambda_s}\right)\right], \quad (2)$$

$$L_\perp = L_0\left[1+\frac{\pi R^2}{a^2}\left(1+\frac{R}{2\lambda_s}\right)\right], \quad (3)$$

as well as formulas which relate the diffusion coefficient for a continuous medium D_0 with the effective diffusion coefficients $D_\parallel$ and $D_\perp$ characteristic of a medium with channels:

$$D_\parallel = D_0\left[1+\frac{\pi R^2}{a^2}\left(1+\frac{3\pi}{4}\frac{R}{\lambda_s}\right)\right], \quad (4)$$

$$D_\perp = D_0\left[1+\frac{\pi R^2}{a^2}\left(1+\frac{R}{\lambda_s}\right)\right]. \quad (5)$$

In Eqs. (2)-(5) πR^2 is the cross-sectional area of a channel of radius R; a^2 is the area of a square cell which is constructed about one channel; λ_s is the mean scattering length for thermal neutrons in a continuous medium with channels.

Sobolev has given a more exact expression for the effective neutron diffusion coefficient along the channels

$$D_\parallel = D_0\left[1+\frac{\pi R^2}{a^2}\left(1+2\frac{R}{\lambda_s}\right)\right], \quad (6)$$

which differs from Eq. (4) by the factor which multiplies $\frac{R}{\lambda_s}$ in the curved brackets. This factor is 15% smaller than the corresponding factor in the formula given by Fursov. The difference arises in the calculation of the additional flux due to the presence of channels in the infinite medium. However, in most important cases the formulas for $D_\parallel$ and $L_\parallel$ given by Fursov and Sobolev are essentially the same; the results which they yield do not differ by more than 0.5-1%*. The work in the present paper is motivated by the desire to make an experimental verification of these formulas as applied to one of these cases. Reported briefly below are the results of this test, which was carried out at the First Soviet Nuclear Reactor [2] immediately after its completion.

EXPERIMENTS AND RESULTS

The experiments designed to verify the theory of neutron diffusion in a medium with channels were carried out in graphite. The geometric parameters of the channel lattice are as follows: $\frac{R}{\lambda_s} = 0.88$, $\frac{\pi R^2}{a^2} = 3.8\cdot10^{-2}$. The ratios between $D_\parallel$ and $D_\perp$, $L_\parallel$ and $L_\perp$, and D_0, L_0 (computed from the formulas given by Fursov) are

$$\frac{L_\parallel}{L_0} = 1{,}077, \quad (2') \qquad \frac{L_\perp}{L_0} = 1{,}055, \quad (3')$$

$$\frac{D_\parallel}{D_0} = 1{,}116, \quad (4') \qquad \frac{D_\perp}{D_0} = 1{,}071. \quad (5')$$

*The formulas given by Fursov and Sobolev are in agreement with the more general formulas reported in the work of Behrens [1], which was published later.

The greatest differences are between $D_{\parallel}$ and D_0. Hence, in order to minimize the effect of experimental errors Eq. (4'), which relates the effective diffusion coefficient $D_{\parallel}$ in a medium with channels (in the direction of the channels) with the diffusion coefficient D_0 for a continuous medium, was chosen.

The effect of the channels on neutron diffusion is essentially the production of an additional neutron flux, in which the channels contribute individually. Hence it is possible to study neutron diffusion in a single channel and an area a^2 independently of the other cells.

According to the calculations carried out by Fursov the neutron flux along the channel is

$$j_{\parallel} = D_0 \left(1 + \frac{3\pi}{4}\frac{R}{\lambda_s}\right) \operatorname{grad} n_{\parallel}, \qquad (7)$$

in a continuous medium; in the same direction, as is well known, the flux is given by

$$j_0 = D_0 \operatorname{grad} n_0. \qquad (8)$$

A comparison of these fluxes indicates that when the neutron-density gradients are the same, the flux in the medium with channels will be 3.07 times $\left(1+\frac{3\pi}{4}\frac{R}{\lambda_s}\right)$ greater than the flux in the same direction through the same area in a continuous medium.

Sobolev has computed the mean flux due to a channel (for a flux close to a channel axis); in the present case, it is larger than the flux in the continuous medium by a factor of 2.76.

It will be apparent that a measurement of the ratio $\frac{j_{\parallel}}{j_0}$ for the two fluxes will be a rather sensitive method for verifying the theory of neutron diffusion in a medium with channels. This was the method employed in the present work and the experimental conditions were closer to those assumed in the calculations carried out by Fursov. The flux measurements were carried out as follows. A rectangular graphite prism with vertical channels was placed at the top reflector of the reactor [2]. The reactor dimensions were as follows: base 60 x 60 cm, height 125 cm. Along the axis of the central channel at a distance z = 65 cm from the lower base of the prism in a plane perpendicular to the axis were located two gold-foil indicators (thickness 0.1 mm, see Fig.) separated by cadmium sheets 0.6 mm thick. The sides and top of the prism were covered by cadmium sheets 1 mm thick. During the reactor's time of operation the thermal neutrons diffused into the prism from the graphite reflector through the lower base of the prism, which served as the neutron source.

Since the lower indicator could be activated only by thermal neutrons which were incident from below (the cadmium sheet was opaque for thermal neutrons incident from above) and the upper indicator could be activated only by neutrons incident from above, the difference in the activities of these indicators per unit area was proportional to the neutron flux. By repeating the experiment in the prism with the channels filled by graphite rods it was possible to find the flux at a given point of the prism and in the same direction but for a continuous medium. The activation time of the indicators and the intensity of the neutron source in the experiments must be the same; these factors were monitored by means of special integrating indicators which were located at the base of the prism and at the reflector of the reactor.

The activity of the gold indicator, with a decay period of 2.7 days, was measured with a Geiger counter and computed per unit area (after the introduction of appropriate corrections for the readings and the decay). The results of these measurements are given in the Table (c.f. page 197). The ratio of the measured fluxes was found to be $\frac{109 \pm 1.5}{38 \pm 1.5} = 2.9 \pm 0.12$, with a mean-square error of ± 4%.

Since the transverse dimensions of the indicators and the cadmium sheet used to separate them were small (approximately 1 cm), the perturbation of the neutron field, as computed by well-known formulas [3], was less than 10 - 13 %. For this reason and because of the fact that the cadmium sheet was uniformly close to both indicators the experimental ratio which has been obtained should be very close to the true ratio.

We may compute a more exact ratio of the fluxes determined by Eq. (7) and Eq. (8). Assuming that the Z-axis is in the direction of the channels we have

$$\frac{j}{j_0} = \left(1 + \frac{3\pi}{4}\frac{R}{\lambda_s}\right)\frac{dn_{\parallel}}{dn_0}. \qquad (9)$$

The factor $\frac{Dn_{\parallel}}{Dn_0}$, which represents the ratio of the gradients for the neutron density along the Z-axis in a medium with channels and in a continuous medium, varies as a function of the distance z from the point being considered to the source but is only a very weak function of the dimensions of the medium and the shape of the source. As a matter of fact, with z = 65 cm, $L_0 \approx 53$ cm, and the channel geometry corresponding to the present experiment, we find:

1) for a point source in an infinite medium

$$\frac{dn_{\parallel}}{dn_0} = \frac{\frac{d}{dz}\left(\frac{c\exp\left(-\frac{z}{L_{\parallel}}\right)}{4\pi D_{\parallel} z}\right)}{\frac{d}{dz}\left(\frac{c\exp\left(-\frac{z}{L_0}\right)}{4\pi D_0 z}\right)} =$$

$$= \frac{D_0\left(\frac{z}{L_{\parallel}}+1\right)}{D_{\parallel}\left(\frac{z}{L_0}+1\right)} \exp\left[-z\left(\frac{1}{L_{\parallel}}-\frac{1}{L_0}\right)\right] = 0{,}94;$$

2) for a infinite plane source in an infinite medium

$$\frac{dn_{\parallel}}{0} = \frac{\frac{d}{dz}\left(\frac{L_{\parallel}\exp\left(-\frac{z}{L_{\parallel}}\right)}{2D_{\parallel}}\right)}{\frac{d}{dz}\left(\frac{L_0\exp\left(-\frac{z}{L_0}\right)}{2D_0}\right)} =$$

$$= \frac{D_0}{D_{\parallel}} \exp\left[-z\left(\frac{1}{L_{\parallel}} - \frac{1}{L_0}\right)\right] = 0{,}97;$$

3) for an infinite plane source in a medium of finite thickness equal to the effective height (127 cm) of the prism which was used

$$\frac{dn_{\parallel}}{dn_0} = 0{,}98;$$

4) for a point source in a rectangular prism equivalent to that which was used

$$\frac{dn_{\parallel}}{dn_0} = 0{,}99 \div 1{,}00.$$

For the actual conditions in the experiment which was carried out [intermediate between cases 3) and 4)], the ratio of the gradients may be taken as 0.99 ± 0.01. Thus, the ratio of the fluxes determined from Eq. (9) is 3.03 ± 0.03. The experimentally measured ratio 2.9 ± 0.12 is in good agreement with these values and gives a value $\frac{D_{\parallel}}{D_0} = 1.11 \pm 0.005$ (mean-square error of 0.5%) for the diffusion coefficient ratio. Thus, it is apparent that the experimental value of $D_{\parallel}$, within the limits of the experimental errors, is in agreement with that computed theoretically.

The theoretical formulas (2) - (6) do not take account of the air in the channels. If account is taken of this air, we must introduce a correction which tends to reduce the difference between $L_{\parallel}$, $L_{\perp}$, and L_0. However, for the present medium this correction is negligibly small (0.3 %) for the diffusion lengths and is unimportant for the diffusion coefficients.

The background of thermal neutrons which are scattered in the reactor cannot affect the results of the measurements because the prism is covered by cadmium sheets. The fast-neutron background is negligibly small. This situation was verified by means of special control experiments in which the graphite prism was enclosed in a layer of paraffin (10 cm thick) in addition to the cadmium; this paraffin layer served as a moderator for fast neutrons.

We have also carried out experiments to verify Eq. (2'). In this case, measurements were made of the diffusion length $L_{\parallel}$ in a graphite prism with channels. Then the channels were filled by graphite rods so that the prism became continuous and a measurement was made of the quantity L_0. The prism dimensions were 140 x 140 x 360 cm. The results of the measurements are in agreement with the theoretical calculations made on the basis of Eq. (2). However, the mean-square error in the measurements of $L_{\parallel}$ and L_0 were of the order of 3%; hence the flux measurement experiments are more convincing.

CONCLUSIONS

Using a graphite medium with parallel cylindrical channels of radius $R\left(\frac{R}{\lambda_s} = 0.88\right)$ located at the corners of a square lattice with spacing $a\left(\frac{\pi R^2}{a^2} = 3{,}8 \times 10^{-2}\right)$, we have experimentally verified the formulas which relate the effective diffusion coefficients and the diffusion lengths for a medium with channels with the parameters which characterize the dimensions of the channels and their location, and the diffusion coefficients and diffusion length for a continuous medium.

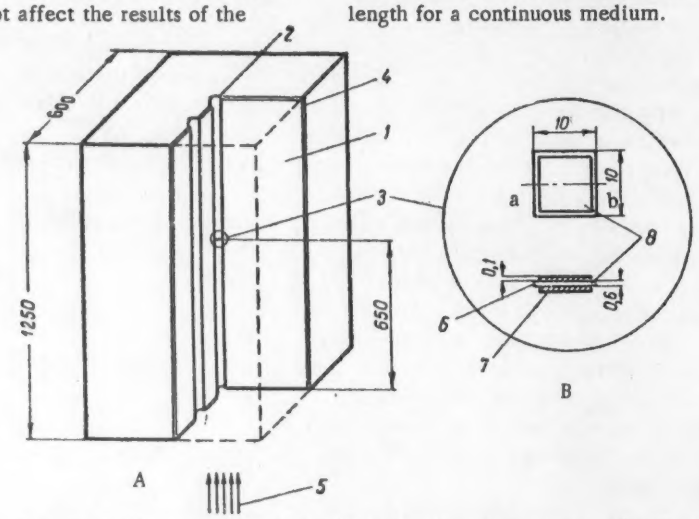

Experimental geometry. a) graphite prism located on the reflector of the reactor; b) compound indicator (plan and section along AB); 1) graphite; 2) channel; 3) indicator; 4) cadmium cover for the prism; 5) direction of the neutron flux in the prism from the reflector of the reactor; 6, 7) indicator made of gold foil 0.1 mm thick; 8) cadmium sheet which separates the gold indicators. Dimensions are given in millimeters.

Results of the Measurements of the Activity of the Gold Indicators

Experimental conditions	Reduced indicator activity (in arbitrary units)			Difference in activities (flux)	Flux reduced to the same integrated exposure
	integrated	lower	upper		
Irradiation of the indicators in the center of a graphite prism with channels	100,0±0,34	443±1	334±1	109±1,4	109±1,5
Irradiation of the indicators in the center of a continuous graphite prism (channels filled with rods)	97±0,34	345±1	308±1	37±1,4	38±1,5

In conclusion, the author wishes to take the opportunity to express his gratitude to V. S. Fursov for his continued interest in this work.

LITERATURE CITED

[1] D. J. Behrens, Proc. Phys. Soc. 62, 358 A, 10, 607 (1949).

[2] V. S. Fursov, Conference of the Academy of Sciences, USSR, on the Peaceful Uses of Atomic Energy (Plenary Session) [in Russian] (Academy of Sciences Press, USSR, 1955) p. 15.

[3] W. Bothe, Z. Phys. 120, 437 (1943).

Received September 4, 1958

NEUTRON ACTIVATION ANALYSIS OF SAMPLES OF ROCK AND ORE CONCENTRATES

D. I. Leipunskaya, Z. E. Gauér, and G. N Flerov

Neutron activation analysis consists of irradiating the samples of rock, ore, or concentrates to be analyzed with (Po-Be) -sources and then measuring the induced activity with scintillation and other counters. A method was developed for measuring aluminum, manganese, vanadium, and indium in ores of complex composition with reasonable concentrations of these elements. The use of its short-lived isotope as an indicator of the element determined makes it possible to achieve a rapid analysis method. The great sensitivity and accuracy of the method makes its application promising.

In prospecting and surveying mineral resources and also for controlling the enrichment of ore concentrates, it is very important to be able to determine a series of elements in samples of rock and concentrates rapidly and quite accurately. For this purpose, neutron activation analysis is extremely promising, since it allows identification and determination of the elements examined by measurement of the radiation from their radioactive isotopes, formed under the action of neutron irradiation.

The extreme sensitivity of neutron activation analysis for a series of elements with anomalously high activation cross sections is well known [1]. An advantage of this analysis is also its high accuracy, which hardly depends on the concentration of the given element in the sample, in contrast, for example, to chemical analysis, with which low concentrations cannot be measured accurately, or to spectral analysis, which is unsuitable for determining high concentrations. These factors determine the expediency of using the given method in prospecting and surveying mineral resources.

For rapidity and convenience in activation analysis both in laboratories and especially under field conditions, it should be carried out without the laborious stage of chemical separation of the irradiated samples. The intensity requirement in the neutron sources used for irradiating the samples is then reduced since the induced activity can be measured directly after irradiation. In addition, by using short-lived radioactive isotopes of the elements determined as indicators of these elements, it is possible to measure the content of these elements in rocks and ore concentrates rapidly.

Due to the complexity of the chemical composition of rocks and ore concentrates, it was impossible to estimate beforehand the extent to which this form of neutron activation analysis could be applied to measurement of certain elements in the widest range of types of rock. In the present work we describe experimental investigations of the possibility of applying this analysis to definite forms of rock, soils, and ore concentrates. The elements determined gave isotopes with comparatively short half-lives (from several minutes to several hours) on activation.

The conditions for irradiation and recording of the induced activity were chosen so as to give the sharpest separation of the activity of the isotope of the element that was to be determined. The sensitivity of the analysis in relation to the intensity of the neutron source was estimated and we determined which elements and to what extent they would interfere with the determination of the given element.

The samples were irradiated in a channel in a paraffin block by means of (Po-Be)-sources. The intensity of the sources used was several curies of polonium, i.e., of the order of 10^7 neutrons/sec. As long as we were not determining extremely low concentrations of the elements examined, this intensity was sufficient to obtain results of the required accuracy.

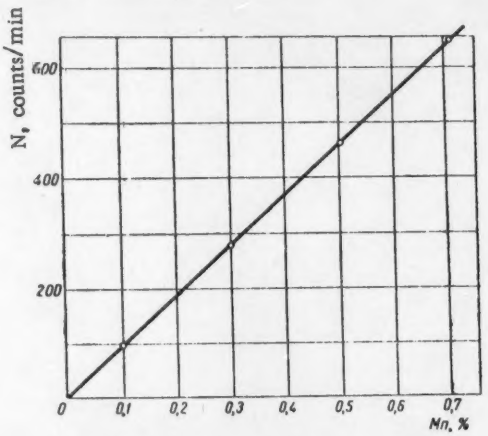

Fig. 1. Relation of β-activity of irradiated mixture to manganese content.

For activation of isotope-indicators, (n, p)-reactions were used together with (n, γ)-reactions. In this case, the irradiation conditions were changed slightly so as to increase the fraction of fast neutrons in the total flux (the moderator, which was normally set between the sample and the source, was removed).

The induced radioactivity was measured both from the β-radiation by means of normal counter tubes and from the γ-radiation by means of a scintillation counter with a single-channel amplitude analyzer. The induced radioactivity was small and therefore for β-radiation, measurements, powdered rock was loaded into cylindrical

cells with double walls made from nonactivateable material (plexiglass or polyethylene); the inner wall of the cell was made from a thin film. The thickness of the sample layer in the cell was greater than the maximum range of the β-rays (infinitely thick layer) and the length of the cell was ~8 cm.

For counting, the cell was slipped over the counter. For measurement of the γ-radiation, the sample layers were thin (with respect to the γ-rays). Standards for the measurements were prepared from rock samples with a known content of the element determined or by means of additions and in certain cases artificial mixtures were used.

Figure 1 shows the relation of the β-particle count rate to the manganese content of irradiated artificial mixtures with quartz. The intensity of the neutron source was $\sim 2 \cdot 10^7$ neutrons/sec, the irradiation time 20 minutes, and the speed of counting 5 minutes (after irradiation). The graph showed a strictly linear relation to the manganese content. Similar graphs were obtained for mixtures containing vanadium, chlorine, indium, etc.

In measuring rock samples by this method, it is very important to satisfy oneself that certain elements do not distort the results of measuring the element determined. This was checked by neutron activation analysis on definite types of rock.

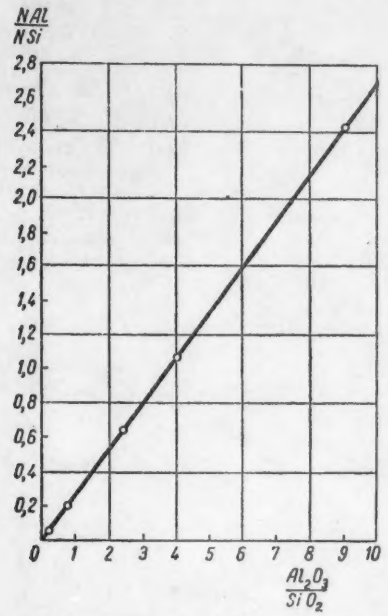

Fig. 2. Correlation of the ratio of aluminum and silicon contents, determined from the induced radioactivity, with the contents of these elements in artificial mixtures.

Considering these factors, we developed a method for determining aluminum in bauxites, aluminosilicate minerals, and soils. The induced radioactivity was counted by the β-radiation. With the use of (Po-Be)-neutron sources with an intensity of about 1.5 curies of polonium, the irradiation time was 5 minutes and the count, 10 minutes. Under these conditions, it was possible to determine the aluminum content of samples, beginning from approximately 3%, with a relative accuracy of 3-5%. In analyzing aluminosilicate rocks, their silicon contents were estimated simultaneously. Since there were slow and fast neutrons in the irradiation channel, Al^{28} ($T_{1/2}$ = = 2.3 min) was obtained not only due to activation of aluminum by slow neutrons, but also due to activation of silicon, for which the reaction $Si^{28}(n, p)Al^{28}$ occurs with fast neutrons [2]. Therefore, to evaluate the effect of silicon, we also irradiated samples shielded from the effect of slow neutrons with a cadmium shield. The Al^{28} activity thus obtained was a measure of the amount of silicon in the sample. It was thus possible to determine the ratio of the aluminum content to the silicon content, which is very important for industrial evaluation of aluminum raw materials. For accurate determinations of this ratio, the irradiation conditions were chosen so that the contribution from the (n, p)-reaction was increased.

The neutron activation analysis was checked by chemical analyses of aluminum and silicon in clays, kaolins, nephelines, bauxites, etc. Figure 2 shows the results of evaluating the ratio by means of data from measurement of the induced radioactivity. The ratio of the Al_2O_3 and SiO_2 concentrations in standards is plotted along the abscissa and the ratio of the measured activities of aluminum to silicon along the ordinate.

In the same way, it is possible to evaluate the ratio between manganese and iron in iron ores, which, under irradiation with neutrons from (Po-Be)-sources, give the isotope Mn^{56} by activation of the manganese from the action of slow neutrons, while the same isotope is also formed as a result of the nuclear reaction $Fe^{56}(n, p)Mn^{56}$ on iron by the action of fast neutrons [3]. However, in this case the ratio of the sensitivity of the determination of iron to manganese is very much less than for aluminum to silicon (in activity, a 0.1% manganese content is equivalent to 40% of iron, while a 1% aluminum content is equivalent to 2.5% of silicon).

The manganese content of rock and soil samples, independent of the iron content, is most conveniently determined by irradiation under conditions giving the minimum dose of fast neutrons in the total neutron flux. Then the induced radioactivity due to Mn^{56} will be strictly proportional to the manganese content of the sample.

By irradiation with (Po-Be)-sources with an intensity of $\sim 10^7$ neutrons/cm and recording the Mn^{56} β-rays, it is possible to determine the manganese content from a few hundredths of a percent upwards. In investigating geochemical anomalies above oil deposits, by this method we measured the Clarke content of manganese in soils. Higher manganese contents could be measured in iron ores, aluminosilicates, and other types of rock, not containing noticeable amounts of nickel or rare earths. Nickel and

Summary of Results of Neutron Activation Analysis of Rock and Ore Concentrate Samples

Element determined	Radioactive isotope of element determined and its characteristics [5]	Sensitivity of determination, %	Intensity of (Po-Be) - source, n/sec	Possible "interfering" elements with similar activation characteristics	Radioactive isotopes of "interfering" elements and their characteristics [5]	Amt. of "interfering" elements giving approximately the same induced activity as 1 g of the element determined, g	Possible methods of allowing for "interfering" elements
Aluminum	Al^{28} $T_{1/2}$=2.3 min E_β=2.87 Mev E_γ=1.77 Mev	~5	$3 \cdot 10^6$	Silicon	Al^{28} $T_{1/2}$=2.3 min E_β=2.87 Mev E_γ=1.77 Mev	2,5	By comparison of the activations with fast and slow neutrons
—	—	—	—	Vanadium	V^{52} $T_{1/2}$=3.9 min E_β=2.7 Mev E_γ=1.46 Mev	0.1	By the decay of the induced activity with time and by the γ-ray energies
—	—	—	—	Silver	Ag^{108} $T_{1/2}$=2.3 min E_β=1.8 Mev E_γ=0.62 Mev (0,8%)	0.04	By comparison of the β- and γ-radiations
Silicon	Al^{28} $T_{1/2}$=2.3 min	7—10	10^7	Aluminum (mainly)	Al^{28} $T_{1/2}$=2.3 min	1.5	By comparison of the activations with fast and slow neutrons
Vanadium	V^{52} $T_{1/2}$=3.9 min E_β=2.7 Mev E_γ=1.46 Mev	10^{-1}	$2 \cdot 10^7$	Aluminum	Al^{28} $T_{1/2}$=2.3 min	10	By the decay of the induced activity with time and by the γ ray energies
—	—	—	—	Copper	Cu^{66} $T_{1/2}$=5.1 min E_β=2.5 Mev E_γ=1.04 Mev(9%)	15	By comparison of the β- and γ-radiations
—	—	—	—	Silver	Ag^{108} $T_{1/2}$=2.3 min E_β=1.8 Mev E_γ=0.62 Mev (0,8%)	0.4	The same
Indium	In^{116} $T_{1/2}$=5.4 min E_β=0.6—1 Mev E_γ=0.1—2 Mev	10^{-2}	$2 \cdot 10^7$	Zinc	Zn^{69} $T_{1/2}$=52 min E_β=0.85 Mev E_γ—none	400	"
—	—	—	—	Chlorine	Cl^{38} $T_{1/2}$=38 min E_β=1.2—4,8 Mev E_γ=1.2—2,1 Mev	300	By the decay of the induced activity with time

Element determined	Radioactive isotope of element determined and its characteristics [5]	Sensitivity of determination, %	Intensity of (Po-Be) - source, n/sec	Possible "interfering" elements with similar activation characteristics	Radioactive isotopes of "interfering" elements and their characteristics [5]	Amt. of "interfering" element giving approximately the same induced activity as 1 g of the element determined, g	Possible methods of allowing for "interfering" elements
—	—	—	—	Manganese	Mn^{56} $T_{1/2}$=2,58 hours E_β=1,8—3 Mev E_γ=0,85—3 Mev	5	By the decay of the induced activity with time
—	—	—	—	Tin	Sn^{123} $T_{1/2}$=40 min E_β=1,26 Mev E_γ=0,15 Mev	20000	The same
Manganese	Mn^{56} $T_{1/2}$=2,58 hours E_β=1,8—3 Mev E_γ=0,85—3 Mev	10^{-2}	$2 \cdot 10^7$	Nickel	Ni^{65} $T_{1/2}$=2,56 hours E_β=0,4—2,1 Mev E_γ=0,4—1,5 Mev (43%)	50	By comparison of the β- and γ-radiations and by the γ-ray energies
—	—	—	—	Dysprosium	Dy^{165} $T_{1/2}$=2,4 hours E_β=1,25 Mev E_γ=0,09—0,7 Mev (25%)	0,05	By the γ-ray energies
—	—	—	—	Silicon	Si^{31} $T_{1/2}$=2,62 hours E_β=1,48 Mev E_γ— none	2000	By comparison of the β- and γ-radiations

dysprosium are "interfering" elements in the determination of manganese by the neutron activation method, since on activation with slow neutrons, they give isotopes with half-lives close to the half-life of Mn^{56}, namely, Ni^{65} ($T_{1/2}$ =2,56 hours) and Dy^{165} ($T_{1/2}$ = 2,4 hours).

We used neutron activation analysis for the rapid determination of the vanadium content of iron ores or the products of their treatment. The isotope V^{52} ($T_{1/2}$ = 3.9 minutes) was used for the determination. Comparison of the neutron activation method of determining vanadium in samples of various iron ores (titano-magnetites) limonites, etc.) with quantitative chemical and spectral methods showed that by the first method it was possible to determine 0,1% of vanadium and above in ore. With a large amount of aluminum present in the ore, the determination became less accurate since the specific activation per g of aluminum is only a factor of 10 less than the activation of vanadium and they can only be distinguished from the character of the decay of the induced radioactivity in the sample with time or, more accurately, by means of the scintillativity in the sample with time or, more accurately, by means of the scintillation spectrometer mentioned above, since the γ-ray energy of V^{52} (1,46 Mev) differs from the γ-ray energy of Al^{28} (1,77 Mev).

A procedure was developed for determining indium in polymetallic ores and concentrates. Indium has a comparatively high activation cross section (145 barns) and the radioactive isotope In^{116} ($T_{1/2}$ = 54 minutes) is convenient for radiometric measurements. Indium is a disperse element and in most known deposits, its content is in hundredths and, more rarely, in tenths of a percent. However, in a series of cases even such low contents may be measured, using the usual (Po-Be)-neutron sources [4].

The radioactivity of In^{116} was recorded by measurement of the γ-rays so as to avoid errors due to the presence of large amounts of zinc in sphalerite ores [on activation with thermal neutrons, zinc gives the isotope Zn^{69} ($T_{1/2}$ = = 52 min), which is a pure β-emitter]. Neutron activation analysis of indium is particularly convenient for controlling processes for the preparation of indium from appropriate ores and concentrates. Here the indium content may be very great. The value of the method lies in the

fact that in a short time it is possible to determine with reasonable accuracy both low and high concentrations of indium without chemical decomposition of the samples.

The results obtained indicate that the method described may be used for determining the content of certain elements in samples of complex composition, at least with not too small concentrations of these elements. The use of a short-lived isotope as an indicator for the element determined makes it possible to develop rapid analysis methods.

The table shows data characterizing the sensitivity of determinations by the method developed, for the elements considered in this work, and also the possible "interfering" elements and methods of allowing for them are given.

Apparently, this method may be used for the control of enrichment and purification processes in the preparation of certain elements, giving, on neutron activation, suitable radioative isotopic indicators (rhodium, rhenium, etc.).

Neutron activation analysis may be applied to rock samples and also in drilling and mining, i.e., under their natural stratification conditions.

In order to measure not only comparatively high, but also low concentrations of elements by the method described, it is necessary to use neutrons sources of higher intensity than the usual (Po-Be)-sources. Now small-size, portable neutron multipliers have been developed, and these will increase the density of a neutron flux by a factor of hundreds [6]. By means of such a source, the sensitivity of the neutron activation method can be increased by 1,5-2 orders, and due to this, the range of measureable concentrations in prospecting and surveying a series of valuable mineral resources sometimes becomes sufficient for the required set of analytical determinations and also for analytical control purposes in the production of valuable elements.

In conclusion, we would like to thank F. A. Alekseev for interest in the work and participating in the discussion of the results.

LITERATURE CITED

[1] Yu. V. Yakovlev, "Investigations in the fields of geology, chemistry, and metallurgy," Reports of the Soviet delegation at the International Conference on the Peaceful Uses of Atomic Energy [in Russian] Acad. Sci. USSR Press, 1955), p. 90; A. A. Smales, "The use of radioactive isotopes in industry, medicine, and agriculture," loc. cit., p. 152; Weiss, Chem. Techn. 9, 262 (1957); E. N. Jenkins and A. A. Smales, Quart. Rev. London, 10, 1, 83 (1956); I. P. Alimarin, Yu. V. Yakovlev, O. E. Zvyagintsev, A. I. Kulak, N. K. Kukharenko, Yu. S. Shimelevich et al., Petroleum Economy 3 (1956); D. I. Leipunskaya and Z. E. Gauér, Sci. Tech. Information Bulletin [in Russian] (State Geo. Tech. Press) 1, 40 (1958).

[2] R. Caldwell, World Petroleum 27, 4, 59 (1956).

[3] J. Terrel and D. M. Holm, Phys. Rev. 109, 6, 20, 31 (1958).

[4]. A. A. Smales, J. V. Smith, and H. Irving, Analyst 8, 539 (1957).

[5] B. S. Dzhelepov and L. K. Peker, Decay Schemes of Radioactive Isotopes [in Russian] (Moscow, Acad. Sci. USSR Press, 1957).

[6] G. N. Flerov, Sessions on the Peaceful Uses of Atomic Energy [in Russian] (Div. Phys. and Math. Sci., Acad. Sci. USSR Press, 1955) p. 170.

Received August 12, 1958

SCINTILLATING GLASS FOR THE DETECTION OF SLOW NEUTRONS*

V. K. Voitovetskii, N. S. Tolmacheva, and M. I. Arsaev

A scintillating glass was prepared and investigated. The glass, with the composition $Li_2O \cdot 2SiO_2$(Ce) may be used for the detection of slow neutrons. The scintillation efficiency of the glass relative to NaI(Tl) under electron excitement, was 1.4%. The ratio of the scintillation yields for electrons and α-particles was 3.8-4. The de-excitation time constant was ~0.15 μ sec. The efficiency of glass 0.1 cm thick, containing lithium with an Li^6 concentration of 90.5%, for thermal neutrons was 82%. For neutrons with an energy of 10 ev, the efficiency of glass 0.5 cm thick was 40%.

All the known solid inorganic scintillators have a crystalline structure. However, in analogy with photoluminescence, one might conjecture that there would also be appreciable light output from certain inorganic compounds, which were not monocrystals or crystalline powders.

We put forward the hypothesis that some types of photoluminescent glasses with a specially chosen composition would be quite efficient scintillators.†

The possibility of using a glass as a scintillator is extremely attractive since the chemical stability and transparency of glass is coupled with great freedom of choice of the chemical composition and relative simplicity of technology, making it possible to obtain blocks of various dimensions and arbitrary form. It is known that among inorganic photoluminescent substances, glasses, as a rule, have the least de-excitation time [3].

The purpose of the present work was the preparation of a scintillating glass, in particular, a high-efficiency slow neutron detector.

A glass for the detection of slow neutrons must contain a certain amount of lithium or boron. One would expect that for a glass the light yield for excitation by electrons to the light yield for excitation by heavy particles would be similar to the ratio characteristic of other inorganic scintillators. To reduce the sensitivity to gamma radiation, it was desirable that the base of the glass did not contain elements of high atomic number.

In choosing the activator and base of the scintillating glass, it was natural to be guided by data on the photoluminescence of glasses. The scintillation characteristics of such glasses obtained later (dependence of scintillation efficiency on the content of the oxygen component; dependence of scintillation efficiency on glass thickness, directly connected with the radiation and absorption spectra; de-excitation time, etc.) were found to be close to the corresponding photoluminescence characteristics and confirmed the possibility of such an approach.

According to Weyl, luminescent glasses may be divided into four groups according to the nature of the fluorescent centers [4]. In glasses belonging to the first three groups, the glass itself does not participate in the luminescence process and the centers of luminescence are: 1) active crystals (crystals of a phosphor of the type ZnS(Ag) dispersed in a glass-like medium)‡ 2) activated crystals (the glass-like medium contains fragments of crystallophosphors, which adsorb activators present in the glass); 3) molecules or atoms, energetically isolated from the glass-like medium.** In glasses of the fourth group the fluorescent centers are ions forming part of the glass.

The scintillating glasses investigated in the present work have ionic fluorescent centers and belong to the fourth group. The structure of such glasses is composed of $(SiO_4)^{-4}$ tetrahedra or of a $(PO_4)^{-3}$ lattice, in whose holes are arranged ions of alkali or alkaline earth elements and activator ions [6].

The composition and the activator of the scintillating glass must be chosen so that the spectrum of the radiation lies in the region of maximum sensitivity of the photomultiplier and does not noticeably overlap the absorption spectrum. The maximal sensitivity of spectrometric photomultipliers with Sb - Cs cathodes (FÉU-C and FÉU-29) corresponds to 3800 - 4200 A [7, 8].

Silicate glasses activated by cerium have a bright blue fluorescence. The absorption spectrum of such a glass lies in the ultraviolet region [9]. Lithium may be introduced into such a glass as the alkali component. On the basis of these considerations, a lithium silicate glass, activated by cerium, was chosen for recording slow neutrons.

* The work was reported at the Second All-Union Conference on Scintillators, November 1957, Kharkov.

† There is little data in the literature on the luminosity of glasses under the action of charged particles. There are few papers on cathodoluminescence of glasses [1]. In discussing work on scintillating glasses, we were told of experiments by S. F. Rodionov, A. L. Osherovich, and B. B. Orlovskii who observed a weak luminosity in a $Na_2B_4O_7$(Tl) glass under the action of an intense beam of α-particles. There is also a report [2] on the use of glass containing uranium for recording of fission fragments.

‡ The $Li_2O \cdot 2SiO_2$(Tl) glass that we obtained belongs to the first group. The recording efficiency for thermal neutrons by such a scintillator 0.2 cm thick was ~10% at quite a low sensitivity to γ-radiation. The de-excitation time constant was ~10 μ sec. The microcrystalline structure of the glass (enamel type) limits the thickness of a transparent layer to 0.2 cm.

** The phosphate and borate glasses, in which an organic scintillator is dissolved, that are described in paper [5], belong to this group.

The carbonates of lithium (analytical grade), calcium, sodium, potassium (chemically pure), and rubidium (pure) and silicon dioxide were used for the preparation of the glasses. Lithium carbonate was recrystallized from water twice. The silicon dioxide was prepared by the following procedure: methyl silicate was synthesized from silicon tetrachloride and methyl alcohol; a fraction with b.p. = 120° and the composition $Si(OCH_3)_4$ was distilled and hydrolyzed with an aqueous solution of ammonia. The silicic acid precipitate was carefully washed with water, dried for 10 - 15 hrs at 120° and fired for 30 min at 600°.

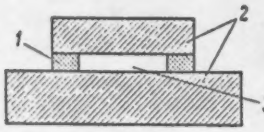

Fig. 1. Form for preparation of glass samples: 1) aluminum ring; 2) chromium plated metal disks; 3) glass.

According to spectral analysis data, the purified Li_2CO_3 and SiO_2 did not contain foreign ions apart from traces of aluminum and magnesium. A weakly acid solution of trivalent cerium ($CeCl_3$) was used for activation of the glass.

The alkali metal carbonates and silicon dioxide were mixed in calculated proportions; to the mixture was added a titrated solution of activator and a certain amount of distilled water. The thick mass obtained was ground in a porcelain mortar for an hour (with a charge of 20 g), dried at 100° and fired for 20 minutes at 800°.

The glass was fused in corundum crucibles in a furnace with a Silit heater at 1250 - 1300°. The completion of the fusion was determined by the clarification of the melt, which usually began 2 - 3 hr after loading of the charge. The prepared glass was poured into a cold metal form (Fig. 1). Samples of glass in the form of disks were rapidly transferred to a muffle furnace, preliminarily heated to 500°, and annealed for 30 min.

By this method we prepared glasses with the compositions:

$$Li_2O \cdot SiO_2,\ Li_2O \cdot 2SiO_2,\ \tfrac{1}{2}Li_2O \cdot \tfrac{1}{2}Na_2O \cdot 2SiO_2,$$
$$\tfrac{1}{2}Li_2O \cdot \tfrac{1}{2}K_2O \cdot 2SiO_2,\ \tfrac{1}{2}Li_2O \cdot \tfrac{1}{2}Rb_2O \cdot 2SiO_2,$$
$$Li_2O \cdot CaO \cdot 2SiO_2.$$

Figure 2 shows the differential amplitude spectrum of pulses from a scintillation counter (photomultiplier FEU-C) with an $Li_2O \cdot 2SiO_2$ glass (1 mole % of cerium), placed in a beam of slow neutrons from a (Po + Be)-source. The peak in the amplitude distribution of the pulses corresponds to the $Li^6(n, \alpha)T$ reaction, whose reaction energy Q = 4.79 Mev. Figure 2 shows that by separating the region corresponding to the peak in the differential or integral spectrum, it is possible to record slow neutrons.

For choosing the optimal glass composition, the dependence of the scintillation efficiency on the silicon oxide content, the character of the alkali component and the activator concentration was determined. The relative change in the scintillation efficiency was characterized by a shift in the peak in the amplitude distribution of the pulses (the glass was excited by the reaction products of neutrons with lithium).

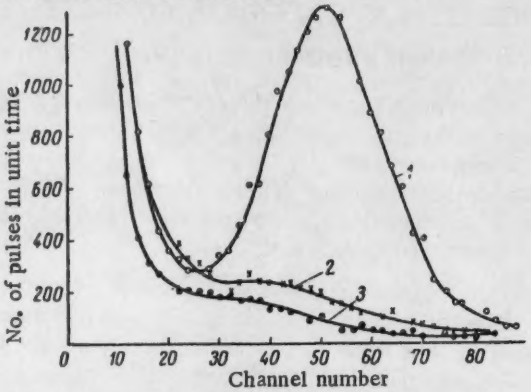

Fig. 2. Amplitude distribution of pulses from scintillation counter: 1) neutrons of a (Po + Be)-source, moderated with paraffin, fast neutrons and C^{12*} γ-quanta (4.45 Mev) recorded; 2) the same conditions but with the counter shielded with a layer of cadmium; 3) paraffin removed, counter shielded with cadmium.

In accordance with the characteristic rule for photoluminescent glasses [10], a glass with the composition $Li_2O \cdot 2SiO_2$ surpasses an $Li_2O \cdot SiO_2$ glass in intensity of luminosity. Apparently, an increase in the SiO_2 content leads to a further increase in the intensity of luminosity. Partial replacement of lithium by other alkali elements or calcium shifts the radiation spectrum into the longwave region and noticeably lowers the light output.

The effect of activator concentration on the scintillation efficiency was investigated on a series of glasses with the composition $Li_2O \cdot 2SiO_2$, 0.2 cm thick, with cerium concentrations of 0.1 - 5.0 mole % (Fig. 3). In the concentration range 0.7 - 1.5 mole %, the change in scintillation efficiency was insignificant. Increasing the

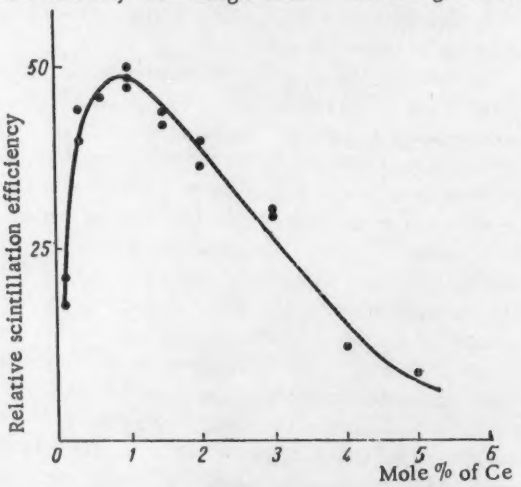

Fig. 3. Dependence of scintillation efficiency on the cerium concentration in the glass.

activator concentration leads to the glass acquiring a yellow color and at a concentration of 5 mole %, the scintillation efficiency is reduced to ½ of the value at the maximum. The results obtained are similar to data on photoluminescence, according to which, the maximal intensity of luminosity is shown by a glass with a cerium content of about 2.0 mole % [11]. A glass with a 1% activator concentration was chosen as the optimal.

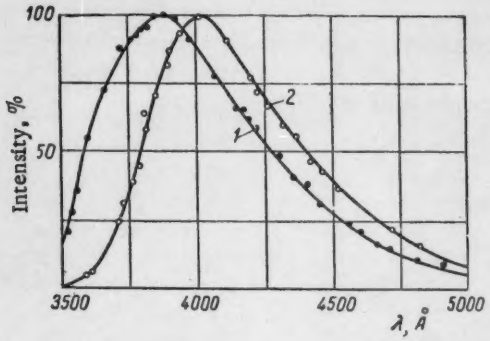

Fig. 4. Radiation spectra of $Li_2O \cdot 2SiO_2$ glass (1 mole % of cerium): 1) sample thickness 0.1 cm; 2) sample thickness 0.5 cm.

The radiation spectra of the glass (Fig. 4) were plotted on a spectrograph with a low pressure mercury lamp, giving predominantly two lines: 2537 and 3650 A ††. The glasses had plane-parallel surfaces and mat sides. For a sample 0.1 cm thick, the radiation maximum lay in the region 3850 - 3900 A . A shift in the maximum of the

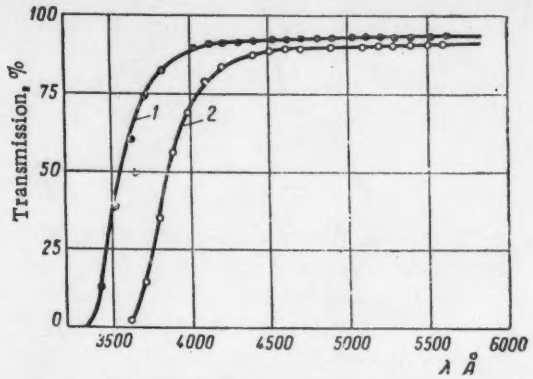

Fig. 5. Absorption spectra of $Li_2O \cdot 2SiO_2$ (1 mole % of cerium): 1) sample thickness 0.1 cm; 2) sample thickness 0.5 cm.

radiation spectrum of a sample 0.5 cm thick may be explained by self-absorption. This agrees with the character of the absorption spectra plotted on an SF-4 spectrophotometer with an incandescent lamp (Fig. 5). The radiation is transmitted quite well by glass of both thicknesses in the maximum sensitivity region of the multiplier.

Figure 6 shows the dependence of scintillation efficiency on glass thickness. The measurements were made with samples (0.2 - 1.6 cm thick), prepared from a single batch by successive castings. With glasses prepared in this way there was some variation (approximately 15%) in the values of the scintillation efficiency for samples of the

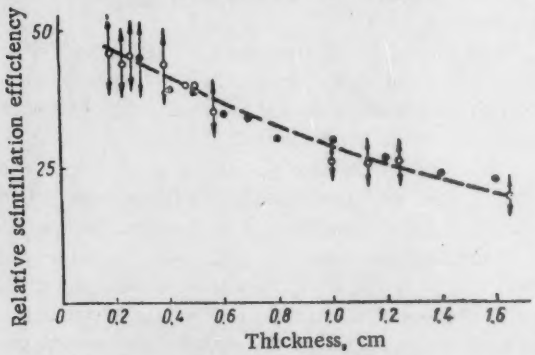

Fig. 6. Dependence of scintillation efficiency on glass thickness: O) experimental data; ●) calculated data.

same thickness, which is apparently explained by unequal distribution of the activator in the melt. It is interesting to note that the experimental values of the scintillation efficiency agree with calculated values (Fig. 6) obtained from the absorption spectra and spectra of radiation under photoexcitation (see Figs. 4 and 5) and the spectral sensitivity of the photomultiplier (Fig. 7).

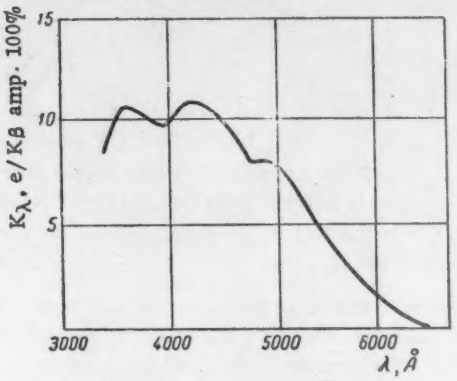

Fig. 7. Spectral sensitivity of an FEU-C spectrometric photomultiplier.

The scintillation efficiency of the glass under electron excitation was compared with the scintillation efficiency of an NaI(Tl) crystal. These measurements were made on a Compton scintillation spectrometer with Co^{60} as a source of gamma radiation; the scattered gamma radiation was registered with an NaI(Tl) crystal and the Compton electrons, in turn, by an NaI(Tl) crystal and the glass. From amplitude analysis of the pulses from monochromatic electrons (920 and 1070 kev), separated by coincidences with gamma quanta scattered through approximately 150° (Fig. 8), it follows that the scintillation efficiency of the glass under excitation by electrons is 1.4% relative to NaI(Tl).

†† The radiation and absorption spectra of glass samples were plotted by M. I. Épshtein, whom we would like to thank.

When the glass was irradiated with alpha particles (the glass was excited with Pu^{239} alpha particles) or simultaneously excited with alpha particles and tritium nuclei (the $Li^6(n, \alpha)T$ reaction), the scintillation yield was reduced by a factor of 3.8 - 4.

By means of DÉSO -1 oscillograph (upper limit of amplifier transmission band approximately 60 Mc/s), the de-excitation time of the glass was measured. The de-excitation time constant was approximately 0.15 μsec.

The efficiency of slow neutron registration by the scintillating glass was determined by the Li^6 content. The calculated efficiency was checked experimentally (measurement accuracy approximately 7%). We determined the coefficient k, the ratio of the number of reactions of thermal neutrons with Li^6 in the glass, leading to pulses from the scintillation counter in the region of the peak to the total number of reactions.

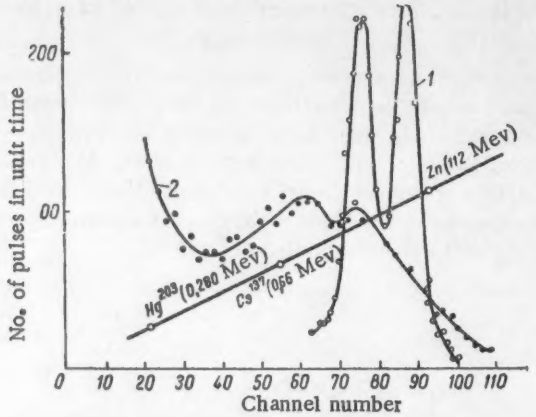

Fig. 8. Amplitude distribution of pulses from electrons with energies of 920 and 1070 kev: 1) for an NaI(Tl) crystal (amplification 320); 2) for glass 0.2 cm thick (amplification 5).

The scintillation counter with the glass was placed in a flux of neutrons from a (Po + Be)-source, moderated with paraffin. The position of the glass was fixed. The number of pulses from the counter in the region of the peak was compared with the number of reactions produced by neutrons in gold foil, irradiated with the same geometry. In the calculation we used the different effect of measurements carried out with a cadmium shield (0.025 cm) and without it. The activity of the gold foil was determined with a scintillation counter with an NaI(Tl) crystal (the counter was calibrated by the beta-gamma-coincidence method and by counting electrons with 4π geometry).

The thickness of the gold foil was chosen so that $N_{Au}\sigma_{Au} = N_{Li}\sigma_{Li^6}$ (N is the number of nuclei per cm^2 and σ the cross section for the interaction of thermal neutrons with Au and Li^6). In this case the equation

$$k = \frac{N_1 - N_1'}{\beta\left(N_2 \frac{e^{0,01t_2}}{1-e^{-0,01t_1}} - N_2' \frac{e^{0,01t_2'}}{1-e^{-0,01t_1'}}\right)} \cdot \frac{S_2}{S_1},$$

is accurate, where N_1 and N_1' are the numbers of pulses from the scintillation counter in unit time, N_2 and N_2' are the numbers of pulses from the gamma-radiation of the gold foil in unit time, t_1 and t_1' are the irradiation times of the gold foil (in hr), t_2 and t_2' are the times between the end of irradiation of the foil and the beginning of the measurements (in hrs), S_1 is the area of the scintillating glass, S_2 is the area of the foil, and beta is the calibration constant of the scintillation counter for gamma-radiation. The symbols without indexes correspond to measurements without a cadmium shield and symbols with indexes, to measurements with a cadmium shield. Within the limits of experimental accuracy, the coefficient k did not differ from unity.

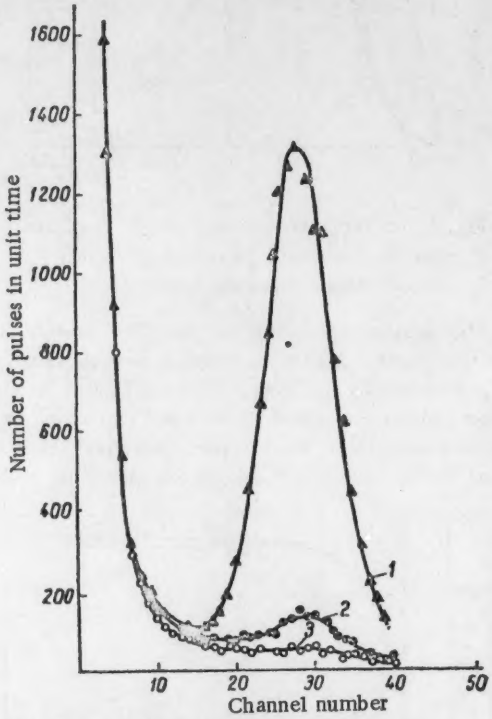

Fig. 9. Amplitude distribution of pulses from a scintillation counter with glass, whose composition contains lithium, enriched in Li^6: 1) registration of neutrons with an energy of 2.5 Mev (D + D reaction), moderated with paraffin, and fast neutrons; 2) scintillation counters shielded with a cadmium layer; 3) scintillation counter shielded with a boron-containing filter.

Glasses were prepared containing lithium with a 90.5 % of the isotope Li^6. Figure 9 shows the amplitude distribution of pulses from a scintillation counter with such a glass, 0.2 cm thick, recording slow neutrons.

The table shows calculated values of the efficiency of scintillating glasses of various thicknesses for a flux of slow neutrons perpendicular to the plane of the glass.

The possibility of detecting slow neutrons over a gamma-radiation background was evaluated experimentally. The

gamma-radiation of a calibrated Co^{60} source (1.17 and 1.33 Mev) was recorded on a scintillation counter with a glass thickness of 0.1 cm with an efficiency of 0.25% (the number of pulses in the region of the peak from the reaction $Li^6(n, \alpha)T$ was determined). Consequently, if thermal neutrons are recorded over a γ-radiation background ($E_\gamma \simeq 1$ Mev) at a ratio of gamma-ray to neutron flux of 10 : 1, then at an 80% efficiency for neutrons (an Li^6 content of 90.5% in the lithium), the contribution of pulses from gamma-rays to the total number of pulses recorded will be 3%.

The sensitivity of the glass for fast neutrons is largely determined by the lithium cross section and for neutrons with an energy of 2.5 Mev with a glass thickness of 0.1 cm the efficiency does not exceed 0.05%.

Efficiency of Scintillating Glasses of Various Thicknesses

Neutron energy, ev	Efficiency of glass with lithium of natural isotopic composition, %				Efficiency of glass with lithium containing 90.5% of the isotope Li^6, %			
	thickness of glass, cm							
	0.1	0.2	0.5	1.0	0.1	0.2	0.5	1.0
thermal	13	24	49	74	82	97	100	100
0.1	7	13	29	50	59	83	99	100
1.0	2.5	5	12	22	27	47	80	96
10	0.8	1.5	4	8	9.5	18	40	64
100	0.3	0.6	1.5	3	3	6	15	27

The authors would like to thank Z. M. Karpova for help in preparing the glasses.

LITERATURE CITED

[1] N. F. Zhirov, Luminophores [in Russian] (Moscow, Defense Industry State Press, 1940) p. 282.

[2] O. Z. Kovacevic and N. V. Kostic, Ceram. Abs., mars 51 (1956).

[3] A. V. Moskvin, Cathodoluminescence, Vol. 1[in Russian] (State Tech. Press, Moscow - Leningrad, 1949) p. 270.

[4] W. Weyl, Industr. Eng. Chem. 34, 1035 (1942).

[5] P. A. Egelstaff. Nucl. Instrum. 1, 197 (1957).

[6] N. I. Kreidl. J. Opt. Soc. Am. 35, 249 (1959).

[7] Electrovacuum Apparatuses, Handbook. Supplement (in Press).

[8] I. Ya. Breido, B. M. Glukhovskii, and L. G. Leiteizen, Radiotechnology and Electronics 10, 1344 (1956).

[9] G. Jaekel, Z. f. Techn. Phys. 7, 301 (1926).

[10] V. V. Vargin and T. I. Veinberg, Bull. Acad. Sci. USSR, Phys. Div. 9, 566 (1945); 12, 203 (1949).

[11] Trans. Sec. Devoted to Memory of Acad. S. I. Vavilov [in Russian] (Moscow, Defense Industry State Press, 1953) p. 134.

Received October 25, 1958

LETTERS TO THE EDITOR

APPARATUS FOR FINE PURIFICATION OF INERT GASES FROM OXYGEN AND WATER VAPOR

N. S. Grachev and P. L. Kirillov

The presence of oxides in apparatuses using sodium and alloys of sodium with potassium strongly increases corrosion of the loop, and, in individual cases, may cause blockage of the passage. In such apparatuses it is necessary to have over the surface of the metal, an atmosphere of inert gases containing the minimal amounts of oxygen and water vapor, to protect the metal from oxidation. The inert gas is used also as a separating medium between the metal and the sensitive elements of the apparatus in measuring the pressure.

Argon, nitrogen, and helium may be used as shielding gases. Argon is the most convenient of them for experimental apparatuses due to its high specific gravity in comparison with air. This makes it possible to open separate parts of the apparatus for a short time (oxidation of the metal does not occur then). For industrial apparatuses, it is advantageous to use nitrogen. It is apparently not advantageous to use helium due to its fluidity, low specific gravity, and high cost. These inert gases contain a definite amount of oxygen and water vapor and may themselves be a source of contamination of the metal with oxides. Thus, "pure" argon contains 0.05-0.1 vol. % of oxygen according to specification data and "technical" nitrogen contains 0.5-1 vol. %. A special apparatus was constructed for purifying these gases to remove oxygen and water vapor.

Principle of action of apparatus. Fine purification from oxygen was based on the chemical interaction of oxygen present in the inert gas first with copper and then with molten alkali metals (sodium and alloys of sodium and potassium). The copper was deposited on silica gel [1]. This absorber was in the form of finely porous balls, ~10 mm in diameter, the surface of which was covered with a thin layer of copper. Copper-covered silica gel has a series of advantages over other solid and liquid absorbers of oxygen and water. Firstly, this preparation is not consumed during operation, since copper oxide is readily reduced with hydrogen. Secondly, it is simultaneously an absorber of water vapor, making it possible to reduce the purification volume. Thirdly, it does not require high-temperature furnaces and raising the operating temperature is not harmful to the preparation. Fourthly, the preparation is cheap and may be prepared readily. Copper-covered silica gel was used for preliminary purification of the gas. Further purification consisted of bubbling the inert gas through liquid sodium or an alloy of sodium and potassium at temperatures of 200-250°. A method of purifying gas in small amounts with a sodium-potassium alloy was described in paper [2].

Construction of apparatus. The apparatus (Fig. 1) consisted of two vessels, filled with the absorbers and installed in a furnace, and one unheated vessel. Vessel I was a cylinder made from steel of grade 1Kh18N9T, 105 mm in diameter and 2.5 m long. Ten kg of copper-covered silica gel was loaded into it. Vessel III was similar to vessel I in dimensions and construction, only with the difference that the inlet tube extended to the bottom. Into vessel III there was poured 5-7 liters of sodium or sodium-potassium alloy. To raise the efficiency of the absorber, this vessel was filled with Raschig rings or bunches of stainless steel wire. The buffer vessel II protected the copper-covered silica gel from metal reaching it in case of a fall in pressure at the gas inlet. A filter 14 for trapping sodium vapor was placed at the outlet of vessel III. The purified inert gas was collected in a receiver, designed for a pressure of 10 atm. The capacity of the receiver was 0.6 m^3. The water seal 18 was used in thereduction of the coppered silica gel. The apparatus was evacuated with a fore-vacuum pump 17.

Operation of apparatus. Before operation, all the spaces in the apparatus filled with air were pumped out with the fore-vacuum pump, then filled with inert gas and again pumped out. The absorbing vessels were heated to 200-250°. With the valves 4, 5, and 6 open, gas was passed through the reducer and into the purifying vessels. The gas flow was controlled with the rotameter R_1. The purified gas was collected in the receiver, from which it was withdrawn as required.

For reduction of the spent (oxidized) coppered silica gel, hydrogen from tank 15 was passed through a reducer and a rotameter R_2 into vessel 1. Valves 8 and 9 were open. The hydrogen consumption was 40 liters/hour. When vessel I had been flushed through with hydrogen for 10 min, the heater of this vessel was switched on. Vigorous reduction of the copper oxide began at temperatures of 250-300°C. The tube connecting vessel I to the water seal became very hot due to steam condensing in it. The water was collected in the water seal and unreacted hydrogen passed out into the atmosphere. The reduction was carried out after purification of 200 m^3 of gas and required about 8 hours. During the reduction of the copper oxide, after approximately each hour vessel I was freed from water vapor by vigorous flushing with a stream of hydrogen. The completion of reduction was

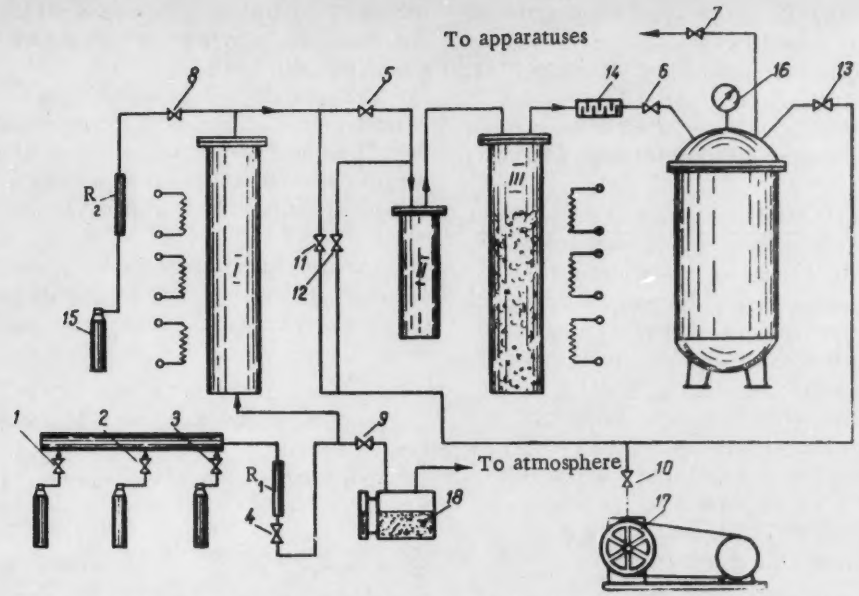

Fig. 1. Plan of apparatus: I) vessel with coppered silica gel; II) buffer vessel; III) vessel with sodium-potassium alloy; R_1 and R_2) rotameters; 1-13) valves; 14) trap for sodium vapor; 15) tank with hydrogen; 16) manometer; 17) fore-vacuum pump; 18) water seal.

easily determined by the fall in temperature of the tube carrying away the hydrogen.

Analysis for oxygen. For determining small amounts of oxygen in the gas we used the known colorimetric method based on the change in color of an ammonia solution of cuprous chloride in contact with oxygen. Flask 2 (Fig. 2), with a previously determined volume, was filled with gas. Then a determined amount of an ammonia solution of cuprous chloride was run from flask 1 into vessel 4. After this, taps 6 and 8 were closed and the solution from vessel 4 was poured into flask 2. The solution was shaken vigorously for several minutes and then run into vessel 4 for comparison with standards.

The percentage oxygen content of the gas analyzed was calculated by the formula

$$\% O_2 = \frac{ak \cdot 100}{V \cdot f},$$

where a is the amount of oxygen, corresponding to the color of the standard solution, k is the correction coefficient for reducing the solution to 0.5 N, V is the volume

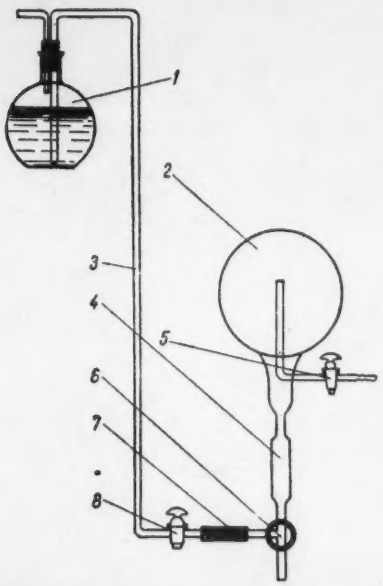

Fig. 2. Apparatus for determining oxygen content: 1) flask with ammonia solution of cuprous chloride; 2) reaction flask (Mugden); 3) connecting tube; 4) vessel for comparison with standard; 5, 6, and 8) taps; 7) connector.

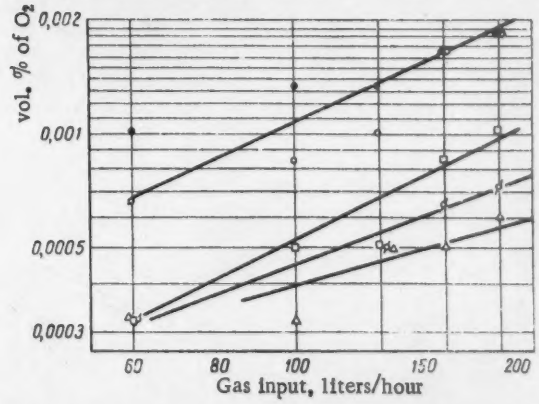

Fig. 3. Dependence of gas purity on rate of passage through the apparatus in the vessel with coppered silica gel at various temperatures (°C).

of the flask in ml, and f is the factor for reducing the gas volume to standard conditions.

The time required for such an analysis was 15-20 minutes. The sensitivity of the method may be raised to 10^{-5}%, which is quite sufficient for analytical purposes. The apparatus was washed with distilled water after the analysis.

Investigation of working conditions for the apparatus. To determine the efficiency of the apparatus under different working conditions, we measured the characteristics, i.e., the dependence of the purity of the gas on the rate at which the latter passed through the apparatus and on the temperature in the absorber vessels. Data from the analyses are presented in Fig. 3, which shows that at an argon input of 60 liters/hour, the oxygen content of the purified gas (argon) was 0.0003 vol. %.

The temperature in the vessel with coppered silica gel was 250-300° and in the vessel with the sodium-potassium alloy, 150-200°. The temperature in the vessels was kept constant while the characteristics were determined. Three analyses were carried out for each set of conditions and the average value of the characteristic was calculated.

The apparatus described has been used over a period of three years. It is simple in operation and at an input of 60 liters/hour guarantees purification of argon to an oxygen content of 0.0003 vol. % and purification of nitrogen at the same input to an oxygen content of 0.003 vol. %.

The apparatus is extremely economical (the sodium-potassium alloy is only replaced after six months operation) and may be used in industry where pure gases are required.

LITERATURE CITED

[1] L. M. Kontorovich and F. M. Rapoport, Factory Lab., 5, 632 (1951).

[2] E. R. Harrison, J. Scient. Instrum. 29, 9,295 (1952).

Received June 21, 1958

PREPARATION OF HEAVY ISOTOPES OF CARBON, SULFUR, KRYPTON, AND NEON BY DIFFUSION IN A VAPOR STREAM

I. G. Gverdtsiteli and V. K. Tskhakaya

An investigation was made of the separation of isotopes in a stream of vapor [1] on a cascade consisting of 80 glass separating pumps. The diaphragm was a steel cylinder, 50 mm high and 16 mm in diameter, and the diaphragm thickness was 0.3 mm. The number of openings, 0.4 mm in diameter, was 500. The total length of the cascade was approximately 6 m. Mercury was used as the operating liquid. The power of the electrical heater, consumed in the separation, was on an average 140 watts.

The separating pumps were connected in cascade by the classical scheme. Gas transfer between pumps was achieved without additional circulating pumps due to the presence of a hydrodynamic drop in pressure across the separating diaphragm. The isotopes were separated at a pressure of 7 - 25 mm Hg.

About 90 cc of gas at S.T.P. was required to fill the cascade to a pressure of 10 mm Hg. As follows from the theory of cascade apparatuses, the time to establish a stationary state was determined by the actual conditions of the separation process.

In the present work, isotopes of sulfur (using SO_2), carbon (using CH_4), and kryton were separated at a pressure of 12 mm Hg. The time to establish equilibrium did not exceed 15 hr.

Since we were not concerned with obtaining a large amount of highly enriched isotopes and the starting gases were present in sufficient amounts, there was no need for a stripping section and practically the whole of the cascade was used as an enrichment section. The container with the mixture to be enriched was connected to the end of the cascade where the light fraction concentrated (the so-called light end).

By means of a special evaporation-condensation system, which made it possible to regulate the magnitude of the currents and the gas pressure in the cascade, the isotope mixture to be separated was circulated through the line of the heavy fraction of the first pump in the cascade. After definite time intervals, when the concentration of the enriched isotope had fallen below a previously calculated value, the starting isotopic mixture was completely replaced by a new portion.

For determing the separation factor, at the first stage the cascade was operated under non take-off conditions. As a result of many measurements of the total separation factor, the average value of this factor for one stage was calculated. The separation factors obtained in the enrichment of various isotope mixtures are shown below.

The values of the separation factors obtained for $C^{13}H_4$-$C^{12}H_4$, Kr^{86}-Kr^{84}, and Ne^{22} – Ne^{20} agree with the rules observed for various isotope systems [1]. The separation factor for sulfur isotopes was somewhat lower than the expected value.

Isotope system	Separation factor for one stage
$S^{34}O_2$—$S^{32}O_2$	1,036
$S^{36}O_2$—$S^{32}O_2$	1,057
$C^{13}H_4$—$C^{12}H_{14}$	1,095
Kr^{86}—Kr^{84}	1,033
Ne^{22}—Ne^{20}	1,16—1,2

Sulfur isotopes were separated in two cycles. In the first cycle sulfur dioxide was enriched in the isotopes S^{34} to 20% (original concentration 4.18%) and S^{36} to 0.66% (original concentration 0.016%). The take-off of the enriched mixture was 80 cc/day. In the second cycle, the concentration of $S^{34}O_2$ was raised to 45% and that of $S^{36}O_2$ to 5.5%. Here, in the first space, the concentration of $S^{34}O_2$ was 12% and that of $S^{36}O_2$, 0.14%.

Kr^{86} was also concentrated in two cycles. In the first cycle, krypton was taken off with a Kr^{86} concentration of 60% (original concentration 17.5%). The take-off was 60 cc/day. In the second cycle the Kr^{86} had a concentration of ~92% and the take-off was 30 - 40 cc/day. In the separation of carbon isotopes, methane with a $C^{13}H_4$ concentration of 2.7% was used as the starting material. In contrast to the previous work, the enrichment was carried out on a cascade of 70 separating pumps. At a take-off of 30 cc/day, the maximum concentration of $C^{13}H_4$ was approximately 90% and at a take-off of 130 cc/day, approximately 75%.

In order to prepare absolute isotopic standards, the isotope Ne^{22} was concentrated. The natural isotope mixture of neon was used as the starting material. The separation was carried out at a pressure of 25 mm Hg. A vessel of 1.1 liters capacity was connected to the circulating loop of the penultimate separating pump and the isotope Ne^{22} accumulated in this. The volume of the reservoir at the light end was 40 liters. When the Ne^{22} concentration had been reduced (<1%), the starting vessel was pumped out and filled with the normal isotope mixture. After two replacements of the volume, the Ne^{22} concentration reached >99.99%.

The approximate values of the separation factor on the cascade at a pressure of 25 mm Hg. was > 10^5. The cascade apparatus was used successfully for the preparation of highly enriched and valuable isotopes, required in small amounts.

The specific separating power of the cascade apparatus was approximately two orders higher than that of analogous apparatuses described in paper [2].

LITERATURE CITED

[1] I. G. Gverdtsiteli and V. K. Tskhakaya, "The separation of isotopes by diffusion in vapors," Collection of Reports to the All-Union Scientific and Technical Conference on the Use of Radioactive and Stable Isotopes and Radiation in the National Economy [in Russian] (Moscow, 1958).

[2] G. Hertz, Z. Phys. 91, 810 (1934); R. J. Sherr, Chem. Phys. 6, 251 (1938); F. Dunn, J. Modli, and R. Potter, Analyt. Chem. 27, 1, 63 (1955).

Received August 9, 1958

PREPARATION OF PLASTIC SCINTILLATORS

E. E. Baroni and V. M. Shoniya

The investigation of the physics of high-energy particles often requires scintillators of large dimensions. In these investigations, wide use is made of the large volume of liquid organic scintillators. A description of methods of preparing and using plastic scintillators (PS) is only given in a few papers, for example [1 and 2].

In comparison with liquid scintillators, PS have a series of advantages, in particular, they are not inflammable and with them there is no evaporation of organic solvents harmful to health. PS may be given any form by mechanical treatment.

For the preparation of PS it is necessary to use a special device, making it possible to carry out the polymerization in the desired volumes. Certainly, such a method presupposes standardization of dimensions, and, to some extent, mass production. In the two-stage process for the production of PS [1], i.e., preliminary polymerization (to form a thick polymerizate) and pouring the thickened mass into a metal mold for the final polymerization, involves a danger of oxidation of the low polymers formed by contact with air.

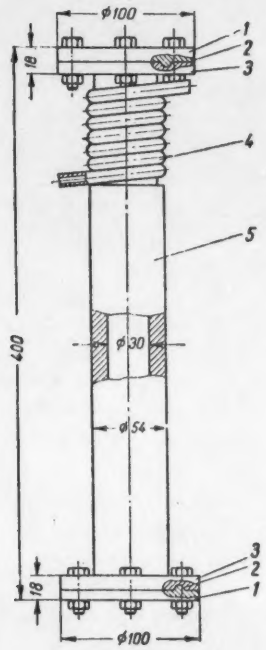

Fig. 1. Mold for preparing plastic scintillators in the form of rods: 1 and 3) flanges; 2) lead washer; 4) coil; 5) metal tube.

In the preparation of large-sized PS by another method [2], organic compounds, in particular, zinc stearate, with a harmful effect on the physical and optical properties of the scintillators were added to the mass to be polymerized. The continuous passage of purified nitrogen or another inert gas through the vessel during the polymerization is undesirable. In addition, in all cases the production of PS with good transparency required additional mechanical treatment of the blank on a lathe. After polymerization, PS of large dimensions required cooling and annealing to remove internal stresses set up during thermal polymerization.

On the basis of results we obtained previously, a method was developed for the preparation of PS by thermal polymerization directly in closed metal vessels. Two forms of metal mold were used (Figs. 1 and 2).

The inside surface of the mold was chromium plated* and carefully polished. A hermetically sealed outlet tube

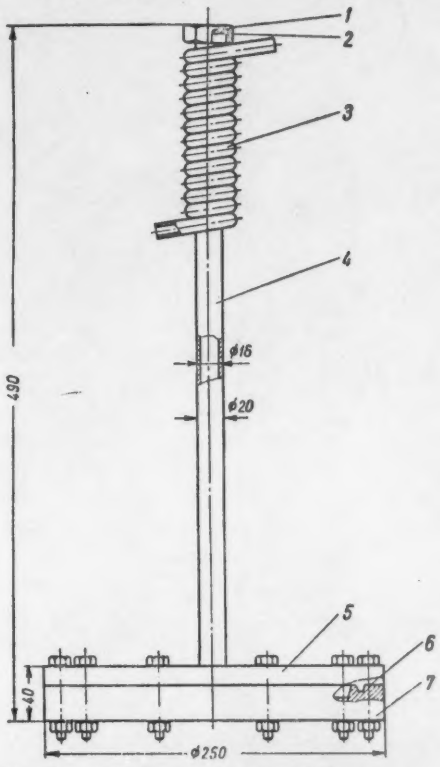

Fig. 2. Mold for preparation of plastic scintillators in the form of disks: 1) nut; 2 and 6) lead washers; 3) coil; 4) metal tube; 5 and 7) flanges.

*Nickel plating is not recommended, since in this case the layer is too soft.

in the upper part of the mold served as a condenser for styrene vapor and low-boiling polymers. A copper coil was used to maintain a constant temperature for cooling the vapor. To prevent the polystyrene from sticking, the surface of the mold was rubbed with cotton wadding, or flannel, soaked with a 1% solution of pure, dehydrated glycerol or polyglycol in pure alcohol. Purified (by distillation under nitrogen at a pressure of ~40 mm Hg) styrene with the luminescing additives dissolved in it was poured into the mold and after the latter had been sealed and the air flushed out with nitrogen, the polymerization was carried out in a glycerol or air bath by gradual heating to 140°C. Cooling water was passed through the coil on the outlet tube. An exothermal reaction proceeded for two hours and then the bath temperature was raised to 200°C, and at this temperature the polymerization process was complete in 20 hours. The temperature was maintained by means of a contact thermometer and a relay. At the end of the polymerization process, the mold was slowly cooled at 100°C and the samples annealed directly in these molds at 80°C for 6 hr, after which the samples were readily withdrawn from the molds at room temperature. The polymerizates obtained in this way were clear, colorless, and homogeneous and did not contain bubbles. The polymerizates were stable in light and air. Additional mechanical treatment of the samples on a lathe was not required. The fluorescent properties of such PS correspond with data presented in paper [3].

LITERATURE CITED

[1] V. K. Kosmachevskii and M. S. Ainutdinov, Apparatus and Experimental Technique, 3, 49 (1956).

[2] G. W. Clark, F. Scherb, and W. V. Smith, Rev. Sci. Instr. 28, 6, 433 (1957); W. L. Buck, and R. K. Swank, Nucleonics, 11, 11, 48 (1953); J. Fischer, Nucleonics 13, 5, 52 (1955).

[3] E. A. Andreeshchev, E. E. Baroni, K. A. Kovyrzina, I. É. Pani, I. M. Rozman, and V. M. Shoniya, Apparatus and Experimental Technique, 1, 32 (1956).

Received August 19, 1958

β-DOSIMETRIC APPLICATIONS OF SEVERAL STANDARD γ-COUNTERS

B. P. Bulatov

The dosimetric characteristics of a 400-SBM-2-type counter (diameter 17.5 mm, length 103 mm, thickness of the steel wall 40-45 mg/cm^2), intended for measurements of low intensities of γ-radiation of a complex or time-varying spectral composition, were examined in reference [1].

As is known [2-5], the sensitivity of C/I (i.e., the ratio of the counting rate C (pulses/sec) to the intensity of the incident radiation I (Mev/cm^2-sec) of counters whose casings are made of a homogeneous material (aluminum, copper, lead) depends a great deal on the spectrum of the radiation.

In order to obtain improved characteristics of the counters, a suitable shield was selected in the above-mentioned work [1], which consisted of tin foil 0.12 mm thick and lead foil 0.25 mm thick separated by an aluminum lining 1.5 mm thick.

In the present work, investigations were made of the dosimetric characteristics of the following standard β-counters, which are in widespread use in laboratory practice: an STS-5 (diameter 10 mm, length of working part 65 mm, thickness of the steel wall 48.5 mg/cm^2), an STS-6 (diameter 18 mm, length of working part 130 mm, thickness of the steel wall 48.5 mg/cm^2), and an MST-17-type end-window counter (diameter 20 mm, thickness of the mica entrance window 5 mg/cm^2).

The counters were shielded by tin foil 87 mg/cm^2 thick and lead foil 280 mg/cm^2 thick. An aluminum lining 1.5 mm thick was placed between the foil sheets.

Radioisotopes from the following group were used as sources of monochromatic γ-radiation: Hg^{197} (0.08 Mev), Hg^{203} (0.28 Mev), Cr^{51} (0.33 Mev), Au^{198} (0.41 Mev), Cu^{64} (0.51 Mev), Cs^{134} (~ 0.72 Mev), Co^{60} (~ 1.25 Mev), Na^{24} (1.38 and 2.76 Mev). The determination of the radiation spectrum of the isotopes was made with the used part of an absorption method under conditions of so-called "good geometry".

The intensity of the incident γ-radiation was measured with a bakelite ionization chamber, the inner conducting surface of which was covered with carbon. The chamber was calibrated with a standard Co^{60} source. In taking the difference between Z_{eff} of the chamber wall and the atmosphere into account, a correction in accordance with the data given in [6] was introduced.

The variation of C/I = $f(E_\gamma)$ is plotted in Fig. 1 for the STS-5 and MST-17 counters, and in Fig. 2 for the STS-6 and 400-SBM-2 counters (the parameters of the latter are approximately the same as the parameters of the STS-6 counter).

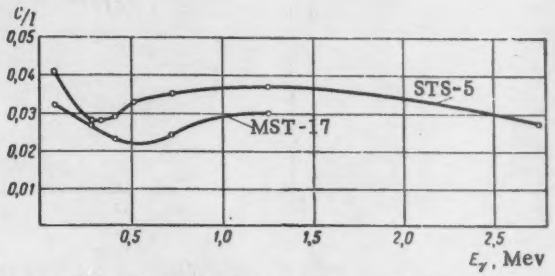

Fig. 1 Dependence of the sensitivity of the STS-5 and MST-17 counters on the energy of the radiation E_γ.

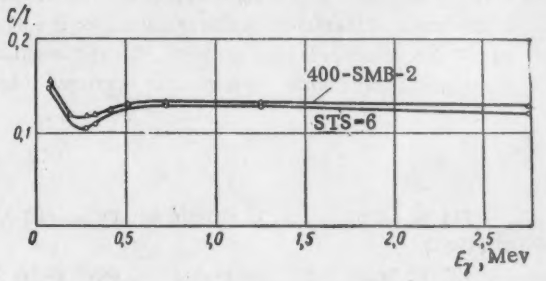

Fig. 2. Dependence of the sensitivity of the STS-6 and 400-SBM-2 counters on the energy of the radiation E_γ.

The deviation in C/I from its average value for the STS-5 counter does not exceed ± 17% for E_γ < 500 kev and ± 18% for E_γ > 500 kev. This deviation for the STS-6 counter is at most ± 15% for E_γ < 500 kev and ± 3.5% for E_γ > 500 kev; for the MST-17 counter, it is ± 16% for E_γ < 500 kev and ± 12% for E_γ > 500 kev.

With the aid of the detectors which have been described, it was possible to determine the intensity of the γ-radiation of a complex spectral composition according to the formula

$$I \text{ Mev/cm}^2\text{-sec} = \frac{C}{\epsilon} \text{ pulses/sec.}$$

The values of ε are listed in the table.

Type of counter	ε	
	E_γ < 500 kev	E_γ > 500 kev
STS-5	0,033 ± 17%	0,033 ± 18%
STS-6	0,12 ± 15%	0,12 ± 4%
MST-17	0,027 ± 16%	0,027 ± 12%

The results listed are applied to the case of normal incidence of the γ-quanta on the lateral faces of the

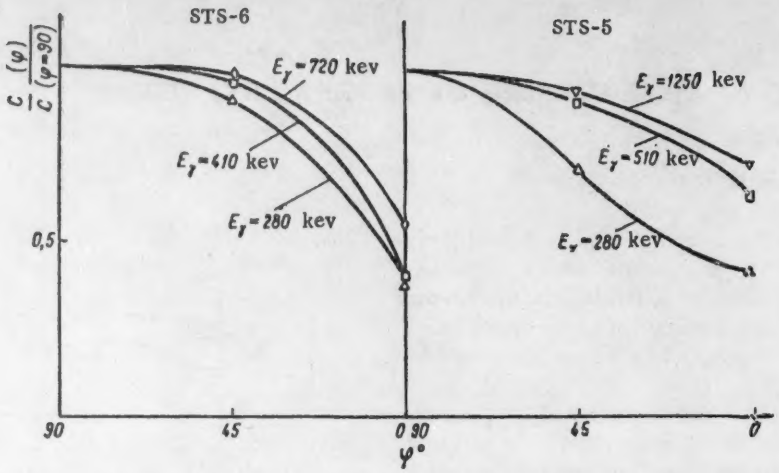

Fig. 3. Dependence of counting rate C on angle of incidence φ, for STS-5 and STS-6 counters.

STS-5 and STS-6 counters or the entrance window of the MST-17 counter. The dependence of the counting rate of the angle of incidence of the radiation for the STS-5 and STS-6 counters is plotted in Fig. 3. The angular functional dependences are somewhat improved if only the working surface is shielded, by leaving the ends of the counters open.

The author is indebted to V. N. Sakharov for his interest in the experiments and in the discussion of the results.

LITERATURE CITED

[1] V. N. Sakharov, J. Atomic Energy (USSR) 3, 7, 61 (1957).

[2] H. Bradt and P. Gugelot, Helv. phys Acta, 19, 77 (1946).

[3] N. Marty, J. phys. et radium 8, 29 (1947).

[4] P. Renard, J. phys. et radium 9, 212 (1948).

[5] W. K. Sinclair, Nucleonics 7, 6, 21 (1950).

[6] H. Laurence, Can. J. Research 15, sec. A, 5, 73, (1937).

Received August 26, 1958

SHIELDING AGAINST γ-RADIATION LEAVING THROUGH THE BASE OF A CYCLINDRICAL SOURCE

D. P. Osanov

Little data has been published concerning the attenuation of the γ-radiation leaving sources of relatively large dimensions. The laws of attenuation are known only for such geometric forms as the truncated cone, the disk, and also for lines and semi-infinite space [1-3]. At the same time, the law of attenuation of radiation has as yet not been formulated for the case of the cylinder, a type of source form which is one of those most frequently encountered in practice. Therefore, shielding calculations for such a source are made by using approximate formulas, which are based on the substitution of a truncated cone [3] (or another geometric solid similar in form to a cylinder) for the cylinder.

A method is considered below for calculating the attenuation of γ-radiation emerging through the base of a cylindrical source. The following assumptions are made in the derivation of the calculating formulas: 1) the active substance is distributed uniformly throughout the volume of the source, 2) each elementary volume dv in the source emits γ-quanta of the same energy.

Let us first consider a nonabsorbing ($\mu_1 = 0$) cylindrical source. The dosage rate at point A (of the figure) is determined by the expression

$$P_A^x = Kq \int_{\varphi} \int_{\theta} \int_{r} \sin\theta \cdot \exp(-\mu_2 h \sec\theta)\, d\varphi\, d\theta\, dr, \qquad (1)$$

where K is the gamma-constant of the radioisotope; q is the specific activity of the source; μ_2 is the linear coefficient of absorption for a narrow beam.

Equation (1) is obtained on the assumption that the center of a spherical system of coordinates is at point A, which is an arbitrary point on the axis of the cylinder. Two cases must be differentiated in integrating with respect to the variable r: 1) for $0 \le \theta \le \operatorname{arctg}^* \frac{R}{b+H}$, r varies from b sec θ to (b + H) sec θ; 2) for $\operatorname{arctg} \frac{R}{b+H} \le \theta \le \operatorname{arctg} \frac{R}{b}$, r varies from b sec θ to R cosec θ.

Thus,

$$P_A^x = 2\pi Kq \int_0^{\operatorname{arctg}\frac{R}{b+H}} \sin\theta \exp(-\mu_2 h \sec\theta)\, d\theta \times \int_{b\sec\theta}^{(b+H)\sec\theta} dr + 2\pi Kq \int_{\operatorname{arctg}\frac{R}{b+H}}^{\operatorname{arctg}\frac{R}{b}} \sin\theta \exp(-\mu_2 h \sec\theta)\, d\theta \times \int_{b\sec\theta}^{R\operatorname{cosec}\theta} dr = P'_x + P''_x. \qquad (2)$$

Equation (1) breaks up into two separate integrals, which correspond to the calculated dosage rate at point A from two bodies: the truncated cone (P'_x), and the solid of rotation with which one must supplement the truncated cone in order to obtain the cylinder (P''_x).

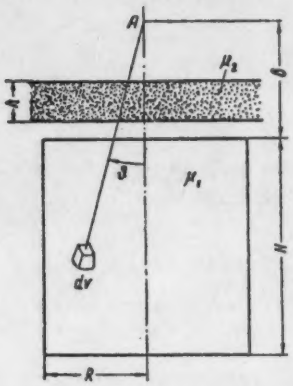

Geometry of the calculation: μ_1-coefficient of absorption of source material; μ_2-coefficient of absorption of shielded material; H- height of source; R- radius of source; b-distance from source to point of measurement; h-thickness of shield; A- point of measurement.

The law of attenuation of γ-radiation from a truncated cone is obtained in a general form in [1]. Consequently, to set up the law of attenuation of γ-radiation for a cylindrical source it is necessary to determine only the second component of sum (2), i.e., the contribution of the solid of rotation to the dosage rate at point A.

By integrating over r and making suitable simplifications, we obtain for the solid of rotation

$$P''_x = 2\pi Kq \int_{\theta_1}^{\theta_2} R \exp(-\mu_2 h \sec\theta)\, d\theta - 2\pi Kq \int_{\theta_1}^{\theta_2} b \operatorname{tg}\theta \exp(-\mu_2 h \sec\theta)\, d\theta = 2\pi Kq \{R \cdot F(\theta_1, \theta_2, \mu_2 h) - b[E_i(-\mu_2 h \sec\theta_2) - E_i(-\mu_2 h \sec\theta_1)]\}, \qquad (3)$$

where $F(\theta_1, \theta_2, \mu_2 h) = \int_{\theta_1}^{\theta_2} \exp(-\mu_2 h \sec\theta)\, d\theta$ is the so-

*tg = tan, Publisher's note.

called Sivert integral, for which detailed tables are available [2]. The integral $\int_{\theta_1}^{\theta_2} \operatorname{tg}\theta \exp(-\mu_2 h \sec\theta)\, d\theta$ is reduced to the exponential integral function Ei. For the sake of brevity, we shall henceforth use the symbols

$$\theta_1 \equiv \operatorname{arctg}\frac{R}{b+H}, \quad \theta_2 \equiv \operatorname{arctg}\frac{R}{b}.$$

For the case of the nonabsorbing truncated cone, the calculations lead to the following result:

$$P'_x = Kq \int_0^{2\pi} d\varphi \int_0^{\theta_1} \sin\theta \exp(-\mu_2 h \sec\theta)\, d\theta \times$$
$$\times \int_{b\sec\theta}^{(b+H)\sec\theta} dr = 2\pi Kq H \{Ei(-\mu_2 h \sec\theta_1) - Ei(-\mu_2 h)\}. \quad (4)$$

One can now write down the expression for the dosage rate created beyond the shield by the nonabsorbing cylindrical source:

$$P_A^x = 2\pi Kq \{R \cdot F(\theta_1, \theta_2, \mu_2 h) +$$
$$+ (H+b) Ei(-\mu_2 h \sec\theta_1) - H \cdot Ei(-\mu_2 h) -$$
$$- b \cdot Ei(-\mu_2 h \sec\theta_2)\}. \quad (5)$$

The efflux of γ-radiation from the nonabsorbing cylinder, i.e., the dosage rate under the previous conditions, but without the presence of the protecting shield, can be obtained in the form

$$P_A^0 = 2\pi Kq \{R(\theta_2 - \theta_1) +$$
$$+ (H+b) \ln\sec\theta_1 - b \ln\sec\theta_2\}. \quad (6)$$

Multiple Compton scattering of the γ-rays in the shield was not taken into account in any of the relations which were given. An exact calculation of this scattering in a finite geometry is impossible at the present time if only for the reason that the dosage accumulation factors for the scattered radiation are known only for an infinite medium and some materials. However, in a number of cases, the multiple scattering of γ-rays can be taken into account for lead, iron, concrete, and water with an accuracy which is completely sufficient for practical work. For this purpose one can employ an analytic representation of of the accumulation factor in the form of a sum of exponentials [4].

In the case of a cylindrical source with self-absorption, one must add another assumption to the ones made earlier: the source material only absorbs, and does not scatter the γ-quanta (the law of absorption in a narrow beam).

The dosage rate at point A (see the figure) created by the cylindrical source (for $\mu_1 \neq 0$) is expressed in the following forms

$$P_A^x = 2\pi Kq \int_0^{\theta_1} \sin\theta \exp(-\mu_2 h \sec\theta)\, d\theta \times$$
$$\times \int_{b\sec\theta}^{(b+H)\sec\theta} \exp[-\mu_1 (r - b\sec\theta)]\, dr +$$
$$+ 2\pi Kq \int_{\theta_1}^{\theta_2} \sin\theta \exp[-\mu_2 h \sec\theta]\, d\theta \times$$
$$\times \int_{b\sec\theta}^{R\operatorname{cosec}\theta} \exp[-\mu_1 (r - b\sec\theta)\, dr = P'_x + P''_x, \quad (7)$$

where P'_x and P''_x are the dosage rates due to the absorbing truncated cone and the solid of rotation, respectively. As was done previously, let us perform the integration over the variable r:

$$P''_x = \frac{2\pi Kq}{\mu_1} \left\{ \int_{\theta_1}^{\theta_2} \sin\theta \exp(-\mu_2 h \sec\theta)\, d\theta - \right.$$
$$- \int_{\theta_1}^{\theta_2} \sin\theta \exp[-\mu_2 h \sec\theta - \mu_1 R \operatorname{cosec}\theta \times$$
$$\left. \times (1 - \operatorname{tg}\theta_2 \operatorname{tg}\theta)]\, d\theta \right\}. \quad (8)$$

It is known that the first integral in Eq. (8) can be expressed with the help of the King functions as:

$$\Phi(x) = \exp(-x) - x \int_x^{\infty} \exp(-t) \frac{1}{t}\, dt.$$

(Tables of the values of the King function are given in [1], [6], and [7].) Then

$$P''_x = \frac{2\pi Kq}{\mu_1} \{\cos\theta_1 \Phi(\mu_2 h \sec\theta_1) - \cos\theta_2 \Phi(\mu_2 h \sec\theta_2) -$$
$$- J_{\theta_1, \theta_2}(\mu_2 h, \mu_1 R)\}, \quad (9)$$

where J_{θ_1, θ_2} represents the integral $\int_{\theta_1}^{\theta_2} \sin\theta \exp \times [-\mu_2 h \sec\theta - \mu_1 R \operatorname{cosec}\theta (1 - \operatorname{tg}\theta_2 \operatorname{tg}\theta)]\, d\theta$. This integral is not expressible in finite form. In connection with this, a fast electronic computer (the "Strela") was used to obtain values of the integral $J(\theta_1\theta_2) =$

$$\int_0^{\theta_1} \sin\psi \exp[-\mu_2 h \sec\psi - \mu_1 R \operatorname{cosec}\psi (1 - \operatorname{tg}\theta_2 \operatorname{tg}\psi)]\, d\psi$$

for a sufficiently wide selection of values of $\mu_2 h$, $\mu_1 R$, and θ_2. The error of the machine calculations was at most 1%. The table lists part of the calculated values of $J(\theta_1, \theta_2)$. It is possible to obtain the necessary value of the integral involved in Eq. (9) by taking appropriate differences from this table, since $J_{\theta_1, \theta_2} = \int_{\theta_1}^{\theta_2} = \int_0^{\theta_2} - \int_0^{\theta_1}$ $= J(\theta_2) - J(\theta_1, \theta_2)$. By combining Eq. (9) with expression (62) for a truncated cone (given in ref. [1]), we determine the dosage rate on the axis of a cylindrical source with account being taken of the self-absorption in the source and attenuation in the shield:

Values of the Integral

θ_2	θ_1	μ_3/h					
		0	1	3	5	7	10
		$\mu_1 R=3$					
arctg 0,3	3	0,0	0,0	0,0	0,0	0,0	0,0
	5	$1{,}884\cdot10^{-12}$	$5{,}662\cdot10^{-13}$	$6{,}787\cdot10^{-14}$	$9{,}089\cdot10^{-15}$	$1{,}217\cdot10^{-15}$	$5{,}967\cdot10^{-17}$
	10	$1{,}209\cdot10^{-5}$	$4{,}386\cdot10^{-7}$	$5{,}771\cdot10^{-8}$	$7{,}593\cdot10^{-9}$	$9{,}991\cdot10^{-10}$	$4{,}769\cdot10^{-11}$
	15	$1{,}923\cdot10^{-3}$	$6{,}837\cdot10^{-4}$	$8{,}640\cdot10^{-5}$	$1{,}092\cdot10^{-5}$	$1{,}380\cdot10^{-6}$	$6{,}201\cdot10^{-8}$
	arctg 0,3	$6{,}118\cdot10^{-3}$	$2{,}166\cdot10^{-3}$	$2{,}714\cdot10^{-4}$	$3{,}402\cdot10^{-5}$	$4{,}264\cdot10^{-6}$	$1{,}893\cdot10^{-7}$
arctg 0,43	5	0,0	0,0	0,0	0,0	0,0	0,0
	10	$5{,}771\cdot10^{-8}$	$2{,}093\cdot10^{-8}$	$2{,}754\cdot10^{-9}$	$3{,}624\cdot10^{-10}$	$4{,}769\cdot10^{-11}$	$2{,}763\cdot10^{-12}$
	15	$8{,}640\cdot10^{-5}$	$3{,}071\cdot10^{-5}$	$3{,}881\cdot10^{-3}$	$4{,}911\cdot10^{-7}$	$6{,}201\cdot10^{-8}$	$2{,}788\cdot10^{-9}$
	20	$2{,}666\cdot10^{-3}$	$9{,}284\cdot10^{-4}$	$1{,}126\cdot10^{-4}$	$1{,}366\cdot10^{-5}$	$1{,}657\cdot10^{-3}$	$7{,}001\cdot10^{-8}$
	arctg 0,43	$1{,}454\cdot10^{-2}$	$4{,}966\cdot10^{-3}$	$5{,}797\cdot10^{-4}$	$6{,}771\cdot10^{-5}$	$7{,}913\cdot10^{-6}$	$3{,}165\cdot10^{-7}$
arctg 1	5	0,0	0,0	0,0	0,0	0,0	0,0
	10	$1{,}217\cdot10^{-9}$	$3{,}624\cdot10^{-10}$	$4{,}769\cdot10^{-11}$	$6{,}275\cdot10^{-12}$	$8{,}257\cdot10^{-13}$	$3{,}941\cdot10^{-14}$
	15	$1{,}380\cdot10^{-5}$	$4{,}906\cdot10^{-7}$	$6{,}201\cdot10^{-8}$	$7{,}840\cdot10^{-9}$	$9{,}912\cdot10^{-10}$	$4{,}457\cdot10^{-11}$
	20	$3{,}921\cdot10^{-5}$	$1{,}366\cdot10^{-5}$	$1{,}657\cdot10^{-6}$	$2{,}011\cdot10^{-7}$	$2{,}442\cdot10^{-8}$	$1{,}033\cdot10^{-9}$
	25	$4{,}500\cdot10^{-4}$	$1{,}515\cdot10^{-4}$	$1{,}720\cdot10^{-5}$	$1{,}954\cdot10^{-6}$	$2{,}219\cdot10^{-7}$	$8{,}548\cdot10^{-9}$
	30	$2{,}329\cdot10^{-3}$	$7{,}563\cdot10^{-4}$	$7{,}989\cdot10^{-5}$	$8{,}458\cdot10^{-6}$	$8{,}977\cdot10^{-7}$	$3{,}118\cdot10^{-8}$
	35	$8{,}972\cdot10^{-3}$	$2{,}767\cdot10^{-3}$	$2{,}642\cdot10^{-4}$	$2{,}540\cdot10^{-5}$	$2{,}457\cdot10^{-6}$	$7{,}490\cdot10^{-8}$
	40	$2{,}616\cdot10^{-2}$	$7{,}608\cdot10^{-3}$	$6{,}490\cdot10^{-4}$	$5{,}606\cdot10^{-5}$	$4{,}907\cdot10^{-6}$	$1{,}305\cdot10^{-7}$
	arctg 1	$6{,}796\cdot10^{-2}$	$1{,}829\cdot10^{-2}$	$1{,}348\cdot10^{-3}$	$1{,}020\cdot10^{-4}$	$7{,}938\cdot10^{-6}$	$1{,}823\cdot10^{-7}$
		$\mu_1 R=5$					
arctg 0,5	5	0,0	0,0	0,0	0,0	0,0	0,0
	10	$7{,}683\cdot10^{-12}$	$2{,}786\cdot10^{-12}$	$3{,}662\cdot10^{-13}$	$4{,}814\cdot10^{-14}$	$6{,}329\cdot10^{-15}$	$3{,}017\cdot10^{-16}$
	15	$8{,}299\cdot10^{-7}$	$2{,}944\cdot10^{-7}$	$3{,}704\cdot10^{-8}$	$4{,}661\cdot10^{-9}$	$5{,}866\cdot10^{-10}$	$2{,}619\cdot10^{-11}$
	20	$1{,}242\cdot10^{-4}$	$4{,}312\cdot10^{-5}$	$5{,}201\cdot10^{-6}$	$6{,}273\cdot10^{-7}$	$7{,}567\cdot10^{-8}$	$3{,}171\cdot10^{-9}$
	25	$6{,}241\cdot10^{-3}$	$2{,}086\cdot10^{-3}$	$2{,}333\cdot10^{-4}$	$2{,}611\cdot10^{-5}$	$2{,}924\cdot10^{-6}$	$1{,}097\cdot10^{-7}$
	arctg 0,5	$1{,}354\cdot10^{-2}$	$4{,}491\cdot10^{-3}$	$4{,}942\cdot10^{-4}$	$5{,}443\cdot10^{-5}$	$5{,}998\cdot10^{-6}$	$2{,}197\cdot10^{-7}$
arctg 0,71	5	0,0	0,0	0,0	0,0	0,0	0,0
	10	$3{,}662\cdot10^{-13}$	$1{,}328\cdot10^{-13}$	$1{,}745\cdot10^{-14}$	$2{,}295\cdot10^{-15}$	$3{,}017\cdot10^{-16}$	$1{,}437\cdot10^{-17}$
	15	$3{,}704\cdot10^{-8}$	$1{,}314\cdot10^{-8}$	$1{,}650\cdot10^{-9}$	$2{,}081\cdot10^{-10}$	$2{,}619\cdot10^{-11}$	$1{,}169\cdot10^{-12}$
	20	$5{,}201\cdot10^{-6}$	$1{,}806\cdot10^{-6}$	$2{,}179\cdot10^{-7}$	$2{,}628\cdot10^{-8}$	$3{,}172\cdot10^{-9}$	$1{,}330\cdot10^{-10}$
	25	$2{,}333\cdot10^{-4}$	$7{,}805\cdot10^{-5}$	$8{,}737\cdot10^{-6}$	$9{,}787\cdot10^{-7}$	$1{,}097\cdot10^{-7}$	$4{,}124\cdot10^{-9}$
	30	$2{,}785\cdot10^{-3}$	$8{,}962\cdot10^{-4}$	$9{,}294\cdot10^{-5}$	$9{,}651\cdot10^{-6}$	$1{,}004\cdot10^{-6}$	$3{,}374\cdot10^{-8}$
	arctg 0,71	$2{,}725\cdot10^{-2}$	$8{,}251\cdot10^{-3}$	$7{,}585\cdot10^{-4}$	$6{,}998\cdot10^{-5}$	$6{,}481\cdot10^{-6}$	$1{,}841\cdot10^{-7}$
arctg 1,67	10	0,0	0,0	0,0	0,0	0,0	0,0
	15	$5{,}866\cdot10^{-10}$	$2{,}081\cdot10^{-10}$	$2{,}619\cdot10^{-11}$	$3{,}296\cdot10^{-12}$	$4{,}148\cdot10^{-13}$	$1{,}853\cdot10^{-14}$
	20	$7{,}567\cdot10^{-8}$	$2{,}628\cdot10^{-8}$	$3{,}172\cdot10^{-9}$	$3{,}827\cdot10^{-10}$	$4{,}619\cdot10^{-11}$	$1{,}937\cdot10^{-11}$
	25	$2{,}924\cdot10^{-6}$	$9{,}786\cdot10^{-7}$	$1{,}097\cdot10^{-7}$	$1{,}231\cdot10^{-8}$	$1{,}382\cdot10^{-9}$	$5{,}205\cdot10^{-12}$
	30	$2{,}994\cdot10^{-5}$	$9{,}651\cdot10^{-6}$	$1{,}004\cdot10^{-6}$	$1{,}045\cdot10^{-7}$	$1{,}090\cdot10^{-8}$	$3{,}681\cdot10^{-10}$
	35	$2{,}024\cdot10^{-4}$	$6{,}166\cdot10^{-5}$	$5{,}739\cdot10^{-6}$	$5{,}366\cdot10^{-7}$	$5{,}040\cdot10^{-8}$	$1{,}464\cdot10^{-9}$
	40	$8{,}638\cdot10^{-44}$	$2{,}474\cdot10^{-4}$	$2{,}042\cdot10^{-5}$	$1{,}699\cdot10^{-6}$	$1{,}428\cdot10^{-7}$	$3{,}542\cdot10^{-9}$
	45	$3{,}150\cdot10^{-3}$	$8{,}270\cdot10^{-4}$	$5{,}781\cdot10^{-5}$	$4{,}125\cdot10^{-6}$	$3{,}009\cdot10^{-7}$	$6{,}199\cdot10^{-9}$
	50	$9{,}538\cdot10^{-3}$	$2{,}263\cdot10^{-3}$	$1{,}308\cdot10^{-4}$	$7{,}859\cdot10^{-6}$	$4{,}935\cdot10^{-7}$	$8{,}489\cdot10^{-9}$
	55	$2{,}856\cdot10^{-2}$	$5{,}848\cdot10^{-3}$	$2{,}596\cdot10^{-4}$	$1{,}256\cdot10^{-5}$	$6{,}678\cdot10^{-7}$	$9{,}766\cdot10^{-9}$
	arctg 1,67	$6{,}710\cdot10^{-2}$	$1{,}190\cdot10^{-2}$	$4{,}109\cdot10^{-4}$	$1{,}641\cdot10^{-5}$	$7{,}671\cdot10^{-7}$	$1{,}019\cdot10^{-8}$

Continued

θ_2	θ_1	$\mu_2 h$					
		0	1	3	5	7	10
		$\mu_1 R=7$					
	10	0,0	0,0	0,0	0,0	0,0	0,0
	15	$4{,}254\cdot10^{-10}$	$1{,}507\cdot10^{-10}$	$1{,}393\cdot10^{-11}$	$2{,}377\cdot10^{-12}$	$2{,}985\cdot10^{-13}$	$1{,}328\cdot10^{-14}$
	20	$2{,}725\cdot10^{-7}$	$9{,}451\cdot10^{-8}$	$1{,}137\cdot10^{-8}$	$1{,}367\cdot10^{-9}$	$1{,}644\cdot10^{-10}$	$6{,}850\cdot10^{-12}$
arctg 0,7	25	$4{,}738\cdot10^{-5}$	$1{,}578\cdot10^{-5}$	$1{,}753{,}10^{-6}$	$1{,}947\cdot10^{-7}$	$2{,}164\cdot10^{-8}$	$8{,}028\cdot10^{-10}$
	30	$1{,}218\cdot10^{-3}$	$3{,}904\cdot10^{-4}$	$4{,}009\cdot10^{-5}$	$4{,}122\cdot10^{-6}$	$4{,}241\cdot10^{-7}$	$1{,}402\cdot10^{-8}$
	arctg 0,7	$1{,}967\cdot10^{-2}$	$5{,}953\cdot10^{-3}$	$5{,}452\cdot10^{-4}$	$5{,}022\cdot10^{-5}$	$4{,}628\cdot10^{-6}$	$1{,}301\cdot10^{-7}$
	10	0,0	0,0	0,0	0,0	0,0	0,0
	15	$1{,}893\cdot10^{-11}$	$6{,}707\cdot10^{-12}$	$8{,}423\cdot10^{-13}$	$1{,}057\cdot10^{-13}$	$1{,}328\cdot10^{-14}$	0,0
	20	$1{,}137\cdot10^{-8}$	$3{,}941\cdot10^{-9}$	$4{,}740\cdot10^{-10}$	$5{,}702\cdot10^{-11}$	$6{,}859\cdot10^{-12}$	$2{,}862\cdot10^{-13}$
arctg 1	25	$1{,}753\cdot10^{-6}$	$5{,}842\cdot10^{-7}$	$6{,}491\cdot10^{-8}$	$7{,}217\cdot10^{-9}$	$8{,}028\cdot10^{-10}$	$2{,}982\cdot10^{-11}$
	30	$4{,}010\cdot10^{-5}$	$1{,}286\cdot10^{-5}$	$1{,}322\cdot10^{-6}$	$1{,}361\cdot10^{-7}$	$1{,}402\cdot10^{-8}$	$4{,}647\cdot10^{-10}$
	35	$6{,}048\cdot10^{-4}$	$1{,}823\cdot10^{-4}$	$1{,}659\cdot10^{-5}$	$1{,}515\cdot10^{-6}$	$1{,}387\cdot10^{-7}$	$3{,}870\cdot10^{-9}$
	40	$4{,}808\cdot10^{-3}$	$1{,}357\cdot10^{-3}$	$1{,}085\cdot10^{-4}$	$8{,}727\cdot10^{-6}$	$7{,}057\cdot10^{-7}$	$1{,}642\cdot10^{-8}$
	arctg 1	$3{,}313\cdot10^{-2}$	$8{,}534\cdot10^{-3}$	$5{,}704\cdot10^{-4}$	$3{,}856\cdot10^{-5}$	$2{,}640\cdot10^{-6}$	$4{,}857\cdot10^{-8}$
	15	0,0	0,0	0,0	0,0	0,0	0,0
	20	$1{,}644\cdot10^{-10}$	$5{,}702\cdot10^{-11}$	$6{,}859\cdot10^{-12}$	$8{,}252\cdot10^{-13}$	$9{,}929\cdot10^{-14}$	$4{,}144\cdot10^{-15}$
	25	$2{,}164\cdot10^{-8}$	$7{,}217\cdot10^{-9}$	$8{,}028\cdot10^{-10}$	$8{,}935\cdot10^{-11}$	$9{,}950\cdot10^{-12}$	$3{,}023\cdot10^{-13}$
	30	$4{,}241\cdot10^{-7}$	$1{,}361\cdot10^{-7}$	$1{,}402\cdot10^{-8}$	$1{,}446\cdot10^{-9}$	$1{,}493\cdot10^{-10}$	$4{,}964\cdot10^{-12}$
	35	$5{,}011\cdot10^{-6}$	$1{,}515\cdot10^{-6}$	$1{,}387\cdot10^{-7}$	$1{,}275\cdot10^{-8}$	$1{,}176\cdot10^{-9}$	$3{,}314\cdot10^{-11}$
	40	$3{,}076\cdot10^{-5}$	$8{,}726\cdot10^{-6}$	$7{,}057\cdot10^{-7}$	$5{,}742\cdot10^{-8}$	$4{,}704\cdot10^{-9}$	$1{,}118\cdot10^{-10}$
arctg 2,33	45	$1{,}538\cdot10^{-4}$	$3{,}982\cdot10^{-5}$	$2{,}699\cdot10^{-6}$	$1{,}858\cdot10^{-7}$	$1{,}302\cdot10^{-8}$	$2{,}503\cdot10^{-10}$
	50	$5{,}850\cdot10^{-4}$	$1{,}365\cdot10^{-4}$	$7{,}583\cdot10^{-6}$	$4{,}344\cdot10^{-7}$	$2{,}577\cdot10^{-8}$	$4{,}004\cdot10^{-10}$
	55	$2{,}147\cdot10^{-3}$	$4{,}299\cdot10^{-4}$	$1{,}806\cdot10^{-5}$	$8{,}143\cdot10^{-7}$	$3{,}976\cdot10^{-8}$	$5{,}020\cdot10^{-10}$
	60	$7{,}320\cdot10^{-3}$	$1{,}213\cdot10^{-3}$	$3{,}630\cdot10^{-5}$	$1{,}250\cdot10^{-6}$	$5{,}047\cdot10^{-8}$	$5{,}450\cdot10^{-10}$
	65	$3{,}011\cdot10^{-2}$	$3{,}650\cdot10^{-3}$	$6{,}560\cdot10^{-5}$	$1{,}623\cdot10^{-6}$	$5{,}545\cdot10^{-9}$	$5{,}535\cdot10^{-10}$
	arctg 2,33	$3{,}876\cdot10^{-2}$	$4{,}455\cdot10^{-3}$	$7{,}255\cdot10^{-5}$	$1{,}684\cdot10^{-6}$	$5{,}600\cdot10^{-8}$	$5{,}539\cdot10^{-10}$

$$P_x=\frac{2\pi Kq}{\mu_1}\{\Phi(\mu_2 h)-\Phi(\mu_2 h+\mu_1 H)+$$
$$+\cos\theta_1\Phi[(\mu_2 h+\mu_1 H)\sec\theta_1]-$$
$$-\cos\theta_2\Phi(\mu_2 h\sec\theta_2)+J(\theta_1,\theta_2)-J(\theta_2)\}. \quad (10)$$

It is important that only tabulated functions are involved in Eq. (10). We now determine the efflux of γ-radiation from an absorbing cylinder at the same point A on its axis. The following expression is obtained for the contribution of the solid of rotation to the dosage rate of γ-radiation:

$$P_0''=\frac{2\pi Kq}{\mu_1}\left\{\cos\theta_1-\cos\theta_2-\int_{\theta_1}^{\theta_2}\sin\theta\exp\times\right.$$
$$\left.\times[-\mu_1(R\operatorname{cosec}\theta-b\sec\theta)]\,d\theta\right\}=$$
$$=\frac{2\pi Kq}{\mu_1}\{\cos\theta_1-\cos\theta_2-J_0(\theta_1,\theta_2)-J_0(\theta_2)\}. \quad (11a)$$

The contribution of the truncated cone to the dosage rate is determined by the expression

$$P_0'=\frac{2\pi Kq}{\mu_1}\{1-\cos\theta_1-\Phi(\mu_1 H)+\cos\theta_1\Phi(\mu_1 H\sec\theta_1)\}. \quad (11b)$$

The addition of expressions (11a) and (11b) gives the expression for the dosage rate on the axis of an absorbing cylinder without a shield:

$$P_0=\frac{2\pi Kq}{\mu_1}\{1-\Phi(\mu_1 H)+\cos\theta_1\Phi(\mu_1 H\sec\theta_1)-$$
$$-\cos\theta_2+J_0(\theta_1,\theta_2)-J_0(\theta_2)\}. \quad (12)$$

Consideration of multiple scattering in the shield for a cylinder with self-absorption can be made analogously to the case of the nonabsorbing cylinder by introducing an analytical expression for the accumulation factor under the sign of the inside integrals in Eqs. (7) and (8).

A simultaneous calculation of the multiple scattering in the cylindrical source itself and in the shield requires a study of the spectral composition of the scattered radiation from the source and the subsequent detection of the "fate" of each of its "lines" in the shield. Since the spectrum of the scattered radiation is complex, even an approximate solution of this problem is very unwieldy. However, in those cases in which the thickness of the shield made of heavy material is sufficiently large, and the energy of the γ-radiation is less than the critical energy for this material, i.e., the energy at which the linear coefficient of attenuation has a minimum value, one may neglect the effect of multiple scattering, inasmuch as the coefficient of attenuation of the multiply scattered components is considerably larger in most cases than the coefficient of attenuation of the primary γ-radiation. The part played by the scattering in the source may prove to be unimportant also in the case in which the dimensions of the source are not very large. Under similar conditions in the calculation of the dosage rate beyond the shield, it is possible to confine the calculation to the self-absorption in the source and the absorption and scattering in the shield.

In conclusion, it must be noted that the rule of the additivity of sources of γ-radiation, which is correct in the case of a nonabsorbing (and consequently, a nonscattering) source, is also correct for the case of a source in which there is self-absorption and self-scattering, at least to within an error of at most 5%. This assertion is based on the results of measurements we made with a cylinder of large dimensions. Of course, this does not refer to cases in which the parts of the source from which is determined the additive dose are shielding each other.

From the expressions obtained for the γ-radiation dosage rate one can determine the amount of error which arises as a result of replacing the cylinder by the truncated cone and the contribution P''_0 or P''_x (which is being determined) to the γ-radiation dosage rate from the solid of rotation. The error can be considerable, as is shown by the calculations. Thus, for example, for a nonabsorbing cylinder with a radius of 0.5 m and a height of 1 m, the the contribution to the dosage rate from the solid of rotation at a point 0.5 m distant from the surface of the base of the cylinder amounts to roughly 150% of the contribution of the truncated cone. If the same cylinder is subsequently filled with an aqueous solution of radioactive cobalt (Co^{60}, $h\bar{\nu}$ = 1.25 Mev), the contribution to the dosage rate from the solid of rotation becomes still larger, and reaches 335% of the contribution from the truncated cone, which is due to the difference in the self-absorption of the truncated cone and the solid for rotation.

LITERATURE CITED

[1] G. V. Groshkov, Gamma-Radiation of Radioactive Bodies [in Russian] (Izd. Leningrad State University, 1956).

[2] R. M. Sivert, Acta Radiol. Suppl. XIV (1932).

[3] Reactor Shielding Design Manual, ed. by Rockwell, N. Y., 1956.

[4] J. Taylor, Application of γ-rays Build-up Data to Shield Design, WARD RM-217 (1954).

[5] H. Goldstein and J. Wilkins, Calculation of the penetration of γ-rays, Final Report, AEC, USA, (1954).

[6] L. King, Phil. Mag. (6), 23, 242 (1912).

[7] N. G.Gusev, Handbook of Radioactive Radiations and Shielding [in Russian] (Medgiz, 1956).

Received January 3, 1958

A NUMERICAL METHOD FOR SOLVING TWO-DIMENSIONAL DIFFUSION EQUATIONS

N. I. Buleev

The investigation of a large number of stationary diffusion processes leads to the solution of a differential equation of the second order

$$\frac{1}{r^{\alpha}}\frac{\partial}{\partial r}r^{\alpha}A\frac{\partial\varphi}{\partial r}+\frac{\partial}{\partial y}A\frac{\partial\varphi}{\partial y}-C\varphi=-F \qquad (1)$$

with linear boundary conditions on a contour

$$m_1\frac{\partial\varphi}{\partial n}+m_2\varphi=U \qquad (2)$$

and conditions on the boundary separating two media

$$[\varphi]=0, \qquad (3)$$

$$\left[A\frac{\partial\varphi}{\partial n}\right]=0 \qquad (4)$$

Here r and y are the independent variables; A, C, F, and U are several piecewise continuous functions of the variables r and y (in which A and C are everywhere positive); the exponent of α is equal to zero or one; the symbol [ ] indicates the difference in the values of the function from one side of the surface of separation to the other; n is the normal to the surface of separation between the different media.

The iteration method of solution is the one in most widespread use. Equations (1)-(4), when written in the form of finite differences, become

$$p_{ik}\varphi_{ik}=a_{ik}\varphi_{i-1,\,k}+c_{ik}\varphi_{i+1,\,k}+b_{ik}\varphi_{i,\,k-1}+d_{ik}\varphi_{i,\,k+1}+f_{ik} \qquad (5)$$

and the n-th approximation for the function φ_{ik} is calculated according to the (n-1)th approximation for the function φ in the neighborhood of the point (i, k) (see for example, [1]). However, the iteration, as described by Eq. (5), converges in many cases quite slowly.

M. V. Keldysh, I. M. Gel'fand, and O. V. Lokutsievskii have developed a method of matrix factorization for solving two-dimensional difference equations of the elliptic type. The difference equation of type (5) is put into difference-matrix form, and is then solved by the method of difference factorization for the one-dimensional diffusion equation [2]. Conveniently, for the case of Eq. (5), the method of matrix factorization proves effective in the case for which the number of net points for one of the independent variables is small

In the present article, a relaxation method (which is a combination of the methods of factorization and successive approximation) for solving the problem will be briefly described.

By a change of variables in Eqs. (1)-(4), their solution by means of finite differences can be reduced to the solution of a system of difference equations of the form

$$-a_{ik}\varphi_{i-1,\,k}-c_{ik}\varphi_{i+1,\,k}-b_{ik}\varphi_{i,\,k-1}-d_{ik}\varphi_{i,\,k+1}+p_{ik}\varphi_{ik}=f_{ik}, \qquad (6)$$

in which the coefficients of these equations satisfy the conditions

$$a_{ik}+b_{ik}+c_{ik}+d_{ik}\leqslant p_{ik}.$$

For simplicity's sake, we will take the region under consideration in the chosen system of coordinates to be rectangular; i.e., the indices i, k in Eq. (6) assume the values

$$i=1,\,2,\,\ldots,\,M,\quad k=1,\,2,\,\ldots,\,N.$$

Since Eq. (6) takes account of boundary conditions (2), we shall assume that

$$a_{1k}=c_{Mk}=b_{i1}=d_{iN}=0. \qquad (7)$$

We shall reduce the solution of Eq. (6) to the solution of a system of first-order difference equations. In order to do this, we shall add to the right and left sides of Eq. (6) the expression

$$\psi_{ik}=r_{ik}\varphi_{i-1,\,k+1}+s_{ik}\varphi_{i+1,\,k-1}-\theta_{ik}(r_{ik}+s_{ik})\varphi_{ik}, \qquad (8)$$

where the coefficient r_{ik} and s_{ik} are for the present arbitrary, while the values of the parameter θ_{ik} are fixed $0\leq\theta_{ik}\leq 1$.

We shall replace the equation obtained by an equivalent system of the form

$$\left.\begin{aligned} z_{ik}&=\alpha_{ik}z_{i-1,\,k}+\beta_{ik}z_{i,\,k-1}+\gamma_{ik}(f_{ik}+\psi_{ik}),\\ \varphi_{ik}&=\xi_{ik}\varphi_{i+1,\,k}+\delta_{ik}\varphi_{i,\,k+1}+z_{ik}.\end{aligned}\right\} \qquad (9)$$

In order that system (9) be equivalent to Eq. (6), the coefficients α_{ik}, β_{ik}, ξ_{ik}, δ_{ik}, r_{ik}, s_{ik} must have the values

$$\left.\begin{aligned} &\alpha_{ik}=a_{ik}\gamma_{ik};\ \beta_{ik}=b_{ik},\ \gamma_{ik};\ \xi_{ik}=c_{ik}\gamma_{ik};\\ &\delta_{ik}=d_{ik}\gamma_{ik};\\ &r_{ik}\gamma_{ik}=\alpha_{ik}\delta_{i-1\ \ k};\ s_{ik}\gamma_{ik}=\beta_{ik}\xi_{i,\,k-1},\end{aligned}\right\} \qquad (10)$$

while the coefficients γ_{ik} are determined by the recurrence formula

$$\gamma_{ik}=\frac{1}{p_{ik}-a_{ik}(c_{i-1,\,k}+\theta_{i,\,k}d_{i-1,\,k})\gamma_{i-1,\,k}-b_{ik}(d_{i,\,k-1}+\theta_{ik}c_{i,\,k-1})\gamma_{i,\,k-1}}. \qquad (11)$$

We will solve the system of equations (9) by the method of successive approximations. In order to obtain the first approximation to φ_{ik}, we shall assign values for φ_{ik} which enter into the right side of the equation for

z_{ik}; in obtaining the second approximation for φ_{ik}, the values of ψ_{ik} are calculated by use of the first approximation, etc. The relative role of the component ψ_{ik} in equations (9) and the convergence of the successive approximations will be determined by the choice of the parameter θ_{ik}.

If the sum of the coefficients a_{ik}, b_{ik}, c_{ik}, and d_{ik} is not much different from p_{ik}, then it is possible to show that the iteration process (9) only converges for values of θ_{ik} near zero. At the same time, one iteration with system (9) is equivalent to 5 or 6 ordinary iterations with Eq (5). The convergence of the iteration process (9) for $\theta_{ik} = 0$ was proved by S. M. Ermakov.

If the value $\theta_{ik} \approx 0.5$ is placed in Eqs. (11) and (9), and the formula of the ordinary iteration (5) is added to Eq. (9), then the iteration process obtained

$$\left.\begin{aligned} &z_{ik}=\alpha_{ik}z_{i-1,\,k}+\beta_{ik}z_{i,\,k-1}+\gamma_{ik}(f_{ik}+\psi_{ik});\\ &v_{ik}=\xi_{ik}v_{i+1,\,k}+\delta_{ik}v_{i,\,k+1}+z_{ik};\\ &\varphi_{ik}=\frac{1}{p_{ik}\gamma_{ik}}(\alpha_{ik}v_{i-1,\,k}+\beta_{ik}v_{i,\,k-1}+\\ &+\xi_{ik}v_{i+1,\,k}+\delta_{ik}v_{i,\,k+1}+\gamma_{ik}f_{ik}) \end{aligned}\right\} \quad (12)$$

will prove quite effective. Practice in solving problems shows that in this case one iteration is equivalent to 10 or 12 iterations of (5).

A sufficient condition for the convergence of the iteration process (12) is the satisfaction of the inequality

$$|z_{ik}^{(m)}| \leqslant \frac{1}{p_{ik}\gamma_{ik}}(P_{ik}+Q_{ik}) < 1, \quad (13)$$

where the functions P_{ik} and Q_{ik} are calculated by the recurrence formulas:

$$\left.\begin{aligned} &Q_{ik}=\xi_{ik}(Q+A)_{i+1,\,k}+\delta_{ik}(Q+A)_{i,\,k+1}+\Sigma''_{ik},\\ &P_{ik}=\alpha_{ik}Q_{i-1,\,k}+\beta_{ik}Q_{i,\,k-1}+A_{ik}, \end{aligned}\right\} \quad (14)$$

in which

$$A_{ik}=\alpha_{ik}A_{i-1,\,k}+\beta_{ik}A_{i,\,k-1}+\Sigma'_{ik}, \quad (15)$$

$$\begin{aligned} \Sigma'_{ik}=&\alpha_{ik}\mu_{i-1,\,k}+\beta_{ik}\nu_{i,\,k-1}+|\beta_{ik}\mu_{i,\,k-1}-\\ &-\alpha_{ik}\theta_{i-1,\,k}(\mu+\nu)_{i-1,\,k}|+\\ &+|\alpha_{ik}\nu_{i-1,\,k}-\beta_{ik}\theta_{i,\,k-1}(\mu+\nu)_{i,\,k-1}|, \end{aligned} \quad (16)$$

$$\begin{aligned} \Sigma''_{ik}=&\xi_{ik}\nu_{i+1,\,k}+\delta_{ik}\mu_{i,\,k+1}+\\ &+|\delta_{ik}\nu_{i,\,k+1}-\xi_{ik}\theta_{i+1,\,k}(\mu+\nu)_{i+1,\,k}|+\\ &+|\xi_{ik}\mu_{i+1,\,k}-\delta_{ik}\theta_{i,\,k+1}(\mu+\nu)_{i,\,k+1}|, \end{aligned} \quad (17)$$

and

$$\mu_{ik}=\alpha_{ik}\delta_{i-1,\,k},\ \nu_{ik}=\beta_{ik}\xi_{i,\,k-1}.$$

As an example of the application of the scheme of (12), we shall give the results of the solution of a problem which is typical in calculations of the spatial distribution of density of thermal neutrons in a reactor (with small absorption of neutrons):

x	0	0.1429	0.2857	0.4286	0.5714	0.7142	0.8571	1.00
$(1-x^2)(1-y^2)$	1.000	0.9796	0.9184	0.8163	0.6735	0.4899	0.2654	0
1st approximation	0.2131	0.2168	0.2010	0.1812	0.1554	0.1190	0.0697	0
2nd approximation	0.3916	0.3905	0.3664	0.3309	0.2810	0.2115	0.1196	0
3rd approximation	0.5335	0.5284	0.4964	0.4464	0.3756	0.2796	0.1556	0
6th approximation	0.7936	0.7802	0.7322	0.6536	0.5428	0.3979	0.2175	0
1st approximation by Eq. (5)	0.0204	0.0202	0.0196	0.0186	0.0171	0.0152	0.0129	0

$$\frac{\partial^2\varphi}{\partial x^2}+\frac{\partial^2\varphi}{\partial y^2}=-2(2-x^2-y^2), \quad (18)$$

$$\left.\begin{aligned} &\frac{\partial\varphi}{\partial n}=0 \quad \text{for} \quad x=0 \quad \text{or} \quad y=0,\\ &\varphi=0 \quad \text{for} \quad x=1 \quad \text{or} \quad y=1. \end{aligned}\right\} \quad (19)$$

[The exact solution of the problem is $\varphi = (1-x^2)(1-y^2)$].

The spacing taken between the coordinate network lines along the x and y axes was $\Delta x = \Delta y = 1/7$, and as a result, a numerical solution for φ was found at 49 points of the region. At points along the x and y axes, the values of θ_{ik} were taken equal to zero, while at the remaining points they were taken equal to 0.5. For the indicated values of the parameter θ_{ik} and the chosen number of computational nodes, the coefficient of convergence of the successive approximations $\lambda_1 = 0.75$. In the solution of the 49 difference equations by the method of ordinary iterations (5), the coefficient of convergence $\lambda_1 = 0.975$. Since $0.75 \approx (0.975)^{11}$ in the present case, one iteration by formula (12) is equivalent to 11 iterations by Eq. (5).

The table lists the values of several approximations for the desired function φ at nodes along the x axis. The first approximation obtained by Eq. (5) is listed for comparison.

In conjunction with extrapolation procedures, and with the help of Eq. (12), the solution of equations of type (18)-(19) can be obtained with sufficient accuracy by about 10-15 iterations.

If the boundary conditions in the original system of equations (1)-(4) have the form $m_2\varphi = U$, then one can apply a more economical scheme of difference factorization for the solution of the problem, in which two systems of form (9) are used alternately. Such a scheme has been investigated by the author previously [3].

The method described for solving two-dimensional diffusion equations can be generalized and applied to diffusion equations in space.

LITERATURE CITED

[1] V. N. Faddeeva, Computational Methods of Linear Algebra [in Russian] (Goztekhizdat, 1948).

[2] O. V. Lokutsievskii, Usp. Matem. Nauk 11, 3, 224 (1956).

[3] G. I. Marchuk, Suppment Nos. 3-4 to the journal "J. Atomic Energy (U.S.S.R.)" (Atomizdat, 1958, chap. 9).

Received October 18, 1958

SCIENTIFIC AND TECHNICAL CONFERENCE ON APPLICATIONS OF RADIOACTIVE ISOTOPES AND RADIATIONS IN AUTOMOTIVE AND TRACTOR ENGINEERING

A. I. Nisnevich and D. I Vysotskii

A professional scientific and technical conference on the applications of radioactive isotopes and radiations in automotive and tractor engineering, convened in Moscow, November 12-15, 1958, called on the initiative of the NAMI (Automobile and Automotive Scientific Research Institute) and NATI (Tractor Scientific Research Institute).

The conference was opened up by M. A. Parshin, director of NAMI, who gave a rundown on the basic trends followed in the use of isotopes and radiations in automotive and tractor engineering practice.

Over 100 participants at the conference, representing scientific research organizations, factories, and institutions of higher learning in various cities of the country, heard and discussed 23 papers presented.

The bulk of the reports were devoted to problems of radioactive isotope applications in the study of wear on automobile, truck, and tractor engine parts. The use of radioactive tracers in that field of research has not only greatly reduced the wear lifetimes of machines, but also provided the possibility of clarifying and studying a whole series of new regularities governing the wear of parts. For example, in a paper entitle "Application of the Technique of Radioactive Isotopes for Determining Wear on D-6 Engine Piston Rings," submitted by I. M. Primakov, the measurement of the rate of piston ring wear during startup of the engine was treated in detail.

The following approach was used in the experiment. Cylindrical radioactive probes, known as "wear tracers," and made from material containing the radioactive isotope Co^{60}, were applied to the outer cylindrical surface (the face) of the piston ring. The dimensions of the probes were: diameter 0.1-1.0 mm, height 1.0-1.5 mm. Fitted onto each piston ring were 12 probes. To record short-term changes in the amount of wear, a Geiger counter (MS-4) was mounted on the lubrication drain path. Recording of radioactive particles in the lubricating oil was carried out by means of a direct-recording device.

Data were given in the report on the amount of wear as a function of lube oil viscosity, crankshaft rpm, and other factors.

Wear on piston-ring sides, which acquires particular importance in engine operation at high speeds, was considered in a paper by B. P. Pakhomov, " The Effect of Operating Conditions of a Diesel Engine on Wear on the Sides of Top Compression Rings."

Activation of the piston rings was accomplished by fitting radioactive probes onto the bottom sides.

On each ring 10 probes were placed. The over-all activity of the material making up the probes amounted to about 10 mC. Part of the engine lubrication oil passed through a reactive oil centrifuge, with the radioactive wear debris being deposited on the walls of the centrifuge. For convenience in recording the emissions of the radioactive particles, the centrifuge was installed at a distance of 1 meter from the engine in a special measuring attachment consisting of MS-4 counters. Variations in the rate of radiation were recorded by a direct-writing recorder.

Piston-ring wear was investigated at different lead angles of fuel injection and at different exhaust-gas, lube-oil, and water temperatures.

The report stated a number of recommendations for the engine under study. It was demonstrated, in particular, that deviations from the rated lead angles of fuel injection could not be permitted at high-speed engine operation; in order to reduce wear on the rings, the engine might be speeded up on the basis of shaft rpm, etc.

A similar arrangement for the measurement of the amount of wear particles (using filter sensors) was described in a paper by A. Kh. Eliava et al., "Study of the Effect of Heating of Fuel Mixture on the Wear of Carburetor Engine Parts." Since a filter from the M-20 engine was used as the filter-sensor, the amount of radioactive wear particles in the lubricating oil was monitored before and after filtration. The authors resorted to a somewhat novel method for activating the piston rings: a groove 0.6 × 0.5 mm, filled with Zn^{65}, was cut into the outer cylindrical surface of a repair-size piston ring. After hot zinc-plating, the series of rings was machined to specifications.

The report furnished data on the effect of heating of the fuel mixture, crankshaft rpm, loading, and of other parameters on engine wear.

B. A. Zakharenko reported on engine wear at intermediate speeds. Tests were performed on engines with the filters removed. Wear on the upper compression piston ring, subjected to prior neutron bombardment, was measured. The specific activity of the piston-ring material was of the order of 0.05 mC/g. To enhance the effectiveness attained in recording the radiation from wear products located in the lubricating oil, the volume of the oil in the measuring gear was taken commensur-

able with the amount of lube oil present in the engine. The temperature of the lube oil in the measuring apparatus was maintained in the neighborhood of +30°C, using an attachment for cooling and heating the oil. The paper gave data on the effect of engine idling time, on the amount of wear during the following start-up period, for engines working with different oils. It was shown, for example, that wear in an engine using MS-20 oil, started cold, is identical to the wear over 4.82 hr of engine operation under normal conditions, and when started warmed-up, is equivalent to wear over 2.22 hr.

The conference heard a paper by D. M. Aronov and V. I. Golov, "Study of the Effect of Anti-Knock Additives on Wear on Engine Piston Rings," and one by R. M. Khromushkin, "Use of the Method of Radioactive Tracers in Research Work on Engines," etc.

Problems involving techniques for studying the wear resistance of the crankshaft connecting rod journal were dealt with in a paper submitted by V.I. Stetsenko and M. M. Rutgaizer. Eight apertures, distributed equidistantly over the circumference of the journal, were made by electro-erosion techniques in a tempered shaft main bearing. Radioactive probes were inserted into the openings. Wear on the bearing journal is estimated by the accumulation of wear particulate matter in the paper filter, around which eight MS-4 counters were positioned. The chamber was shielded by the filter and counters, and was air-cooled. The setup was washed and flushed out after each experiment. Data were furnished in the report on main bearing wear when using gaskets fabricated from different materials and autoradiograms of the gaskets obtained after testing outside the engine compartment were presented.

In a paper entitled "Determination of Rate of Wear on Automotive Engine Crankshaft Journal Bearings Using Radioactive Isotopes (e.g., the ZIL-120 Engine)" V. P. Lebedev and N. S. Zolotukhin reported on a different research technique. Although the shaft main bearing surface was also activated by means of radioactive probes in this case, the probes themselves were mounted along the directrix, in the zone of maximum wear. Eight probes each, measuring 1.2 mm in diameter, were placed on each bearing journal. Special oil traps were used to direct the lubricating grease, carrying the radioactive wear debris, from the bearing journal under test to the counter chamber, and after passage of a mixing agent, the grease was returned to the bearing. The installation of that special lubricating system made it possible to reduce the volume of radioactive grease. The report furnished the results of engine tests in operation at various rpm levels, with different radial clearances, etc.

It is generally known that the findings obtained from test-bed engine tests differ considerably from data obtained in road tests. The greatest interest therefore focused naturally on wear-resistance data for engine parts in road tests in a truck or tractor.

The study of the effect of actual performance factors on the rate of wear on piston rings in tractor operation under road conditions was approached in a report by I. N. Velichkin, I. N. Nabiev, and A. I. Nisnevich. The tests were carried out in winter and summer seasons on the DT-54 tractor, widely used throughout the country, the upper piston rings being fitted with activated (Co^{60}) probes. Nine probes with an over-all activity of the order of 4 mC were mounted on each ring. In preliminary experiments, the oil filter was removed from the engine, and piston-ring wear was determined on the basis of measurements of the rate of radiation from wear particles present in the grease. In the second series of experiments, the engine was tested with a reactive oil centrifuge.

The paper provided data on piston-ring wear under actual road conditions. In particular, the conclusion was drawn that it was necessary to improve the quality of performance of the air purifiers, since piston ring wear, even in the presence of low dust concentration in the air (0.12 g/cubic meter), is three times higher than when the tractor is driven under dust-free conditions. The need for a dust-tight intake path of the engine was pointed out, since even a small amount of unfiltered air sucked into the engine passages leads to a sharp increase in wear; it was demonstrated that piston-ring wear at an ambient temperature of less than minus 10° is almost equal to summertime wear under dust-laden conditions. The circumstance last mentioned points to the need for employing special engine heating hoods.

The report also took up a number methodological questions in the use of radioactive tracers for wear studies. It was shown, in particular, that when a centrifugal filter is inserted into the engine-lubricating system, that filter fails to trap all of the wear particles. Therefore, in estimating parts wear, it is necessary to determine the amount of wear particles present not only in the filter, but also in the engine grease.

The report also showed the possibility of employing a scintillation radiometer for continuous recording of radiation from wear particulate matter trapped in the grease; the radiometer is in that case installed directly in the tractor cab.

A paper submitted by a team of authors (A. K. Andrievskii, D. I. Vysotskii, G. I. Beloglazov, V. I. Golov, V. P. Kaznacheev, and Yu. G. Mochalov) was devoted to the study of automotive-parts wear under road conditions. The tests were conducted using a specially designed on-the-road laboratory.

The on-the-road laboratory was equipped with radiometric equipment and devices for measuring engine speeds, dust content in the air, and ambient air temperatures, roadbed strength, etc. The laboratory was designed to service several vehicles with experimental radioactive parts. In that case, the automotive engines were operated without benefit of oil filters.

Inside the specially shielded measuring devices of the automobile laboratory, one or several filters were installed. These filters were used to carry out a periodic purification of the grease in the experimental engines. The authors of the paper assume that all of the wear products settle in the filter as the grease penetrates the engine and that

measurement of filter radioactivity may consequently provide a good measure of the rate of wear on parts.

The paper furnishes data on the results of tests of air purifiers of different types, in response to different levels of dust content in the air. The air purifiers were tested out on the "Moskvich" automobile, with radioactive piston rings installed in the engine.

In one of the reports (by G. M. Azarevich and A. I. Nishnevich), the results of parts wear studies were presented for parts fabricated from nonmetallic materials, in particular for the sealing ring of the hydraulic power cylinder of a tractor suspension. In addition, the paper discussed the use of scintillation counters. It was shown that for a judicious choice of counter chamber geometry and optimum operating conditions for the recording apparatus, the efficiency achieved in recording wear particles present in the grease by means of a scintillation counter is roughly 80-100 times higher than in the case of a Geiger counter.

A paper submitted by R. A. Srapenyants and S. G. Arabyan discussed a method for evaluation of the propensity of diesel oils to cause fouling of the piston rings. A probe containing radioactive Co^{60} was inserted in the catch of a ring. Geiger counters, connected up to a direct-writing recorder, were mounted in two mutually perpendicular planes outside the engine block. The moment of piston ring fouling was established on the basis of the impeding of the piston ring travel in the piston groove. The report gave results of tests on different greases, as well as recommendations on regrease periods for tractor engines.

A study of the factors affecting wear on lubricating surfaces was reported in a paper by V. S. Zavel'skii and R. S. Ramai.

Tests on oils with different additives were carried out on a laboratory stand. One of the samples under study (a bushing) was activated. Wear was determined in terms of the accumulation of radioactive particulate matter in the grease. Several hypotheses on the mechanism involved in parts wear were discussed in the paper.

The use of radioactive emissions in the field of flaw detection are of great significance. This question was treated at the conference in a paper submitted by. S. V. Rumyantsev. A paper by A. Ya. Sergievskii dealt with problems of the use of gammas at the Likhachev Automotive Works.

The conference also heard reports on the use of radioactive isotopes and emissions in the study of processes of metal finishing (A. L. Chestnov), in the study of the pattern of distribution of carbon in casehardened steel (V.G. Kostogonov), for inspection of parts dimensioning during machining operations (V. V. Kondashevskii, A. N. Chertovskikh), for estimating the quality of detergents used in the automotive and tractor industry, etc.

A good deal of attention was devoted at the conference to problems arising in designing and equipping laboratories and establishing safety procedures in carrying out the studies. In addition to a report by N. I. Leshchinskii, E. A. Spitsyn, and A. S. Shtan', entitled "Basic and Technical Solutions in the Design of Laboratories for Machine Parts Wear Studies," those questions were thrashed out in discussions and treated in a number of other communications.

Some of the papers reported on quite novel problems in radioisotope applications. For example, in a paper entitled "Radioactive Isotopes in Automobile and Tractor Practice," (submitted by D. I. Vysotskii, V. S. Zavel'skii, A. I. Nisnevich, and Yu. S. Zaslavskii) a discussion was advanced on the need for developing some "pure" technique for determining wear, based, for example, possibly on the introduction of some element with a large capture cross section for thermal neutrons into the material of the part under study, and subsequent bombardment of the wear particles followed by measurement of the induced radioactivity. In that case, the part under study will not be radioactive, and health physics measures will not be paramount in importance.

A paper by B. A. Zakharenko outlined the principles involved in utilizing pulse-height discrimination for the simultaneous measurement of wear on two different parts, etc.

The conference drew up a balance sheet for the application of radioisotopes and radiations in automotive and tractor engineering, and took note of further measures to be taken in broadening the scope of that work.

SOVIET ELECTRONIC INSTRUMENTS FOR USE IN NUCLEAR PHYSICS ON DISPLAY AT THE 1958 WORLD'S FAIR

Electronic equipment developed and manufactured in the USSR, including instruments widely used in experimental nuclear physics and in nuclear engineering, were demonstrated at the Brussels 1958 World's Fair.

These instruments stimulated a good deal of interest, and were rated highly by foreign specialists. The international Jury of the World's Fair awarded 25 prizes to the Soviet Union for exhibits in the "Radioelectronics" section, including 6 of the highest prizes, the "Grand Prix," six second-order prizes, "Honorary Diplomas of the 1958 World's Fair," 8 gold and 5 silver medals.

World's Fair prizes were awarded to a number of instruments used in experimental nuclear physics and in nuclear engineering.

The third highest award was granted to the following vacuum-tube products:

-a photoelectronic multiplier with a threshold response of up to 10 lamberts and an integral sensitivity over the range of 0.4 - 10,000 amp/lamberts;

-13L0101M millimicrosecond oscillograph tubes, which make it possible to display unit processes 10^{-11} sec in dura-

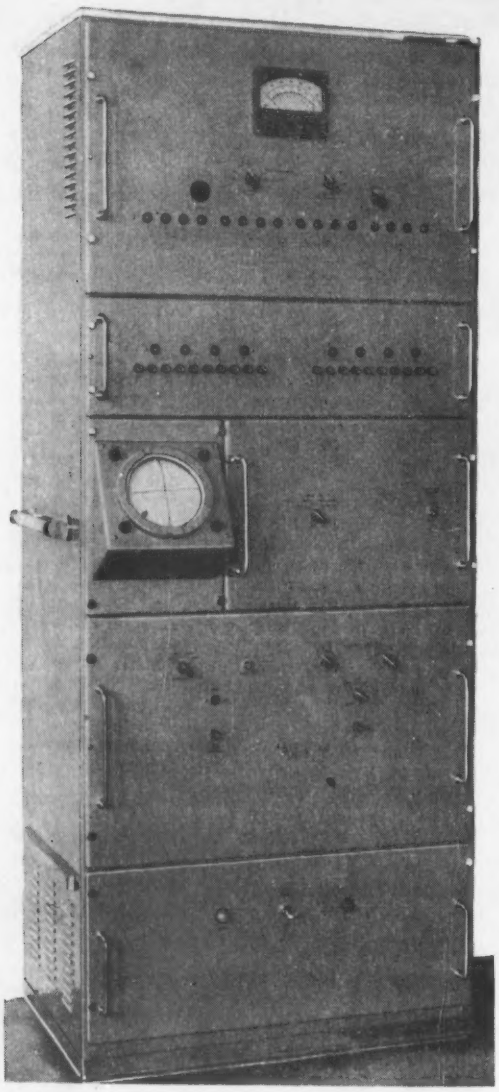

Fig. 1. Hundred-channel pulse amplitude analyzer, AI-100, with ferrite-core memory storage.

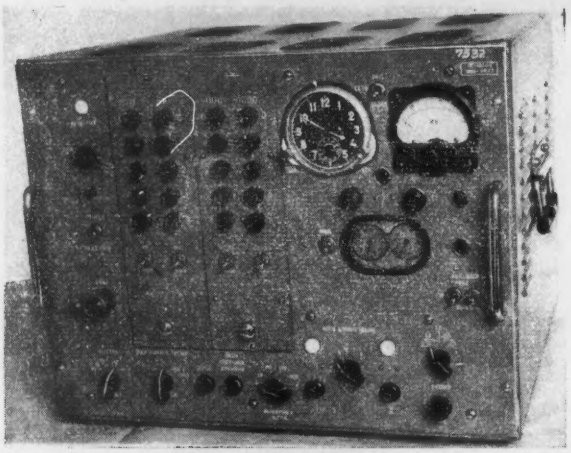

Fig. 2. PS-10000 scaling instrument.

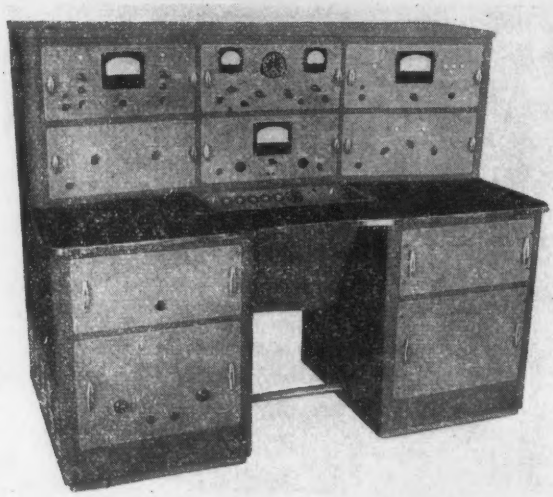

Fig. 3. SGS-1 scintillation gamma spectrometer.

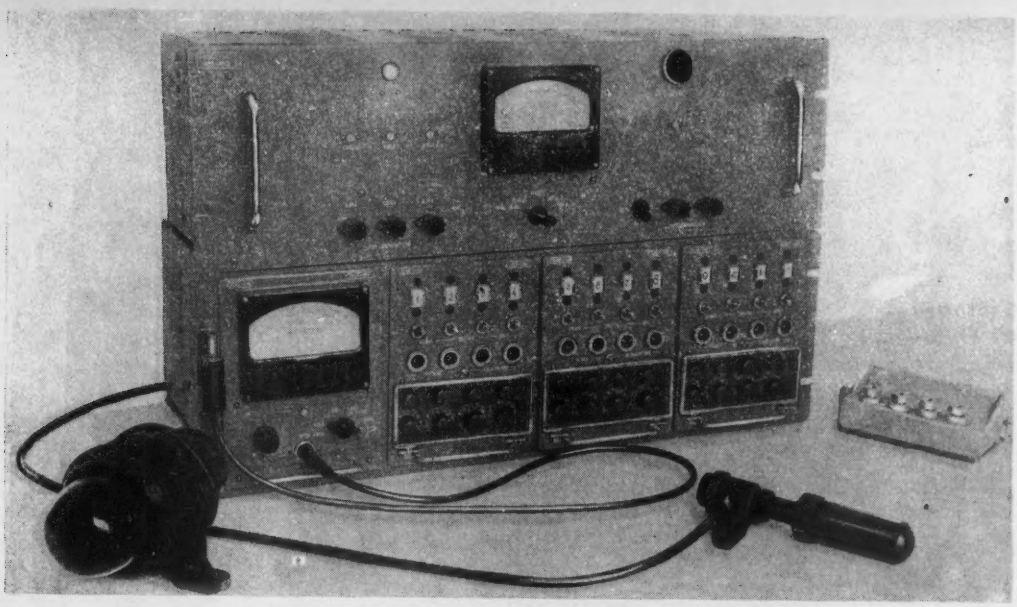

Fig. 4. Signal-measuring USID-1 radiation monitoring equipment.

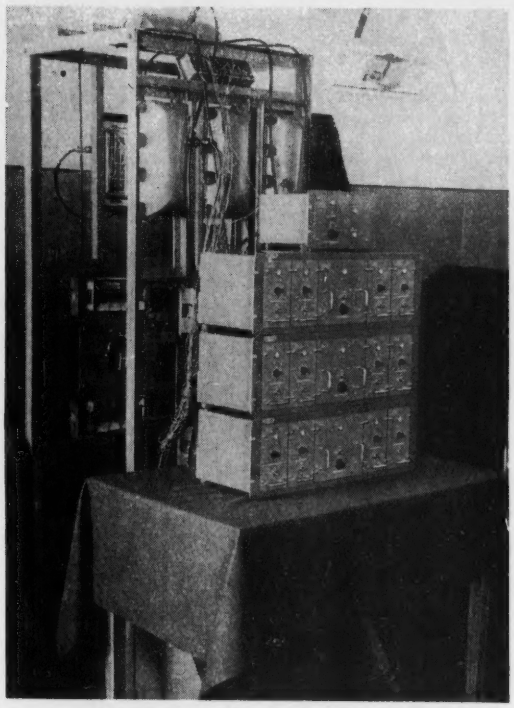

Fig. 5. SU-1 automatic signal device for monitoring radioactive contamination.

tion on the screen. The speed of travel of the flying spot on the screen in those tubes is greater than the speed of light;

-coronal discharge stabilizers, making it possible to stabilize voltages in time up to 0.01%.

Second prizes, i.e., "honorary diploma of 1958 World's Fair," were awarded to the measuring devices:

-GSS-15, GSS-27, and GSS-28, standard signal generators, with a bandwidth of from 16 to 7500 Mc;

-wideband SGShD signal generator, 5 - 10 wt rated power with bandwidth of 30-400 Mc;

-a hundred-channel pulse amplitude analyzer with ferrite-core memory, AI-100 model (Fig. 1). The device has the following engineering specifications: capacity of each channel 10^4 pulses, average dead time 70 microseconds, average input load 10^4 pps, amplitude range of input pulses from 10 mv to 100 v, nonlinearity of amplitude characteristic 2%, instability of channel width ± 1.5%;

-PS-10000 scaling instrument (Fig. 2), with resolving time from 1 to 200 microseconds, and input pulse range from 1 mv to 100 v. Pulse recording by means of electromechanical counter and neon tubes. The instrument incorporates a time relay to enable automatic setting of the counter at intervals of 10, 30 sec, 1, 2, and 5 min;

-broadband USh-2 pulse amplifier, with built-in discriminator. The device makes it possible to amplify pulses of 5 to 40 microseconds width. The gain is controlled within a range of 50-15,000;

-a two-crystal SGS-1 scintillation gamma-ray spectrometer (Fig. 3), with high stability and linearity (up to 100 v across output). The resolving time of the coincidence circuit in this spectrometer is approximately 10^{-7} sec. FEU-S and FEU-11 phototubes may be used as sensors;

-a USID-1 signal measuring radiation monitoring equipment (Fig. 4) designed for determining the level of contamination due to radioactive substances. The device is designed for simultaneous operation on 12 channels;

-an SU-1 automatic signal device for monitoring the contamination of the surface of the body or of the clothes

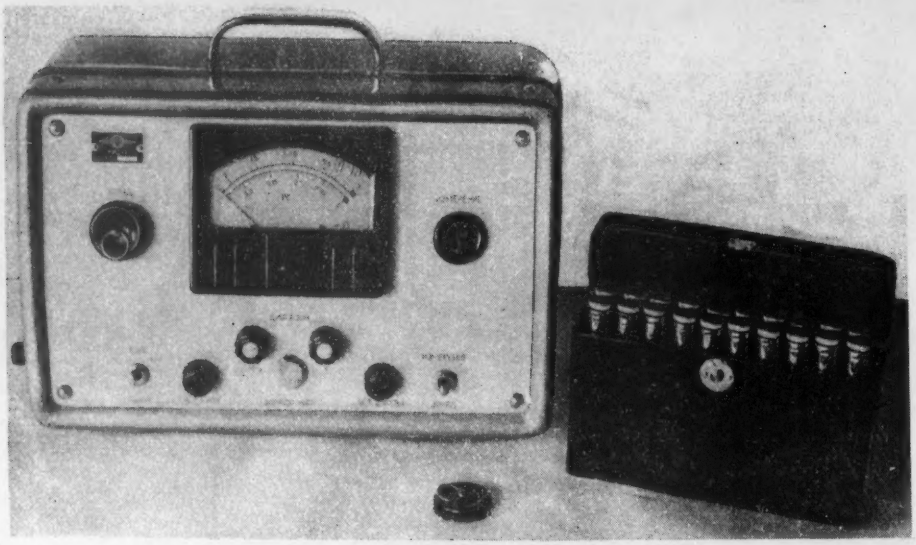

Fig. 6. KID-1 kit for individual radiation monitoring.

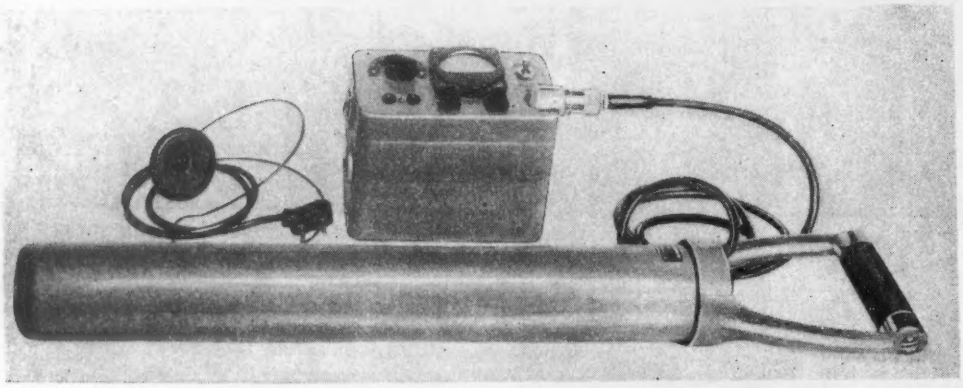

Fig. 7. Portable scintillation prospecting SRP-1 radiometer.

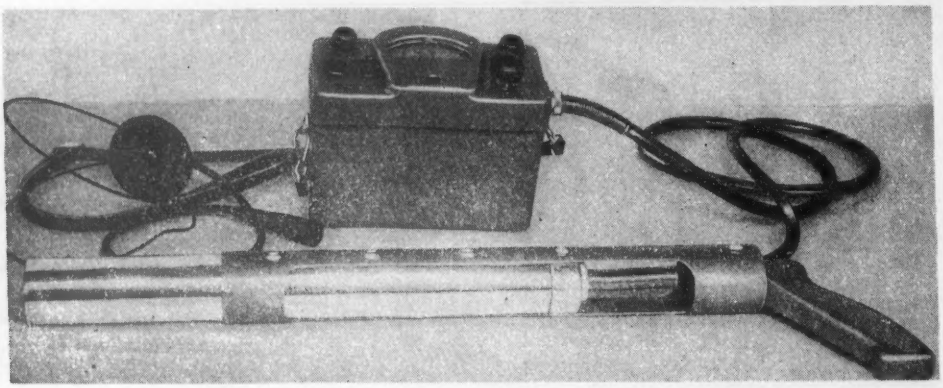

Fig. 8. Portable SRP-2 scintillation prospecting radiometer.

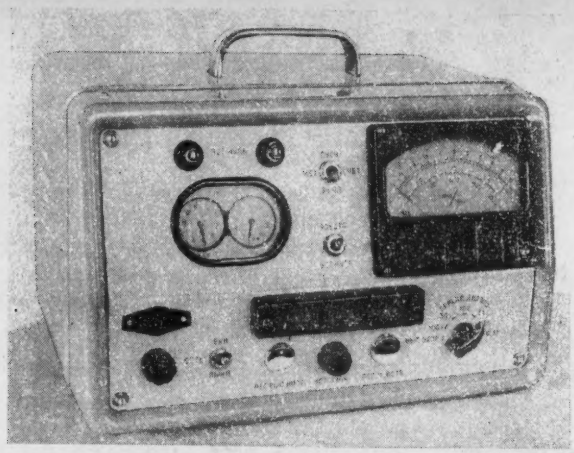

Fig. 9. "TISS" device for measuring contamination of surfaces by alpha and beta emitters.

Fig. 10. RM-1-M medical x-ray meter.

of personnel by beta and gamma emitting substances. The setup consists of a monitoring unit, a high-voltage rectifier, 12 sensors, and a photo resistor chamber. The instrument operates in the presence of an outside gamma-ray background intensity of up to 0.4 millicuries/sec;

-a KID-1 individual radiation monitoring kit (Fig. 6) for measurement of the dosage to which personnel are exposed during a working day, in the presence of x-rays and gammas. The kit consists of a charge-measuring device and a set of back-to-back ionization chambers for individual radiation monitoring. The ranges of total dose measurement are 0.02-0.2 r and 0.2-2 r for the respective chambers. The self-charge of the chambers over a 24-hour period does not exceed 3% of the scale value. The diameter of the double individual chamber is 15 mm, the length 120 mm, weight 25 grams;

-SRP-1 (Fig 7) and SRP-2 (Fig. 8), scintillation prospecting radiometers, designed for discovery of radioactive matter in geological ore prospecting. The radiometers record gammas of 50 kev energy and hard betas. The range of gamma intensity measurement extends to 1250 millicures/hour. The radiometer casings are leaktight and may be immersed in water, along with the cabling, to a depth of 2 meters;

-a "TISS" device (Fig. 9) for measuring contamination of clothing, hands, and surfaces by alpha- and beta-emitting substances. The range of measurement of the mean rate of arrival of pulses extends from 60 to 100,000 ppm. The instrument makes it possible to measure beta contamination of surfaces in the presence of a gamma background, and is equipped with attachments giving an alarm signal when a preset permissible level of contamination is exceeded. ZnS phosphors with the FEU-19 photomultiplier tube and a proportional counter are used as sensors;

-an RM-1-M roentgenometer (Fig. 10) for medical purposes. The device makes it possible to measure doses of x-ray and gamma-ray radiation, and to automatically stop irradiation as soon as the desired dosage is reached. The measurements range is from 0.001 r to 50,000 r.

The Gold Medal was awarded to several radiation measuring devices, including the following:

-a short pulse GKI-4B generator for measuring transients, for testing and adjusting broadband amplifiers, pulse-height analyzers, discriminators, and other electronic equipment. Pulse duration $(7\text{-}100)\cdot10^{-9}$ sec at a pulse repetition rate of 200 cps;

-a GI-ZM pulse generator for controlling and testing various types of pulsing equipment;

-an IBM-2 pulse power measuring device for high-frequency oscillators in the 30 to 1000 Mc bandwidth. Range of power measurement covers 0.5-500 kw.

-an AP-1 attenuator for smooth variation of high-frequency signal power. Signal attenuation is from 15 to 120 db.

-an ASChKh-1 spectrum analyzer and frequency characteristic analyzer for visual observation of the spectrum of periodic oscillations in the 20 –20,000 cps band of sound frequencies. The dynamic resolving power in the subband-widths is 12, 60, 100, and 400 cps, respectively. The device is compact and general-purpose adaptable;

-a portable GTI-2 halide leak detector, with a sensitivity to (freon) leakage of 0.5 gram per year.

HYPERFINE-GRAINED EMULSIONS

At the Radium Institute of the Academy of Sciences of the USSR (laboratory of N. A. Perfilov), three types of hyperfine-grained emulsions have been developed for purposes of nuclear research: P-9o "fragment"; P-9ch "sensitive," and P-R "relativistic," manufacture of the emulsions being assigned to the Kinofabrika [photofilm factory] No. 2.

The general characteristics of all three types of emulsions are: AgBr percentage by weight, 83%; specific weight of emulsion, 3.8 g/cm^3; most probable size of microcrystals in P-9o and P-9ch emulsions, 0.04, 0.06, and 0.08 microns, in P-R emulsion, 0.08 microns; pH of emulsion, 4.2; transparency-half-value layer of 70 microns at a wavelength of 800 millimicrons.

The emulsions are developed by the temperature method, using ID-19 developing agent with reduced soda content.

The photosensitivity of the emulsions in GOST units is, for P-9o, $0.12 \cdot 10^{-3}$, for P-9ch, $2 \cdot 10^{-3}$, and for P-R, $10 \cdot 10^{-3}$. Photosensitivity is determined on the characteristic curve at the point corresponding to a density of 0.2 above the density of fogged film.

The recording properties of the emulsions are entered in the Table. The sensitivity is determined by the minimum energy losses at which a track perceptible against the background fog appears. The discriminating properties of the emulsions are determined by the length and slope of the linear range of the function $\frac{\Delta N}{\Delta R} = f\left(\frac{\Delta E}{\Delta R}\right)$, plotted on semilogarithmic coordinates, since it is precisely in that interval that optimum conditions exist for distinguishing particles of different energies and of different origin. The discriminating power may be different for a given emulsion sensitivity.

The storage life of the emulsions are: for P-9o, over 12 months (without special precautions, under ordinary laboratory conditions); for P-9ch, over 6 - 8 months; and for P-R, over 4 - 5 months after preparation, if sensitization is carried out immediately after irradiation in triethanolamine.

Type of emulsion	Sensitivity kev/μ	Discriminating Properties		Stopping power relative to Ilford emulsion	Average Ag grain size, in particle tracks with minimum ionizing power, μ
		linear interval from $(dE/dR)_{min}$ to $(dE/dR)_{max}$, kev/μ	tangent of slope of linear interval		
P-9o	15–20	15–150	1.45	~0.94	0.26 ± 0.05
P-9ch	1–2	2–12	1.78	~0.94	0.29 ± 0.04
P-R	0.25	0.2–6	1.25	~0.83	0.32 ± 0.04

RADIOGENIC LEAD IN NONRADIOACTIVE MINERALS AS A CRITERION IN EXPLORATION OF URANIUM AND THORIUM DEPOSITS*

Much attention has been devoted recently to the development of geochemical methods in prospecting for radioactive ores. In particular, the possibility of using the isotope abundance of different elements for the evaluation of the capabilities inherent in ore regions is being studied (P/773, P/776). Positive results have been scored in that sense in the use of radiogenic lead present in nonradioactive minerals as a yardstick in prospecting (P/773).

Lead, as we know, exists in four isotopes: Pb^{204}, Pb^{206}, Pb^{207}, and Pb^{208}. As a result of constant radioactive decay going on in the earth's crust, the amount of isotopes Pb^{206}, Pb^{207}, and Pb^{208} is steadily increasing. It has become accepted practice to carry out investigations on the basis of the last three isotopes, since the amount of Pb^{204} available is usually very scanty.

Investigations of lead present in nonradioactive minerals such as galena, etc., originating in occurrences where uranium and thorium are absent, have demonstrated that the data of the isotope assay of the mineral, superposed on a ternary diagram, form a slender sickle-shaped figure OXY (Fig. 1). All leads whose isotope assays may be placed within that figure have been conventionally termed ordinary lead.

The data of the isotope assay of lead in nonradioactive minerals from uranium and thorium occurrences, superposed on a ternary diagram, display a basically different pattern (Fig. 2). We find that they yield a series of figures passing far beyond the confines of the sickle-shaped area assigned to ordinary lead, and spill over into the field assigned to uranium or thorium. Consequently, if in the course of studies of lead present in nonradioactive minerals from some region it is discovered that the isotopic assay data for that lead form figures characteristic of lead in radioactive occurrences, then we may justifiably expect that radioactive ores may be discovered in that area.

Then, if the isotopes analyses fall over into the U field on the ternary diagram, it is most probable that uranium deposits will be discovered in the region; or thorium depos-

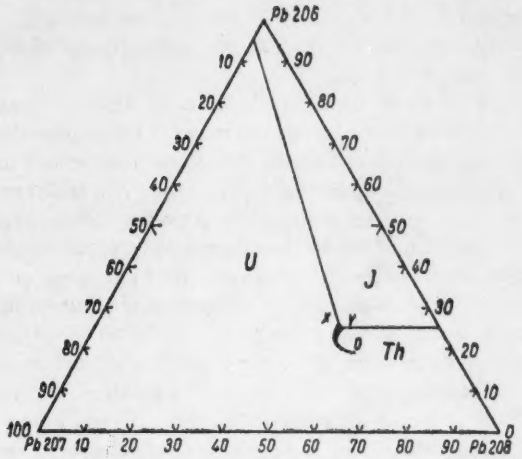

Fig. 1. Diagram of isotopic composition of ordinary lead (OXY field) obtained from nonradioactive occurrences.

*References given as P/773, etc., indicate the number assigned to papers presented at the Second International Conference on the Peaceful Uses of Atomic Energy at Geneva, 1958.

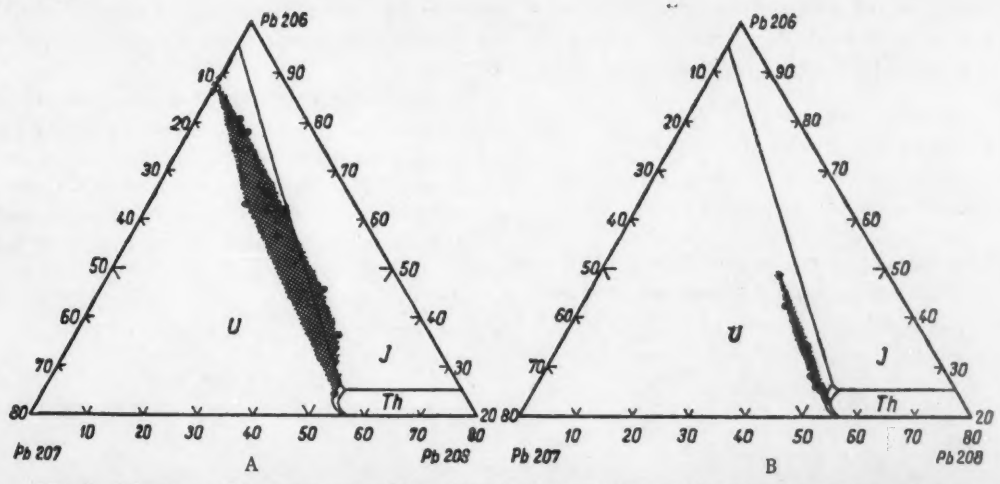

Fig. 2. Diagrams of isotope composition of leads obtained from radioactive occurences. A) Blind River deposit, USA; B) Witwatersranddeposit, Union of South Africa.

its, if the data spill over into the Th field. The location of the isotope analysis data points in the J field provides a less certain orientation, but may be appraised as a yardstick for the possibility of discovering complex uraniferous-thoriferous occurrences.

This technique has yet to be verified in exploration practice. Its use is restricted by the high cost of isotopic assays. However, this approach is beyond any question deserving of the attention of geologists as a new effective method in prospecting for radioactive ores.

BRIEF COMMUNICATIONS

USSR. A facility has been set up at the Joint Institute for Nuclear Research incorporating a diffusion chamber immersed in a magnetic field, designed for studies of interactions of protons and mesons with light-element nuclei or their isotopes (H, D, He). The diameter of the working region of the chamber is 300 mm, the outer diameter is 456 mm. The chamber is designed for operation at pressures up to 25 atm. The magnetic field is set up on the sensitive layer by a MS-4 solenoid magnet, and its field strength reaches 11,200 oersteds in continuous operation and 16,000 oersteds in pulsed operation. The required temperature distribution in the sensitive layer inside the chamber is attained by using an inner plexiglass casing and special electric heaters. The temperature gradient across the outer boundary of the sensitive layer (5/6 cm above the bottom of the chamber) amounts to approximately 8°C/cm and does not exceed 0.3°C/cm in the horizontal planes of the working volume.

USSR. At the Physics Institute of the Academy of Sciences of the USSR, a device has been developed for recording the quantities entering into a correlation function of the form $\Phi_{ik} = \overline{n_i \cdot n_k} - \bar{n}_i \cdot \bar{n}_k$. The measuring time is broken down into ν intervals. In the course of a single interval, the numbers of events n_i of decay events of the i-th type, and n_k of the k-th type, as well as their product $n_i \cdot n_k$, are recorded. The device makes it possible to obtain, with the aid of two PS-10,000 and one PS-64 scalers, values of the number of intervals ν and the total number of decay events of the i-th type in ν_ν intervals, $\sum_1^\nu n_i$; of the k-th type $\sum_1^\nu n_k$ and $\sum_1^\nu n_i \cdot n_k$ directly. On the basis of those values, $\bar{n}_i$, $\bar{n}_k$, and $\overline{n_i \cdot n_k}$ may be computed. The duration of the intervals may be varied over a range of 0.08 to 20 sec. The high speed of response of a single recording channel is 5 μsec, of the second, recording the product $n_i \cdot n_k$, 120 μsec.

USSR. At the Radium Institute of the Academy of Sciences of the USSR, a scaling instrument has been developed, using 10 SG1S decatrons. The resolving time is 12 μ secs, the scaling factor 10^5. The instrument incorporates a device for automatic setting of the counting time (nine set points from 3 sec to 25 min), a rate meter and a quartz calibrator (75 cps frequency). The measurements range for the rate meter is 200, 500, 10^3, $2 \cdot 10^3$, $5 \cdot 10^3$, 10^4, $2 \cdot 10^4$, $5 \cdot 10^4$ ppm, the mean statistical error at a counting rate ≥ 500 ppm is under 1%. The scaling instrument functions normally in response to power supply voltage swings of 200 to 240 volts.

USSR. At the Kharkov branch of the All-Union Scientific Research Institute of chemical reagents for large-scale scintillator inspection, a simple design has been worked out for a single-channel pulse height analyzer. The analyzer provides automatic recording of the gamma spectrum, rapid determination of the half-width of the photopeak in percentage and determination of the relative light output on a graduated circle. The curve of the gamma spectrum is recorded by a self-recording device in a TSShchPr-154-type galvanometer; duration of the trace, with a Cs^{137} source of 0.05 mc activity, is 15 min. The device provides for the possibility of taking the curves of the gamma spectra by the usual method of counting pulses over the channels. The device may be also used in testing photomultipliers.

China. Over 30 different types of radioactive isotopes, including Co^{60}, Na^{24}, P^{32}, Ca^{45}, and others, have been produced in the recently commissioned nuclear research reactor, China's first, constructed with the aid of the Soviet Union in 1958.

China. At the Nangkang Polytechnic Institute (at Tientsin), a homogeneous research reactor delivering 3 watts power has been assembled and started up by the efforts of the faculty and students. The neutron flux is approximately $4.5 \cdot 10^6$ neutrons per cm^2 per sec. The reactor was designed for research and training purposes, and for the production of isotopes.

INFORMATION AND BIBLIOGRAPHY

Fuel element (teplovydelyayushchii element). The basic component of the design of the core or active zone of a power heterogeneous nuclear reactor, containing nuclear fuel. The chief purpose of the fuel element in a power reactor is the generation of heat. The use of this term would be most correct when applied only to power reactors.

Fuel element (toplivnyi element). The basic component of the design of the core or active zone of a research nuclear reactor, containing nuclear fuel. The chief purpose of the fuel element in a research reactor is to sustain the chain reaction initiated in the core; generation of heat in the fuel element of a research reactor is undesirable in a number of instances. The term "toplivnyi element", underscoring its function as fuel (toplivo) for the sustenance of the chain reaction, is properly applied in reference to research reactors.

Coolant (teplonositel'). A substance used for abstraction of the heat developed in the core or active zone, reflector or shielding of a reactor. The equivalent terms "khladoagent" and "okhladitel'" are sometimes employed. However, the term "teplonositel'" most fully characterizes the intended design function of the substance, which is to carry off the heat ["teplonositel'" = heat-transfer agent] (especially when applied to power reactors). It would be most correct to use only this one term.

Natural uranium (prirodnyi uran). Uranium encountered in ores which is characterized by a certain isotope composition (U^{234} = 0.0056%, U^{235} = 0.718%, and U^{238} = 99.276%). The terms "estestvennyi" and "naturalnyi" are frequently used in the literature. They are identical to the term "prirodnyi." For standardization of terminology, it would be most expedient to use the term "prirodnyi uran".

NEW LITERATURE

Books, Symposia, Periodicals

A. D. Galanin, Theory of Thermal Nuclear Reactors (Teoriya yadernykh reaktorov na teplovykh neitronakh). (Atomizdat, 1959) 384 pp., 12 rubles, 40 kopeks. Second revised edition.

The book is devoted to the theory of nuclear reactors working with thermal neutrons. Most of the chapters are based on the work of other authors; some sections contain original material. The exposition not only of the general aspects of the theory, but also of particular details makes this book a useful handbook in practical design work on power reactors and experimental reactors. Appended to the text are experimental data on constants useful in reactor design.

The book will prove useful to engineers and physicists engaged in nuclear reactor design, to servicing personnel in atomic power stations and experimental reactors, and also to students specializing in the field of nuclear power and reactor design.

A. N. Komarovskii, Structural Design of Nuclear Reactors (Stroitel'nye konstruktsii yadernykh reaktorov), (Atomizdat, 1958) 164 pp., 7 rubles, 40 kopeks.

Extensive experience accumulated at home and abroad in the design and construction of the biological shielding of stationary-plant nuclear reactors is generalized in the present book. The foundations of the biological shielding and of the reactors themselves, the construction of lateral and upper biological shielding units, experimental and other apertures in the shielding, etc. are discussed; recommendations are given on the design of shielding facilities for different types of reactors. The book is illustrated with a large number of diagrams and photographic plates showing the structural features of nuclear reactors. An appendix gives the design layout of the biological shielding of a reactor, as well as a long list of literature pertaining to the topic.

A. N. Komarovskii, Structural Design of Accelerators (Stroitel'nye konstruktsii uskoritelei) (Atomizdat, 1958) 112 pp., 6 rubles.

Literature and design materials on the construction of charged-particle accelerator facilities in the Soviet Union and abroad are compiled in the book.

The book is aimed at engineers engaged in accelerator design, as well as students in advanced courses.

A. N. Komarovskii, Structural Materials for Shielding from Radiations Emitted by Nuclear Reactors and Accelerators (Stroitel'nye materialy dlya zaschchity ot izluchenii yadernykh reaktorov i uskoritelei) (Atomizdat, 1958) 124 pp., 5 rubles, 30 kopeks.

The book discusses the shielding and technological properties, as well as the particular applications of structural materials used in shielding from nuclear reactor and accelerator radiations. Most of the attention is devoted to special heavy and hydrated concretes. The shielding properties of ordinary concretes, as well as the conditions for obtaining peak density and homogeneity in the concrete structure, are considered.

The results of a number of investigations at home and abroad and experience accumulated in the practice of erecting shielding for nuclear reactor and accelerator radiations are compiled, symstematized, and generalized in the book.

The book is written for engineers engaged in designing the structural aspects of such facilities, and also those engaged in construction work on radiation shielding.

N. G. Gusev, V. P. Mashkovich, and P. V. Obvintsev, Gamma Radiation of Radioactive Isotopes and Fission Products (theory and tables) [in Russian] (Gostekhizdat, 1958) 208 pp., 10 rubles, 75 kopeks.

The book is a reference manual; it contains data on gamma radiation emitted by radioactive isotopes and mixtures of products of U^{235} fission, the data being necessary for the practical use of the isotopes, in particular with reference to shielding needs.

The following data are available: gamma constants of 400-odd isotopes, gamma activity in terms of 1 mC per milligram equivalent of radium, rate of stopping power, β - λ-activity and spectral composition of gamma radiation from products of U^{235} fission as a function of the length of exposure in the reactor.

IN PRESS

A. K. Val'ter et al., Electrostatic Generators [in Russian] (Atomizdat, 1959) 240 pp., 9 rubles.

A symposium of the reports compiled by a team of authors headed up by Acting Member of the Academy of Sciences of the USSR A. K. Val'ter, and devoted to the general principles of the construction of high-voltage electrostatic generators and specific problems in their design, testing, and operation.

A number of articles in the symposium deal with components of electrostatic generators, as well as with some of the research work carried out using the generators.

The edition is written for scientific workers, engineers, designers, and students in advanced courses.

Catalog. Isotopes, Radiation Sources, and Radioactive Materials. (Katalog. Izotopy, istochniki izlucheniya i radioaktivnye materialy) (Atomizdat, 1959) 336 pp., 22 rubles.

The first part of the catalog contains information on methods for the production of radioactive isotopes and techniques for measuring their radiations, as well as tagged compounds and products incorporating them. Health physics requirements are dealt with. Most of the space is given to Tables and the technical characteristics of isotopes, compounds incorporating them, and radiation sources. The features of radiation sources and sample emitters are described. A description is given of the packing and crating to be used in transporting and handling isotopes.

The second section of the catalog provides, for the first time, information of irradiation of different samples of materials and machine parts in the customer's packaging, inside reactors.

The third section of the catalog is devoted to production techniques and methods for using stable isotopes, the characteristics of stable isotopes, labeled compounds, and isotope targets produced in the USSR.

The fourth part of the catalog furnishes information on conditions and procedure to be followed in ordering isotopes and products incorporating isotopes.

ARTICLES IN THE PERIODICAL LITERATURE

M. M. Aleksandrovskaya, "Some data on the effects of ionizing radiation on the morphology of the central nervous system in animals," Trudy inst. vyssh. nervnoi deyatel'nosti akad. nauk SSSR. Seriya patofiziol. 4 (1958).

O. S. Andreeva, "Some data on investigations of contamination and deactivation of personnel laundry in working with radium salts", Gigiena i sanitariya 10 (1958).

"An Atomic Miniaturized Battery", (based on articles in Radio und Fernsehen, 24 (1957). Radio 10 (1958).

A. S. Belitskii, "Evaluation of underground water supply sources under conditions of contamination of the watershed by radioactive products of uranium fission", Gigiena i sanitariya 10 (1958).

K. S. Bogolyubov, "Photographic recording of nuclear radiations", Khim. nauka i promyshlennost' 3, 5 (1958).

Ya. M. Varshavskii et al., "Equilibrium distribution of deuterium in hydrogen exchange with liquid hydrogen chloride", Doklady akad. nauk SSSR 112, 5 (1958).

I. V. Volkind, "Zirconium production in the USA", tsvetnye metally 11 (1958).

H. F. Galanin, "All-Union conference on assay techniques for the determination of trace amounts of radioactive substances in the ambient medium (Leningrad, February, 1958)", Gigiena i sanitariya 10 (1958).

G. I. Glatova et al., "Comparison of plasma decay rates in hydrogen and in deuterium," Zhur. eksptl. i. teoret. fiz. 35, 12 (1958).

V. P. Granil'shchikov and G. M. Parkhomenko, "Experience in using three-zone planning in working with radium", Gigiena i sanitariya 10 (1958).

I. I. Gusarov and V. K. Lyapidevskii, "Technique for measuring natural radioactivity of air, on the basis of radon decay products", Gigiena i sanitariya 10 (1958).

V. N. Gus'kova and A. N. Bragina, "Contribution to the question of the hygenic characteristics of the natural radioactive background of the soil", Gigiena i sanitariya 10 (1958).

I. Dem'yanikov, "Achievements of nuclear physics in the service of the national economy", Narodnoe khozyaistvo Kazakhstana 9 (1958).

Yu. N. Denisov, "Universal nuclear magnetometer," Pribory i tekhnika eksperimenta 5 (1958).

A. I. Zhernovoi et al., "New method for measuring homogeneous and nonhomogeneous magnetic fields on the basis of proton magnetic resonance," Pribory i tekhnika eksperimenta. 5 (1958).

A. . Zil'berberg, "Rational design of containers and storage vessels for ampules containing radioactive isotopes (Quality control of seam welds by gamma rays)", Stroitel'stvo turboprovodov [Pipeline Construction] 10 (1958).

A. S. Zykova et al., "Contribution to the question of determination of natural radioactive aerosols in atmospheric air", Gigiena i sanitariya 10 (1958).

R. S. Kalinova, "Health problems in the transportation of radioactive isotopes", Gigiena i sanitariya 10 (1958).

T. V. Kirillova and R. F. Byurig, "On the results of measurement of underwater radiation in Lake Sevan," Trudy glav. geofiz. obs., 78 (1958).

T. V. Kirilova, "Radiation budget of Lake Balkhash," Trudy. glav. geofiz. obs. 78 (1958).

J. Cockcroft, John Cockcroft on Perspectives of Atomic Science (Interview with the British scientist), Novoye Vremya 48 (1958).

J. Cockcroft, Nuclear Energy, the Power of the Future [Report presented to the British conference on problems of electricity and power in Brussels (May, 1958)]. Elektr. stantsii 10 (1958).

A. S. Kompaneyets, "Radio frequency emissions from an atomic explosion", Zhur. eksptl. i teoret. fiz. 35, 12 (1958).

V. N. Kotlyar, "On the genesis of uranium mineralization of ancient conglomerates", Sbornik nauchn. trud. Mosk. inst. tsvetnykh met. i zolota, 28 (1958).

S. P. Kruglov, "Calorimetric measurement of energy flux of gamma rays from a synchrotron," Zhur. tekhn. fiz. 28, 10 (1958).

A. N. Marei, "Radioactive wastes", Priroda 12 (1958).

V. V. Nikolaev et al., "Radioactive densitometer for measurement of the density of petroleum products in pipelines in series pumping," Neftyanoe khozyaistvo 10 (1958).

A. A. Nichiporovich, "Photosynthesis and the technique of labeled atoms", Priroda 12 (1958).

Yu. F. Orlov and E. K. Tarasov, "Excitation of oscillations in an electron cyclic accelerator by quantum radiation fluctuations", Pribory i tekhnika eksperimenta 5 (1958).

M. S. Osipova, "On some changes in protein metabolism in the brain in response to Co^{60} gammas," Report no. 1. Trudy inst. vyssh. nervnoi deyatel'nosti akad. nauk SSSR. Seriya patofiziol. 4 (1958).

B. P. Peregud, "Stabilization of the field of an electromagnet", Pribory i tekhnika eksperimenta 5 (1958).

B. P. Peregud, "Stabilization of constant current and voltage using the field of a permanent magnet as a reference", Pribory i tekhnika eksperimenta 5 (1958).

I. A. Piontovskii, "Basic trends in radiobiological research at the institute of higher nervous activity of the Academy of Sciences of the USSR," Seriya patofiziol 4, (1958).

A. A. Saukov, "All-Union conference on geochemical and radiometric techniques in prospecting and exploration of petroleum and gas deposits", Geokhimiya 6 (1958).

G. V. Smirnitskaya and E. M. Renkhrudel', "Kinetics of electrons in the electromagnetic field of a magnetic ioni-

zation manometer and an ion pump", Vestnik Mosk. gos. universiteta 2 (1958).

I. E. Starik and I. A. Skul'skii, "Adsorption of trace amounts of radio elements on non-ion exchange adsorbents", Izvestiya akad. nauk SSSR. Otdel. khim. nauk 10 (1958).

P. S. Stroganov and M. M. Telitchenko, "Accumulation and distribution of some radioactive substances in water organisms," Byul. Mosk. obshchestva ispyt. prirody. Otdel. biol. 4 (1958).

S. I. Syrovatskii, "On the stability of shock waves in magnetohydrodynamics," Zhur. eksptl. i teoret. fiz. 35, 12 (1958).

A. V. Terman, "Use of radioactive tracers in health research," Gigiena i sanitariya 10 (1958).

N. M. Tomson, "Technique for assaying the radioactivity of atmospheric dust", Gigiena i sanitariya 10 (1958).

G. K. Ul'yanov and K. N. Vinogradov, "Measurement of nonhomogeneous magnetic fields", Pribory i tekhnika eksperimenta 5 (1958).

Jao Kei-Hua, "Surface oscillations of a discharge pinch in a longitudinal magnetic field", Zhur. eksptl. i teoret. fiz. 12 (1958).

S. S. Yastrebov, "Automatic sweep of a magnetic field for the MS-2M mass spectrometer", Pribory i tekhnika eksperimenta 5 (1958).

ACADEMY OF SCIENCES OF THE USSR, DIVISION OF PHYSICS AND MATHEMATICAL SCIENCES

CONTEST FOR THE S. I. VAVILOV GOLD MEDAL

The division of physics and mathematical sciences of the Academy of Sciences of the USSR announces that the contest for the S. I. Vavilov Gold Medal has been carried over from 1958 into 1959.

The S. I. Vavilov Gold Medal is awarded once every three years for outstanding work in the field of physics.

The right to compete for the S. I. Vavilov Gold Medal is open to all Soviet scientists. Only individuals may participate in the contest, on a personal basis.

Promotion of candidates for the Gold Medal competition may be undertaken by scientific institutions in the USSR and sister republics (by scientific research institutions and laboratories), by design offices, advanced educational institutions, scientific and engineering societies, honorary members, acting members and corresponding members of the Academy of Sciences of the USSR.

Organizations and individual persons promoted as candidates in the Gold Medal competition must present the following materials to the Commission of Experts on the S. I. Vavilov Gold Medal:

1) published scientific papers, materials relating to a scientific discovery or invention, in triplicate;

2) materials on discussion of the papers presented by the scientific community;

3) an abstract of the paper;

4) concise biographical information on the candidate with a list of his basic scientific work.

Papers previously receiving recognition in the competition will not be accepted.

Papers addressed to the S. I. Vavilov Gold Medal contest should be directed to the S. I. Vavilov Gold Medal Commission of Experts at the following address: Moscow, Leninskii prospekt, 53, Physics Institute of the Academy of Sciences of the USSR.

The deadline for submission of papers is September 15, 1959.

The Division of Physics and Mathematical Sciences

A PUBLICATION OF **POLYTECHNIC PRESS**
OF THE POLYTECHNIC INSTITUTE OF BROOKLYN

Exploring the Most Advanced Industrial Practices in Communication . . .

Writing in Industry . . . Volume I

Edited by Siegfried Mandel, Associate Professor of English, Polytechnic Institute of Brooklyn.

This new, outstanding work incorporates the highlights of the 1959 conference on Writing and Publication in Industry which was sponsored by Polytechnic Institute of Brooklyn. Exploring the most advanced industrial practices in communication, the authors present clearly and concisely, the most effective techniques in proposal writing and science reporting, as well as the design and production problems in engineering publications.

This "first" from Polytechnic Press will prove to be fascinating reading for all technical writers and editors, and will be a valuable addition to all libraries.

Contents are as follows:

PREFACE

INTRODUCTION: THE CHALLENGE TO WRITERS IN INDUSTRY, by Siegfried Mandel, *Associate Professor of English, Polytechnic Institute of Brooklyn.*

THE RELATIONSHIP OF ENGINEERING AND TECHNICAL WRITING, by Robert T. Hamlett, *Director of Training and Personnel, Sperry Gyroscope Company.*

EVERYDAY EDITORIAL PROBLEMS OF AN ENGINEER-SUPERVISOR, by Ronald J. Ross, *Engineering Section Head for Advanced Studies, Sperry Gyroscope Company.*

TECHNIQUES AND PRACTICES OF PROPOSAL WRITING, by David L. Caldwell, *Proposal Manager, Process Plants Division, Foster-Wheeler Corporation.*

WRITING FOR PUBLICATIONS: WHY AND HOW?, by George R. Wheatley, *Department Chief, Public Relations, Western Electric Co., Inc.*

PRODUCTION AND DESIGN PROBLEMS IN ENGINEERING PUBLICATIONS, by Arthur Eckstein, *Eckstein-Stone, Inc.*

JOURNALISTIC ASPECTS OF SCIENCE WRITING, by William L. Laurence, *Science Editor, New York Times.*

1959 bound 128 pages illus. $2.75

Send all orders and inquiries to:

PLENUM PRESS, INC. • 227 W. 17 St., New York 11, N. Y.

A Milestone in Scientific Communication...

Advances in Cryogenic Engineering

VOLUME 1
VOLUME 2
VOLUME 3
VOLUME 4
VOLUME 5

Edited by K. D. Timmerhaus

These 5 volumes, the proceedings of the Cryogenic Engineering Conferences held since 1954, form the only authoritative collection on the research and development to date in this new and exciting field.

A working tool for industry!

ROCKETRY • MISSILES • LIQUEFACTION OF GASES • FREE RADICALS SPECTROSCOPY • ELECTRONICS • MINIATURIZATION • AIR SEPARATION • PURIFICATION • INSULATION • ATOMIC ENERGY

are all vitally affected by the rapid research progress in low-temperature technology.

In order to meet the growing demand for more information about cryogenics, Plenum Press has reprinted Volumes 1-4 in new hard-cover editions and presents

(Special rate of $35 for first four volumes)

VOLUME 5
(Proceedings of the Fifth National Conference on Cryogenic Engineering, 1959)

Foreign price Volumes 1-5 $15.00 Volumes 1-4 (set) $40.00

for the first time.

cloth illustrated over 350 pages in each volume $13.50 per volume

PLENUM PRESS 227 WEST 17TH STREET, NEW YORK 11, N. Y.
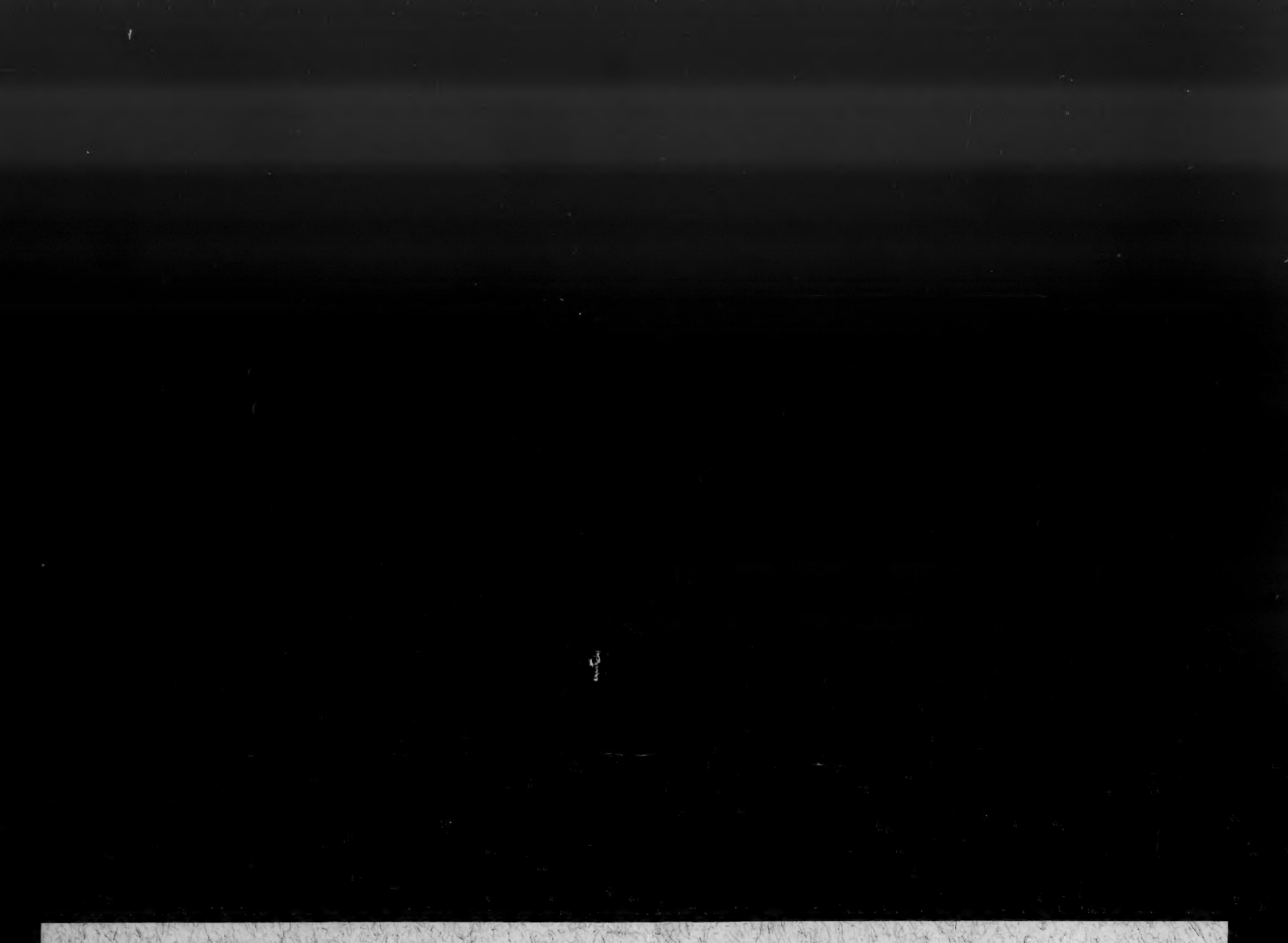
A subsidiary of Consultants Bureau Enterprises, Inc.